Mono Basin
Annual Monitoring Reports

May 2025

Prepared for State Water Resources Control Board

In Accordance with the Terms and Conditions of Amended License Nos. 10191 and 10192

Contents

Section I. Mono Basin Fisheries Monitoring Report
Rush, Lee Vining, and Walker Creeks 2024

Prepared by Ross Taylor and Associates

Mono Basin Fisheries Monitoring Report
Rush, Lee Vining, and Walker Creeks
2024

Prepared by Ross Taylor and Associates for

The State Water Resources Control Board, the Los Angeles Department of Water and Power and the Mono Basin Monitoring Administration Team

April 9, 2025

Table of Contents

Executive Summary

The 2024 fisheries sampling was the third of ten years of biological monitoring of the Stream Ecosystem Flows (SEF), with oversight from the Mono Basin Monitoring Administration Team (MAT) as directed by the California State Water Resource Control Board's (SWRCB) amended Licenses 10191 and 10192. This monitoring continues a 25-year history of monitoring ordered by the SWRCB under Orders 98-05 and 98-07. The six reaches sampled in 2024 were similar in length to those sampled annually between 2009 and 2023, except the Lee Vining Creek side channel was dropped in 2022. Sample site selection has evolved over time, with more sites annually sampled in 1999 through 2008 as the Fisheries Team investigated potential differences in fish production based on proximity to the Grant Lake Reservoir (GLR) dam and varying channel slopes and confinement. For example, in Rush Creek, the Mono Gate One Return Ditch (MGORD) was selected because of its tail water condition below the dam and its propensity to support older and larger Brown Trout. Upper Rush was selected for its moderately-sloped channel and its location just downstream of a confined, gorge-like section. The Bottomlands section was selected for its location in a low-gradient area that historically had more potential for the formation of meanders, deeply scoured pools, and side-channels. In 2023, three locations in a multi-thread channel reach were sampled in lower Rush Creek because they were heavily influenced by beaver dams.

The 2024 Runoff Year (RY) was 103% of normal and classified as a Normal RY type, as measured on April 1st. The range of runoff that defines Normal RY is 82.5% - 107% (40% - 60% exceedance). The preceding 15 years included an Extreme-Wet RY of 226% in 2023, Dry RY of 60% in 2022, Dry RY of 58% in 2021, Dry-Normal-1 RY of 71% in 2020, a Wet RY of 140% in 2019, a Normal RY of 85% in 2018, a record Extreme-wet RY of 206% in RY 2017 and five consecutive below "Normal" RY's (RY 2016 was 74% of normal, RY 2015 was 25% of normal, RY 2014 was 48% of normal, RY 2013 was 66% of normal and RY 2012 was 55% of normal).

Because 2024 was an even-year, two-pass electrofishing for generating mark-recapture population estimates was conducted in the Lee Vining Creek main channel section and in three sections of Rush Creek – the MGORD, Upper Rush and the Bottomlands. Multiple-pass depletion electrofishing was conducted in Walker Creek. Single-pass electrofishing was conducted in the 8-Channel, in the area associated with beaver dams in lower Rush Creek.

Annual Monitoring Metrics

As in previous even-years, the annual monitoring metrics included population estimates of three size classes of trout (<125 mm, 125-199 mm, and ≥200 mm in total length), density estimates (number of fish/ha) of age-0 and age-1+ trout, and total standing crop estimates (kg/ha). As in all years, condition factors, growth rates (in length and weight) from recaptures of previously PIT tagged trout, and relative stock densities (RSD) for three size classes of catchable trout were computed with the 2024 fisheries data (Table 1).

Table 1 provides a concise view of comparisons of the 2024 monitoring metrics versus 2022 and 2023 results. Comparisons of population estimates and metrics derived from population estimates require using the even-year data from 2022 and 2024. The Results section provides more detail regarding the decreases and increases of all monitoring metrics (Table 1).

PIT Tagging – New Tags and Recaptures

In 2024, a total of 979 trout received PIT tags and adipose fin clips in Rush, Lee Vining, and Walker Creeks. In addition, one recaptured adipose fin-clipped fish had shed its original tag and was re-tagged, thus a total of 980 PIT tags were implanted during the 2024 fisheries sampling. Of the 979 new trout tagged and clipped, 742 were age-0 Brown Trout and 180 were age-1 and older Brown Trout. For Rainbow Trout, 56 age-0 fish and one older fish were tagged and clipped. One-hundred-eighty of the 238 Brown Trout tagged in the MGORD section were 164 mm to 225 mm in total length and were presumed to be age-1 fish. In addition, 58 age-0 Brown Trout were tagged in the MGORD.

In 2024, a total of 52 previously tagged trout (that retained their tags) were recaptured in the Rush Creek watershed. Fourteen of the recaptures occurred in the Upper Rush section, followed by 12 recaptures in Walker Creek, 11 recaptures in the 8-Channel section, nine recaptures in the MGORD, and six recaptures in the Bottomlands section. A total of four previously tagged Brown Trout (that retained their tags) were recaptured in the Lee Vining Creek main channel section. During the 2024 sampling, only one previously tagged Rainbow Trout was recaptured (in the Upper Rush section), thus very limited growth rate information was available for Rainbow Trout in Rush Creek, and none was available for Lee Vining Creek.

The 2024 growth rates of most PIT-tagged recaptured age-1 and age-2 Brown Trout were relatively high, most likely due to the mostly favorable summer water temperatures in Rush Creek.

Summer Water Temperatures in Rush Creek

In 2024, the water temperature monitoring was again conducted by the MLC. The extended elevated flows during the 78-day spill out of GLR resulted in the loss of the data logger at the Rush Creek/Above Parker location (no data for 2024). At the Rush/County Road location the data logger was deployed on July 12th and this data logger also was exposed when flows dropped in August. Thus, during the 92-day period of July-September when summer water temperatures were examined, the County Road site was missing 29 days of data (July 1st through 12th and August 8th through 24th).

In 2024, the Normal RY with GLR at high storage levels and a 78-day spill resulted in mostly favorable summer thermal conditions, with peak water temperatures exceeding 70^{o}F at only the Above Damsite (11 days) and County Road (one day) monitoring locations. In 2024, daily average temperatures and average daily maximum temperatures were relatively low and within

the range typical of wetter RY types and/or when a full GLR spills for extended periods. At most Rush Creek temperature monitoring locations, the maximum diurnal fluctuations were relatively large, yet appeared to be influenced by lower lows, as opposed to higher daily maximums.

Proposed Fisheries Sampling for 2025 Season

During the development of the post-settlement monitoring scope and budget, RTA proposed that the annual fisheries sampling was reduced to conduct population estimate sampling every other year (in even-years). In the odd-years, single-pass electrofishing sampling would occur to collect data to evaluate population age-class structure, compute condition factors, generate growth data from recaptures of previously tagged fish, and implant PIT tags in new cohorts of fish.

We intend to conduct single-pass sampling in the fall of 2025. In addition to conducting single-pass sampling at the annually sampled locations, RTA proposes sampling the 8-Channel section of Rush Creek to continue sampling the area adjacent to the area once occupied by beavers.

Table 1. Summary of Mono Basin Brown Trout annual monitoring metrics; changes between sampling years 2023 and 2024. N/A = not applicable or not available. The percentage increases/decreases between 2023 and 2024 are provided in parentheses. For population estimates and for metrics based on population estimates (density and standing crop), the comparisons are between 2022 and 2024 values. For growth rates, increases/decreases between 2023 and 2024 are provided in millimeters or grams.

Annual Monitoring Metrics	Rush Creek - MGORD	Rush Creek - Upper	Rush Creek - Bottomlands	Walker Creek	Lee Vining Creek
Population Estimate <125 mm	N/A to 481	Increase (91%)	Increase (87%)	Decrease (81%)	Increase (842%)
Population Estimate 125-199 mm	N/A to 265	Decrease (21%)	Decrease (87%)	Decrease (98%)	Decrease (81%)
Population Estimate ≥200 mm	Increase (202%)	No change	Increase (74%)	Decrease (13%)	Decrease (25%)
Density Estimate (fish/ha) Age-0	N/A to 254	Increase (82%)	Increase (53%)	Decrease (86%)	Increase (631%)
Density Estimate (fish/ha) Age-1+	Increase (236%)	Decrease (33%)	Decrease (62%)	Decrease (73%)	Decrease (64%)
Standing Crop (kg/ha)	Increase (220%)	Increase (13%)	Decrease (7%)	Decrease (36%)	Decrease (12%)
Condition Factor	Decrease	Decrease	Increase	Increase	Decrease
Growth Rate (mm) of Age-1 Recaptures	Increase (23 mm)	Decrease (32 mm)	Decrease (27 mm)	N/A	N/A
Growth Rate (g) of Age-1 Recaptures	Increase (32 g)	Decrease (49 g)	Decrease (28 g)	N/A	N/A
Growth Rate (mm) of Age-2 Recaptures	N/A	N/A	N/A	Increase (11 mm)	Increase (4 mm)
Growth Rate (g) of Age-2 Recaptures	N/A	N/A	N/A	Increase (14 g)	Increase (9 g)
RSD-225	Decrease	Decrease	Increase	N/A	Increase
RSD-300	Decrease	Increase	Increase	N/A	Increase
RSD-375	Decrease	Decrease	Decrease	N/A	N/A

Introduction

Study Area

Between September 15th and 25th 2024, Ross Taylor (the SWRCB's Fisheries Scientist) and a staff of six fisheries biologists conducted the annual fisheries monitoring surveys in six reaches along Rush, Lee Vining, and Walker Creeks in the Mono Lake Basin. The 2024 fisheries sampling was the third of ten post-settlement years of biological monitoring of the Stream Ecosystem Flows (SEF), with oversight from the Mono Basin Monitoring Administration Team (MAT). The SEFs are an integral part of the amended water licenses in SWRCB's Order WR-2021-0086. Five of the six reaches sampled in 2024 were similar in length to those sampled between 2009 and 2023. The sixth reach sampled was the Rush Creek 8-Channel, which was sampled for the first time in 2023. Aerial photographs of the sampling reaches are provided in Appendix A.

Hydrology

The 2024 Runoff Year (RY) was 103% of normal and classified as a Normal RY type, as measured on April 1st. The range of runoff that defines Normal RY is 82.5% - 107% (40% - 60% exceedance). The preceding 15 years included an Extreme-Wet RY of 226% in 2023, Dry RY of 60% in 2022, Dry RY of 58% in 2021, Dry-Normal-1 RY of 71% in 2020, a Wet RY of 140% in 2019, a Normal RY of 85% in 2018, a record Extreme-wet RY of 206% in RY 2017 and five consecutive below Normal RY's (RY 2016 was 74% of normal, RY 2015 was 25% of normal, RY 2014 was 48% of normal, RY 2013 was 66% of normal and RY 2012 was 55% of normal).

Following the flow regimes developed for the Los Angeles Department of Water and Power's (LADWP) State Water Resources Control Board Order WR-2021-0086, in Normal runoff years, SEFs in Rush Creek were defined in Table 2-11 of the Synthesis Report (Table 2). However, given the compromised condition of the roto-valve, LADWP was unable to release the prescribed 380 cfs down the MGORD in 2024. For the actual 2024 Rush Creek hydrograph, the red line in Figure 1 depicts both snowmelt runoff and Southern Cal Edison (SCE) ramping in Rush Creek upstream of Grant Lake Reservoir (GLR). The purple line depicts releases by LADWP into the top end of the MGORD, with a maximum release of 171 cfs on 7/02/24 (Figure 1). The blue bars depict the 78-day spill over the dam spillway, which included 16 days of spills >200 cfs and seven days >300 cfs (Figure 1). The light-tan dotted line in Figure 1 depicts the combined flows below GLR of the SEF release plus the spill, which included a peak of 501 cfs on 6/15/24 and nine days of flows >400 cfs (Figure 1). The dashed blue line in Figure 1 depicts flows in lower Rush Creek with unregulated accretions from Parker and Walker Creeks, which included a peak of 569 cfs on 6/14/24 and 15 days of flows >400 cfs (Figure 1). The brown dashed line depicts storage elevations in GLR (Figure 1).

For RY 2024 in Lee Vining Creek, LADWP followed the diversion rate table (when diverting) and fall/winter baseflows consistent with the SEF regime defined in WR-2021-0086 (Figure 2). In 2024, multiple peaks occurred in Lee Vining Creek above the intake, with a peak of 259 cfs on

6/6/24 (Figure 2). The difference between the blue line and the red bars depicts LADWP's diversions from Lee Vining Creek into GLR (Figure 2). The erratic blue line peaks throughout the summer/fall/winter months were most likely SCE's ramping for power generation. Starting in early October, LADWP's diversions maintain the steady SEF fall/winter baseflow (Figure 2).

Table 2. Rush Creek SEFs for Normal runoff year type as defined in the Synthesis Report.

Table 2-11. Rush Creek recommended SEFs for NORMAL runoff year types.

NORMAL RUNOFF YEAR					
Hydrograph Component	Start Date	End Date	Streamflow (cfs)	Duration (days)	Rate of Change
Spring Baseflow	April 1	April 30	40	30	
Spring Ascension	May 1	May 14	40-80	14	5%
Spring Bench	May 15	June 11	80	28	
Snowmelt Ascension	June 12	June 14		3	10%
Snowmelt Bench	June 15	July 14	120	14	
Snowmelt Flood	June 19	July 4	120-380-120	16	20%
Snowmelt Peak (release)	June 25	June 27	380	3	
Snowmelt Peak (spill)					
Fast Recession					10%
Medium Recession (Node)	July 15	July 26	120-58	12	6%
Slow Recession	July 27	August 16	58-27	21	3%
Summer Baseflow	August 17	September 30	27	45	
Fall Baseflow	October 1	November 30	27	61	
Winter Baseflow	December 1	March 31	27	121	

Grant Lake Reservoir (GLR)

In 2024, storage elevation levels in GLR fluctuated from a high of 7,131.8 ft on June 13th through 15th to a low of 7,119.4 ft on December 31st (Figure 1). In 2024, GLR spilled for 78 consecutive days, between April 23rd and July 9th (Figure 1). This spill had flows >200 cfs for 16 days, including seven days >300 cfs (Figure 1). In 2024, GLR filled from January until mid-June, then dropped steadily through September, and then dropped at a steeper rate the remainder of the year as LADWP started their exports (Figure 1). The extended spill and relatively high storage levels throughout the summer months resulted in mostly favorable water temperatures for Brown Trout.

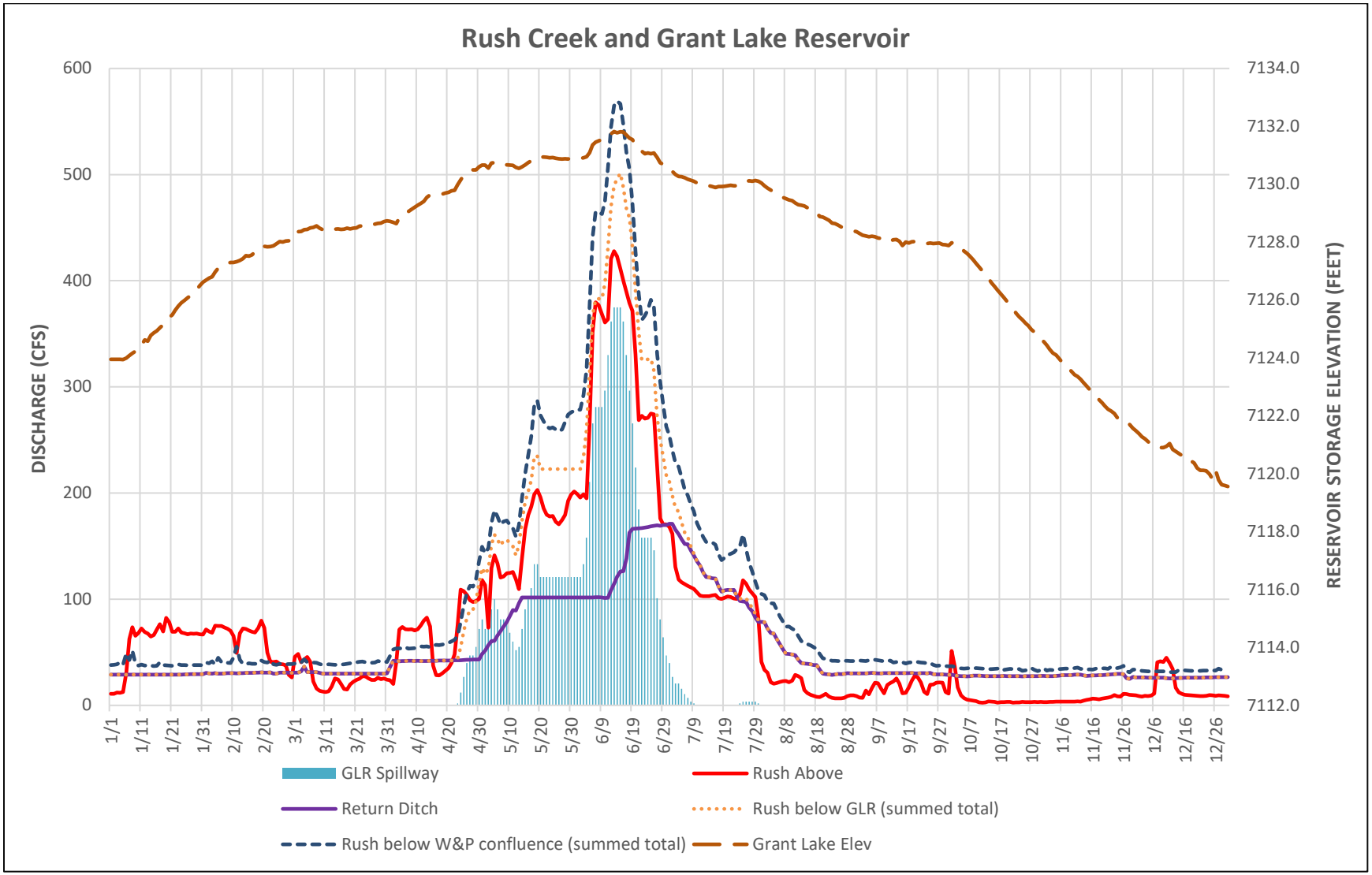

Figure 1. Rush Creek hydrographs and GLR storage levels between January 1st and December 31st of 2024 (chart provided by LADWP).

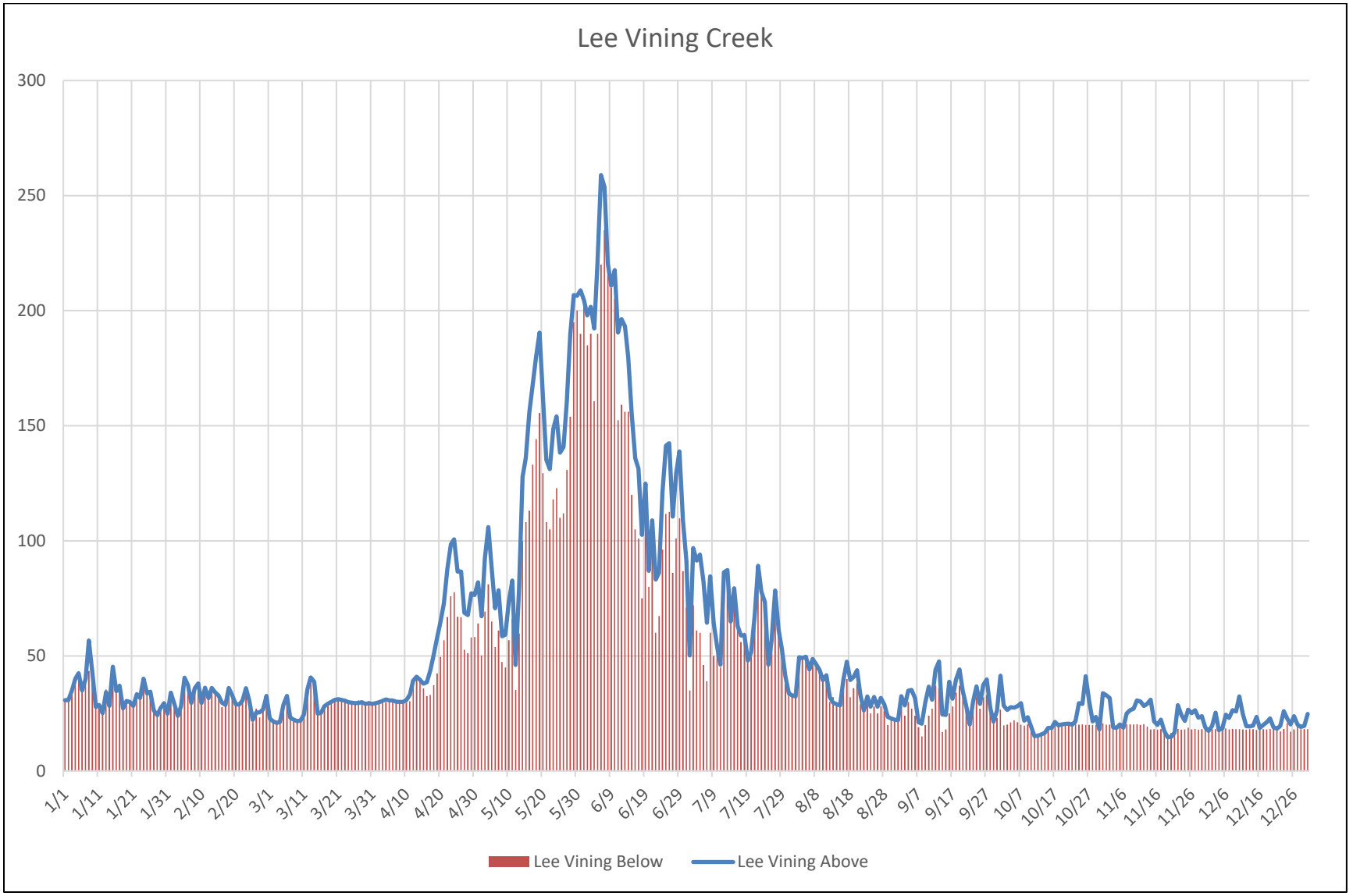

Figure 2. Lee Vining Creek hydrograph between January 1st and December 31st of 2024 (chart provided by LADWP).

Methods

The annual fisheries monitoring was conducted between September 15th and 25th of 2024. The sampling was conducted by Ross Taylor of Ross Taylor and Associates (RTA), Lawrance Vernallis, Zane Taylor and Ty Seay (RTA employees), and three sub-consultants to RTA: Beth Chasnoff-Long, Tyler Rose, and Olivia Vosburg. Closed population mark-recapture and depletion methods were utilized to estimate trout abundance. The mark-recapture method was used on the MGORD, Upper and Bottomlands sections of Rush Creek and on the Lee Vining Creek main channel section. The multiple-pass depletion method was used on the Walker Creek section. The 8-Channel on Rush Creek was sampled on a single-pass with the electrofishing barge.

For the mark-recapture method to meet the assumption of a closed population, semi-permanent block fences were installed at the upper and lower ends of each section. The semi-permanent fences were 48 inches tall, constructed with ½-inch mesh hardware cloth, t-posts, and rope. Hardware cloth was stretched across the entire width of the creek and t-posts were then driven at roughly five-foot intervals through the cloth on the upstream side approximately one foot from the edge. Rocks were placed on the upstream (lower) edge of the fence to prevent trout from swimming underneath the fence. Rope was secured across the tops of the T-posts and anchored to both banks upstream of the fence. The hardware cloth downstream of the T-posts was raised and secured to the rope with bailing wire. Fences were raised the morning of the mark-run and left in place for seven days until the recapture-run was finished. To prevent failure, all fences were cleaned of leaves, twigs, pine needles, and checked for mortalities at least twice daily (morning and evening). The seven days between the mark-run and recapture-run allowed fish caught on the mark run to fully reintegrate back into the population of fish within the sample section (another prerequisite of the mark-recapture methodology).

The Walker Creek depletion estimate only required a temporary blockage to prevent fish movement in and out of the study area while conducting the survey. Temporary blockage of the sections was achieved with 3/16 inch-mesh nylon seine nets installed across the channel at the upper and lower ends of the study areas. Rocks were placed on the lead line to prevent trout from swimming underneath the seine net. A long T-post was laid across the channel, on top of the banks, and then the cork line of the seine net was zip-tied to the T-post. Both ends of the seine net were weighed with rocks to hold it in place.

Equipment used to conduct mark-run electrofishing on Rush Creek included a seven-foot plastic barge that contained the Smith-Root© 2.5 GPP electrofishing system, an insulated cooler, and battery powered aerators. The Smith-Root© 2.5 GPP electrofishing system included a 5.5 horsepower Honda© generator which powered the 2.5 GPP control box. Electricity from the 2.5 GPP control box was introduced into the water via two anodes. The electrical circuit was completed by the metal plate cathode attached to the bottom of the barge.

Mark-recapture runs on Rush Creek consisted of a single downstream pass starting at the upper block fence and ending at the lower block fence. In 2024, the field crew consisted of a barge operator, two anode operators, and four netters: two for each anode. The barge operator's job consisted of carefully maneuvering the barge down the creek and ensuring overall safety of the entire crew. The anode operators' job was to safely shock and hold trout until they were netted. The netters' job was to net and transport fish to the insulated cooler and monitor trout for signs of stress. Once the cooler was full of fish, electrofishing was temporarily stopped to process the trout. The trout were then transferred from the cooler to live pens and placed back in the creek. The trout were then processed in small batches and then returned to a recovery live pen in the creek. Once all the trout were processed at a sub-stop, the crew resumed electrofishing until the cooler was once again full. Once a section was completed, the trout in the recovery live pens were released back into the sub-section in which they were captured.

The mark-recapture runs on the Lee Vining Creek main channel consisted of an upstream pass starting at the lower block fence to the upper block fence, a short 15–20-minute break, and then a downstream pass back down to the lower fence. The electrofishing crew consisted of two crew members operating Smith-Root© LR-20B and Model-12 POW backpack electrofishers, three netters, and one bucket carrier who transported the captured trout and periodically transferred trout into holding live pens.

Due to the depth of the MGORD, all electrofishing and netting was done from inside a drift boat. The drift boat was held perpendicular to the flow by two crew members who walked it down the channel. The electrofishing barge was tied off to the upstream side of the drift boat and a single throw anode was used. A single netter used a 10-foot-long handle dipnet to net the stunned trout, which were then placed in an insulated cooler equipped with aerators. A safety officer sat at the stern of the drift boat whose job was to monitor the trout in the cooler, the electrofishing equipment, the electrofishing crew, and shut off the power should the need arise. Once the cooler was full, the trout were moved to a live pen and placed back in the creek for the shore-based crew to process before continuing the electrofishing effort. Any time the electrofishing crew unloaded fish into a live car ahead of the processing crew, the live pen's location was marked with bright-colored survey flagging at the edge of the MGORD road.

For the Walker Creek depletion, a single pass was considered an upstream pass from the lower seine net to the upper seine net followed by a downstream pass back to the lower seine net. One member of the electrofishing crew operated an LR-20B electrofisher; another member was the primary netter, and a third member was the backup netter/bucket carrier. The other crew members processed the trout captured during the first pass while the electrofishing crew was conducting the second pass. Processed first-pass fish were temporarily held in a live pen until the second pass was completed. If it was determined that only two passes were required to generate suitable estimates, all fish were then released. If additional passes were needed, fish from each pass were held in live pens until we determined that no additional electrofishing passes were required to generate reasonable population estimates.

To process trout during the mark-run, small batches of fish from the live pen were transferred to a five-gallon bucket equipped with aerators. Trout were then anesthetized, identified as

either Brown Trout or Rainbow Trout, measured to the nearest millimeter (total length), and weighed to the nearest gram on an electronic balance. Trout were then "marked" with a small (< 3 mm) fin clip for identification during the recapture-run. Trout captured in the Rush Creek MGORD and Bottomlands sections received anal fin clips and trout captured in the Upper Rush section received lower caudal fin clips. Before placing trout into the aerated recovery bucket, each fish was examined for a missing adipose fin. Trout missing their adipose fin were then scanned for their Passive Integrated Transponder (PIT) tag number. Any trout missing their adipose fin that failed to produce a tag number when scanned were recorded as having "shed" the PIT tag; in most instances these fish were retagged. Partially regenerated adipose fins of fish with PIT tags were reclipped for ease of future identification. PIT tags were implanted in most age-0 trout between 70 mm and 124 mm, and in most trout captured in the MGORD up to 225 mm in total length (with the intent to tag only known age-0 and presumed age-1 trout). Once recovered, fish were then moved from the recovery bucket to a live pen to be held until the day's sampling effort was completed. This was done to prevent captured fish from potentially moving downstream into the actively sampled section. At the end of the electrofishing effort, fish were released from the live pens back into the sub-sections in which they had been captured. Fish were then provided with a seven-day period to remix back into the section's population prior to conducting the recapture run.

During the recapture-run, fish were designated as either new fish or recaptured fish. New fish were measured and weighed and scanned for PIT tags if their adipose fin was missing. Recaptured fish, identified by the fin clip made a week earlier, were only measured since they had been weighed during the mark-run. The ratio of new fish to recaptured fish caught on the recapture-run determined the capture efficiency for each size class of trout (<125 mm, 125-199 mm, and ≥200 mm).

All data collected in the field were written on data sheets and entered into Excel spreadsheets using a field laptop computer. Hard copy data collection was used to provide a crucial back-up in case of in-field technical issues with the laptop. These data sheets were then used to proof-check the Excel spreadsheets.

Calculations

To calculate the area of each sample section, channel lengths and wetted widths were measured within the sample reaches. Wetted widths were measured at approximately 10-meter intervals to 0.1-meter accuracy within each reach. Average wetted widths and reach lengths were used to generate sample section areas (in hectares), which were then used to calculate each section's estimates of trout biomass (kg/ha) and density (# of fish/ha).

Mark-recapture population estimates were derived from the Chapman modification of the Petersen equation (Ricker 1975 as cited in Taylor and Knudson 2012). Depletion estimates and condition factors were derived from MicroFish 3.0 software program. Estimates were generated for three size groups of trout: <125 mm in length, 125-199 mm in length, and ≥200 mm in length (200 mm is approximately eight inches).

Mortalities

For the purpose of conducting the mark-recapture methodology, accounting for fish that died during the sampling process was important. Depending on when the fish died (i.e. whether or not they were sampled during the mark-run), dictated how these fish were treated within the estimation process.

All fish that died during the mark-run and were consequently unavailable for sampling during the recapture-run, were considered as "morts" in the mark-run for the purposes of mark-recapture estimates. These fish were removed from the mark-run data and then were added back into the total estimate after computing the mark-recapture estimate.

During the seven-day period between the mark-run and the recapture-run, when the block fences were cleaned twice daily, fence cleaners also looked for additional dead fish, primarily on the lower fences, inside the bounded study sections. When "marked" morts were found on the fences, we went back into the mark-run data and assigned block-fence morts on a one-to-one basis as "morts" to individual fish on the mark-run based on species and size. When this occurred, a comment was added to the individual fish, such as "assigned as fence mort". These marked morts were then removed from the mark-run data since they were unavailable for sampling during the recapture-run. Because of fin deterioration on some morts, exact lengths were not always available. Fortunately, it was not critical to match the exact length when assigning these marked fence morts to fish from the mark-run, but it was important that the fence morts were placed within the proper size class for which estimates were computed. As with fish that died during the mark-run, these marked fence morts were added back into the total estimate after the mark-recapture estimate was computed.

Unmarked fence morts (dead fish in the block fences that had not been caught and clipped during the mark-run) were measured and tallied by the three size classes for which estimates were computed. These fish were then added to the total number of morts (for each size class), which were then added back into the mark-recapture estimates to provide unbiased total estimates for each size class.

PIT tags were removed from all morts with previously implanted tags. The PIT tag database was updated to confirm these morts and “tag pulled” was noted, because these tags were reused.

Length-Weight Relationships

Length-weight regressions (Cone 1989 as cited in Taylor and Knudson 2012) were calculated for all Brown Trout greater than 100 mm in all sections of Rush Creek. Regressions using Log_{10} transformed data were used to compare length-weight relationships by year and by section.

Fulton-type condition factors were computed in MicroFish 3.0 using methods previously reported (Taylor and Knudson 2012) for Brown Trout 150 to 250 mm. A trout condition factor of 1.00 was considered the demarcation between poor and average condition (Reimers 1963; Barnham and Baxter 1998; Blackwell et al. 2000). The literature considers a trout condition

factor of <1.00 as poor, a condition factor of 1.00-1.19 as average, and a condition factor >1.20 as good (Barnham and Baxter 1998).

Relative Stock Density (RSD) Calculations

Relative stock density (RSD) is a numerical descriptor of length frequency data (Hunter et al. 2007; Gabelhouse 1984). RSD values are the proportions (percentage x 100) of the total number of Brown Trout ≥150 mm in length that are also ≥225 mm or (RSD-225), ≥300 mm (RSD-300) and ≥375 mm (RSD-375). A primary purpose of generating RSD values is to describe the structure of a fish population in terms of recreational fishing satisfaction. For Rush and Lee Vining Creeks this would be a descriptor of an eastern Sierra trout stream; as in, out of the estimated numbers of catchable trout (≥150 mm or ≈6 inches) what proportion are "stock" length (≥225 mm or ≈9 inches), "memorable" length (≥300 mm or ≈12 inches), or "trophy" length (≥375 mm or ≈15 inches). These three RSD values are calculated by the following equations:

RSD-225 = [(# of Brown Trout ≥225 mm) ÷ (# of Brown Trout ≥150 mm)] x 100
RSD-300 = [(# of Brown Trout ≥300 mm) ÷ (# of Brown Trout ≥150 mm)] x 100
RSD-375 = [(# of Brown Trout ≥375 mm) ÷ (# of Brown Trout ≥150 mm)] x 100

Water Temperature Monitoring

Water temperatures were recorded (in degrees Fahrenheit) at various locations within Rush and Lee Vining Creeks as part of the Fisheries Monitoring Program. Data loggers were deployed by Robbie Di Paolo of the Mono Lake Committee (MLC) in January and recorded data throughout the year in one-hour time intervals. Data loggers were downloaded at the end of the year and the data were summarized in spreadsheets. Water temperature data loggers were deployed at the following locations in 2024:

1. Rush Creek – Above Damsite
2. Rush Creek – top of MGORD.
3. Rush Creek – bottom of MGORD.
4. Rush Creek – at Upper Rush/Old Highway 395 Bridge.
5. Rush Creek – above Parker Creek.
6. Rush Creek – below Narrows.
7. Rush Creek – at County Road arch-culvert crossing.
8. Lee Vining Creek – at County Road crossing.

For the Fisheries Monitoring Program, the year-long data sets were edited to focus on the 2024 summer water temperature regimes (July – September) in Rush Creek. Analysis of summer water temperature included the following metrics:

1. Daily mean temperature.
2. Average daily minimum temperature.

3. Average daily maximum temperature.
4. Number of days with daily maximums exceeding 70^{o}F.
5. Number of hours with temperatures exceeding 66.2^{o}F.
6. Number of good/fair/poor potential growth days, based on daily average temperatures.
7. Number of bad thermal days based on daily average temperatures.
8. Maximum diurnal fluctuations.
9. Average maximum diurnal fluctuations for a consecutive 21-day period.

Results

Channel Lengths and Widths

Differences in wetted widths between years can be due to several factors such as magnitude of spring peak flows, stream flows at time of measurements, and locations of where the measurements were taken. Lengths, widths, and areas from 2023 were provided for comparisons (Table 3).

Table 3. Total length, average wetted width, and total surface area of sample sections in Rush, Lee Vining, and Walker Creeks sampled between September 15-25, 2024. Values from 2023 provided for comparisons.

Sample Section	Length (m) 2023	Width (m) 2023	Area (m^2) 2023	Length (m) 2024	Width (m) 2024	Area (m^2) 2024	Area (ha) 2024
Rush – Upper	381	7.2	2,743.2	375	7.7	2,887.5	0.2888
Rush - Bottomlands	437	7.6	3,321.2	485	7.7	3,811.5	0.3812
Rush – MGORD	2,230	8.5	18,955.0	2,230	8.5	18,955.0	1.8955
Lee Vining – Main	255	5.9	1,504.5	261	6.1	1,592.1	0.1592
Walker Creek	178	2.9	516.2	194	2.8	543.2	0.0543

Trout Population Abundance

Upper Rush Creek Section

In 2024, a total of 477 Brown Trout ranging in size from 62 mm to 357 mm were captured on the two mark-recapture electrofishing passes in the Upper Rush section (Figure 3); 252 of these fish were caught on the mark-run (Table 4). For comparison, in 2023 a total of 160 Brown Trout were caught on the single electrofishing pass. In 2024, age-0 Brown Trout (<125 mm) comprised 63% of the total catch (compared to 35% in 2023 and 53% in 2022). The Upper Rush section supported an estimated 1,449 age-0 Brown Trout in 2024 compared to 757 age-0 Brown Trout in 2022 (a 91% increase) (Table 4).

In 2024, the 88 Brown Trout captured in the 125-199 mm size class comprised 18% of the total catch in the Upper Rush section (compared to 6% in 2023). The Upper Rush section supported an estimated 206 Brown Trout in the 125-199 mm size class in 2024, compared to 262 fish in 2022 (a 21% decrease) (Table 4).

The 89 Brown Trout ≥200 mm in length comprised 19% of the Upper Rush total catch in 2024 (compared to 59% in 2023). In 2024, Upper Rush supported an estimated 159 Brown Trout ≥200 mm in length compared to an estimate of 159 fish in 2022 (Table 4). In 2024, 11 Brown Trout ≥300 mm in length were captured in the Upper Rush section (Figure 3).

A total of 85 Rainbow Trout were captured in the Upper Rush section comprising 15% of the section's total catch of 562 fish in 2024 (Table 4); Rainbow Trout comprised 15% of the total catch in 2023 and 12% of the total catch in 2022. The 85 Rainbow Trout ranged in length from 54 mm to 339 mm and 65 of these were age-0 fish (Figure 4). Most of the Rainbow Trout appeared to be of naturally produced origin. For Rainbow Trout <125 mm in length, only one recapture was caught, which resulted in a population estimate of 541 fish with a very high standard error (Table 4). No recaptures were made of Rainbow Trout in the 125-199 mm size class; thus, no estimate was possible for 2024 (Table 4). For Rainbow Trout >200mm one recapture was caught, which resulted in a population estimate of 17 fish with a high standard error (Table 4).

Bottomlands Rush Creek Section

In 2024, a total of 402 Brown Trout ranging in size from 57 mm to 319 mm were captured on the two mark-recapture electrofishing passes in the Bottomlands section of Rush Creek (Figure 5); 189 of these fish were caught on the mark-run (Table 4). For comparison, in 2023 a total of 69 Brown Trout were caught on the single electrofishing pass. Brown Trout <125 mm in length comprised 82% of the total catch in 2024 versus 20% of the total catch in 2023. The Bottomlands section supported an estimated 1,156 Brown Trout <125 mm in length in 2024 versus 617 fish in 2022 (an 87% increase).

Brown Trout 125-199 mm in length comprised 3% of the total catch in the Bottomlands section in 2024 versus 30% of the total catch in 2023. This section supported an estimated 27 Brown Trout 125-199 mm in length in 2024 (Table 4) compared to 200 fish in 2022 (an 87% decrease). This low estimate was due to poor recruitment of age-0 trout during the record runoff in 2023.

Brown Trout ≥200 mm in length comprised 15% of the total catch in the Bottomlands section in 2024 (versus 50% in 2023) with the largest trout 319 mm in total length (Figure 5). The Bottomlands section supported an estimated 113 Brown Trout ≥200 mm in 2024 compared to 65 trout in 2022 (a 74% increase).

MGORD Rush Creek Section

Within the MGORD section of Rush Creek a total of 651 Brown Trout were captured in 2024, with 341 fish caught on the mark-run (Table 3). In comparison, a total of 111 Brown Trout were caught in a single electrofishing pass in 2023. In 2024, Brown Trout ranged in size from 82 mm to 543 mm (Figure 6). A total of 73 Brown Trout <125 mm in length were captured in 2024, which comprised 11% of the total catch of Brown Trout (19 age-0 fish were caught in 2023). The 2024 estimate of Brown Trout <125 mm was 481 fish, with a high standard error due to only two recaptures (Table 4).

In 2024, a total of 88 Brown Trout 125-199 mm in length were caught during the mark-recapture sampling and comprised 14% of the total Brown Trout catch in the MGORD section (one fish was caught in 2023). The 2024 estimate of Brown Trout in the 125-199 mm size class was 265 fish (Table 4).

In 2024, a total of 490 Brown Trout ≥200 mm in length were caught during the mark-recapture sampling and comprised 75% of the total catch in the MGORD section (91 fish were caught in 2023). The MGORD supported an estimated 1,508 Brown Trout in the ≥200 mm size class in 2024 (Table 4), compared to 498 fish in 2022, an increase of 203%.

In 2024, 124 Brown Trout ≥300 mm were captured in the MGORD (28 fish ≥300 mm were captured in 2023 and 23 fish in 2022). Fourteen Brown Trout ≥375 mm in length were captured in 2024 (compared to nine fish in 2023 and six fish in 2022). In 2024, eight of these Brown Trout were >400 mm in length (Figure 6).

In 2024, 56 Rainbow Trout were captured in the MGORD section (Figure 7). In the previous 10 years, the Rainbow Trout catch in the MGORD has ranged from zero to 40 fish. Most of the Rainbow Trout captured in 2024 appeared to be of natural origin, with several larger fish exhibiting signs of hatchery origin.

For the past 19 sampling years, electrofishing passes through the MGORD have produced the following total catch values (all size classes of Brown and Rainbow Trout):

- 2024 – Mark run = 362 trout. Recapture run = 345 trout. Two pass average = 353.5 fish.
- 2023 – Single pass = 135 trout.
- 2022 – Mark run = 100 trout. Recapture run = 148 trout. Two pass average = 124 fish.
- 2021 – Mark run = 273 trout. Recapture run = 387 trout. Two pass average = 330 fish.
- 2020 – Single pass = 457 trout.
- 2019 – Single pass = 361 trout.
- 2018 – Mark run = 233 trout. Recapture run = 188 trout. Two-pass average = 210.5 fish.
- 2017 – Single pass = 203 trout.
- 2016 – Mark run = 121 trout. Recapture run = 110 trout. Two-pass average = 115.5 fish.
- 2015 – Single pass = 176 trout.
- 2014 – Mark run = 206 trout. Recapture run = 268 trout. Two-pass average = 237 fish.
- 2013 – Single pass = 451 trout.
- 2012 – Mark run = 606 trout. Recapture run = 543 trout. Two-pass average = 574.5 fish.
- 2011 – Single pass = 244 trout.
- 2010 – Mark run = 458 trout. Recapture run = 440 trout. Two-pass average = 449 fish.
- 2009 – Single pass = 649 trout.
- 2008 – Mark run = 450 trout. Recapture run = 419 trout. Two-pass average = 434.5 fish.
- 2007 – Single pass = 685 trout.
- 2006 – Mark Run = 283 trout. Recapture run = 375 trout. Two-pass average = 329 fish.

Table 4. Rush Creek mark-recapture estimates for 2024 showing total number of trout marked (M), total number captured on the recapture run (C), total number recaptured on the recapture run (R), and total estimated number and its associated standard error (S.E.) by stream, section, date, species, and size class. Mortalities (Morts) were those trout that were captured during the mark run, but died prior to the recapture run. Mortalities were not included in mark-recapture estimates and were added back in for accurate total estimates. NP = estimate not possible. BNT = Brown Trout. RBT = Rainbow Trout. * = biased due to low recaps.

Stream Section-Species Date Size Class (mm)	M	C	R	Morts	**Mark - Recapture Estimate** **Estimate**	S.E.
Rush Creek						
Upper Rush - BNT						
9/15/2024 & 9/22/2024						
0 - 124 mm	148	164	16	4	**1,449**	304
125 - 199 mm	41	58	11	0	**206**	43
≥200 mm	59	47	17	0	**159**	24
Upper Rush - **RBT**						
9/15/2024 & 9/22/2024						
0 - 124 mm	35	29	1	2	**541***	293
125 - 199 mm	5	6	0	0	**NP**	NP
≥200 mm	6	4	1	0	**17***	44
Bottomlands - BNT						
9/16/2024 & 9/23/2024						
0 - 124 mm	149	207	26	1	**1,156**	185
125 – 199 mm	7	6	1	0	**27***	12
≥200 mm	32	37	10	0	**113**	23
MGORD – BNT						
9/18/2024 & 9/24/2024						
0 - 124 mm	36	38	2	1	**481***	222
125 - 199 mm	50	46	8	0	**265**	69
≥200 mm	254	283	47	0	**1,508**	177
Lee Vining Creek						
Main Channel - BNT						
9/19/2024 & 9/25/2024						
0 - 124 mm	102	96	18	3	**528**	95
125 - 199 mm	10	10	4	0	**23***	29
≥200 mm	57	39	31	1	**73**	14

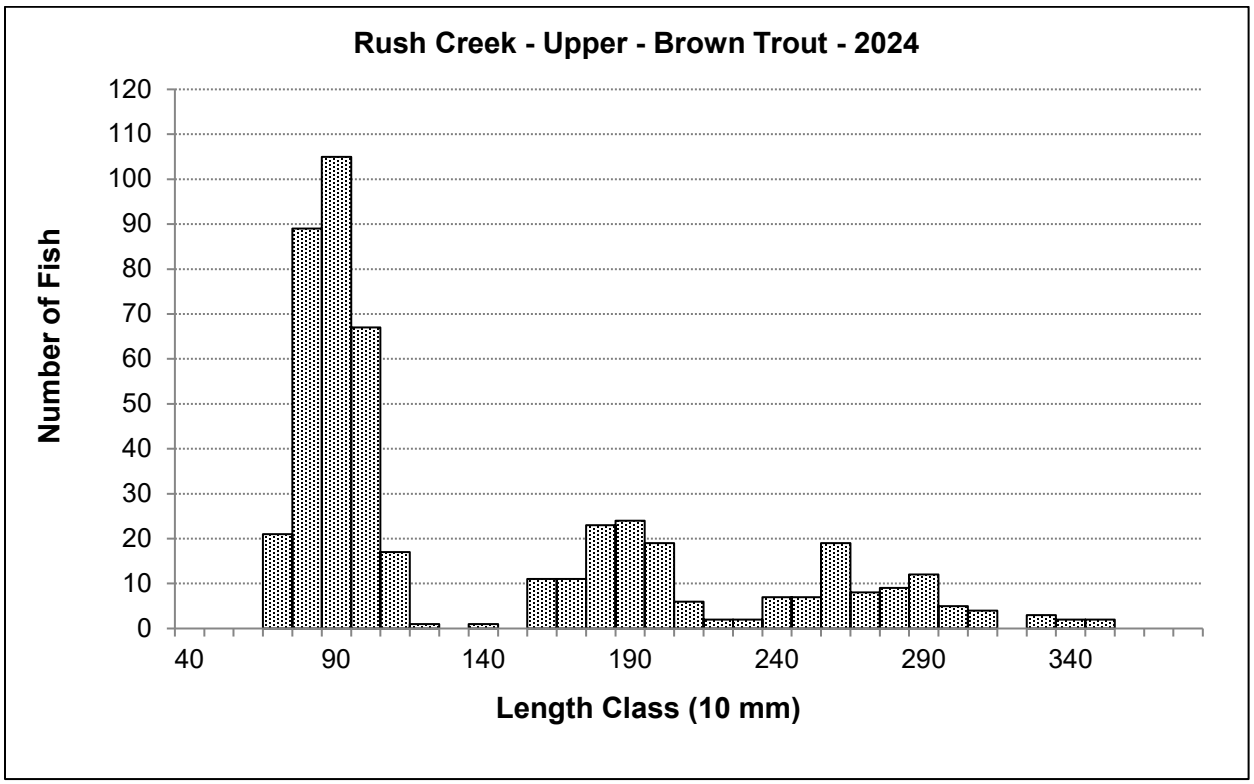

Figure 3. Length-frequency histogram of Brown Trout captured in Upper Rush, September 15th and 22nd, 2024.

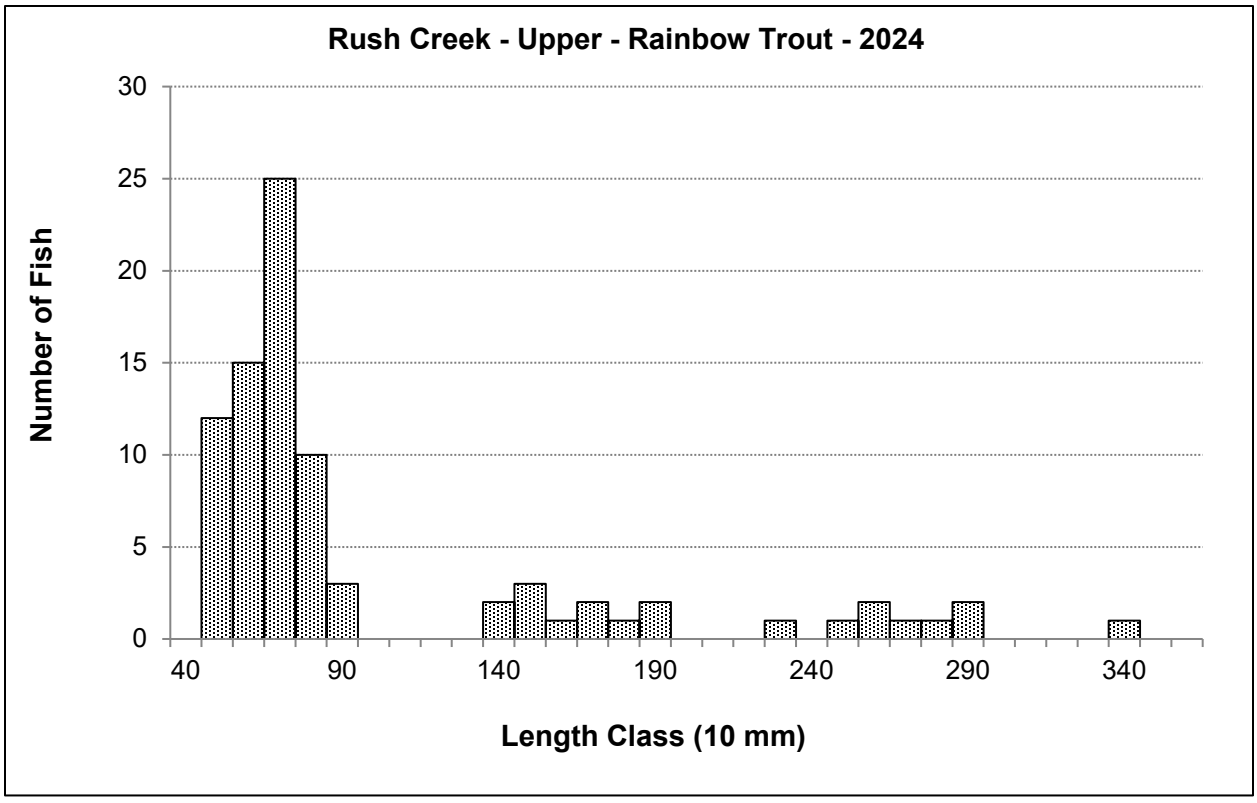

Figure 4. Length-frequency histogram of Rainbow Trout captured in Upper Rush, September 15th and 22nd, 2024.

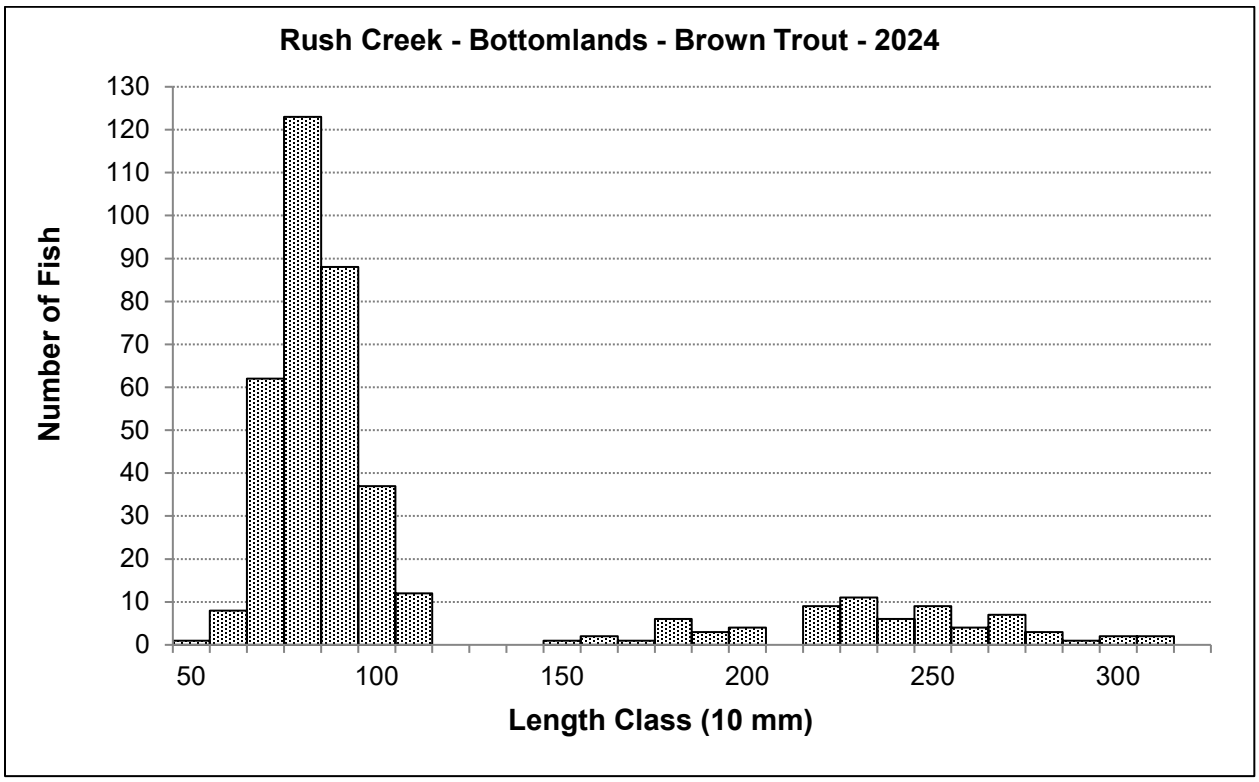

Figure 5. Length-frequency histogram of Brown Trout captured in the Bottomlands section of Rush Creek, September 16th and 23rd, 2024.

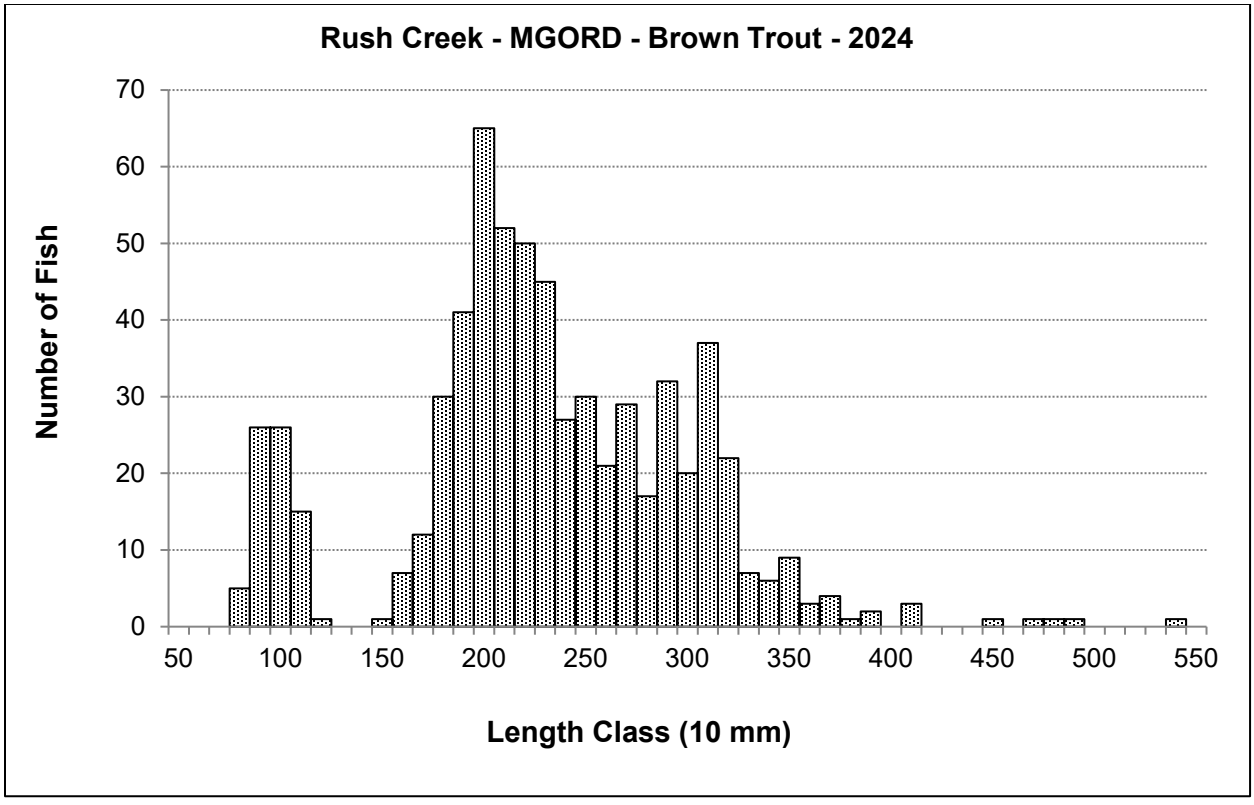

Figure 6. Length-frequency histogram of Brown Trout captured in the MGORD section of Rush Creek, September 18th and 24th, 2024.

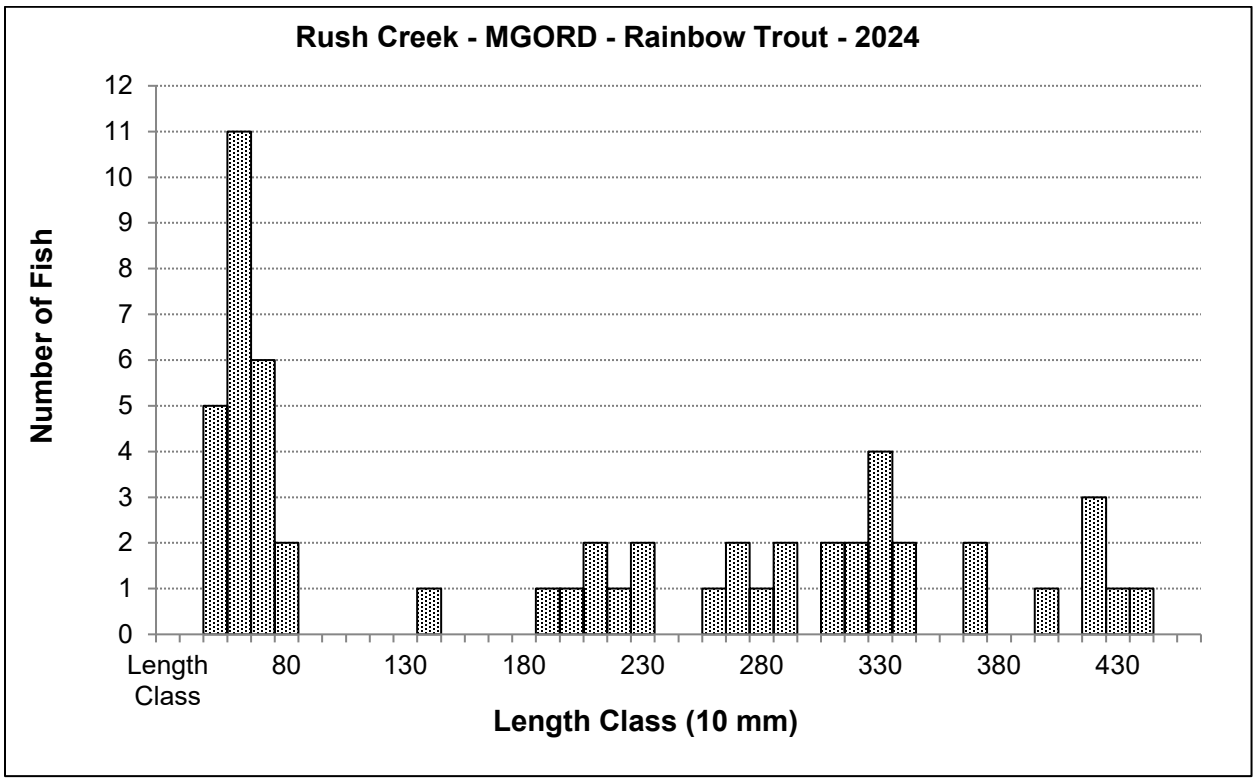

Figure 7. Length-frequency histogram of Rainbow Trout captured in the MGORD section of Rush Creek, September 18th and 24th, 2024.

Lee Vining Creek – Main Channel Section

In 2024, a total of 273 trout were captured on the mark-recapture electrofishing passes made in the Lee Vining Creek main channel section, and nearly all the trout captured (265 fish) were Brown Trout (Table 4). In 2024, 178 fish were caught on the mark run, versus 81 trout caught in a single pass in 2023.

In 2024, Brown Trout ranged in size from 69 mm to 356 mm in length (Figure 8). Fish <125 mm in length comprised 69% of the total Brown Trout catch in 2024, compared to 0% in 2023 and 18% in 2022. In 2024, the Lee Vining Creek's main channel section supported an estimated 528 Brown Trout in the <125 mm size class (Table 4), compared to an estimated 56 fish in 2022; an increase of 842%.

In 2024, Brown Trout 125-199 mm in length comprised 6% of the total Brown Trout catch in Lee Vining Creek's main channel section (versus 32% in 2023). This section supported an estimated 23 Brown Trout 125-199 mm in length in 2024 (Table 4) compared to 119 fish in 2022 (an 81% decrease). The 2024 estimate has a high standard error due to the four recaptures (Table 4).

In 2024, the population estimate of Brown Trout ≥200 mm in Lee Vining Creek's main channel was 73 fish (versus 97 fish in 2022 and 51 fish in 2021) (Table 4). Eight Brown Trout captured in 2024 were >300 mm in length, ranging from 303 mm to 356 mm (Figure 8).

No population estimate was generated for Rainbow Trout in Lee Vining Creek due to insufficient numbers of fish, with only eight fish captured during the mark-recapture electro-fishing passes made in 2024.

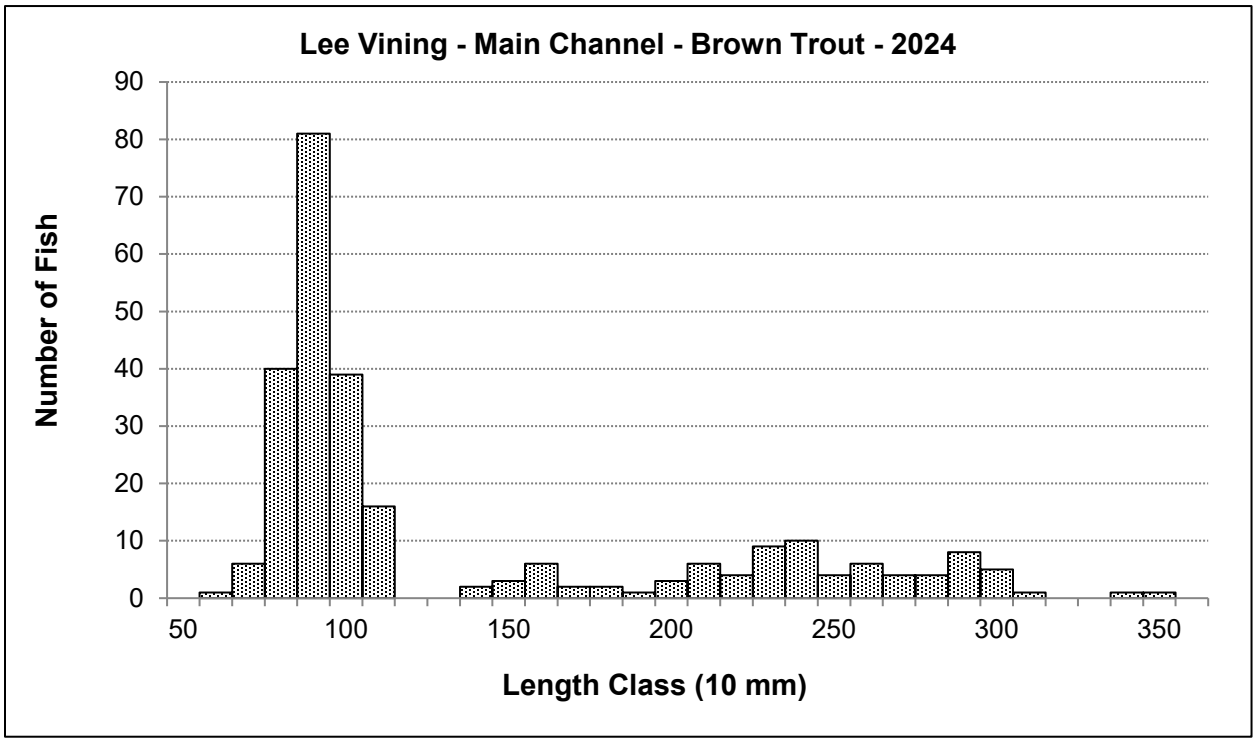

Figure 8. Length-frequency histogram of Brown Trout captured in the main channel section of Lee Vining Creek, September 19th and 25th, 2024.

Walker Creek

In 2024, 70 Brown Trout were captured in two electrofishing passes in the Walker Creek section (Table 5). The capture of 70 Brown Trout in Walker Creek is one of the lowest catches for this section, in comparison, 249 Brown Trout were caught in 2022, 356 were caught in 2021, 362 were caught in 2020, 278 were caught in 2019, and 175 were caught in 2018. Twenty-three of these 70 captured fish, or 33%, were age-0 fish ranging from 72 mm to 122 mm in length (Figure 9). The 2024 estimated population of Brown Trout <125 mm in length was 24 fish (Table 4), compared to 129 fish in 2022, an 81% decrease. For trout <125 mm in length, the probability of capture in 2022 equaled 0.74 (Table 5).

Brown Trout in the 125-199 mm size class (three fish) accounted for 4% of Walker Creek's total catch in 2024, compared to 70% of the catch in 2023. The 2024 population estimate for Brown Trout in the 125-199 mm size class was three trout (a 98% decrease from the 2022 estimate) with a probability of capture of 1.00 (Table 5). The low numbers of Brown Trout in the 125-199 mm size class in 2024 was due to the poor recruitment of age-0 fish in the record runoff of 2023.

Brown Trout ≥200 mm in length (44 fish caught) accounted for 63% of the total catch in 2024. The 2024 population estimate for this size class was 47 Brown Trout with a probability of

capture of 0.73 (Table 5). The largest Brown Trout captured in Walker Creek in 2024 was 278 mm in length (Figure 9).

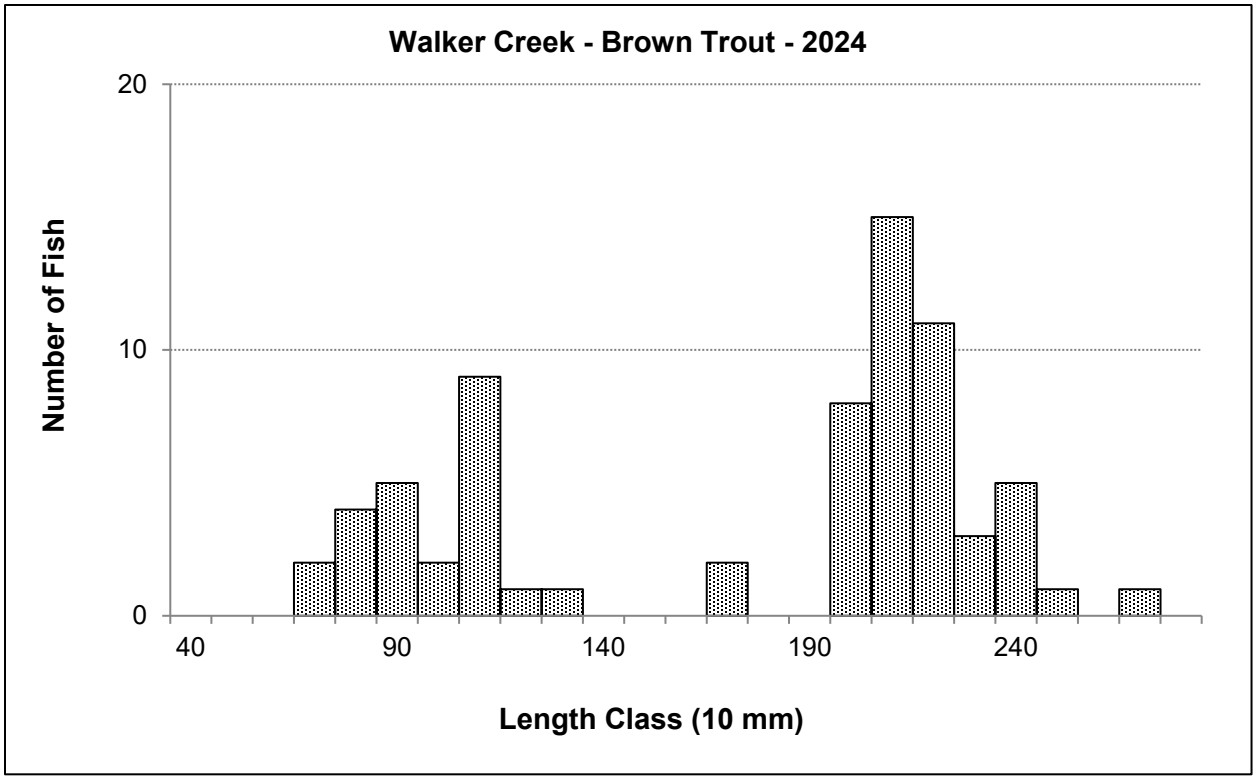

Figure 9. Length-frequency histogram of Brown Trout captured in Walker Creek, September 17th, 2024.

Table 5. Depletion estimates made in Walker Creek during September 2024 showing number of trout captured in each removal pass, estimated number of Brown Trout, and probability of capture (P.C.) by size class.

Stream - Section Date **Species**	Size Class (mm)	Removals	Removal Pattern	**Estimate**	P.C.
Walker Creek - above old Hwy 395 - 9/17/2024					
Brown Trout					
	0 - 124 mm	2	17 6	**24**	0.74
	125 - 199 mm	2	3 0	**3**	1.00
	200 + mm	2	34 10	**47**	0.73

Rush Creek – 8-Channel Single Pass

In 2024, a single electrofishing pass was made down the 8-Channel section of Rush Creek with the electrofishing barge. This section was sampled for the first time in October of 2023 when the 8-Channel was part of a multi-channel system created by extensive beaver dams. In 2023,

three distinct channels were sampled: the 8-Channel, the Jeffrey Connector Channel, and the Old Main Channel (with multiple pools formed by beaver dams). After the 2024 runoff, all of Rush Creek's flow at the time of the fisheries monitoring was concentrated in the 8-Channel.

A total of 210 Brown Trout and eight Rainbow Trout were caught in the 8-Channel. The Brown Trout ranged from 62 mm to 305 mm in total length with 152 fish in the <125 mm size class, 30 fish in the 125-199 mm size class, and 29 fish in the ≥200 mm size class (Figure 10).

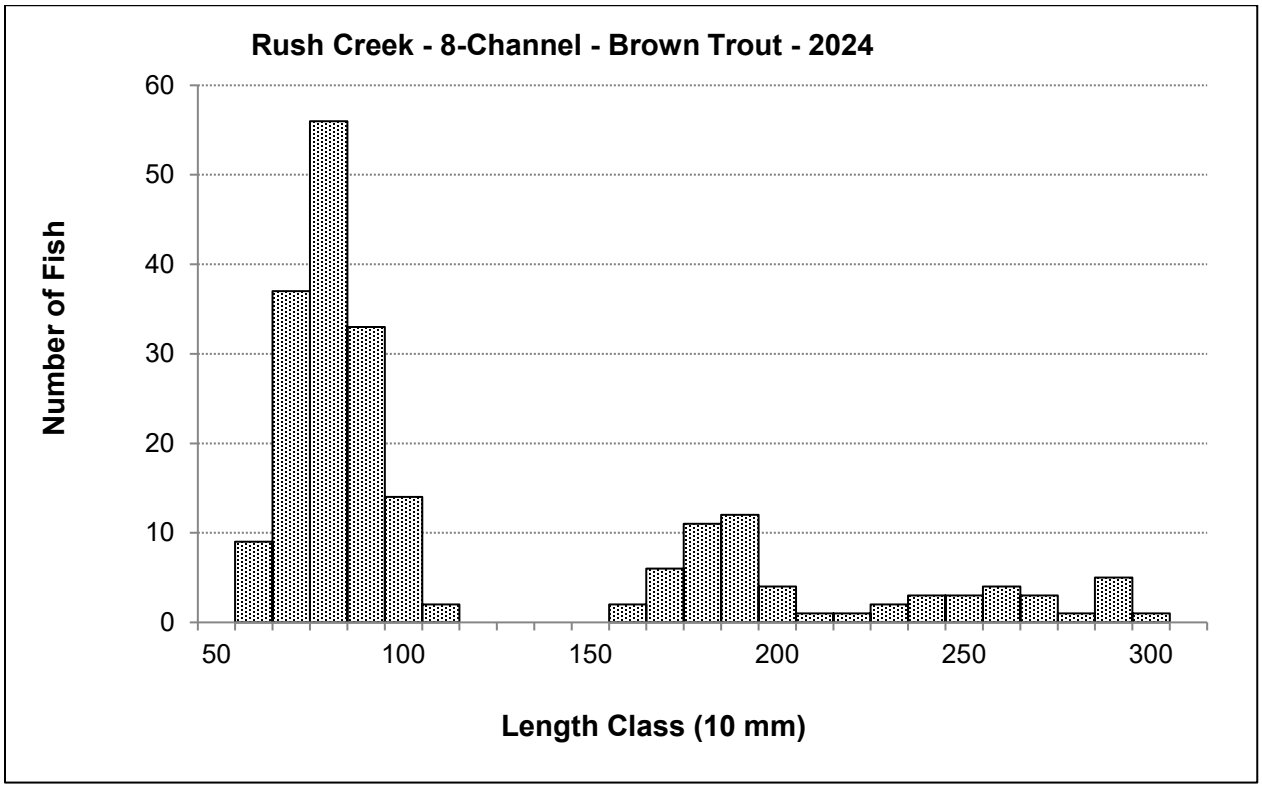

Figure 10. Length-frequency histogram of Brown Trout captured in the 8-Channel of Rush Creek, September 20th, 2024.

Rainbow Trout – 2024 Catch

In 2024, a total of 162 Rainbow Trout were caught: 85 fish in Upper Rush, 56 fish in the MGORD, five fish in the Bottomlands, eight fish in the 8-Channel, and eight fish in Lee Vining Creek. For the four Rush Creek sections, Rainbow Trout comprised 8.1% of the total catch (154 Rainbow Trout ÷ 1,894 total trout). In Lee Vining Creek, Rainbow Trout comprised just 2.9% of the total catch (8 RBT ÷ 273 total trout). Because recaptures of clipped fish were very low, the only population estimates made for Rainbow Trout in 2024 were in the Upper Rush sections, biased estimates for <125 mm and ≥200 mm size classes based on single recaptures.

For the computations of 2024 Rainbow Trout densities and standing crops, the actual numbers of fish caught were used. This method is conservative in that it typically underestimates the actual numbers of fish present. Prior use and discussion of using Rainbow Trout catch numbers has been discussed in previous annual fisheries reports (Taylor and Knudson 2012).

Relative Condition of Brown Trout

Linear regressions of log-length to log-weight for captured Brown Trout ≥ 100 mm indicated strong correlations between length and weight (r^2 values 0.98 and greater; Table 6). Slopes of these relationships were near 3.0 indicating isometric growth, which was assumed to compute fish condition factors, and were reasonable (Table 6).

Table 6. Regression statistics for log_{10} transformed length (L) to weight (WT) for Brown Trout 100 mm and longer captured in Rush Creek by sample section and year. The 2024 regression equations are in ***bold*** type.

Section	Year	N	Equation	r^2	P
Bottomlands	***2024***	***131***	***$Log_{10}(WT) = 2.9939*Log_{10}(L) – 5.0233$***	***0.99***	***<0.01***
	2023	62	$Log_{10}(WT) = 3.1294*Log_{10}(L) – 5.3820$	0.98	<0.01
	2022	253	$Log_{10}(WT) = 3.1013*Log_{10}(L) – 5.2251$	0.98	<0.01
	2021	205	$Log_{10}(WT) = 3.0091*Log_{10}(L) – 5.0526$	0.98	<0.01
	2020	223	$Log_{10}(WT) = 2.9792*Log_{10}(L) – 4.9754$	0.98	<0.01
	2019	310	$Log_{10}(WT) = 2.9631*Log_{10}(L) – 4.9409$	0.99	<0.01
	2018	226	$Log_{10}(WT) = 2.9019*Log_{10}(L) – 4.8059$	0.99	<0.01
	2017	160	$Log_{10}(WT) = 3.0398*Log_{10}(L) – 5.0998$	0.99	<0.01
	2016	132	$Log_{10}(WT) = 3.0831*Log_{10}(L) – 5.2137$	0.99	<0.01
	2015	301	$Log_{10}(WT) = 3.0748*Log_{10}(L) – 5.1916$	0.99	<0.01
	2014	238	$Log_{10}(WT) = 3.0072*Log_{10}(L) – 5.0334$	0.98	<0.01
	2013	247	$Log_{10}(WT) = 2.7997*Log_{10}(L) – 4.5910$	0.98	<0.01
	2012	495	$Log_{10}(WT) = 2.8149*Log_{10}(L) – 4.6206$	0.98	<0.01
	2011	361	$Log_{10}(WT) = 2.926*Log_{10}(L) – 4.8580$	0.99	<0.01
	2010	425	$Log_{10}(WT) = 2.999*Log_{10}(L) – 5.0050$	0.99	<0.01
	2009	511	$Log_{10}(WT) = 2.920*Log_{10}(L) – 4.8210$	0.99	<0.01
	2008	611	$Log_{10}(WT) = 2.773*Log_{10}(L) – 4.5240$	0.99	<0.01
Upper Rush	***2024***	***198***	***$Log_{10}(WT) = 2.9982*Log_{10}(L) – 5.0095$***	***0.99***	***<0.01***
	2023	131	$Log_{10}(WT) = 3.044*Log_{10}(L) – 5.0950$	0.99	<0.01
	2022	392	$Log_{10}(WT) = 2.9632*Log_{10}(L) – 4.9305$	0.99	<0.01
	2021	441	$Log_{10}(WT) = 2.9851*Log_{10}(L) – 4.9837$	0.98	<0.01
	2020	426	$Log_{10}(WT) = 2.9187*Log_{10}(L) – 4.8382$	0.99	<0.01
	2019	686	$Log_{10}(WT) = 2.9667*Log_{10}(L) – 4.9298$	0.99	<0.01
	2018	391	$Log_{10}(WT) = 2.9173*Log_{10}(L) – 4.8237$	0.99	<0.01
	2017	309	$Log_{10}(WT) = 3.0592*Log_{10}(L) – 5.1198$	0.99	<0.01
	2016	176	$Log_{10}(WT) = 3.0702*Log_{10}(L) – 5.1608$	0.99	<0.01

Table 6 (continued).

Section	Year	N	Equation	r^2	P
Upper Rush	2015	643	$Log_{10}(WT) = 2.9444*Log_{10}(L) - 4.8844$	0.99	<0.01
	2014	613	$Log_{10}(WT) = 2.9399*Log_{10}(L) - 4.8705$	0.99	<0.01
	2013	522	$Log_{10}(WT) = 2.9114*Log_{10}(L) - 4.8160$	0.99	<0.01
	2012	554	$Log_{10}(WT) = 2.8693*Log_{10}(L) - 4.7210$	0.99	<0.01
	2011	547	$Log_{10}(WT) = 3.006*Log_{10}(L) - 5.0140$	0.99	<0.01
	2010	420	$Log_{10}(WT) = 2.995*Log_{10}(L) - 4.9941$	0.99	<0.01
	2009	612	$Log_{10}(WT) = 2.941*Log_{10}(L) - 4.8550$	0.99	<0.01
	2008	594	$Log_{10}(WT) = 2.967*Log_{10}(L) - 4.9372$	0.99	<0.01
	2007	436	$Log_{10}(WT) = 2.867*Log_{10}(L) - 4.7150$	0.99	<0.01
	2006	485	$Log_{10}(WT) = 2.99*Log_{10}(L) - 4.9802$	0.99	<0.01
	2005	261	$Log_{10}(WT) = 3.02*Log_{10}(L) - 5.0203$	0.99	<0.01
	2004	400	$Log_{10}(WT) = 2.97*Log_{10}(L) - 4.9430$	0.99	<0.01
	2003	569	$Log_{10}(WT) = 2.96*Log_{10}(L) - 4.8920$	0.99	<0.01
	2002	373	$Log_{10}(WT) = 2.94*Log_{10}(L) - 4.8670$	0.99	< 0.01
	2001	335	$Log_{10}(WT) = 2.99*Log_{10}(L) - 4.9630$	0.99	< 0.01
	2000	309	$Log_{10}(WT) = 3.00*Log_{10}(L) - 4.9610$	0.98	< 0.01
	1999	317	$Log_{10}(WT) = 2.93*Log_{10}(L) - 4.8482$	0.98	< 0.01
MGORD	***2024***	***626***	$\boldsymbol{Log_{10}(WT) = 2.9152*Log_{10}(L) - 4.8039}$	***0.98***	***<0.01***
	2023	108	$Log_{10}(WT) = 3.0180*Log_{10}(L) - 4.9965$	0.99	<0.01
	2022	229	$Log_{10}(WT) = 3.1344*Log_{10}(L) - 5.3145$	0.99	<0.01
	2021	498	$Log_{10}(WT) = 2.9447*Log_{10}(L) - 4.8871$	0.99	<0.01
	2020	383	$Log_{10}(WT) = 3.0144*Log_{10}(L) - 5.0575$	0.98	<0.01
	2019	314	$Log_{10}(WT) = 2.9774*Log_{10}(L) - 4.9282$	0.98	<0.01
	2018	350	$Log_{10}(WT) = 3.0023*Log_{10}(L) - 5.0046$	0.98	<0.01
	2017	159	$Log_{10}(WT) = 3.0052*Log_{10}(L) - 5.0205$	0.99	<0.01
	2016	183	$Log_{10}(WT) = 3.0031*Log_{10}(L) - 5.3093$	0.99	<0.01
	2015	172	$Log_{10}(WT) = 3.131*Log_{10}(L) - 5.0115$	0.99	<0.01
	2014	399	$Log_{10}(WT) = 2.9805*Log_{10}(L) - 4.9827$	0.98	<0.01
	2013	431	$Log_{10}(WT) = 2.8567*Log_{10}(L) - 4.6920$	0.98	<0.01
	2012	795	$Log_{10}(WT) = 2.9048*Log_{10}(L) - 4.8081$	0.99	<0.01
	2011	218	$Log_{10}(WT) = 2.917*Log_{10}(L) - 4.8230$	0.98	<0.01
	2010	694	$Log_{10}(WT) = 2.892*Log_{10}(L) - 4.7563$	0.98	<0.01

Table 6 (continued).

Section	Year	N	Equation	r^2	P
MGORD	2009	689	$Log_{10}(WT) = 2.974*Log_{10}(L) - 4.9330$	0.99	<0.01
	2008	862	$Log_{10}(WT) = 2.827*Log_{10}(L) - 4.6020$	0.98	<0.01
	2007	643	$Log_{10}(WT) = 2.914*Log_{10}(L) - 4.8254$	0.98	<0.01
	2006	593	$Log_{10}(WT) = 2.956*Log_{10}(L) - 4.8722$	0.98	<0.01
	2004	449	$Log_{10}(WT) = 2.984*Log_{10}(L) - 4.9731$	0.99	<0.01
	2001	769	$Log_{10}(WT) = 2.873*Log_{10}(L) - 4.7190$	0.99	<0.01

Condition factors of Brown Trout >150 mm in length in 2024 increased from the 2023 values in the Bottomlands section of Rush Creek and in the Walker Creek section (Figure 11). Between 2023 and 2024, condition factors of Brown Trout >150 mm in length decreased in the MGORD and Upper Rush sections of Rush Creek and decreased in the Lee Vining Creek main channel section (Figures 11 and 12).

Brown Trout in the Upper Rush section had a condition factor of 0.94 in 2024, a decrease from 1.02 in 2023 (Figure 11). The Upper Rush section has had Brown Trout condition factors ≥1.00 in 12 of 24 sampling seasons (Figure 11).

Brown Trout in the Bottomlands section of Rush Creek had a condition factor of 0.97 in 2024, a slight increase from 0.94 in 2023 (Figure 11). In 17 years of sampling the Bottomlands section, 2022 was the only sampling year that the Brown Trout condition factor was ≥1.00 (Figure 11).

The MGORD's 2024 Brown Trout condition factor equaled 0.99, a decrease from 1.15 in 2023 (Figure 11). In 2024, condition factors for larger Brown Trout in the MGORD were also computed: fish ≥300 mm had a condition factor of 0.97 and fish ≥375 mm had a condition factor of 0.92.

In 2024, the condition factor for Brown Trout in Lee Vining Creek's main channel was 0.97, a decrease from 1.05 in 2023 (Figure 12). The Lee Vining Creek main channel section has had Brown Trout condition factors ≥1.00 in 15 of 24 sampling seasons. In 2024, the Rainbow Trout condition factor for the Lee Vining Creek main channel was 1.01, a slight decrease from 1.02 in 2023. In both 2023 and 2024, only three Rainbow Trout >150 mm in length were captured.

In Walker Creek, Brown Trout had a condition factor of 0.98 in 2024, an increase from 0.94 in 2023 and 0.88 in 2022 (Figure 11). Brown Trout condition factors in Walker Creek have been ≥1.00 in 12 of the 25 sampling years; however, in the past 10 years only the 2018 sampling year had a condition factor ≥1.00 (Figure 11).

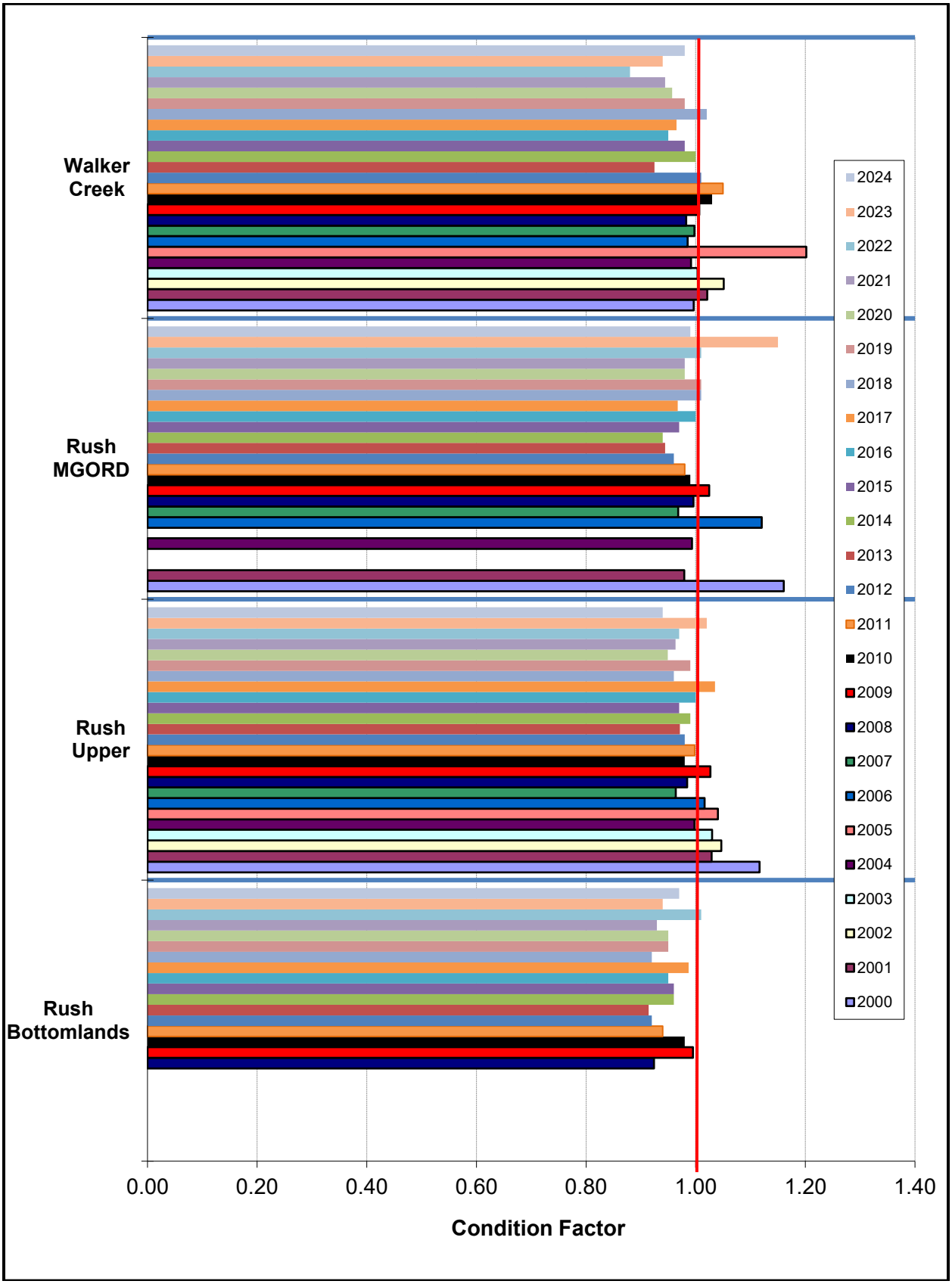

Figure 11. Condition factors for Brown Trout >150 mm in length from sample sections of Rush Creek and Walker Creeks from 2000 to 2024.

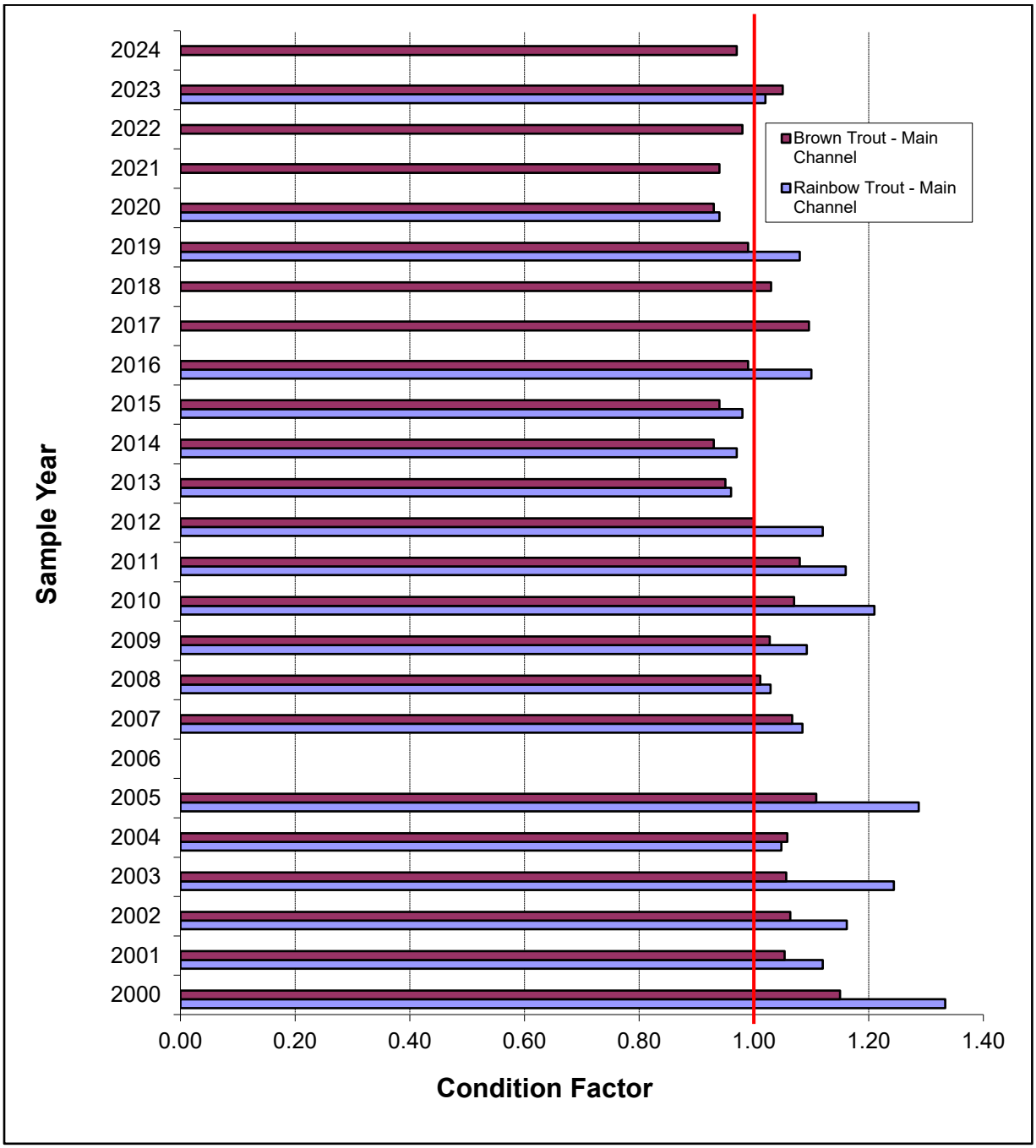

Figure 12. Condition factors for Rainbow Trout and Brown Trout >250 mm in length from the main channel section of Lee Vining Creek from 2000 to 2024. Main channel was not sampled in 2006 due to high flows.

Estimated Trout Densities Expressed in Numbers per Hectare

Age-0 Brown Trout

The Upper Rush section had an estimated density of 5,017 age-0 Brown Trout/ha in 2024, an increase of 82% from the 2022 estimate of 2,760 age-0 trout/ha and an increase of 203% from the 2021 estimate of 1,657 age-0 trout/ha (Figure 13). The Upper Rush section has a 24-year average of 5,500 age-0 Brown Trout/ha.

The Bottomlands section of Rush Creek had a density estimate of 3,033 age-0 Brown Trout/ha in 2024, a 53% increase from the 2022 estimate of 1,988 age-0 trout/ha and an increase of 29% from the 2021 estimate of 2,347 age-0 trout/ha (Figure 13). The Bottomlands section has a 16-year average of 2,168 age-0 Brown Trout/ha.

In Walker Creek, the 2024 density estimate of 442 age-0 Brown Trout/ha was an 86% decrease from the 2022 estimate of 3,193 age-0 trout/ha and a 91% decrease from the 2021 estimate of 5,147 age-0 trout/ha (Figure 13). The 2024 density estimate of age-0 trout in Walker Creek was the lowest estimate for the section over the past 18 years. This section has a 24-year average of 3,434 age-0 Brown Trout/ha.

In 2024, the estimated density of age-0 Brown Trout in the main channel of Lee Vining Creek was 3,317 age-0 trout/ha, which was a 631% increase from the 2022 density estimate of 454 age-0 trout/ha and an increase of 692% from the 2021 estimate of 419 age-0 trout/ha (Figure 14). This section has a 24-year average of 1,731 age-0 Brown Trout/ha and typically experiences low recruitment of age-0 trout in wetter runoff years.

Age-1 and older (aka Age-1+) Brown Trout

The Upper Rush section had an estimated density of 1,264 age-1+ Brown Trout/ha in 2024, a decrease of 17% from the 2022 estimate of 1,535 age-1+ trout/ha and a 45% decrease from the 2021 estimate of 2,302 trout/ha (Figure 15). For the Upper Rush section, the 25-year long-term average equaled 1,525 age-1+ Brown Trout/ha.

The Bottomlands section of Rush Creek had an estimated density of 367 age-1+ Brown Trout in 2024, a 62% decrease from the 2022 estimate of 966 age-1+ trout/ha and a 73% decrease from the 2021 estimate of 1,338 age-1+trout/ha (Figure 15). The 2024 density estimate of age-1+ Brown Trout was the lowest for the past seven years and the second lowest for the 16 years of available data (Figure 15). For the Bottomlands section, the 16-year long-term average equaled 1,069 age-1+ Brown Trout/ha.

The estimated density of age-1+ Brown Trout in the MGORD section of Rush Creek in 2024 was 935 fish/ha, a 236% increase from the 2022 estimate of 278 age-1+trout/ha and a 128% increase from the 2021 estimate of 411 age-1+trout/ha (Figure 15). The 2024 density estimate of age-1+ Brown Trout in the MGORD was the highest estimate ever generated for this section

(Figure 15). Since 2001, for the 13 seasons where density estimates were computed for the MGORD, the long-term density estimate of age-1+ Brown Trout averaged 480 fish/ha.

The 2024 density estimate for age-1+ Brown Trout in Walker Creek was 921 age-1+ trout/ha which was a 73% decrease from the 2022 estimate of 3,391 age-1+ trout/ha and a 70% decrease from the 2021 estimate of 3,061 age-1+ trout/ha (Figure 15). The 2024 density estimate of age-1+ Brown Trout in Walker Creek was the lowest estimate for this section over the past 17 years (Figure 15). For Walker Creek, the 25-year long-term average equaled 1,998 age-1+ Brown Trout/ha.

The 2024 density estimate for age-1+ Brown Trout in the Lee Vining Creek main channel section was 603 trout/ha, a 64% decrease from the 2022 estimate of 1,660 age-1+ trout/ha and an 82% decrease from the 2021 estimate of 3,350 age-1+trout/ha (Figure 16). For the Lee Vining Creek main channel section, the 24-year long-term average equaled 1,214 age-1+ Brown Trout/ha.

Age-0 and Age-1+ Rainbow Trout

The Upper Rush section supported an estimated density of 430 age-0 Rainbow Trout/ha in 2024. This section also supported an estimated density of 127 age-1+ Rainbow Trout/ha in 2024.

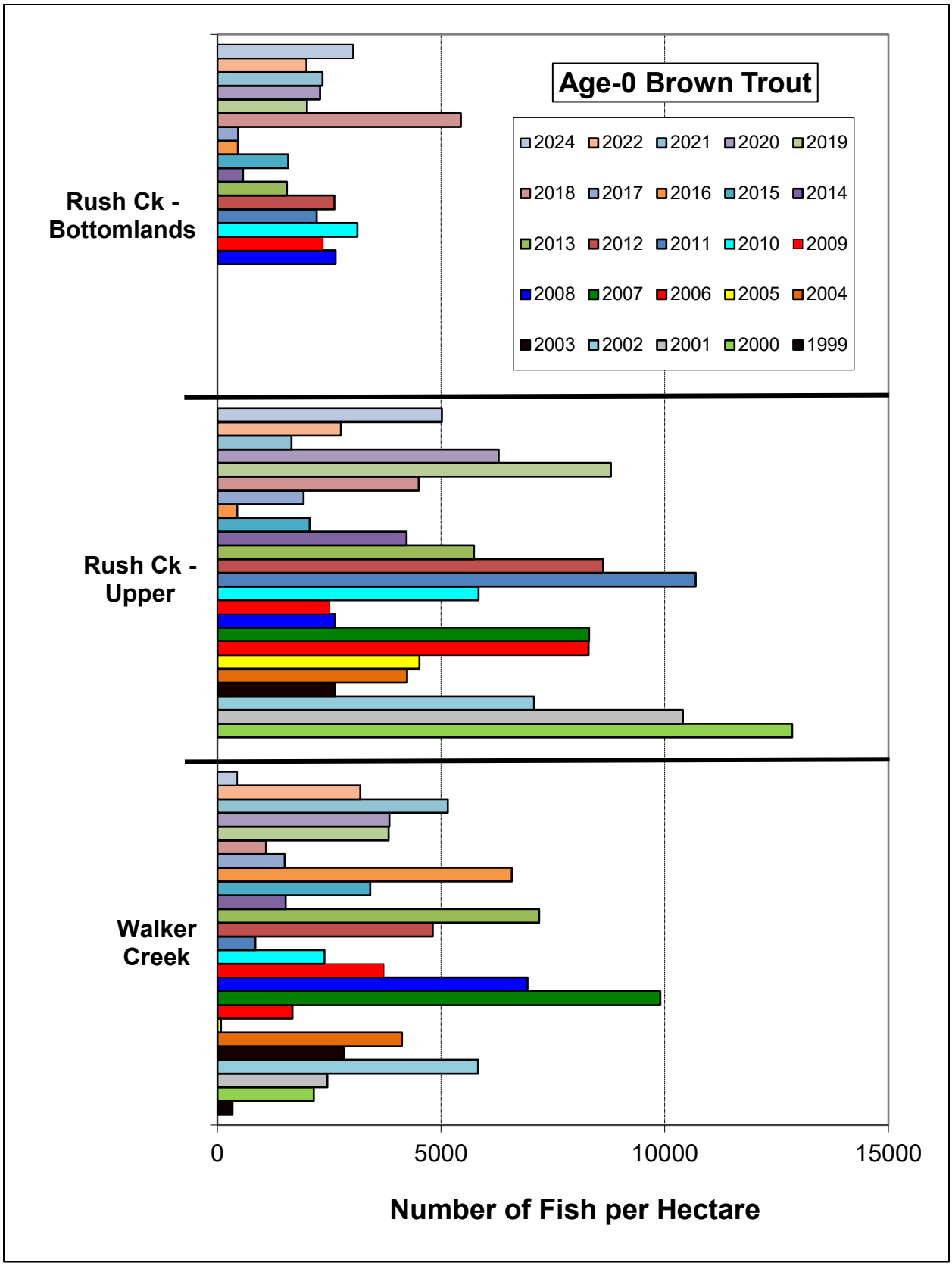

Figure 13. Estimated number of age-0 Brown Trout per hectare in Rush Creek and Walker Creek from 1999 to 2024.

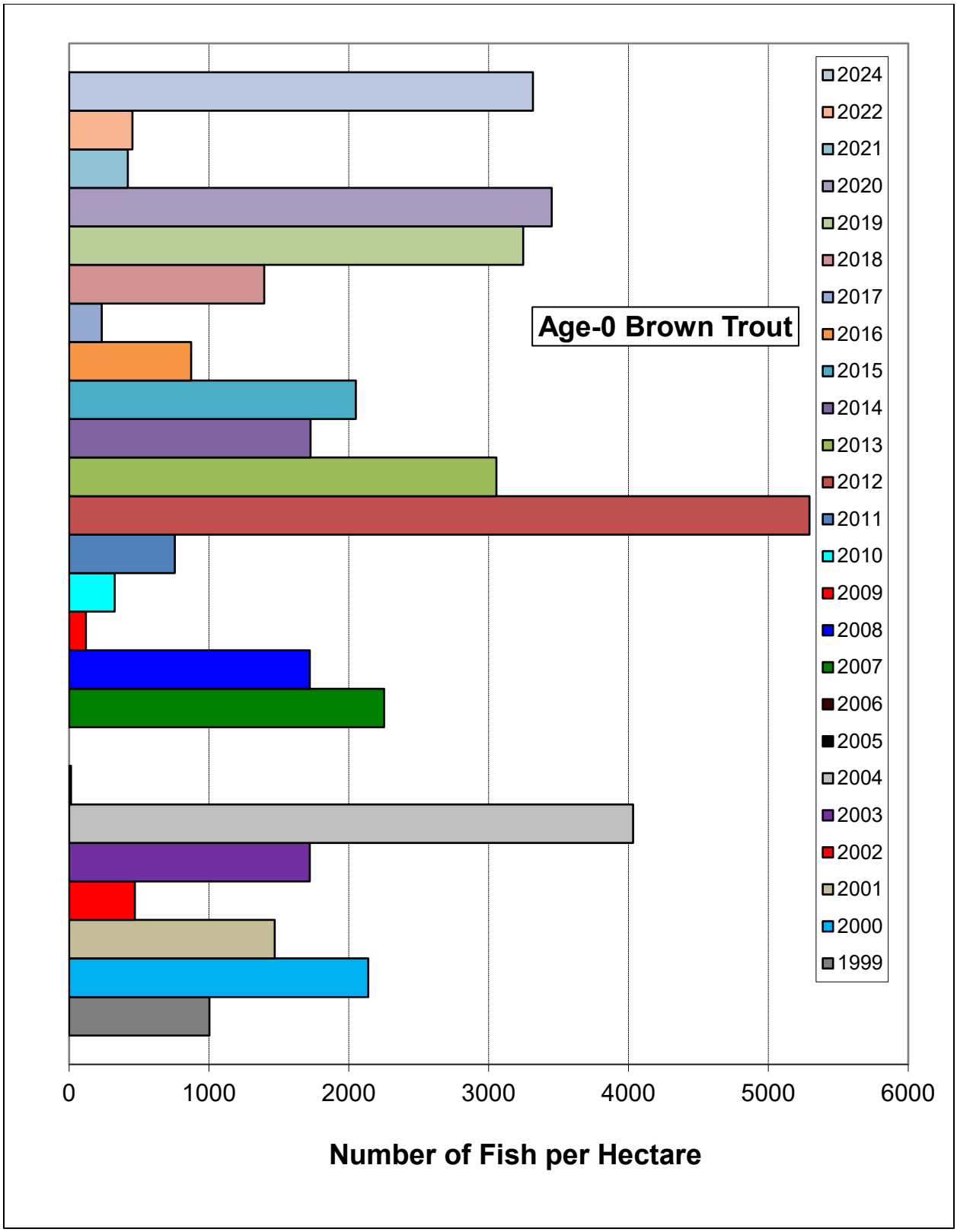

Figure 14. Estimated number of age-0 Brown Trout per hectare in the Lee Vining Creek main channel from 1999 to 2024.

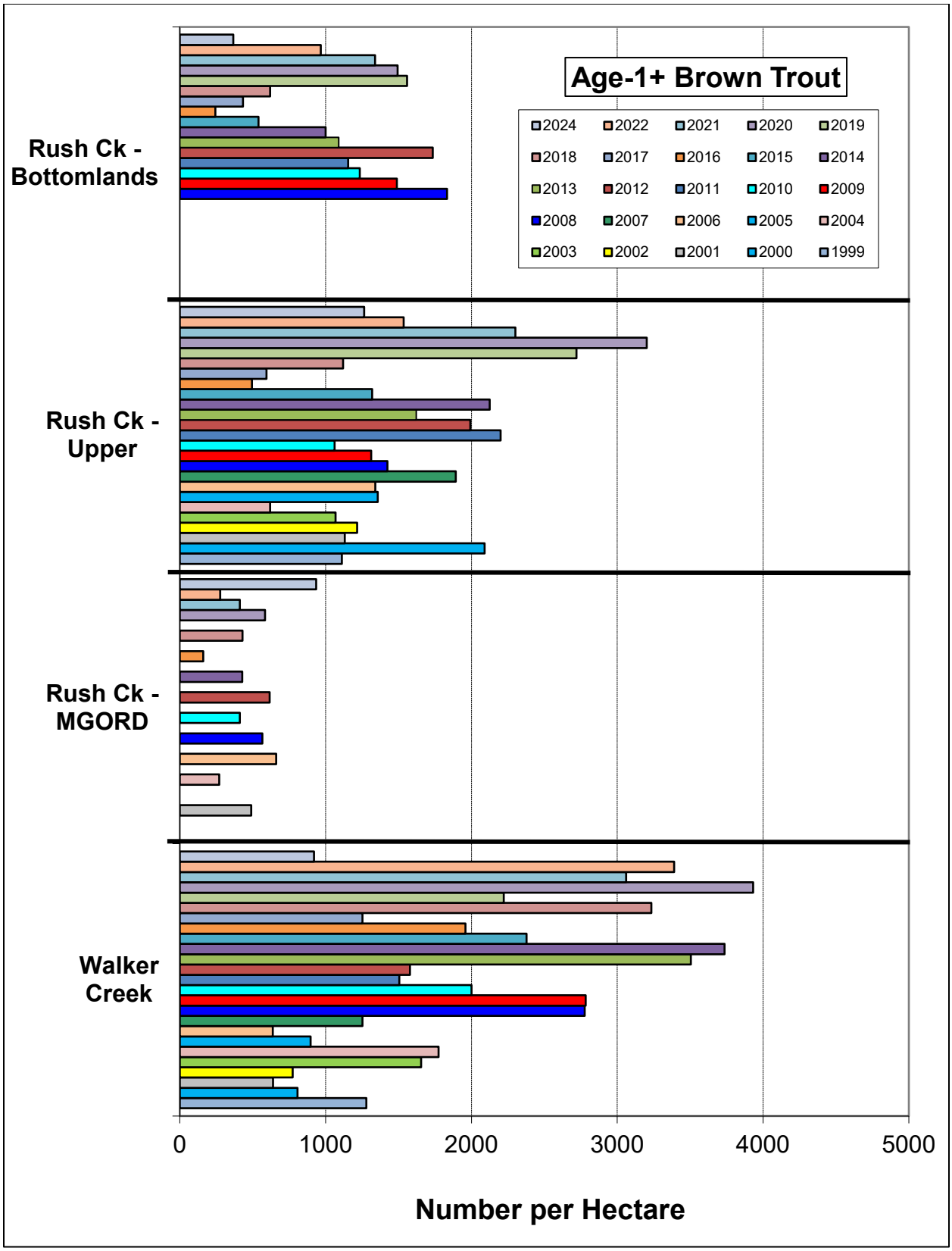

Figure 15. Estimated number of age-1 and older Brown Trout per hectare in sections of Rush and Walker Creeks from 1999 to 2024.

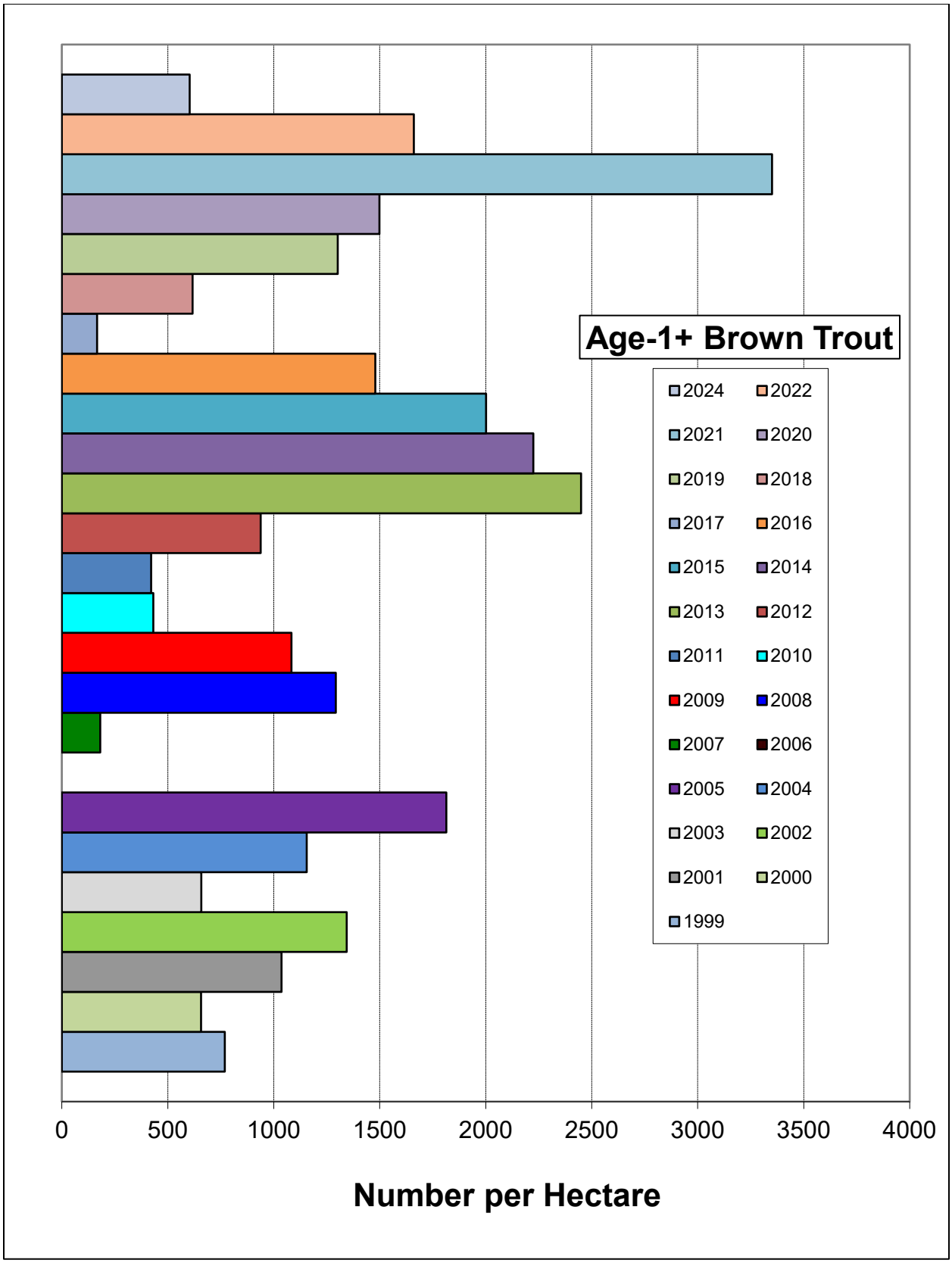

Figure 16. Estimated number of age-1 and older Brown Trout per hectare in the Lee Vining Creek main channel from 1999 to 2024.

Estimated Trout Standing Crops (kg/ha)

The total (Brown and Rainbow Trout) estimated standing crop in the Upper Rush section was 193 kg/ha in 2024, a 19% increase from 162 kg/ha in 2022 and a 40% increase from 138 kg/ha in 2021 (Table 7 and Figure 17). Rainbow Trout comprised 10.2 kg/ha of the 2024 standing crop estimate versus 15.9 kg/ha in 2022 (Figure 17). For the Upper Rush section, the 24-year average standing crop of Brown and Rainbow Trout equaled 158 kg/ha.

The estimated standing crop for Brown Trout in the MGORD section of Rush Creek was 173 kg/ha in 2024, a 220% increase from 54 kg/ha in 2022 (Figure 17). The 2024 Brown Trout standing crop estimate was the first estimate >100 kg/ha since 2012 and the second highest estimate for the 13 years of available data (Figure 17). For the 13 seasons where Brown Trout standing crop estimates were generated for the MGORD, the average value equaled 90 kg/ha.

The estimated standing crop for Brown Trout in the Bottomlands section of Rush Creek was 70 kg/ha in 2024, a 7% decrease from 75 kg/ha in 2022 (Table 7 and Figure 18). For the Bottomlands section of Rush Creek, the 16-year average standing crop of Brown Trout equaled 80 kg/ha.

The estimated standing crop for Brown Trout in Walker Creek was 103 kg/ha in 2024, a 36% decrease from the 2022 estimate of 160 kg/ha (Table 7 and Figure 18). The 2024 Brown Trout standing crop in Walker Creek was the second lowest estimate for this section over the past 18 years (Figure 18). For Walker Creek, the 25-year average standing crop of Brown Trout equaled 143 kg/ha.

The estimated total standing crop (Brown Trout and Rainbow Trout) in the Lee Vining Creek main channel section in 2024 was 124 kg/ha; a decrease of 9% from the 2022 estimate of 136 kg/ha (Table 8 and Figure 19). In 2024, Rainbow Trout comprised 3.8 kg/ha of the standing crop estimate (Table 8 and Figure 19). The long-term average for the 24 -year sampling period is 125 kg/ha.

Table 7. Comparison of Brown Trout standing crop (kg/ha) estimates between 2018 and 2024 for Rush Creek and Walker Creek sections. These six years include one Normal RY 2018, a Wet RY 2019, Dry-Normal-1 RY 2020, a Dry RY 2021, a Dry RY 2022, and a Normal RY 2024.

Collection Location	2018 Total Standing Crop (kg/ha)	2019 Total Standing Crop (kg/ha)	2020 Total Standing Crop (kg/ha)	2021 Total Standing Crop (kg/ha)	2022 Total Standing Crop (kg/ha)	2024 Total Standing Crop (kg/ha)	Percent Change Between 2022 and 2024
Rush Creek – MGORD	95	N/A	81	67	54	180[+]	+233%
Rush Creek – Upper	188*	291**	195***	138[#]	162[##]	193[###]	+19%
Rush Creek - Bottomlands	103	91	84	78	75	70	-7%
Walker Creek	245	179	240	158	160	103	-36%

+ includes 6.5 kg/ha of Rainbow Trout *Includes 18.7 kg/ha of Rainbow Trout **includes 36.5 kg/ha of Rainbow Trout ***Includes 24.4 kg/ha of Rainbow Trout [#]Includes 10.8 kg/ha of Rainbow Trout [##]Includes 15.9 kg/ha of Rainbow Trout [###]includes 10.2 kg/ha of Rainbow Trout.

Table 8. Comparison of total (Brown and Rainbow Trout) standing crop (kg/ha) estimates between 2018 and 2024 for the Lee Vining Creek main channel section. These six years include one Normal RY 2018, a Wet RY 2019, Dry-Normal-1 RY 2020, a Dry RY 2021, a Dry RY 2022, and a Normal RY 2024.The Rainbow Trout portion of the main channel's total estimated biomass is provided within the parentheses.

Collection Location	2018 Total Standing Crop (kg/ha)	2019 Total Standing Crop (kg/ha)	2020 Total Standing Crop (kg/ha)	2021 Total Standing Crop (kg/ha)	2022 Total Standing Crop (kg/ha)	2024 Total Standing Crop (kg/ha)	Percent Change Between 2022 and 2024
Lee Vining Creek - Main Channel	70 (0)	192 (4.6)	96 (0.6)	146 (0)	136 (0)	124 (3.8)	-9%

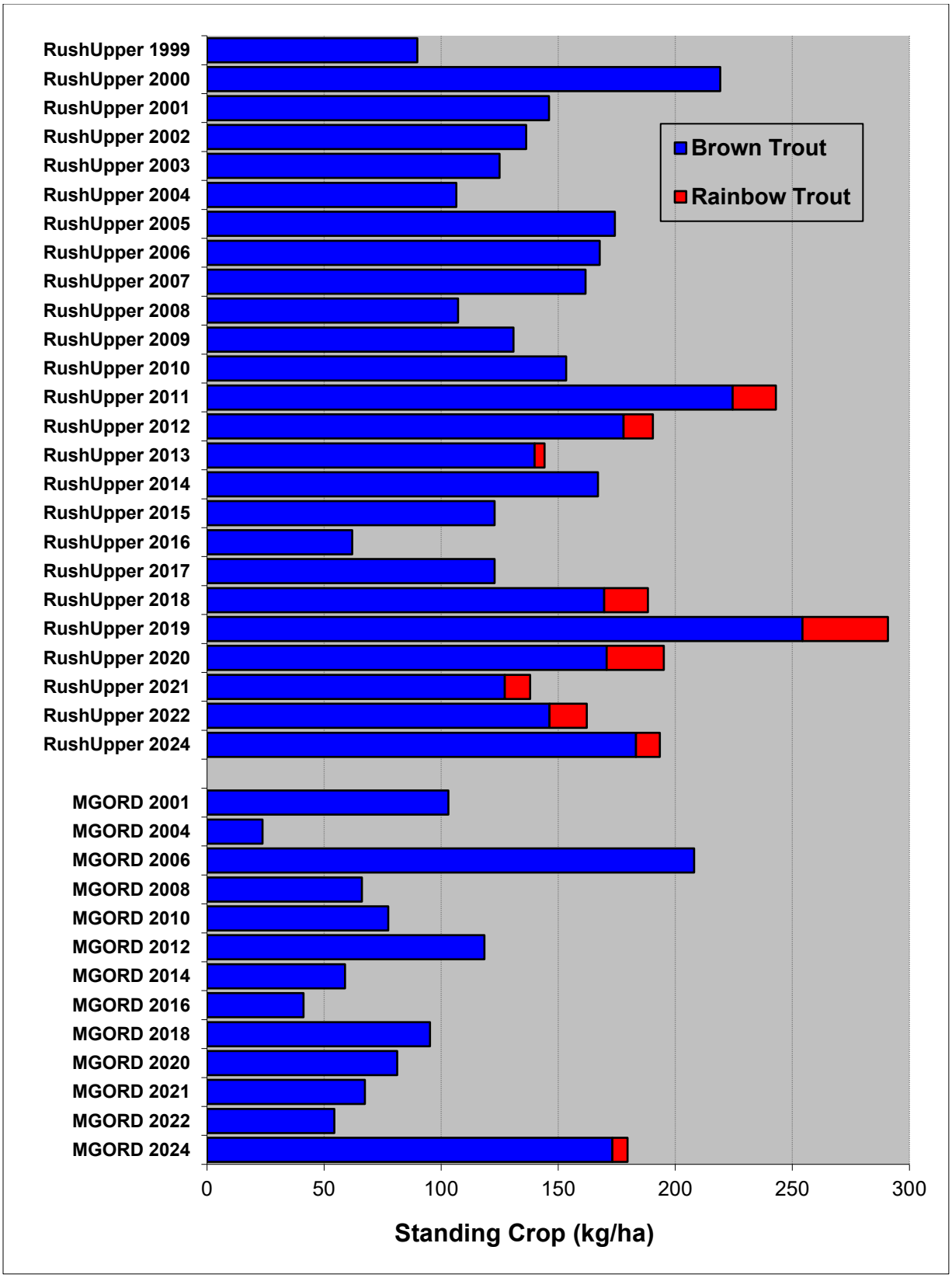

Figure 17. Estimated total standing crop (kilograms per hectare) of Brown Trout and Rainbow Trout in the Upper and MGORD sample sections of Rush Creek from 1999 to 2024.

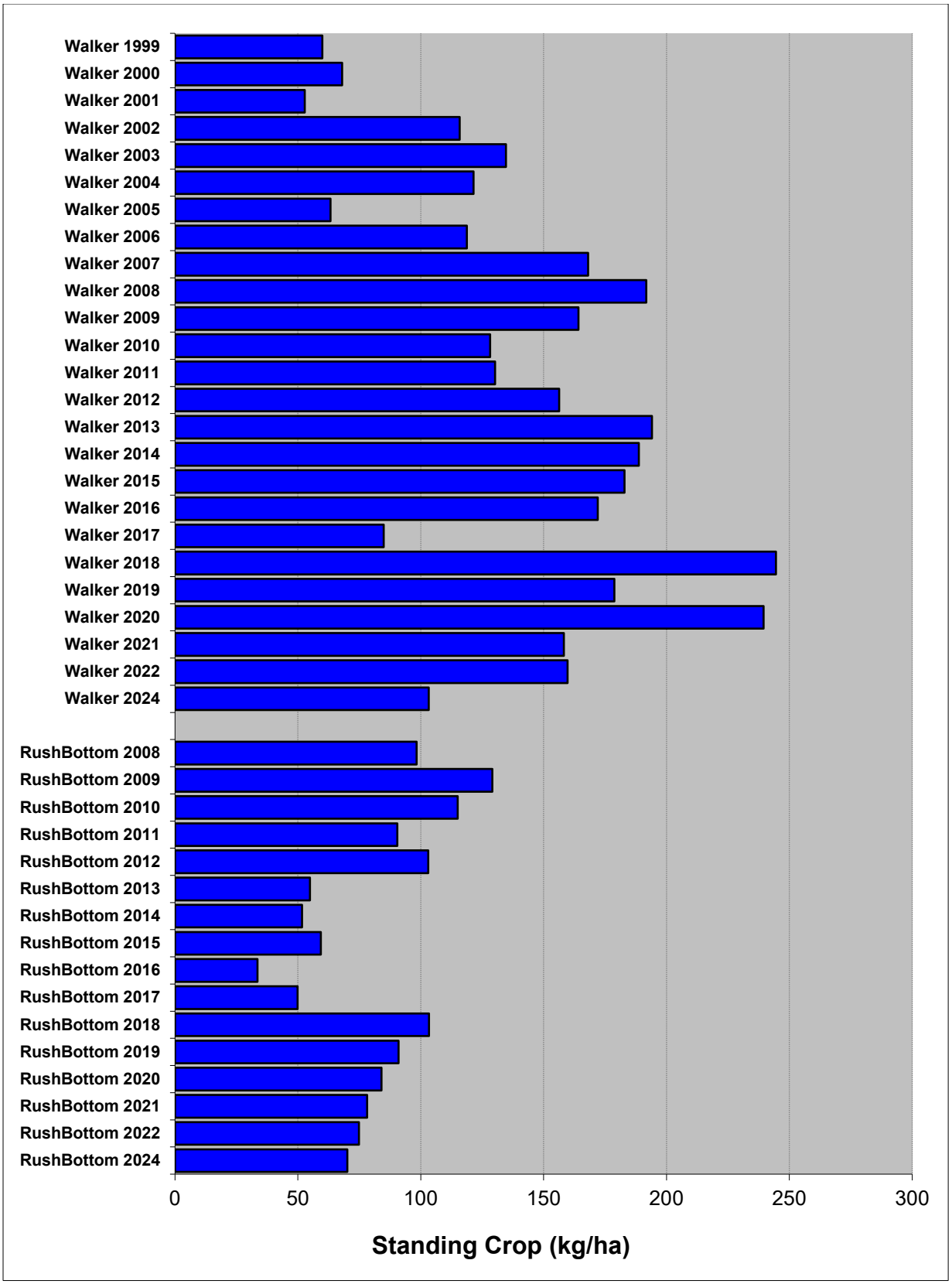

Figure 18. Estimated total standing crop (kilograms per hectare) of Brown Trout in Walker Creek and the Bottomlands sections of Rush Creek from 1999 to 2024.

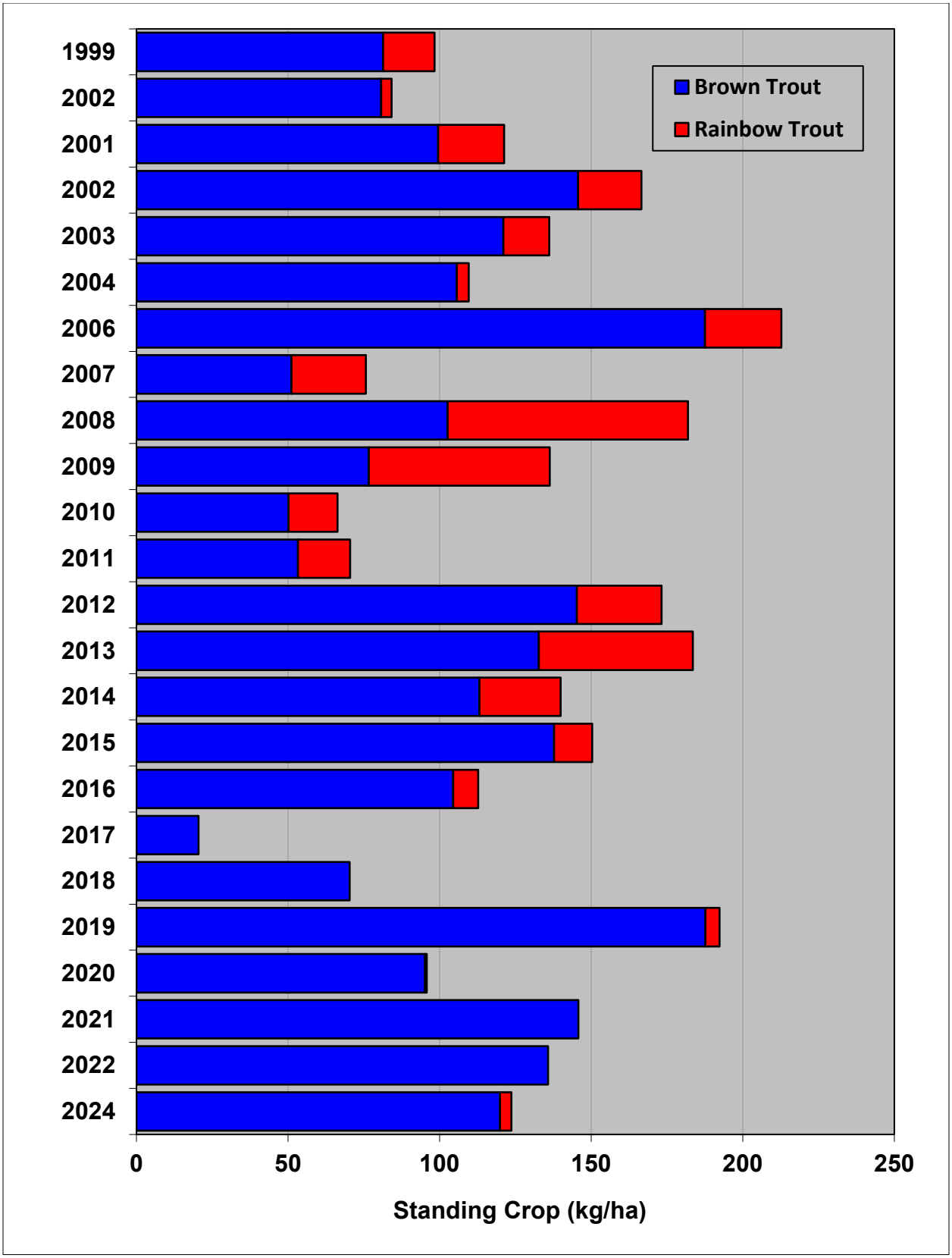

Figure 19. Estimated total standing crop (kilograms per hectare) of Brown Trout and Rainbow Trout in the Lee Vining Creek main channel sample section from 1999 to 2024.

Relative Stock Density (RSD) for Rush and Lee Vining Creeks

In the Upper Rush section, the RSD-225 equaled 45 for 2024, down from the RSD-225 of 58 in 2023 (Table 9). The 2024 RSD-225 value was influenced by greater numbers of fish in the 150 to 224 mm size class than in the ≥225 mm size class (Table 9). The RSD-300 value was 6 in 2024, the highest RSD-300 value over the past six sampling seasons and double the 2023 RSD-300 value (Table 9). Over 25 sampling years, a total of 169 Brown Trout ≥300 mm were captured in the Upper Rush Creek section, an average of 6.8 fish ≥300 mm per year (Table 9).

In the Bottomlands section of Rush Creek, the RSD-225 for 2024 equaled 72, the highest value for this section for the 17 years of available data (Table 9). The Bottomlands 2024 RSD-225 value was most likely influenced by an increase in the numbers of fish ≥225 mm, more than twice as many fish as in the 150 to 224 mm size class (Table 9). The RSD-300 value was 6 in 2024, because of the four Brown Trout ≥300 mm captured in the Bottomlands section (Table 9). Over the 17 sampling years, a total of 32 Brown Trout ≥300 mm were captured in the Bottomlands section, an average of 1.9 fish ≥300 mm per year (Table 9).

In the MGORD, the RSD-225 value decreased from a record value of 93 in 2023 to 61 in 2024 (Table 9). In 2024, the RSD-300 value was 21, four less than the 2023 value (Table 8). The RSD-375 value dropped from 10 in 2023, to 2 in 2024 (Table 9). The large number of Brown Trout captured ≥150 mm in 2024 (578 fish) and the large proportion between 150 and 224 mm (226 fish) influenced the drop in all RSD values (Table 9). The 2024 mark-recapture electrofishing passes in the MGORD included 124 fish ≥300 mm in length and 14 of these fish were ≥375 mm in length (Table 9). For sampling conducted between 2001 and 2012, the annual average catch of Brown Trout ≥300 mm equaled 180 fish/year; then for the past 12 sampling years the annual average catch of Brown Trout ≥300 mm equaled 45 fish/year (Table 9). This 75% decline in larger Brown Trout coincided with the five years of drier RY's and poor summer thermal regimes within the MGORD in 2012-2016. However, in the eight seasons following the five-year drought, the recruitment of larger, older fish appears to be a relatively slow process, possibly because for the three years of 2020-2022 summer water temperatures were generally unfavorable for Brown Trout growth and survival in the MGORD (Table 9). However, 2024 was the first year since 2012 in which more than 100 Brown Trout ≥300 mm in length were captured during the annual sampling (Table 9).

RSD values were computed for the Caddis Channel (aka the 8-Channel) in 2023 and 2024. For the 8-Channel, the RSD-225 equaled 66 in 2023 and 37 in 2024. The RSD-300 was 6 in 2023 and equaled 2 in 2024. In 2024, a larger proportion of the fish ≥150 mm were in the 150 to 224 mm size class, thus lowering the RSD-225 value. The number of Brown Trout ≥300 mm in length also dropped from five fish to two fish in 2024, this lowering the RSD-300 value.

The RSD-225 value for the Lee Vining Creek main channel was 71 in 2024, the largest RSD-225 value in this section for the 25 years of available data (Table 10). In 2024, eight Brown Trout greater than 300 mm in length were captured in Lee Vining Creek main channel, thus the RSD-300 value was 8, the highest value for the 25 years of data (Table 10).

Table 9. RSD values for Brown Trout in Rush Creek sections from 2000 to 2024.

Sampling Location Rush Creek	Sample Year	Number of Trout ≥150 mm	Number of Trout 150-224 mm	Number of Trout 225-299 mm	Number of Trout 300-374 mm	Number of Trout ≥375 mm	RSD-225	RSD-300	RSD-375
Upper Rush	**2024**	**176**	**97**	**68**	**11**	**0**	**45**	**6**	**0**
Upper Rush	2023	104	44	57	2	1	58	3	1
Upper Rush	2022	235	196	37	2	0	17	1	0
Upper Rush	2021	274	257	13	4	0	6	1	0
Upper Rush	2020	148	129	18	1	0	13	1	0
Upper Rush	2019	503	406	85	11	1	19	2	0
Upper Rush	2018	254	155	75	24	0	39	9	0
Upper Rush	2017	130	28	82	19	1	78	15	1
Upper Rush	2016	103	74	26	1	2	28	3	2
Upper Rush	2015	289	246	41	0	2	15	1	1
Upper Rush	2014	366	331	31	4	0	10	1	0
Upper Rush	2013	336	288	45	3	0	14	1	0
Upper Rush	2012	354	284	66	3	1	20	1	0
Upper Rush	2011	498	381	110	6	1	23	1	0
Upper Rush	2010	308	202	97	7	2	34	3	1
Upper Rush	2009	372	322	43	5	2	13	2	1
Upper Rush	2008	227	189	31	6	1	17	3	0
Upper Rush	2007	282	210	61	9	2	26	4	1
Upper Rush	2006	233	154	69	10	0	34	4	0
Upper Rush	2005	202	139	56	5	2	31	3	1
Upper Rush	2004	179	112	64	2	1	37	2	1
Upper Rush	2003	264	216	45	2	1	18	1	0
Upper Rush	2002	220	181	35	1	2	18	2	1
Upper Rush	2001	223	190	27	6	0	15	3	0
Upper Rush	2000	182	158	22	2	0	13	1	0
Bottomlands	**2024**	**71**	**20**	**47**	**4**	**0**	**72**	**6**	**0**
Bottomlands	2023	55	39	15	0	1	29	2	2
Bottomlands	2022	145	123	22	0	0	15	0	0
Bottomlands	2021	121	110	10	1	0	9	1	0
Bottomlands	2020	128	117	11	0	0	9	0	0
Bottomlands	2019	220	202	17	1	0	8	0	0
Bottomlands	2018	140	90	41	9	0	36	6	0
Bottomlands	2017	82	29	49	4	0	65	5	0
Bottomlands	2016	66	52	11	1	2	21	5	3
Bottomlands	2015	115	88	26	0	1	23	1	1

Table 9 (continued).

Sampling Location Rush Creek	Sample Year	Number of Trout ≥150 mm	Number of Trout 150-224 mm	Number of Trout 225-299 mm	Number of Trout 300-374 mm	Number of Trout ≥375 mm	RSD-225	RSD-300	RSD-375
Bottomlands	2014	154	152	1	0	1	1	1	1
Bottomlands	2013	128	123	5	0	0	4	0	0
Bottomlands	2012	325	290	34	1	0	11	0	0
Bottomlands	2011	267	218	46	3	0	18	1	0
Bottomlands	2010	307	225	81	1	0	27	0	0
Bottomlands	2009	379	321	56	1	1	15	1	0
Bottomlands	2008	160	141	19	0	0	12	0	0
MGORD	**2024**	**578**	**226**	**228**	**110**	**14**	**61**	**21**	**2**
MGORD	2023	91	6	62	14	9	93	25	10
MGORD	2022	198	56	114	22	6	72	14	3
MGORD	2021	431	204	180	35	12	53	11	3
MGORD	2020	322	167	112	37	6	48	13	2
MGORD	2019	275	145	102	24	4	47	10	1
MGORD	2018	326	98	162	51	15	70	20	5
MGORD	2017	104	12	64	17	11	88	27	11
MGORD	2016	179	46	95	18	20	74	21	11
MGORD	2015	116	33	54	20	9	72	25	8
MGORD	2014	388	184	175	19	10	53	7	3
MGORD	2013	411	237	118	41	15	42	14	4
MGORD	2012	694	176	319	173	26	75	29	4
MGORD	2011	216	36	117	55	8	83	29	4
MGORD	2010	694	252	292	115	35	64	22	5
MGORD	2009	643	156	338	123	26	76	23	4
MGORD	2008	856	415	301	118	22	52	16	3
MGORD	2007	621	144	191	259	27	77	46	4
MGORD	2006	567	60	200	280	27	89	54	5
MGORD	2004	424	130	197	64	33	69	23	8
MGORD	2001	774	330	217	119	108	57	29	14

Table 10. RSD values for Brown Trout in the Lee Vining Creek main channel section from 2000-2024. Note: the main channel section was not sampled in 2006 due to high flows.

Sampling Location Rush Creek	Sample Year	Number of Trout ≥150 mm	Number of Trout 150-224 mm	Number of Trout 225-299 mm	Number of Trout 300-374 mm	Number of Trout ≥375 mm	RSD-225	RSD-300
LV Main	**2024**	**80**	**23**	**49**	**8**	**0**	**71**	**10**
LV Main	2023	76	32	41	3	0	58	4
LV Main	2022	129	105	24	0	0	19	0
LV Main	2021	175	169	6	0	0	3	0
LV Main	2020	80	69	11	0	0	14	0
LV Main	2019	131	107	22	2	0	18	2
LV Main	2018	51	39	10	2	0	24	4
LV Main	2017	23	17	5	1	0	26	4
LV Main	2016	169	145	24	0	0	14	0
LV Main	2015	210	192	18	0	0	9	0
LV Main	2014	200	173	27	0	0	14	0
LV Main	2013	325	308	16	1	0	5	0
LV Main	2012	111	72	37	2	0	35	2
LV Main	2011	60	31	23	5	1	48	10
LV Main	2010	62	28	32	2	0	55	3
LV Main	2009	137	106	30	1	0	23	1
LV Main	2008	149	138	11	0	0	7	0
LV Main	2007	29	24	5	0	0	17	0
LV Main	2005	60	37	20	2	1	38	5
LV Main	2004	70	60	8	2	0	14	3
LV Main	2003	52	27	23	2	0	48	4
LV Main	2002	100	74	23	3	0	26	3
LV Main	2001	90	71	16	3	0	21	3
LV Main	2000	51	32	18	1	0	37	2

PIT Tag Recaptures

PIT Tags Implanted Between 2009 and 2024

Between 2009 and 2024, a total of 12,379 PIT tags were implanted in Brown Trout and Rainbow Trout within the annually sampled sections of Rush, Lee Vining and Walker Creeks. All PIT tagged fish received adipose fin clips. The numbers of PIT tags implanted each year varied according to fish availability and inventory of PIT tags, with year-specific information for 2009 through 2023 tabulated in Appendix B.

In 2024, a total of 979 trout received PIT tags and adipose fin clips in Rush, Lee Vining, and Walker Creeks (Table 11). In addition, one recaptured adipose fin-clipped fish had shed its original tag and was re-tagged, thus a total of 980 PIT tags were implanted during the 2024 fisheries sampling (Table 11). Of the 979 new trout tagged and clipped, 742 were age-0 Brown Trout and 180 were age-1 and older Brown Trout (Table 11). For Rainbow Trout, 56 age-0 fish and one older fish were tagged and clipped (Table 11). One-hundred-eighty of the Brown Trout tagged in the MGORD section were 164 mm to 225 mm in total length and were presumed to be age-1 fish (Table 11). In addition, 58 age-0 Brown Trout were tagged in the MGORD (Table 11). Tagged and recaptured fish provided empirical information to estimate annual fish growth, tag retention, and fish movements.

Table 11. Total numbers of trout implanted with PIT tags during the 2024 sampling season, by stream, sample section, age-class and species.

Creek Name	Sample Section	Number of Age-0 Brown Trout (<125 mm)	Number of Age-1 and older Brown Trout	Number of Age-0 Rainbow Trout (<125 mm)	Number of Age-1 and older Rainbow Trout	Section Totals
Rush Creek	Upper Rush	229	1*	35	0	**265 Trout**
	Bottomlands	197	0	1	0	**198 Trout**
	MGORD	58	180**	15	1	**254 Trout**
	Caddis or 8-Channel	85	0	0	0	**85 Trout**
LV Creek	Main Channel	150	0	5	0	**155 Trout**
Walker Creek	Above old 395	23	0	0	0	**23 Trout**
Species/Age Class Sub-totals:		**742**	**181**	**56**	**1**	**Total Trout: 980**

*shed tag/new tag implanted **164 to 225 mm in total length ***all fish tagged in new sample sections

In September of 2024, a total of 56 previously tagged trout (that retained their tags) were recaptured, 52 fish in the Rush Creek watershed (including Walker Creek) and four fish in Lee Vining Creek (Appendix C). Fourteen of the recaptures occurred in the Upper Rush section, followed by 12 recaptures in Walker Creek, 11 recaptures in the 8-Channel section, nine recaptures in the MGORD, and six recaptures in the Bottomlands section (Appendix C). In

September of 2024, a total of four previously tagged Brown Trout (that retained their tags) were recaptured in the Lee Vining Creek main channel section (Appendix C). During the 2024 sampling, only one previously tagged Rainbow Trout was recaptured (in the Upper Rush section), thus very limited growth rate information was available for Rainbow Trout in Rush Creek, and none was available for Lee Vining Creek.

In the following text, growth between 2023 and 2024 will be referred to as 2024 growth rates. A 2024 trout refers to a fish recaptured in September of 2024. The age of a PIT tagged trout reflects its age during the sampling year. For instance, an age-1 trout in 2024 was a trout tagged in October 2023 at age-0 and its length and weight were remeasured in September 2024 when it was recaptured.

Also note there is a separate results section for reporting growth rates of recaptures from the MGORD section of Rush Creek, primarily because most of these fish were tagged at presumed age-1 (based on lengths up to 225 mm), instead of at a known age-0. When captured in the MGORD, age-0 trout were also implanted with PIT tags.

Growth of Age-1 Brown Trout between 2023 and 2024

In 2024, a total of nine known age-1 Brown Trout were recaptured that were tagged as age-0 fish in 2023, for an overall recapture rate of 6.4% (nine recaps/141 age-0 fish tagged in 2023). All nine age-1 recaptures were from Rush Creek sections, no age-1 fish were recaptured in Walker Creek or in Lee Vining Creek. The lack of recaptures in Walker Creek and Lee Vining Creek was due to the extremely low age-0 recruitment during the record runoff of RY2023.

In the Upper Rush section, five age-1 Brown Trout were recaptured in 2024, and the average growth rates of these five trout were 88 mm and 49 g (Table 12). Compared to 2023 rates, the average growth rates of the five age-1 Brown Trout were lower by 32 mm and 49 g (Table 12). Growth rates of age-1 Brown Trout in the Upper Rush section have generally declined annually from 2010 to 2014, but the 2015-2017 growth rates increased each year, with the 2017 growth rates being the largest recorded for this section (Table 12). After the 2017 season, growth rates of age-1 Brown Trout in Upper Rush remained relatively low, with the 2020 and 2021 average growth rates the two lowest rates recorded for the 16 years of available data (Table 12). The 2024 growth rates of age-1 Brown Trout in the Upper Rush section were the second highest rates for the past seven years (Table 12).

In the Bottomlands section of Rush Creek, two age-1 Brown Trout were recaptured in 2024 and the average growth rates of these trout were 77 mm and 40 g (Table 12). Compared to 2023 rates, the growth rates of the two age-1 Brown Trout were lower by 27 mm and by 28 g (Table 12). In terms of length, the 2024 growth rates of age-1 Brown Trout were the third highest rates for the past seven years (Table 12).

Growth of Age-2 Brown Trout between 2023 and 2024

In 2024, a total of five known age-2 Brown Trout were recaptured that were tagged as age-0 fish in 2022, for a recapture rate of 0.8% (five recaps/610 age-0 fish tagged in 2022). Three of these fish were recaptured in Walker Creek and two fish were recaptured in Lee Vining Creek.

In Walker Creek, three age-2 fish were recaptured in 2024 that were tagged as age-0 fish in 2022 (Table 12). Between age-1 and age-2, the average growth rates of these three Brown Trout were 63 mm and 62 g; increases of 11 mm and 20 g from the 2023 age-2 growth rates (Table 12). The 2024 age-2 growth rates were the highest ever recorded in Walker Creek for the 13 years of available data (Table 12).

In the Lee Vining Creek main channel section, two age-2 Brown Trout were recaptured in 2024 that were tagged at age-0 fish in 2022. Between age-1 and age-2, the average growth rates of these two Brown Trout were 71 mm and 73 g, a 14 mm and 9 g increase in average growth rates from the previous year (Table 12). In Lee Vining Creek, the growth rates of age-2 Brown Trout have increased in four consecutive years (Table 12).

Growth of Age-3 Brown Trout between 2023 and 2024

In 2024, four known age-3 Brown Trout were recaptured in Walker Creek that were tagged as age-0 fish in 2021; all four of these fish were also recaptured each year since their initial tagging. Between age-2 and age-3, the average growth rates of these four Brown Trout were 40 mm and 47 g, versus average growth rates of 39 mm and 51 g of age-3 fish in 2023 (Table 12). In Walker Creek, growth rates of age-3 Brown Trout have been made in 12 of 16 years, the most of any of the annually sampled sections (Table 12).

Growth of Age-4 Brown Trout between 2023 and 2024

In 2024, one known age-4 Brown Trout was recaptured in Walker Creek that was tagged as an age-0 fish in 2020. Between age-3 and age-4, the growth rates of this Brown Trout were 29 mm and 44 g (Table 12). At age-4, this fish was 250 mm in total length. This fish has been recaptured every year since being tagged in 2020 (Table 12).

Growth of MGORD Brown Trout between 2023 and 2024

Starting in September of 2017, PIT tagging of Brown Trout in the MGORD section of Rush Creek was focused on known age-0 fish and presumed age-1 fish. Based on past years' length-frequency histograms and growth rates of known age-1 fish (from recaptures of previously tagged age-0 fish), a conservative cut-off of 225 mm in total length was used to define the probable upper limit for age-1 Brown Trout in the MGORD. Thus, moving forward, most re-captures of previously tagged fish within the MGORD will allow us to compute annual growth rates of fish in which their ages are known or accurately presumed.

In 2024, two age-1 Brown Trout were captured in the MGORD that were tagged at age-0 in the MGORD. Between 2023 and 2024, the growth rates of these two fish were 118 mm and 86 g,

compared to average growth rates of 162 mm and 169 g in 2023. At age-1, these two Brown Trout had total lengths of 210 mm and 219 mm.

In 2024, one (presumed age-4) Brown Trout was recaptured in the MGORD that had been PIT tagged (at 190 mm in length) in the MGORD as presumed age-1 fish in 2021 and was also recaptured as presumed age-2 fish in the MGORD in 2022 and at age-3 in 2023. Between age-3 and age-4, this fish grew by 9 mm and lost 46 g in weight; in sharp contrast to its growth between age-2 and age-3, when it grew by 69 mm and 252 g.

In 2024, six previously tagged Brown Trout were recaptured in the MGORD as non-sequential recaptures. All six of these Brown Trout were tagged as age-0 fish in the Upper Rush section and were recaptured in the MGORD at age-2. Between age-0 and age-2, these six fish had average growth rates of 206 mm and 302 g. These age-2 Brown Trout averaged 309 mm in total length, with a range of 289 mm to 346 mm.

Movement of PIT Tagged Trout between Sections

Previous annual fisheries reports have summarized documented movements of PIT tagged fish between the sample sections, with most movements occurring from the Upper Rush section upstream into the MGORD (Taylor 2021). These movements between the Upper Rush section and MGORD were initially documented during the radio telemetry study when approximately 50% of the radio-tagged fish left the MGORD during the fall/early winter spawning period (Taylor et al. 2009). As described in the previous paragraph, in 2024, six of the PIT tagged Brown Trout recaptured in the MGORD had moved upstream from the Upper Rush section, sometime between age-0 and age-2. To date, this is the largest number of PIT tag recaptures we have made in a single sampling year of Brown Trout moving upstream from Upper Rush to the MGORD.

PIT Tag Shed Rate of Trout Recaptured in 2024

In 2024, a total of 64 trout with adipose fin clips were recaptured and eight of these fish failed to produce a PIT tag number when scanned with the tag reader (two from the MGORD, one from Upper Rush, four from the 8-Channel, and one from Bottomlands). Assuming that all these fish were previously PIT tagged, the 2024 calculated shed rate was 12.5% (8 shed tags/64 clipped fish recaptured) versus shed rates of 4.7% in 2023, 3.8% in 2022, 2.3% in 2021 and 6.8% in 2020. Retention rates tend to be higher in juvenile fish because adult salmonids are known to shed tags during spawning (Bateman et al. 2009). The multi-thread channel section in lower Rush Creek was an observed spawning site/habitat in 2023 – the location where four of the eight fish with shed tags were captured in 2024. Also, tag retention rates have been linked to tagger's experience and crew turnover rates, with less experienced taggers resulting in higher shed rates (Dare 2003). For the past nine years, our crew members implanting tags have remained relatively stable, however the 2022-2023 fisheries crew was comprised of mostly new individuals and some with minimal tagging experience, which may explain the higher shed rate.

Table 12a. Average growth (length and weight) of Brown Trout recaptured from 2009 through 2016 by age. Note: *denotes only one PIT tagged fish recaptured.

Stream and Reach	Cohort	Average Annual Growth in Length and Weight (mm/g)							
		2008 -2009	2009 -2010	2010 -2011	2011 -2012	2012 -2013	2013 -2014	2014 -2015	2015 -2016
Upper Rush Creek	Age 1	89/51	81/50	83/48	72/33	67/35		90/55	105/77
	Age 2		58/70	54/73	43/42	41/42		64/69	99/176•
	Age 3				14/29		24/41		
	Age 4					12/-22			
	Age-5								
Rush Creek Bottom-lands	Age 1	84/43	77/40	71/35	58/25	56/24		84/41	94/62
	Age 2		50/54	35/32	30/28	27/22	32/29*	62/62	
	Age 3			13/14	17/16	11/9	35/31		
	Age 4				4/-11		18/20		
	Age-5								
LV Main Channel Brown Trout	Age 1		80/42	72/37	99/52	61/27		73/33	74/40
	Age 2		66/95		77/110	33/34	35/29	47/40	47/49
	Age 3			34/92		23/48*	16/20*	27/32	42/75
	Age 4				21/41*				25/47*
	Age-5								
LV Main Channel RB Trout	Age 1					78/47		80/35	
	Age 2						40/48*	52/50	62/74*
	Age 3								38/82*
	Age 4								
	Age-5								
Walker Creek Above Old 395	Age 1	68/27	51/20	71/34	68/36	59/23		58/24	72/36
	Age 2		31/26	60/56	40/33	27/21	39/35		47/44
	Age 3			28/44	18/12	9/2	20/36	27/29	
	Age 4				7/2	2/-16*		28/45*	
	Age-5						0/-10*		

Table 12b. Average growth (length and weight) of Brown Trout recaptured from 2017 through 2024 by age. Note: *denotes only one PIT tagged fish recaptured. •denotes one fish that moved from Upper Rush to the MGORD.

Stream and Reach	Cohort	Average Annual Growth in Length and Weight (mm/g)							
		2016 -2017	2017 -2018	2018 -2019	2019 -2020	2020 -2021	2021 -2022	2022 -2023	2023 -2024
Upper Rush Creek	Age 1	132/129	83/56	77/43	55/21	66/27	81/41	120/98	88/49
	Age 2	108/239	39/66	48/71	44/55	54/42	68/67*		
	Age 3		11/40*	15/27*	41/49*				
	Age 4					38/144*			
	Age-5						15/-49*		
Rush Creek Bottom-lands	Age 1	118/96	72/42	74/38	64/29	67/26	80/41	104/68	77/40
	Age 2		39/55	36/44*		35/33*	81/84*		
	Age 3				21/20*				
	Age 4								
	Age-5								
LV Main Channel Brown Trout	Age 1	110/92*	103/77	71/41	72/29	63/27	73/33	71/39	
	Age 2	77/128*		60/91*	70/81	46/47	55/54	57/64*	71/73
	Age 3					30/48			
	Age 4						31/67*		
	Age-5								
LV Main Channel RB Trout	Age 1			80/43*				105/71*	
	Age 2								
	Age 3								
	Age 4								
	Age-5								
Walker Creek Above Old 395	Age 1	66/33		55/28	54/24	47/18	53/18	67/30	
	Age 2	37/37	42/52		36/30	25/19	37/23	52/42	63/62
	Age 3	42/59*	25/37	25/37		12/19	22/18	39/51	40/47
	Age 4		27/37*		8/-5		13/-5	103/212*	29/44*
	Age-5							22/36*	

Comparison of Brown Trout Length-at Age amongst Sample Sections

During the September 2024 sampling, five known age-classes of PIT tagged Brown Trout were recaptured within four fisheries monitoring sections of Rush, Walker, and Lee Vining Creeks (Tables 13 and 14). Along with providing age-specific length information for each section, these data allowed comparisons of length-at-age between sample sections and between the years 2013-2024 (Tables 13 and 14).

In Upper Rush, the average length-at-age-1 in 2024 was 191 mm, 31 mm less than the average length-at-age-1 in 2023 (Table 13). In 2024, age-1 Brown Trout in Upper Rush were, on average, 14 mm longer than age-1 fish in the Bottomlands section (Table 13). In the Bottomlands section, the average length-at-age-1 in 2024 was 177 mm, 25 mm less than the 2023 average length-at-age-1 (Table 13).

In Upper Rush, the average length-at-age-2 in 2024 was 273 mm, 3 mm less than the average length-at-age-2 in 2023 (Table 13). In the Bottomlands section, the average length-at-age-2 equaled 244 mm, the second highest value for the eight years of available data (Table 13).

In 2024, one PIT-tagged age-3 Brown Trout was recaptured in the Upper Rush section and this fish was 304 mm in total length (Table 13). No age-3 Brown Trout were recaptured in 2024 in the Bottomlands section of Rush Creek (Table 13). Also, no PIT-tagged age-4 or age-5 Brown Trout were recaptured in either of these sections (Table 13).

For Walker Creek in 2024, no age-1 Brown Trout were recaptured (Table 9). In 2024, three PIT tagged age-2 Brown Trout were recaptured in Walker Creek and the average length-at-age-2 equaled 217 mm, 26 mm longer than the average length-at-age-2 in 2023 (Table 13). In 2024, six PIT tagged age-3 Brown Trout were recaptured in Walker Creek and the average length-at-age-3 equaled 222 mm, 8 mm longer than the 2023 average (Table 13). In 2024, one PIT tagged age-4 Brown Trout was recaptured in Walker Creek and its length-at-age-4 was 250 mm, 20 mm less than the age-4 fish recaptured in 2023 (Table 13). In 2024, one age-5 Brown Trout was recaptured, and this fish was 257 in length; this was the second consecutive year where an age-5 fish was recaptured in Walker Creek (Table 13). In 2023, the age-5 fish was 227 mm in total length.

For the Lee Vining Creek main channel in 2024, no age-1 Brown Trout were recaptured. In 2024, four previously tagged age-2 Brown Trout were recaptured, and the average length-at-age-2 equaled 229 mm, 4 mm longer than in 2023 (Table 14). In 2024, no age-3 or age-4 Brown Trout were recaptured in Lee Vining Creek.

These findings of average lengths by age-class continue to support previous conclusions by the Stream Scientist that very few Brown Trout reach age-4 or older in Rush Creek or Lee Vining Creek (Taylor 2022). Outside of the MGORD, we have never recaptured a PIT tagged Brown Trout older than age-5. The MGORD section continues to be the only section where Brown

Trout lengths consistently approach or exceed 300 mm by age-2 or age-3. In 2024, three age-2 MGORD recaptures had total lengths of 313 mm, 323 mm, and 346 mm.

Table 13. Size range of PIT tagged recaptures in 2013-2024 by age class for Brown Trout at three electrofishing sections on Rush and Walker Creeks. NOTE: years omitted if no tagged fish were recaptured.

Section	Cohort	Size Range (mm)	Average Length (mm)
Upper Rush	Age-1	**2024** = 180-203 **2023** = 193-258 **2022** = 151-189 **2021** = 126-185 **2020** = 124-167 **2019** = 128-202 **2018** = 158-232 **2017** = 224-264 **2016** = 192-237 **2015** = 169-203	**2024** = 191 **2023** = 222 **2022** = 169 **2021** = 154 **2020** = 145 **2019** = 173 **2018** = 193 **2017** = 243 **2016** = 208 **2015** = 187
	Age-2	**2024** = 257-287 **2023** = 267-285 **2022** = 217-237 **2021** = 174-233 **2020** = 209-235 **2019** =203-251 **2018** = 236-305 **2017** = 284-337 **2016** = 289* **2015** = 205-242	**2024** = 273 **2023** = 276 **2022** = 228 **2021** = 198 **2020** = 221 **2019** = 237 **2018** = 274 **2017** = 313 **2016** = 289* **2015** = 217
	Age-3	**2024** = 304 **2021** = 220 **2020** = 287 **2019** = 251 **2018** = 295 **2014** = 226-236 **2013** = 227-263	**2024** = 304 **2021** = 220 **2020** = 287 **2019** = 251 **2018** = 295 **2014** = 231 **2013** = 245
	Age-4	**2021** = 325 **2014** = 288 **2013** = 252-255	**2021** = 325 **2014** = 288 **2013** = 254
	Age-5	**2022** = 340 **2014** = 298	**2022** = 340 **2014** = 298
Bottomlands	Age-1	**2024** = 168-185 **2023** = 177-222 **2022** = 142-204 **2021** = 155 **2020** = 141-187 **2019** = 133-196 **2018** = 166-199 **2017** = 189-246 **2016** = 172-217 **2015** = 150-181	**2024** = 177 **2023** = 202 **2022** = 166 **2021** = 155 **2020** = 155 **2019** = 168 **2018** = 181 **2017** = 221 **2016** = 197 **2015** = 169
	Age-2	**2024** = 235-259 **2022** = 202-236 **2021** = 186 **2019** = 219 **2018** = 251-287 **2015** = 197-239 **2014** = 192 **2013** = 156-196	**2024** = 244 **2022** = 219 **2021** = 186 **2019** = 219 **2018** = 267 **2015** = 219 **2014** = 192 **2013** = 178
	Age-3	**2021** = 214-248 **2020** = 240 **2014** = 194 **2013** = 194-227	**2021** = 231 **2020** = 240 **2014** = 194 **2013** = 204
	Age-4	**2014** = 215-219	**2014** = 216
	Age-5	**2016** = 318	**2016** = 318

*Fish was tagged in Upper Rush but moved to MGORD between age-1 and age-2.

Table 13 (continued).

Section	Cohort	Size Range (mm)	Average Length (mm)
Walker Creek	Age-1	**2023** = 131-187 **2022** = 114-169 **2021** = 121-154 **2020** = 132-170 **2019** = 141-168 **2017** = 151-179 **2016** = 145-187 **2015** = 133-177	**2023** = 159 **2022** = 140 **2021** = 138 **2020** = 151 **2019** = 159 **2017** = 166 **2016** = 167 **2015** = 154
	Age-2	**2024** = 210-225 **2023** = 167-220 **2022** = 151-205 **2021** = 155-187 **2020** = 190-196 **2018** = 191-221 **2017** = 180-224 **2016** = 180-226 **2014** = 168-200 **2013** = 181-208	**2024** = 217 **2023** = 191 **2022** = 175 **2021** = 175 **2020** = 194 **2018** = 210 **2017** = 202 **2016** = 201 **2014** = 186 **2013** = 197
	Age-3	**2024** = 205-236 **2023** = 209-221 **2022** = 180-215 **2021** = 200-212 **2019** = 215-235 **2018** = 204-245 **2017** = 238 **2015** = 211-231 **2014** = 207-222 **2013** = 219-221	**2024** = 222 **2023** = 214 **2022** = 199 **2021** = 205 **2019** = 220 **2018** = 228 **2017** = 238 **2015** = 219 **2014** = 217 **2013** = 220
	Age-4	**2024** = 250 **2023** = 240-299 **2022** =205-221 **2020** = 224-243 **2018** = 265 **2015** = 249 **2014** = 211 **2013** = 219	**2024** = 250 **2023** = 270 **2022** = 213 **2020** = 234 **2018** = 265 **2015** = 249 **2014** = 211 **2013** = 219
	Age-5	**2024** = 257 **2023** = 227 **2014** = 220	**2024** = 257 **2023** = 227 **2014** = 220

Table 14. Size range of PIT tagged fish recaptured in 2013-2024 by age class for Brown Trout and Rainbow Trout on Lee Vining Creek. NOTE: years omitted if no tagged fish were recaptured.

Section	Cohort	Size Range (mm)	Average Length (mm)
Brown Trout in Lee Vining Main Channel	Age-1	**2023** = 154 - 181 **2022** = 145-169 **2021** = 126-182 **2020** = 125-185 **2019** = 142-209 **2018** = 170-194 **2017** = 210 **2016** = 147-186 **2015** = 149-190	**2023** = 170 **2022** = 161 **2021** = 154 **2020** = 155 **2019** = 174 **2018** = 183 **2017** = 210 **2016** = 171 **2015** = 166
	Age-2	**2024** = 218-233 **2023** = 212-250 **2022** = 183-230 **2021** = 163-225 **2020** = 212-270 **2019** = 222-274 **2017** = 247 **2016** = 205-217 **2015** = 176-214 **2014** = 174-195 **2013** = 206-225	**2024** = 229 **2023** = 225 **2022** = 208 **2021** = 195 **2020** = 232 **2019** = 247 **2017** = 247 **2016** = 211 **2015** = 197 **2014** = 188 **2013** = 215
	Age-3	**2023** = 266 **2022** =226-246 **2021** = 246 **2017** = 280-305 **2016** = 210-256 **2015** = 188-228 **2014** = 234-241 **2013** = 238-271	**2022** = 236 **2021** = 246 **2017** = 293 **2016** = 240 **2015** = 215 **2014** = 238 **2013** = 253
	Age-4	**2022** = 277 **2016** = 237	**2022** = 277 **2016** = 237
	Age-5	None captured in past ten years	
Rainbow Trout in Lee Vining Main Channel	Age-1	**2023** = 202 **2019** = 165 **2015** = 140-177	**2023** = 202 **2019** = 165 **2015** = 157
	Age-2	**2016** = 232 **2015** = 195-216 **2014** = 201-229	**2016** = 232 **2015** = 204 **2014** = 215
	Age-3	**2016** = 242	**2016** = 242
	Age-4	None captured in past 10 years. No age-5 fish in the past 10 years either.	

Summer Water Temperature

During the past 13 years, the Mono Basin has experienced a five-year drought (2012-2016), a near-record Extreme-wet RY (2017), a Normal RY with a full GLR (2018), a Wet RY (2019), a Dry-normal-1 RY (2020), a Dry RY (2021), a Dry RY (2022), a record Extreme-wet RY (2023), and a Normal RY in 2024 with a full GLR. These RY types have resulted in a range of summer water temperatures in Rush Creek, from moderate-to-severe stressful conditions in drier RYs to thermal regimes mostly conducive to fair-to-good growth conditions in wetter RYs and/or in average RYs with a full/spilling GLR.

In 2024, the water temperature monitoring was again conducted by the MLC. The extended elevated flows during the 78-day spill out of GLR resulted in the loss of the data logger at the Rush Creek/Above Parker location (no data for 2024). At the Rush/County Road location the data logger was deployed on July 12th and this data logger also was exposed when flows dropped in August. Thus, during the 92-day period of July-September when summer water temperatures were examined, the County Road site was missing 29 days of data (July 1st through 12th and August 8th through 24th). Unfortunately, the missing August data was right as the County Road location started to experience its highest peaks and largest diurnal fluctuations of the summer, metrics important to trout growth rates and condition factors.

In 2024, the Normal RY with GLR at high storage levels and a 78-day spill resulted in mostly favorable summer thermal conditions, with peak water temperatures exceeding 70^{o}F at only the Above Damsite (11 days) and County Road (one day) monitoring locations (Table 15). In 2024, daily mean temperatures and average daily maximum temperatures were relatively low and within the range typical of wetter RY types and/or when a full GLR spills for extended periods (Table 15). At most Rush Creek temperature monitoring locations, the maximum diurnal fluctuations were relatively large, yet appeared to be influenced by lower lows, as opposed to higher daily maximums (Table 15).

Similar to the 2013-2023 annual reports, 2024 Rush Creek summer average daily water temperature data were classified based on its predicted influence on growth of Brown Trout as either: 1) good potential growth days, 2) fair potential growth days, 3) poor potential growth days (daily averages within one degree or less of a “bad thermal day”), or 4) bad thermal days (Table 16). Development of these thermal-based growth criteria were fully described in previous annual reports (Taylor 2013 and 2014). Using these growth prediction metrics, good potential growth days in 2024 varied from 46 to 92 days in Rush Creek out of the 92-day period from July 1 to September 30 (Table 16). For all Rush Creek temperature monitoring locations downstream of GLR, the number of days classified as “fair” potential growth days in 2024 ranged from zero to 26 days (Table 16). In 2024, no days were classified as either poor potential growth days or bad thermal days at the temperature monitoring locations downstream of GLR (Table 16). Conversely, at the Above Damsite location, there were two poor potential growth days (7/31/24 and 8/1/24) and nine bad thermal days (8/3-11/24), which accounted for 12% of the 92-day summer period when water temperature data were evaluated (Table 16).

As was done with the 2013-2023 data, the diurnal temperature fluctuations for July, August and September 2024 were characterized by the one-day maximum fluctuation that occurred each month and by monthly averages (Table 17). Also, for each temperature monitoring location, the highest average diurnal fluctuations over consecutive 21-day durations were determined (Table 17). The diurnal fluctuations throughout the summer of 2024 were relatively low at the Top of MGORD and Bottom of MGORD temperature monitoring locations, but diurnal fluctuations increased at the downstream monitoring locations, most likely due to effects of daily warming and nightly cooling of air temperatures (Table 17). Over the 21-day durations, these larger diurnal fluctuations were above the threshold of 12.6°F considered detrimental to trout growth (Werley et al. 2007) during the summer of 2024 as recorded only at the County Road temperature monitoring location (Table 17). Again, the missing data between August 8th and 24th at the County Road temperature monitoring location hampered a complete picture of the diurnal fluctuations during what was likely the hottest period of the summer. At two other temperature monitoring locations, at the Above Damsite and Below Narrows locations, the 21-day diurnal fluctuations approached, but did not exceed the 12.6°F threshold (Table 17). August into September were when these temperature monitoring locations experienced their highest 21-day diurnal fluctuations, including levels detrimental to trout growth (Werley et al. 2007).

The thermal window bounded by 66.2-71.6°F where Brown Trout may be physiologically stressed and living at the edge of their survival tolerance as defined by Bell (2006) was quantified for each Rush Creek temperature monitoring location in 2013 through 2024. The hourly temperature data for the 92-day (or 2,208-hour) summer period were sorted from low to high and the number of hours where temperatures exceeded 66.2°F were summed by month and entire summer period (Table 18). The values from 2013-2023 were also included to better illustrate the variability that occurred at all the temperature monitoring locations (Table 18). The 2024 data show that all the temperature monitoring stations, located downstream of GLR experienced very few hours in exceedance of the 66.2°F thermal threshold, with seasonal ranges of 0% to 6% of the 2,208-hour summer period (Table 18). At the Above Damsite location, hourly water temperatures exceeded 66.2°F for 212 hours (or 9.6%) of the 2,208-hour summer period (Table 18).

Summer water temperatures in Lee Vining Creek were all within the range of fair-to-good growth potential during 2024. For example, the highest peak temperature recorded at the Lee Vining Creek Ford was 65.4°F on 8/9/24 and was one of two days the entire summer where the daily maximum temperature exceeded 65°F. Regardless of RY type, excessively warm water has not been an issue in Lee Vining Creek, thus detailed analyses were not performed with the 2024 data.

Table 15. Summary of water temperature data during the summer of RY 2024 (July to September). Averages were calculated for daily mean, daily minimum, and daily maximum temperatures between July 1st and September 30th. All temperature data are presented in °F. When available, values for 2013-2023 are provided for comparison.

Temperature Monitoring Location	Daily Mean (°F)	Ave Daily Minimum (°F)	Ave Daily Maximum (°F)	No. Days > 70°F	Max Diurnal Fluctuation (°F)	Date of Max. Fluctuation
Rush Ck. – Above Damsite	2023 = 55.2 **2024 = 60.4**	2023 = 53.0 **2024 = 56.5**	2023 = 58.3 **2024 = 65.6**	2023 = 0 **2024 = 11**	2023 = 10.0 **2024 = 14.9**	9/18/23 **8/27/24**
Rush Ck. – Top of MGORD	2013 = 63.1 2014 = 64.8 2015 = 64.4 2016 = 63.8 2017 = 57.0 2018 = 60.7 2019 = 58.5 2020 = 63.2 2021 = 65.9 2022 = 65.9 2023 = 54.0 **2024 = 57.8**	2013 = 62.7 2014 = 64.6 2015 = 64.1 2016 = 63.0 2017 = 56.5 2018 = 59.6 2019 = 57.2 2020 = 62.1 2021 = 65.2 2022 = 65.0 2023 = 53.3 **2024 = 56.5**	2013 = 63.7 2014 = 65.0 2015 = 64.8 2016 = 64.7 2017 = 58.1 2018 = 61.9 2019 = 59.9 2020 = 64.4 2021 = 66.8 2022 = 67.0 2023 = 55.0 **2024 = 59.3**	2013 = 0 2014 = 0 2015 = 0 2016 = 0 2017 = 0 2018 = 0 2019 = 0 2020 = 0 2021 = 5 2022 = 3 2023 = 0 **2024 = 0**	2013 = 3.4 2014 = 3.9 2015 = 2.1 2016 = 6.5 2017 = 5.4 2018 = 6.7 2019 = 8.2 2020 = 6.4 2021 = 6.5 2022 = 6.6 2023 = 8.2 **2024 = 9.1**	7/09/13 8/13/14 7/03/15 7/07/16 9/07/17 8/20/18 8/10/19 7/02/20 7/13/21 7/12/22 8/31/23 **8/20/24**
Rush Ck. – Bottom of MGORD	2013 = 63.2 2014 = 64.8 2015 = 64.4 2016 = 63.8 2017 = 57.1 2018 = 61.0 2019 = 58.7 2020 = 63.2 2021 = 65.8 2022 = 65.9 2023 = N/A **2024 = 58.1**	2013 = 60.9 2014 = 62.9 2015 = 62.3 2016 = 61.8 2017 = 56.5 2018 =58.9 2019 = 56.6 2020 = 60.5 2021 = 63.4 2022 = 63.7 2023 = N/A **2024 = 55.7**	2013 = 67.1 2014 = 68.5 2015 = 68.0 2016 = 66.9 2017 = 58.5 2018 = 63.9 2019 = 61.3 2020 = 67.5 2021 = 69.8 2022 = 69.5 2023 = N/A **2024 = 61.8**	2013 = 1 2014 = 20 2015 = 20 2016 = 1 2017 = 0 2018 = 0 2019 = 0 2020 = 17 2021 = 44 2022 = 50 2023 = N/A **2024 = 0**	2013 = 9.0 2014 = 8.3 2015 = 8.4 2016 = 8.0 2017 = 6.4 2018 = 8.7 2019 = 8.1 2020 = 10.0 2021 = 8.5 2022 = 8.7 2023 = N/A **2024 = 12.3**	7/09/13 7/13/14 7/06/15 7/04/16 9/07/17 7/05/18 8/10/19 8/03/20 7/24/21 7/29/22 2023 = N/A **8/18/24**
Rush Ck. – Old Highway 395 Bridge/Upper Rush section	2013 = 62.6 2014 = 64.0 2015 = N/A 2016 = 63.5 2017 = 59.0 2018 = 60.9 2019 = 58.7 2020 = 62.6 2021 = 65.0 2022 = 64.7 2023 = 57.4 **2024 = 58.2**	2013 = 58.8 2014 = 60.5 2015 = N/A 2016 = 60.1 2017 = 57.5 2018 = 58.0 2019 = 56.1 2020 = 58.5 2021 = 61.2 2022 = 60.4 2023 = 55.8 **2024 = 54.8**	2013 = 68.7 2014 = 69.8 2015 = N/A 2016 = 68.8 2017 = 61.0 2018 = 65.3 2019 = 62.3 2020 = 68.4 2021 = 70.8 2022 = 70.6 2023 = 59.6 **2024 = 63.3**	2013 = 40 2014 = 51 2015 = N/A 2016 = 47 2017 = 0 2018 = 0 2019 = 0 2020 = 30 2021 = 63 2022 = 55 2023 = 0 **2024 = 0**	2013 = 13.5 2014 = 13.3 2015 = N/A 2016 = 12.5 2017 = 7.6 2018 = 10.9 2019 = 10.7 2020 = 14.0 2021 = 12.8 2022 = 15.2 2023 = 9.6 **2024 = 13.2**	7/09/13 7/13/14 N/A 7/11/16 9/07/17 7/10/18 9/14/19 8/03/20 8/02/21 8/07/22 8/31/23 **8/20/24**

Table 15 (continued).

Temperature Monitoring Location	Daily Mean (°F)	Ave Daily Minimum (°F)	Ave Daily Maximum (°F)	No. Days > 70°F	Max Diurnal Fluctuation (°F)	Date of Max. Fluctuation
Rush Ck. – Above Parker	2016 = 63.2	2016 = 58.8	2016 = 69.4	2016 = 55	2016 = 13.7	7/11/16
	2017 = 59.0	2017 = 57.2	2017 = 61.9	2017 = 0	2017 = 8.6	9/08/17
	2018 = 60.9	2018 = 57.2	2018 = 66.3	2018 = 0	2018 = 13.4	7/10/18
	2019 = 58.4	2019 = 55.5	2019 = 62.3	2019 = 0	2019 = 11.8	9/14/19
	2020 = 62.2	2020 = 57.1	2020 = 68.6	2020 = 40	2020 = 16.1	8/03/20
	2021 = 64.4	2021 = 59.6	2021 = 70.8	2021 = 61	2021 = 14.4	8/02/21
	2022 = 64.5	2022 = 59.4	2022 = 70.7	2022 = 59	2022 = 15.7	8/07/22
	2023 = 57.5	2023 = 55.6	2023 = 60.4	2023 = 0	2023 = 10.7	9/27/23
	2024 = N/A	**2024 = N/A**	**2024 = N/A**	**2024 = N/A**	**2024 = N/A**	**2024 = N/A**
Rush Ck. – below Narrows	2013 = 61.2	2013 = 56.2	2013 = 67.6	2013 = 24	2013 = 16.3	7/19/13
	2014 = 63.2	2014 = 57.1	2014 = 69.4	2014 = 46	2014 = 17.3	7/26/14
	2015 = 62.3	2015 = 58.8	2015 = 66.1	2015 = 0	2015 = 11.5	9/23/15
	2016 = 61.7	2016 = 56.9	2016 = 68.3	2016 = 34	2016 = 14.3	7/13/16
	2017 = 58.4	2017 = 56.3	2017 = 61.3	2017 = 0	2017 = 8.2	9/07/17
	2018 = 60.0	2018 = 56.0	2018 = 65.4	2018 =0	2018 = 12.4	7/10/18
	2019 = 57.8	2019 = 54.4	2019 = 62.2	2019 = 0	2019 = 12.7	9/22/19
	2020 = 61.0	2020 = 55.5	2020 = 67.5	2020 = 16	2020 = 15.7	8/03/20
	2021 = 63.2	2021 = 58.0	2021 = 69.7	2021 = 49	2021 = 14.9	8/12/21
	2022 = 63.2	2022 = 58.0	2022 = 69.5	2022 = 52	2022 = 14.7	7/29/22
	2023 = 57.3	2023 = 55.2	2023 = 60.3	2023 = 0	2023 = 8.9	8/31/23
	2024 = 58.0	**2024 = 53.6**	**2024 = 63.8**	**2024 = 0**	**2024 = 14.2**	**8/16/24****
Rush Ck. – County Road*	2013 = 61.4	2013 = 56.5	2013 = 66.6	2013 = 7	2013 = 14.7	8/02/13
	2014 = 62.0	2014 = 56.7	2014 = 67.8	2014 = 24	2014 = 17.6	7/26/14
	2015 = 62.1	2015 = 59.1	2015 = 65.5	2015 = 2	2015 = 9.2	7/28/15
	2016 = 61.6	2016 = 56.0	2016 = 68.3	2016 = 32	2016 = 16.1	7/11/16
	2017 = N/A	2017 = N/A	2017 = N/A	2017 = N/A	2017 = N/A	N/A
	2018 = N/A	2018 = N/A	2018 = N/A	2018 = N/A	2018 = N/A	N/A
	2019 = 58.2	2019 = 54.0	2019 = 63.6	2019 = 0	2019 = 13.5	9/13/19
	2020 = 61.0	2020 = 54.5	2020 = 68.5	2020 = 42	2020 = 18.2	8/03/20
	2021 = 63.1	2021 = 56.6	2021 = 70.7	2021 = 57	2021 = 17.4	9/02/21
	2022 = 63.3	2022 = 57.5	2022 = 70.2	2022 = 55	2022 = 16.8	7/29/22
	2023 = 61.4	2023 = 56.8	2023 = 63.6	2023 = 0	2023 = 12.6	8/04/23
	2024 = 58.6	**2024 = 53.1**	**2024 = 65.2**	**2024 = 1**	**2024 = 15.7**	**8/26/24**

*logger missed 29 days of data collection in July and August ** also occurred on 8/20/24, 8/26/24 and 8/27/24

Table 16. Classification of 2013-2024 summer water temperature data into good growth days, fair growth days, poor growth days and bad thermal days based on daily average temperatures (92-day period from July 1 to September 30). The percentage (%) designates each thermal day-type's occurrence for the 92-day summer period.

Temperature Monitoring Location	No. of Days for Good Growth Potential – Daily Ave. ≤60.5°F	No. of Days for Fair Growth Potential – Daily Ave. 60.6° – 63.9°F	No. of Days of Poor Growth Potential – Daily Ave. 64.0° - 64.9°F	No. of Bad Thermal Days - Daily Ave. ≥65°F
Rush Ck. – Above Damsite	2023 = 92 (100%) **2024 = 46 (50%)**	2023 = 0 **2024 = 35 (38%)**	2023 = 0 **2024 = 2 (2%)**	2023 = 0 **2024 = 9 (10%)**
Rush Ck. – Top of MGORD	2013 = 14 (15%) 2014 = 5 (6%) 2015 = 7 (8%) 2016 = 10 (11%) 2017 = 66 (71%) 2018 = 47 (51%) 2019 = 65 (71%) 2020 = 6 (6%) 2021 = 0 2022 = 12 (13%) 2023 = 90 (98%) **2024 = 66 (72%)**	2013 = 43 (47%) 2014 = 14 (15%) 2015 = 20 (22%) 2016 = 32 (35%) 2017 = 26 (29%) 2018 = 42 (46%) 2019 = 23 (25%) 2020 = 50 (54%) 2021 = 30 (33%) 2022 = 21 (23%) 2023 = 2 (2%) **2024 = 26 (28%)**	2013 = 17 (18%) 2014 = 25 (27%) 2015 = 5 (5%) 2016 = 17 (18%) 2017 = 0 2018 = 3 (3%) 2019 = 4 (4%) 2020 = 12 (13%) 2021 = 8 (9%) 2022 = 5 (6%) 2023 = 0 **2024 = 0**	2013 = 18 (20%) 2014 = 48 (52%) 2015 = 60 (65%) 2016 = 33 (36%) 2017 = 0 2018 = 0 2019 = 0 2020 = 24 (26%) 2021 = 54 (59%) 2022 = 54 (59%) 2023 = 0 **2024 = 0**
Rush Ck. – Bottom MGORD	2013 = 11 (12%) 2014 = 6 (6%) 2015 = 8 (9%) 2016 = 9 (10%) 2017 = 67 (73%) 2018 = 48 (52%) 2019 = 62 (68%) 2020 = 4 (4%) 2021 = 14 (15%) 2022 = 23 (25%) 2023 = N/A **2024 = 68 (74%)**	2013 = 38 (41%) 2014 = 11 (12%) 2015 = 20 (22%) 2016 = 31 (34%) 2017 = 25 (27%) 2018 = 42 (46%) 2019 = 28 (30%) 2020 = 50 (54%) 2021 = 30 (33%) 2022 = 14 (15%) 2023 = N/A **2024 = 24 (26%)**	2013 = 20 (22%) 2014 = 21 (23%) 2015 = 5 (6%) 2016 = 16 (17%) 2017 = 0 2018 = 2 (2%) 2019 = 2 (2%) 2020 = 18 (20%) 2021 = 13 (14%) 2022 = 7 (8%) 2023 = N/A **2024 = 0**	2013 = 23 (25%) 2014 = 54 (59%) 2015 = 59 (64%) 2016 = 36 (39%) 2017 = 0 2018 = 0 2019 = 0 2020 = 20 (22%) 2021 = 35 (38%) 2022 = 48 (52%) 2023 = N/A **2024 = 0**
Rush Ck. – Old Highway 395 Bridge/Upper Rush section	2013 = 14 (15%) 2014 = 7 (8%) 2015 = N/A 2016 = 16 (17%) 2017 = 75 (82%) 2018 = 36 (39%) 2019 = 64 (70%) 2020 = 17 (18%) 2021 = 24 (26%) 2022 = 29 (32%) 2023 = 77 (89%) **2024 = 78 (85%)**	2013 = 41 (45%) 2014 = 25 (27%) 2015 = N/A 2016 = 24 (26%) 2017 = 17 (18%) 2018 = 56 (61%) 2019 = 28 (30%) 2020 = 48 (52%) 2021 = 30 (33%) 2022 = 17 (18%) 2023 = 10 (11%) **2024 = 14 (15%)**	2013 = 33 (36%) 2014 = 27 (29%) 2015 = N/A 2016 = 19 (21%) 2017 = 0 2018 = 0 2019 = 0 2020 = 17 (18%) 2021 = 11 (12%) 2022 = 7 (8%) 2023 = 0 **2024 = 0**	2013 = 4 (4%) 2014 = 33 (36%) 2015 = N/A 2016 = 33 (36%) 2017 = 0 2018 = 0 2019 = 0 2020 = 10 (11%) 2021 = 27 (29%) 2022 = 39 (42%) 2023 = 0 **2024 = 0**

Table 16 (continued).

Temperature Monitoring Location	No. of Days for Good Growth Potential – Daily Ave. ≤60.5°F	No. of Days for Fair Growth Potential – Daily Ave. 60.6°– 63.9°F	No. of Days of Poor Growth Potential – Daily Ave. 64.0° - 64.9°F	No. of Bad Thermal Days - Daily Ave. ≥65°F
Rush Ck. – Above Parker Ck.	2016 = 17 (18%) 2017 = 65 (71%) 2018 = 28 (30%) 2019 = 67 (73%) 2020 = 24 (26%) 2021 = 30 (33%) 2022 = 31 (34%) 2023 = 81 (88%) **2024 = N/A**	2016 = 26 (28%) 2017 = 27 (29%) 2018 = 64 (70%) 2019 = 25 (27%) 2020 = 41 (45%) 2021 = 34 (37%) 2022 = 16 (17%) 2023 = 11 (12%) **2024 = N/A**	2016 = 24 (26%) 2017 = 0 2018 = 0 2019 = 0 2020 = 21 (23%) 2021 = 10 (11%) 2022 = 7 (8%) 2023 = 0 **2024 = N/A**	2016 = 25 (27%) 2017 = 0 2018 = 0 2019 = 0 2020 = 10 (11%) 2021 = 18 (20%) 2022 = 38 (41%) 2023 = 0 **2024 = N/A**
Rush Ck. – Below Narrows	2013 = 17 (18%) 2014 = 13 (14%) 2015 = 24 (26%) 2016 = 22 (24%) 2017 = 75 (82%) 2018 = 46 (50%) 2019 = 74 (80%) 2020 = 36 (39%) 2021 = 26 (28%) 2022 = 33 (36%) 2023 = 75 (90%) **2024 = 92 (100%)**	2013 = 69 (75%) 2014 = 58 (63%) 2015 = 44 (48%) 2016 = 52 (57%) 2017 = 17 (18%) 2018 = 46 (50%) 2019 = 18 (20%) 2020 = 53 (58%) 2021 = 39 (42%) 2022 = 22 (24%) 2023 = 8 (10%) **2024 = 0**	2013 = 6 (7%) 2014 = 18 (20%) 2015 = 22 (24%) 2016 = 16 (17%) 2017 = 0 2018 = 0 2019 = 0 2020 = 2 (2%) 2021 = 10 (11%) 2022 = 27 (29%) 2023 = 0 **2024 = 0**	2013 = 0 2014 = 3 (3%) 2015 =2 (2%) 2016 = 2 (2%) 2017 = 0 2018 = 0 2019 = 0 2020 = 1 (1%) 2021 = 17 (18%) 2022 = 8 (9%) 2023 = 0 **2024 = 0**
Rush Ck. – County Road*	2013 = 17 (18%) 2014 = 17 (18%) 2015 = 25 (27%) 2016 = 24 (26%) 2017 = N/A 2018 = N/A 2019 = 71 (77%) 2020 = 31 (34%) 2021 = 26 (28%) 2022 = 33 (36%) 2023 = 24 (69%) **2024 = 49 (78%)**	2013 = 64 (70%) 2014 = 59 (65%) 2015 = 39 (42%) 2016 = 50 (54%) 2017 = N/A 2018 = N/A 2019 = 21 (23%) 2020 = 50 (54%) 2021 = 31 (34%) 2022 = 15 (16%) 2023 = 11 (31%) **2024 = 14 (22%)**	2013 = 8 (9%) 2014 = 14 (15%) 2015 =23 (25%) 2016 = 13 (14%) 2017 = N/A 2018 = N/A 2019 = 0 2020 = 10 (11%) 2021 = 9 (10%) 2022 = 8 (9%) 2023 = 0 **2024 = 0**	2013 = 3 (3%) 2014 = 2 (2%) 2015 = 5 (6%) 2016 = 5 (6%) 2017 = N/A 2018 = N/A 2019 = 0 2020 = 1 (1%) 2021 = 26 (28%) 2022 = 36 (39%) 2023 = 0 **2024 = 0**

*logger missed 29 days of data collection in July and August (63 days with data)

Table 17. Diurnal temperature fluctuations in Rush Creek for 2024: maximum daily for month, daily average for month, and highest average for consecutive 21-day duration (92-day period from July 1 to September 30). NOTE: 2023 values in ( ) for comparison.

Temperature Monitoring Location	Maximum and Average Daily Diurnal Fluctuation for July	Maximum and Average Daily Diurnal Fluctuation for August	Maximum and Average Daily Diurnal Fluctuation for September	Highest Average Diurnal Fluctuation for a Consecutive 21-Day Duration
Rush Ck. – Above Damsite	Max = 10.6°F (5.7) Ave = 6.1°F (4.3)	Max = 14.9°F (7.3) Ave = 11.6°F (4.7)	Max = 12.7 °F (10.0) Ave = 9.5°F (7.2)	12.2°F (7.5) Aug 13 – Sept 2
Rush Ck. – Top of MGORD	Max = 5.3°F (3.6) Ave = 3.1°F (1.3)	Max = 9.1°F (8.2) Ave = 4.0°F (2.5)	Max = 3.7°F (3.2) Ave = 1.1°F (1.1)	5.4°F (2.4) Aug 2 – 22
Rush Ck. – End of MGORD	Max = 7.9°F (N/A) Ave = 4.1°F (N/A)	Max = 12.3°F (N/A) Ave = 7.7°F (N/A)	Max = 7.8°F (N/A) Ave = 6.5°F (N/A)	8.6°F (N/A) Aug 7 -27
Rush Ck. – Old Hwy 395 Bridge	Max = 9.8°F (4.3) Ave = 5.8°F (3.0)	Max = 13.2°F (9.6) Ave = 10.5°F (4.0)	Max = 11.5°F (7.8) Ave = 9.1°F (4.6)	11.3°F (4.7) Aug 9 -29
Rush Ck. – Above Parker	Max = N/A (4.6) Ave = N/A (3.4)	Max = N/A (9.7) Ave = 4.8°F (11.5)	Max = N/A (10.7) Ave = N/A (11.3)	N/A (7.2) N/A
Rush Ck. – below Narrows	Max = 10.6°F (5.6) Ave = 7.7°F (7.7)	Max = 14.2°F (8.9) Ave = 11.7°F (5.2)	Max = 13.4°F (7.8) Ave = 11.2°F (5.8)	12.2°F (6.0) Aug 25 – Sept 14
Rush Ck. – County Road*	Max = 14.0°F (7.8) Ave = 10.3°F (6.6)	Max = 15.7°F (N/A) Ave = 14.7°F (N/A)	Max = 15.2°F (N/A) Ave = 12.8°F (N/A)	**13.9°F** (7.0) Aug 25 – Sept 14

*logger missed 29 days of data collection in July and August (63 days with data)

Table 18. Number of hours (percent of hours in parentheses) that temperature exceeded 66.2°F in Rush Creek: by month and for 92-day period from July 1 to September 30, 2013 - 2024. The total number of hours within each month is in parentheses in the column headings.

Temperature Monitoring Location	Number of Hours Temperature exceeded 66.2°F in July (744 hours)	Number of Hours Temperature exceeded 66.2°F in August (744 hours)	Number of Hours Temperature exceeded 66.2°F in Sept. (720 hours)	Number of Hours Temperature exceeded 66.2°F in 92-day period
Rush Ck. – Above Damsite	2023 = 0 hrs **2024 = 34 hrs (5%)**	2023 = 0 hrs **2024 = 157 hrs (21%)**	2023 = 0 hrs **2024 = 21 hrs (3%)**	2023 = 0 hrs **2024 = 212 hrs (10%)**
Rush Ck. – Top of MGORD	2013 = 4 hrs (0.5%) 2014 = 315 hrs (42%) 2015 = 140 hrs (19%) 2016 = 42 hrs (6%) 2017 = 0 hrs 2018 = 0 hrs 2019 = 0 hrs 2020 = 0 hrs 2021 = 488 hrs (66%) 2022 = 246 hrs (33%) 2023 = 0 hrs **2024 = 0 hrs**	2013 = 4 hrs (0.5%) 2014 = 96 hrs (13%) 2015 = 205 hrs (28%) 2016 = 127 hrs (17%) 2017 = 0 hrs 2018 = 6 hrs 2019 = 0 hrs 2020 = 71 hours (10%) 2021 = 588 hrs (79%) 2022 = 728 hrs (98%) 2023 = 0 hrs **2024 = 0 hrs**	2013 = 0 hrs 2014 = 0 hrs 2015 = 0 hrs 2016 = 0 hrs 2017 = 0 hrs 2018 = 0 hrs 2019 = 13 hrs 2020 = 47 hrs (7%) 2021 = 35 hrs (5%) 2022 = 343 hrs (48%) 2023 = 0 hrs **2024 = 0 hrs**	2013 = 8 hrs (0.4%) 2014 = 411 hrs (19%) 2015 = 345 hrs (16%) 2016 = 169 hrs (8%) 2017 = 0 hrs 2018 = 6 hrs (0.3%) 2019 = 13 hrs (0.6%) 2020 = 118 hrs (5%) 2021 = 1,111 hrs (50%) 2022 = 1,317 hrs (60%) 2023 = 0 hrs **2024 = 0hrs**

Table 18 (continued).

Temperature Monitoring Location	Number of Hours Temperature exceeded 66.2°F in July (744 hours)	Number of Hours Temperature exceeded 66.2°F in August (744 hours)	Number of Hours Temperature exceeded 66.2°F in Sept. (720 hours)	Number of Hours Temperature exceeded 66.2°F in 92-day period
Rush Ck. – Bottom MGORD	2013 = 121 hrs (16%) 2014 = 282 hrs (38%) 2015 = 305 hrs (41%) 2016 = 142 hrs (19%) 2017 = 0 hrs 2018 = 0 hrs 2019 = 0 hrs 2020 = 49 hrs (6%) 2021 = 444 hrs (60%) 2022 = 257 hrs (35%) 2023 = N/A **2024 = 0 hrs**	2013 = 229 hrs (31%) 2014 = 248 hrs (33%) 2015 =282 hrs (38%) 2016 = 268 hrs (36%) 2017 = 0 hrs 2018 = 1 hr (0.01%) 2019 = 0 hrs 2020 = 234 hrs (31%) 2021 = 376 hrs (51%) 2022 = 535 hrs (72%) 2023 = N/A **2024 = 11 hrs (2%)**	2013 = 61 hrs (9%) 2014 = 115 hrs (16%) 2015 = 17 hrs (2%) 2016 = 38 hrs (5%) 2017 = 2 hrs (0.3%) 2018 = 1 hr (0.01%) 2019 = 46 hrs (6%) 2020 = 101 hrs (14%) 2021 = 125 hrs (17%) 2022 = 247 hrs (34%) 2023 = N/A **2024 = 14 hrs (2%)**	2013 = 411 hrs (19%) 2014 = 645 hrs (29%) 2015 = 604 hrs (27%) 2016 = 448 hrs (20%) 2017 = 2 hrs (0.09%) 2018 = 2 hrs (0.09%) 2019 = 46 hrs (2%) 2020 = 335 hrs (15%) 2021 = 945 hrs (43%) 2022 = 1,039 hrs (47%) 2023 = N/A **2024 = 25 hrs (1%)**
Rush Ck. – Old 395 Bridge/Upper Rush	2013 = 181 hrs (24%) 2014 = 287 hrs (39%) 2016 = 216 hrs (29%) 2017 = 0 hrs 2018 = 17 hrs (2%) 2019 = 0 hrs 2020 = 113 hrs (15%) 2021 = 351 hrs (47%) 2022 = 252 hrs (34%) 2023 = 0 hrs **2024 = 0 hrs**	2013 = 228 hrs (31%) 2014 = 248 hrs (33%) 2016 = 263 hrs (35%) 2017 = 0 hrs 2018 = 32 hrs (4%) 2019 = 4 hrs (0.5%) 2020 = 241 hrs (32%) 2021 = 328 hrs (44%) 2022 = 350 hrs (47%) 2023 = 0 hrs **2024 = 27 hrs (4%)**	2013 = 73 hrs (10%) 2014 = 117 hrs (16%) 2016 = 53 hrs (7%) 2017 = 3 hrs (0.4%) 2018 = 33 hrs (5%) 2019 = 41 hrs (6%) 2020 = 87 hrs (12%) 2021 = 127 hrs (18%) 2022 = 162 hrs (23%) 2023 = 0 hrs **2024 = 34 hrs (5%)**	2013 = 482 hrs (22%) 2014 = 639 hrs (29%) 2016 = 532 hrs (24%) 2017 = 3 hrs = (0.1%) 2018 = 82 hrs (4%) 2019 = 45 hrs (2%) 2020 = 441 hrs (20%) 2021 = 806 hrs (37%) 2022 = 764 hrs (35%) 2023 = 0 hrs **2024 = 61 hrs (3%)**
Rush Ck. – Above Parker Creek	2016 = 240 hrs (32%) 2017 = 0 hrs 2018 = 70 hrs (9%) 2019 = 0 hrs 2020 = 146 hrs (20%) 2021 = 342 hrs (46%) 2022 = 276 hrs (37%) 2023 = 0 hrs **2024 = N/A**	2016 = 269 hrs (36%) 2017 = 0 hrs 2018 = 68 hrs (9%) 2019 = 11 hrs (2%) 2020 = 257 hrs (35%) 2021 = 316 hrs (42%) 2022 = 348 hrs (47%) 2023 = 0 hrs **2024 = N/A**	2016 = 65 hrs (9%) 2017 = 14 hrs (2%) 2018 = 44 hrs (6%) 2019 = 27 hrs (4%) 2020 = 73 hrs (10%) 2021 = 122 hrs (17%) 2022 = 157 hrs (22%) 2023 = 0 hrs **2024 = N/A**	2016 = 574 hrs (26%) 2017 = 14 hrs (0.6%) 2018 = 182 hrs (8%) 2019 = 38 hrs (2%) 2020 = 476 hrs (22%) 2021 = 780 hrs (35%) 2022 = 781 hrs (35%) 2023 = 0 hrs **2024 = N/A**
Rush Ck. – below Narrows	2013 = 158 hrs (21%) 2014 = 244 hrs (33%) 2015 = 129 hrs (17%) 2016 = 167 hrs (22%) 2017 = 0 hrs 2018 = 36 hrs (5%) 2019 = 0 hrs 2020 = 109 (15%) 2021 = 273 hrs (37%) 2022 = 243 hrs (33%) 2023 = 0 hrs **2024 = 0 hrs**	2013 = 192 hrs (26%) 2014 = 193 hrs (26%) 2015 = 189 hrs (25%) 2016 = 222 hrs (30%) 2017 = 0 hrs 2018 = 42 hrs (6%) 2019 = 13 hrs (2%) 2020 = 204 hrs (27%) 2021 = 267 hrs (36%) 2022 = 265 hrs (36%) 2023 = 0 hrs **2024 = 23 hrs (3%)**	2013 = 55 hrs (7%) 2014 = 105 hrs (15%) 2015 = 0 hrs (0%) 2016 = 49 hrs (7%) 2017 = 0 hrs 2018 = 36 hrs (5%) 2019 = 8 hrs (1%) 2020 = 43 hrs (6%) 2021 = 104 hrs (14%) 2022 = 109 hrs (15%) 2023 = 0 hrs **2024 = 16 hrs (2%)**	2013 = 405 hrs (18%) 2014 = 542 hrs (25%) 2015 = 318 hrs (14%) 2016 = 438 hrs (20%) 2017 = 0 hrs 2018 = 114 hrs (5%) 2019 = 21 hrs (1%) 2020 = 356 hrs (16%) 2021 = 644 hrs (29%) 2022 = 617 hrs (28%) 2023 = 0 hrs **2024 = 39 hrs (2%)**

Table 18 (continued).

Rush Ck. – County Road*	2013 = 197 hrs (27%) 2014 = 222 hrs (30%) 2015 = 174 hrs (23%) 2016 = 212 hrs (28%) 2017 = N/A 2018 = N/A 2019 = 0 hrs 2020 = 195 hrs (26%) 2021 = 301 hrs (40%) 2022 = 290 hrs (39%) 2023 = 0 hrs **2024 = 10 hrs (2%)**	2013 = 172 hrs (23%) 2014 = 195 hrs (26%) 2015 = 119 hrs (16%) 2016 = 233 hrs (31%) 2017 = N/A 2018 = N/A 2019 = 76 hrs (10%) 2020 = 241 hrs (32%) 2021 = 278 hrs (37%) 2022 = 282 hrs (38%) 2023 = 2 hrs **2024 = 48 hrs (13%)**	2013 = 42 hrs (6%) 2014 = 79 hrs (11%) 2015 = 0 hrs (0%) 2016 = 42 hrs (6%) 2017 = N/A 2018 = N/A 2019 = 10 hrs (1%) 2020 = 41 hrs (6%) 2021 = 99 hrs (14%) 2022 = 107 hrs (15%) 2023 = N/A **2024 = 38 hrs (5%)**	2013 = 411 hrs (19%) 2014 = 496 hrs (23%) 2015 = 293 hrs (13%) 2016 = 487 hrs (22%) 2017 = N/A 2018 = N/A 2019 = 86 hrs (4%) 2020 = 477 hrs (22%) 2021 = 678 hrs (31%) 2022 = 679 hrs (31%) 2023 = N/A **2024 = 96 hrs (6%)**

*logger missed 29 days of data collection in July and August (63 days with data)

Discussion

The 2024 sampling was marked by being the third year of fisheries monitoring under the recently issued WR-2021-0086, which amended LADWP's license and signaled the start of the 10-year post-settlement monitoring period. During this 10-year period, all monitoring activities (fisheries, geomorphic/riparian, Mono Lake limnology and waterfowl) will be conducted by consultants, with oversight from the MAT. The purpose of the post-settlement monitoring is to evaluate the effectiveness of the SEF flow regimes and as needed, make recommended changes to these flows (timing and magnitude), as long as the overall quantity of water released by LADWP is not increased from quantities defined by RY type in WR-2021-0086.

Although RY 2024 was classified as Normal, the high storage level in GLR and the 78-day spill from GLR resulted in mostly favorable summer water temperatures in Rush Creek. This exemplifies the importance of entering the spring/summer period with a high storage level in GLR. A discussion of the 2024 trout population metrics is included below.

The 2024 sampling year was also highlighted by news from LADWP that the roto-valve which controls flow releases from GLR into the MGORD (and flow exports) was damaged during the 2023 RY. The maximum allowable flow release (to avoid cavitation) into the MGORD is now 175 cfs, instead of 380 cfs, which has implications on LADWP's ability to deliver SEFs for most RY types. In addition, replacement of the roto-valve and the 80-foot vertical concrete shaft that houses the roto-valve, will require LADWP to most likely dewater the MGORD for two to three years. An extended dewatering of the MGORD will require a massive fish relocation effort, in addition to the loss of the only Rush Creek habitat below GLR that consistently produces larger and older Brown Trout.

Trout Population Metrics

Annual fisheries sampling in Rush and Lee Vining Creeks since 1999 has provided an unusually long-term data set of trout population metrics. The overarching theme of these data is that trout populations respond better to wetter runoff years than to average-to-drier runoff years. The best example of this trend was the recent five-year drought of 2012-2016 in which the recruitment of age-0 Brown Trout decreased by 95% in the Upper Rush section and by 89% in the Bottomlands section. Numbers and condition factors of older trout also decreased during this five-year drought. Then, two good runoff years in 2017 and 2018 with a full GLR, saw trout populations rebound quickly with age-0 recruitment increasing nearly two-fold (200%) in Upper Rush and more than 12-fold (1,200%) in the Bottomlands section. Growth rates and condition factors also improved in the two years post-drought. In fact, growth rates measured in September of 2017 were the highest ever recorded, with elevated streamflows all summer long. High growth rates were also documented in October 2023, after the record snowpack and runoff. Thus, trout numbers, growth rates and conditions factors in Rush and Lee Vining Creeks can oscillate widely depending on RY type. The 2024 Normal RY type coincided with a full GLR and a 78-day-long spill. The relatively cool summer water temperatures in Rush Creek resulted in good recruitment of age-0 Brown Trout, relatively high growth rates, and increased numbers of Brown Trout ≥300 mm in total length.

Although in 2024 we documented modest increases in the numbers of Brown Trout ≥300 mm, our long-term PIT tag data and length-at-age data still shows that Brown Trout in most Rush Creek sections attain lengths ≥300 mm at age-4 or age-5 and that very few trout survive to these ages (with the MGORD section as the exception). In 16 years of implanting PIT tags and recapturing previously tagged fish, we've only documented one age-5 Brown Trout in Upper Rush and have never documented an age-5 Brown Trout in the Bottomlands section. In 2024, the Upper Rush section had an RSD-225 value of 45, meaning of the sub-population of catchable trout (>150 mm), 45% were ≥225 mm (≈9 inches) and the RSD-300 value was 6 or only 6% of the catchable trout were ≥300 mm (≈12 inches). The only two years out of the past 25 years where the RSD-300 was >6 in Upper Rush were 2017 and 2018, the two good runoff years following the five-year drought. In the Bottomlands section of Rush Creek, the RSD-300 in 2024 was also 6, meaning that 6% of the catchable trout were ≥300 mm. This was only the second time in 17 years of available data where the RSD-300 was 6 in the Bottomlands, and in seven of those 17 years, the RSD-300 equaled 0. The MGORD, a trapezoidal diversion canal, is the only section of Rush Creek downstream of GLR that consistently produces Brown Trout of memorable (RSD-300) or trophy (RSD-375) sizes and is the only reach of Rush Creek downstream of GLR that receives much fishing pressure. However, the long-term RSD-300 data for the MGORD documents a decline in the proportion of Brown Trout ≥300 mm. For the years 2001-2012, the RSD-300 ranged from 16 to 54 with an average of 30; whereas between 2013-2024, the RSD-300 ranged from 7 to 27 with an average of 17. However, in 2024 a total of 124 Brown Trout were captured in the MGORD that were ≥300 mm, the highest number of trout caught in this size class since 2012.

In 2023, we electrofished a multi-thread channel section in lower Rush Creek where beavers had modified the creek with a series of dams. We determined that Brown Trout <125 mm from these multi-thread channels were significantly heavier than Brown Trout <125 mm from the Bottomlands and Upper Rush sections (Taylor 2024). The 2024 peak runoff >500 cfs in Rush Creek below the Narrows resulted in numerous channel adjustments, including the loss of the multi-thread channel section we sampled in 2023. In September of 2024, all the flow was concentrated in the 8-Channel (aka the Caddis Channel), and this flow was relatively fast and confined. The single electrofishing pass we made in the 8-Channel in 2024 captured 151 Brown Trout <125 mm and their average weight equaled 6.4 g, down from an average weight of 13.3 g in 2023 (a 54% decrease). In 2024, the average weight of Brown Trout <125 mm in the Bottomlands was 7.0 g and equaled 6.4 g in Upper Rush, these sections also experienced decreases in the average weights of Brown Trout <125 mm, yet these decreases were not as large, 22% and 34%, respectively.

Roto-valve Replacement and Fate of the MGORD

LADWP's infrastructure to divert water from Mono Basin streams into the upper Owens River was constructed in the 1930s and early 1940s, thus many of the dams, valves, diversion canals and associated mechanical structures are 80 to 90+ years old. The Mono Gate One Return Ditch (MGORD) is an approximately 1.4-mile-long trapezoidal diversion canal where water from Grant Lake Reservoir (GLR) is released, that eventually meets up with Rush Creek's natural channel, below GLR's dam and spillway. Flows entering the top of the MGORD are controlled by a roto-

valve encased in a vertical, concrete outlet valve shaft that is 10 feet in diameter and approximately 80 feet tall (or deep). After the record snowpack runoff in 2023, LADWP communicated to the parties involved in the Mono Lake restoration process that the roto-valve was damaged and flow releases into the MGORD could not exceed 175 cfs, instead of its maximum release capacity of 380 cfs. Replacement of the roto-valve is required for the safety of the dam/reservoir system, for LADWP's ability to export water, and for LADWP's ability to meet the Rush Creek flow requirements (SEF's) as defined in their recently amended water licenses.

Prior to replacement of the roto-valve, an inspection is needed of the outlet valve shaft by a diver who must enter the structure when no flow is actively moving through the roto-valve and outlet valve shaft. The duration of this inspection is estimated at four to six hours on one or two days. The purpose of this detailed inspection is to accurately determine the condition of this vertical outlet valve shaft and assess whether this structure also needs to be repaired or replaced. During the actual replacement of the roto-valve (and possibly the outlet valve shaft), flow from GLR to the MGORD through the outlet valve shaft and roto-valve needs to be shut off for at least two to three years.

In recent discussions between LADWP staff and the stream monitoring leads (Bill Trush and Ross Taylor) regarding the fate of the MGORD during roto-valve replacement, Taylor expressed concerns regarding the options discussed and that ultimately the regulatory agencies issuing permits would dictate the procedures to isolate the roto-valve and outlet valve shaft. On 12/3/24, LADWP requested that Taylor draft a document describing the pros and cons of each option and potential effects on the trout populations and aquatic biota within the MGORD.

Prior to evaluating the pros and cons of either pumping into the top of the MGORD or dewatering the MGORD, Taylor developed a summary of the MGORD's Brown Trout population to set the stage of why the MGORD provides unique habitat conditions not found anywhere else in Rush Creek between GLR and Mono Lake. The remainder of this sub-section of the Discussion is the MGORD summary provided to LADWP on December 20, 2024.

The MGORD is a low-gradient trapezoidal canal that's approximately 1.4 miles in length that's dominated by deep, slow-flowing pools and glides with extensive beds of aquatic vegetation. Within the lower 1,200 feet of the MGORD a series of boulder-grade-control weirs step the canal down to its confluence with Rush Creek's natural channel. The slow, deep water and extensive aquatic vegetation beds provide excellent cover and low-velocity habitat for Brown Trout. Aquatic vegetation in the MGORD also supports abundant populations of benthic macroinvertebrates, as well as a robust population of crayfish, all are prey items of Brown Trout.

The fisheries monitoring team first electrofished the MGORD in 2001, followed by annual sampling in 2004 through 2024. Our 20+years of sampling the MGORD has shown that this area is the only location on Rush Creek between GLR and Mono Lake that consistently produces larger and older Brown Trout, of the sizes frequently cited in the pre-1941 references by Eldon Vestal. Our long-term fisheries data has documented that very few Brown Trout live longer

than five years of age in the natural Rush Creek channel downstream of the MGORD, yet from PIT tag recaptures we have documented Brown Trout as old as nine to twelve years of age residing in the MGORD.

During the 2005-2008 radio telemetry movement study (Taylor et al. 2009), 41 large Brown Trout residing in the MGORD were implanted with radio tags (14 fish tagged in 2005 and 27 fish tagged in 2006). A fixed receiving station was installed at the downstream end of the MGORD with two antennas which allowed us to determine direction of movement. We also made near-monthly field trips to radio track fish over a 2.5-year period and download data from the fixed receiver. The radio telemetry movement study illuminated two interesting life history behaviors of radio-tagged Brown Trout in the MGORD:

During two fall/early winter spawning seasons, just over half of the radio-tagged fish left the MGORD and moved downstream for spawning. We relocated some of the tagged fish downstream near the Sheep Herder cabin, some in our Upper Rush study section, and several fish even farther downstream. Radio-tagged females tended to return to the MGORD within days or several weeks post-spawn, whereas some males remained downstream for weeks to months, with some returning to the MGORD the following spring on the start of the snowpack runoff. Because of the high cost of the radio tags (around $350/tag), our sample size was small, yet both years around the same percentage of tagged fish left the MGORD on spawning migrations. During the annual fisheries sampling, we also consistently catch PIT tagged Brown Trout in the MGORD that were tagged as age-0 fish in Upper Rush, another indicator of the influence of larger MGORD Brown Trout on Rush Creek beyond the MGORD.

Second, we documented that many of the radio-tagged Brown Trout had a very small and distinct home range within the MGORD during most of the year (during daytime tracking). Some fish were relocated month after month in literally the exact same location (next to a certain boulder or weed bed or undercut bank). The exception was during the fall/early-winter spawning season; however, we had several of the radio-tagged “home bodies” leave the MGORD, spawn one to several miles downstream, and then return to their exact “home” location within the MGORD. This distinct homing behavior has been documented in other Brown Trout tagging studies – fish tend to stay in a specific “home” location during the day, range widely during the night while foraging, then return “home” prior to sunrise (Meyers et at. 1992; Diana et al. 2004). Again, the exception is more extensive movements during spawning season.

If the MGORD was drained, what would be the fate of larger relocated/displaced Brown Trout? Would they successfully occupy new habitats, or would they attempt to return to the MGORD? Are there locations in Rush Creek below GLR where channel conditions are similar to the MGORD, where larger trout could be relocated to? For example, could the old channel section just below the dam be rewatered? Could this section be mechanically configured to provide habitat conditions consistent with the MGORD? Regarding relocation of Brown Trout and fidelity to home territory, a study showed that radio tagged Brown Trout that were moved 800 to 3,600 meters (up to 2.2 miles) returned to their capture location, with some return

movement commencing within an hour of being released (Armstrong and Herbert 2005). The authors described the displaced Brown Trout homing movements as “directed and rapid”.

If the approved plan for LADWP’s roto-valve replacement includes an extended dewatering of the MGORD, additional fisheries monitoring should include tracking the fate of displaced Brown Trout as well as potential impacts to age-0 recruitment in the Upper Rush section. Post-construction monitoring should evaluate how (or if) the MGORD is re-occupied by a Brown Trout population with a more diverse age class structure. Loss of the MGORD’s older age classes of Brown Trout could have impacts to the long-term viability of Rush Creek’s trout populations below GLR because a diverse age structure, with a mix of young and older individuals, is crucial for a healthy, stable, and resilient ecosystem, as it allows for better adaptation to environmental changes and ensures long-term population viability. A more diverse age class structure often translates to increased genetic diversity, which is also vital to a population’s ability to adapt to changing environmental conditions and resilience to disease.

Methods Evaluation

As in previous years, small variations in wetted channel widths were measured, which resulted in changes to sample section areas. As previously recommended, channel lengths and widths should be remeasured annually.

Starting in 2022, MLC personnel conducted water temperature monitoring, which is extremely helpful having someone local to deploy and retrieve the data loggers. High runoff frequently complicates water temperature monitoring, by either washing away data loggers or having data loggers exposed when flows drop. Deploying duplicate data loggers at the seven Rush Creek water temperature monitoring locations regularly used in the annual fisheries report may reduce the frequency of lost loggers and/or gaps in the data sets. Also, conducting periodic checks of the deployed data loggers as flows drop after peak runoff would likely reduce the occurrence of data gaps caused by loggers being exposed to air temperatures.

The PIT tagging program was continued during the September 2024 sampling; tags were implanted primarily in age-0 fish in all sections and in presumed age-1 fish in the MGORD. The PIT tagging program allowed us to document annual growth rates of trout and assess the ability of fish to reach or exceed lengths of 300 mm. We recommend continuation of the PIT tagging program during the post-settlement Fisheries Monitoring Program.

Trout size classes (<125, 125-199, and ≥200 mm) developed and discussed during the 2008 annual report should continue to be used for calculations of population estimates (Hunter et al. 2008). Using these size classes provides for long-term consistency as well as year-to-year consistency with the annual fisheries data sets. However, we acknowledge that in Walker Creek, some age-1 Brown Trout are occasionally less than 125 mm in total length and in the MGORD some age-0 fish are bigger than 125 mm in total length and some age-1 fish are bigger than 199 mm in total length.

To ensure that electrofishing sampling can be conducted safely and efficiently, flow in Rush Creek should not exceed **35 cfs** and flow in Lee Vining Creek should not exceed **30 cfs** during the annual sampling period. Allowances for flow variances to allow for safe wading conditions and effective sampling were included in the new SWRCB WR-2021-0086.

Also, to ensure the safety of the fisheries crew, there needs to be clear communication between the fisheries stream scientist, the MAT, and LADWP as to when the fisheries sampling is occurring, so that LADWP does not inadvertently schedule the annual cycling of the roto-valve during the fisheries monitoring. The roto-valve cycling on 9/24/24 occurred when the fisheries crew was sampling the MGORD, and they experienced a sudden and significant increase in flow with no forewarning. Fortunately, the electrofishing effort was quickly halted, and everyone safely exited the water.

The 2025 RY will likely be classified as Normal, with a relatively high storage level in GLR. This may result in another summer of mostly favorable summer water temperatures in Rush Creek.

Proposed Fisheries Sampling for 2025 Season

During the development of the post-settlement monitoring scope and budget, RTA proposed that the annual fisheries sampling be reduced to conduct population estimate sampling every other year. In the other years, single-pass electrofishing sampling would occur to collect data to evaluate population age-class structure, compute condition factors, generate growth data from recaptures of previously tagged fish, and implant PIT tags in new cohorts of fish. We intend to conduct single-pass sampling in the fall of 2025. In addition to conducting single-pass sampling at the annually sampled locations, RTA proposes sampling the 8-Channel section of Rush Creek to continue sampling the area adjacent to the area once occupied by beavers; if other channels in this area carry flow in 2025, these would also be sampled.

The Fisheries Stream Scientist continues to recommend that a bathymetric survey of GLR is conducted to assess the amount of sediment infill and to determine the actual storage capacity of GLR. Reduced storage may negate assumptions made in the Synthesis Report about minimum storage levels for suitable summer water temperatures in Rush Creek, as well as affect water availability for future LADWP exports. Bathymetric surveys are commonly used to assess rates of sedimentation in reservoirs and the loss of storage capacity can depend on a number of factors (Iradukunda and Bwanbale 2021). Globally the overall loss of reservoir storage capacity is estimated at 1 to 2% of total storage capacity per year (Iradukunda and Bwanbale 2021). When properly conducted, a bathymetric survey will evaluate reductions in reservoir capacity, in both live storage and dead storage locations and provide an estimate of a reservoir's useful lifespan (Endalew and Mulu 2022). In 1991, the GLR thermal characteristics study by Cullen and Railsback (1993) determined that their reservoir thermal model underpredicted water surface elevations, which corresponded to a storage volume error of approximately 1,000 acre-feet and that sedimentation may likely have caused this discrepancy in their depth-to-volume regression.

Recommended changes to SEF's based on 2024 Fisheries Monitoring

The Fisheries Stream Scientist has no recommended changes to the SEFs based on results of the 2024 fisheries monitoring, other than LADWP should adhere to the SEFs as much as possible with the limited release capacity due to the damaged roto-valve. These include hydrograph components such as the spring ascensions, spring benches, snowmelt ascensions, and snowmelt benches. These pre-peak flows are important components of the hydrograph in meeting spring/early-summer ecological processes described in the Synthesis Report (McBain & Trush and RTA 2010). In runoff years where LADWP is unable to deliver the SEF peaks, extending the receding limb of the hydrograph farther into the summer will deliver the required quantity of water to Mono Lake, as well as likely provide more favorable water temperatures for trout.

Another potential consequence of LADWP's limited capacity to release flows from GLR are unplanned reservoir spills, including spills during times of the year that Rush Creek would not normally experience elevated flows. Spills during fall and winter months could potentially affect Brown Trout spawning, egg incubation and post-spawning survival of adult fish. Flows up to 200-225 cfs would likely not cause bedload movement, a situation to avoid since bedload movement could cause mortality of incubating eggs. Unplanned higher winter flows would also decrease the amount of low-velocity habitat in pools, which is an important habitat type for post-spawn adult Brown Trout recovery and survival. While short-term deviations from SEFs probably have limited impacts to Rush Creek's ecological processes, repeated and/or sustained deviations from the SEFs may negatively impact trout population metrics, riparian recruitment, and/or channel-forming geomorphic processes.

The primary stressor to Rush Creek's trout population still appears to be unfavorable summer water temperatures in drier years and/or when GLR has lower storage going into the summer. At this point, there is no mechanical or operational "fix" to reduce or relieve stressfully warm water temperatures in Rush Creek via manipulation of water releases from GLR, other than heading into each summer season with as full of a reservoir as feasibly possible. Thus, when feasible, LADWP should strive to keep GLR as full as possible heading into each spring and early-summer.

The Fisheries Stream Scientist will work with the Geomorphic/Riparian Stream Scientist in reviewing LADWP's draft AOP for 2025 and provide comments, as needed.

References Cited

Armstrong, J.D. and N.A. Herbert. 2005. Homing movements of displaced stream-dwelling Brown Trout. Journal of Fish Biology 50(2): 445-449.

Barnham, C. and A. Baxter. 1998. Condition factor, K, in salmonid fish. Fisheries Notes #FN0005 State of Victoria, Australia. 3 p.

Bateman, D.S., R.E. Gresswell and A.M. Berger. 2009. Passive integrated tag retention rates in headwater populations of Coastal Cutthroat Trout. North American Journal of Fisheries Management 29: 653-657.

Bell, J.M. 2006. The assessment of thermal impacts on habitat selection, growth, reproduction, and mortality in Brown Trout (*Salmo trutta*): a review of the literature. Vermillion River EPA Grant #WS 97512701-1. 23p.

Blackwell, B.G., M.L. Brown and D.W. Willis. 2000. Relative weight (W_r) status and current use in fisheries assessment and management. Reviews in Fisheries Science, 8(1): 1-44.

Cone, R.S. 1989. The need to reconsider the use of condition indices in fishery science. Transactions of the American Fisheries Society 118: 510-514.

Cullen, R.T. and S.F. Railsback. 1993. Summer thermal characteristics of Grant Lake, Mono County, California. Feasibility Study #2, Trihey and Associates, Concord, CA. 118 p.

Dare, M.R. 2003. Mortality and long-term retention of passive integrated tags by spring Chinook salmon. North American Journal of Fisheries Management 23: 1015-1019.

Diana, J.S., J.P. Hudson, and R.C. Clark. 2004. Movement patterns of large Brown Trout in the mainstream Au Sable River, Michigan. Transactions of the American Fisheries Society 133: 34-44.

Endalew, L. and A. Mulu. 2022. Estimation of reservoir sedimentation using bathymetric survey at Shumburit earth dam, East Gojjam zone Amhara, Ethiopia. Heliyon (8): 15 p.

Gabelhouse, D. W., Jr. 1984. A length-categorization system to assess fish stocks. North American Journal of Fisheries Management 4:273-285.

Hunter, C., R. Taylor, K. Knudson and B. Shepard. 2007. Fisheries Monitoring Report for Rush, Lee Vining, Parker and Walker Creeks 2006. Los Angeles Department of Water and Power. 74 p.

Hunter, C., R. Taylor, K. Knudson and B. Shepard. 2008. Fisheries Monitoring Report for Rush, Lee Vining, Parker and Walker Creeks 2007. Los Angeles Department of Water and Power. 49 p.

Iradukunda, P. and E. Bwambale. 2021. Reservoir sedimentation and its effect on storage capacity – a case study of Murera Reservoir, Kenya. Cogent Engineering 8: 14 p.

McBain & Trush and RTA. 2010. Synthesis of instream flow recommendations to the State Water Resources Control Board and the Los Angeles Department of Water and Power. 159 p.

Meyers, L.S., T.F. Thuemler, and G.W. Kornely. 1992. Seasonal movements of Brown Trout in northeast Wisconsin. North American Journal of Fisheries Management 12:433-441.

Reimers, N. 1963. Body condition, water temperature, and overwinter survival of hatchery-reared trout in Convict Creek, California. Transactions of the American Fisheries Society 92: 39-46.

Ricker, W.E. 1975. Computation and interpretation of biological statistics of fish populations. Journal of the Fisheries Research board of Canada, 191: 1-382.

Taylor, R., K. Knudson, B. Shepard and C. Hunter. 2009. Radio telemetry-movement study of Brown Trout in Rush Creek. Los Angeles Department of Water and Power. 55 p.

Taylor, R. and K. Knudson. 2012. Fisheries Monitoring Report for Rush, Lee Vining, Parker and Walker Creeks 2011. Los Angeles Department of Water and Power. 90 p.

Taylor, R. 2013. Fisheries Monitoring Report for Rush, Lee Vining, Parker and Walker Creeks 2012. Los Angeles Department of Water and Power. 100 p.

Taylor, R. 2014. Fisheries Monitoring Report for Rush, Lee Vining, Parker and Walker Creeks 2013. Los Angeles Department of Water and Power. 89 p.

Taylor, R. 2021. Fisheries Monitoring Report for Rush, Lee Vining, Parker and Walker Creeks 2020. Los Angeles Department of Water and Power. 97 p.

Taylor, R. 2022. Fisheries Monitoring Report for Rush, Lee Vining, Parker and Walker Creeks 2021. Los Angeles Department of Water and Power. 97 p.

Taylor, R. 2024. Fisheries Monitoring Report for Rush, Lee Vining, Parker and Walker Creeks 2023. Los Angeles Department of Water and Power. 85 p.

Werley, K.E., L. Wang and M. Mitro. 2007. Field-based estimates of thermal tolerance limits for trout: incorporating exposure time and temperature fluctuation. Transactions of the American Fisheries Society 136: 365-374.

Appendices for the 2024 Mono Basin Annual Fisheries Report

Appendix A: Aerial Photographs of Annual Sample Sites on Rush, Walker and Lee Vining Creeks

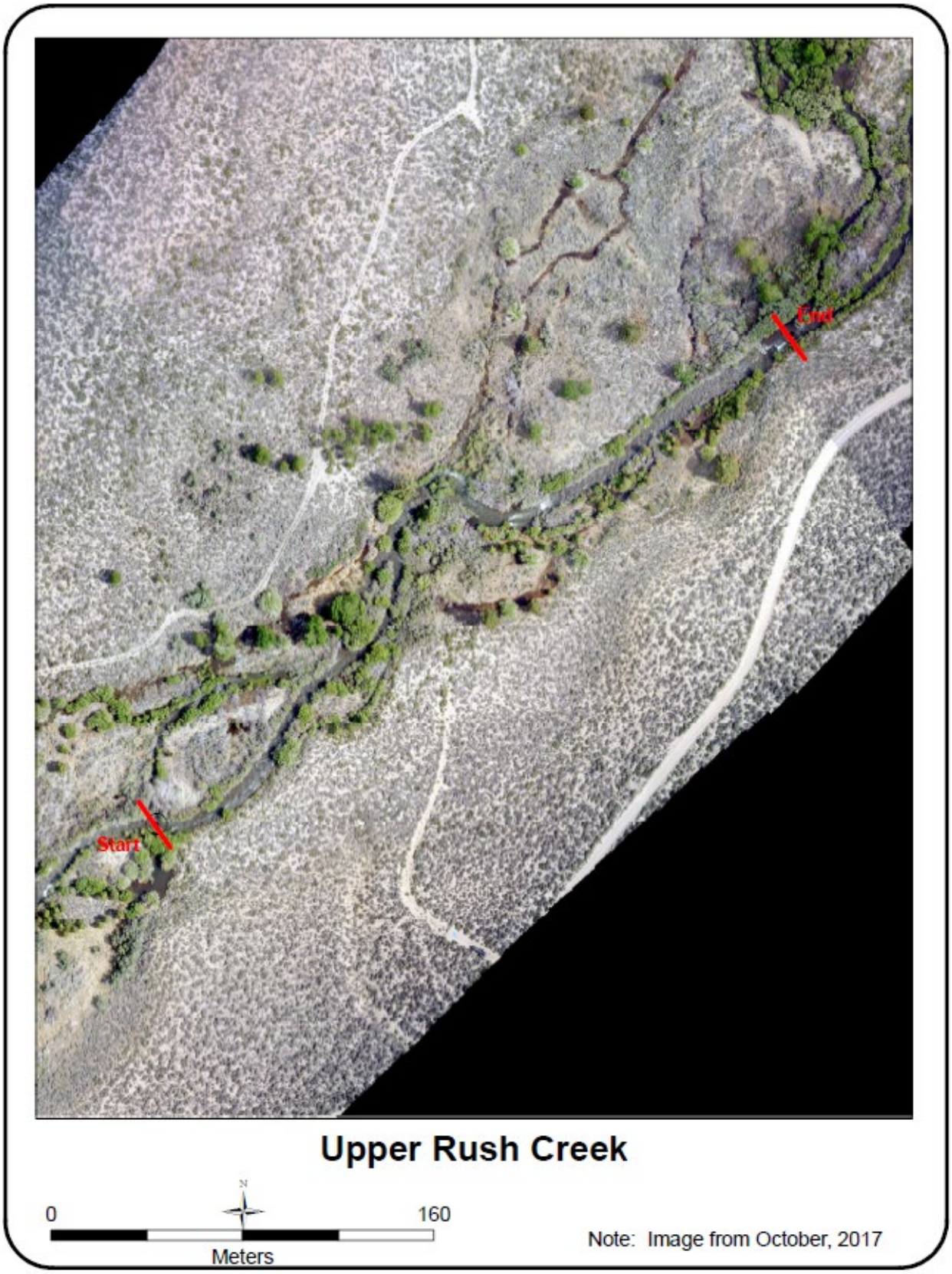
End
Start
Upper Rush Creek
N
0
160
Meters
Note: Image from October, 2017

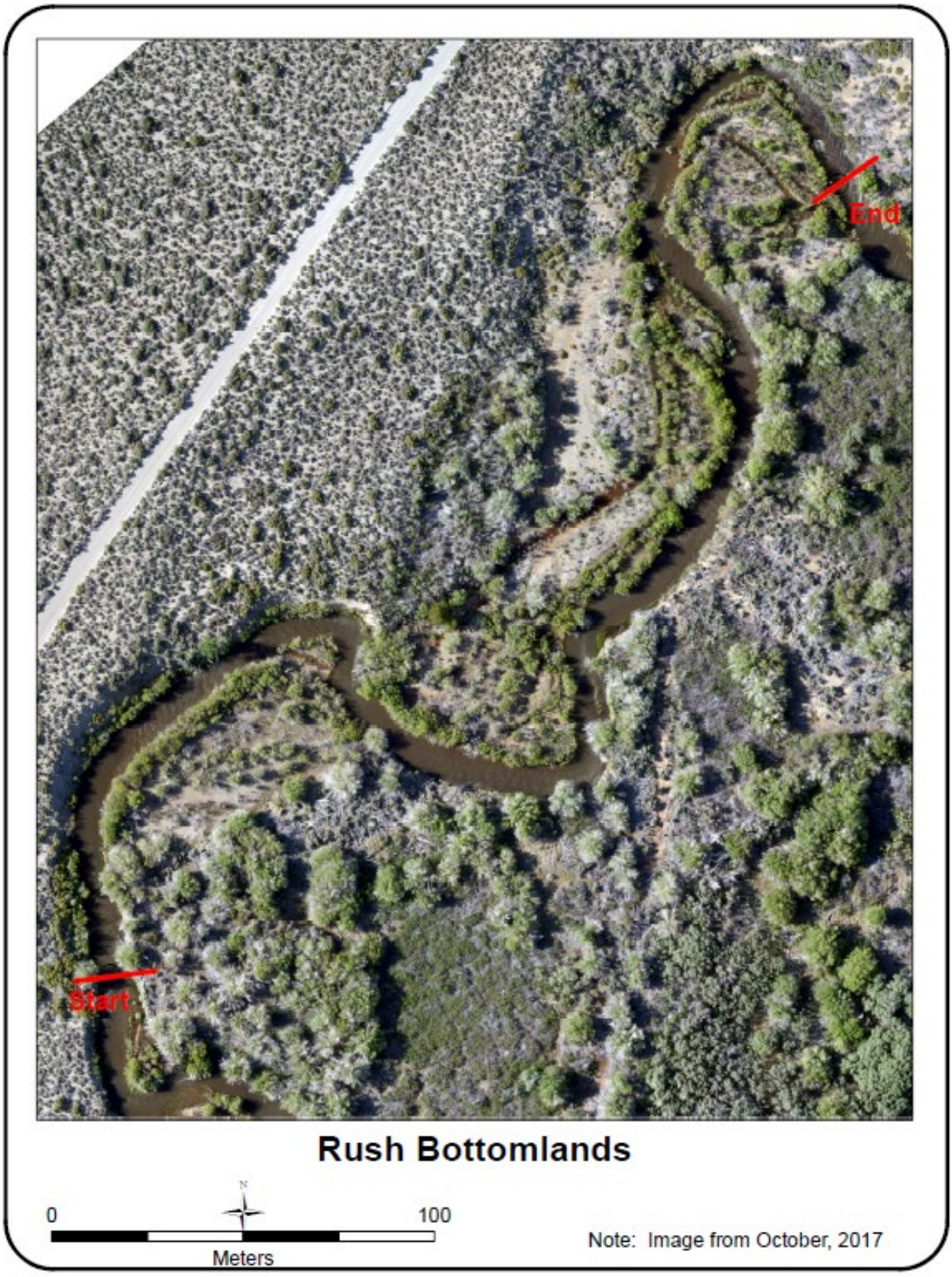
End
Start
Rush Bottomlands
N
0
100
Meters
Note: Image from October, 2017

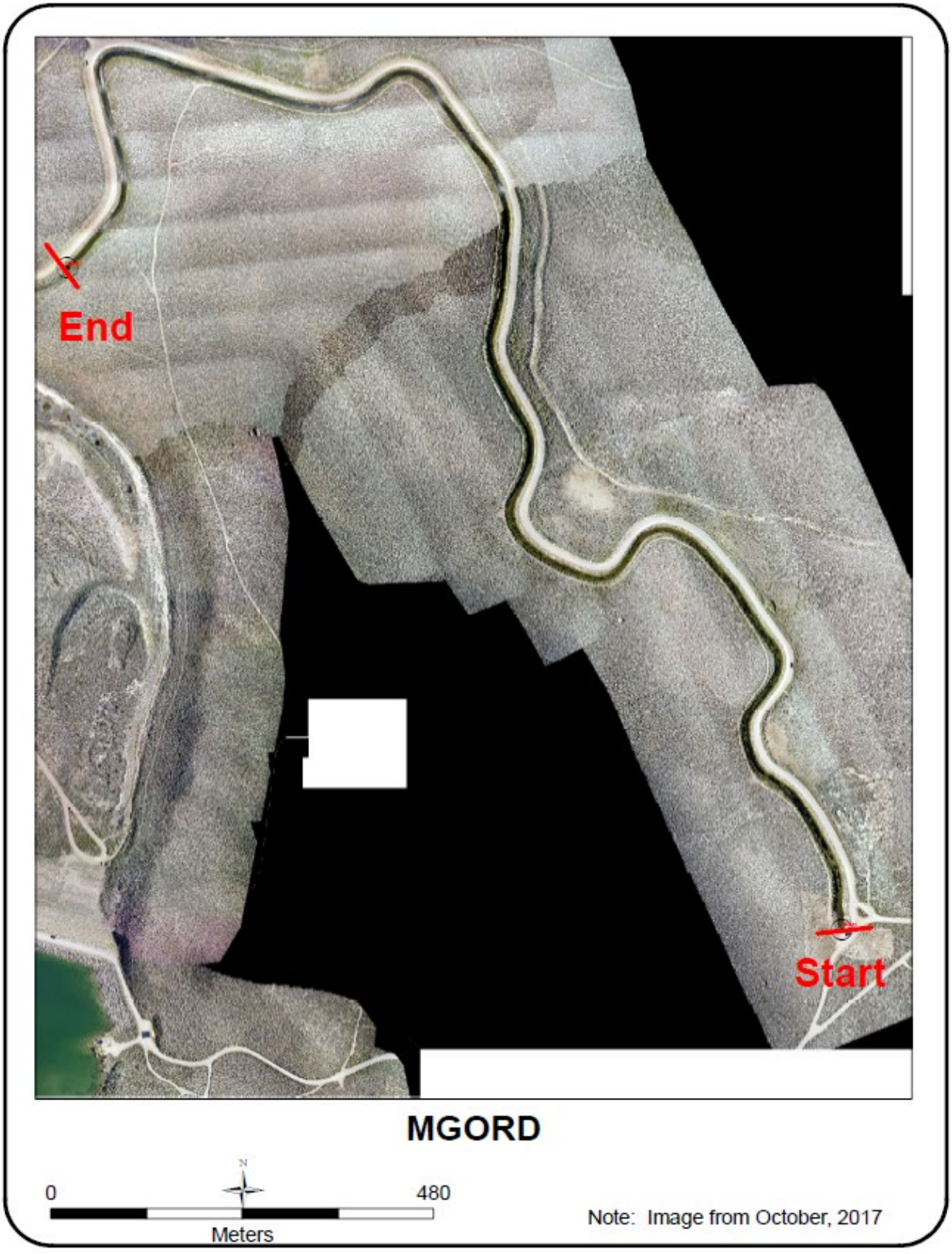
End
Start
MGORD
N
0
480
Meters
Note: Image from October, 2017


End
Start
Walker Creek
N
0
100
Meters
Note: Image from October, 2017

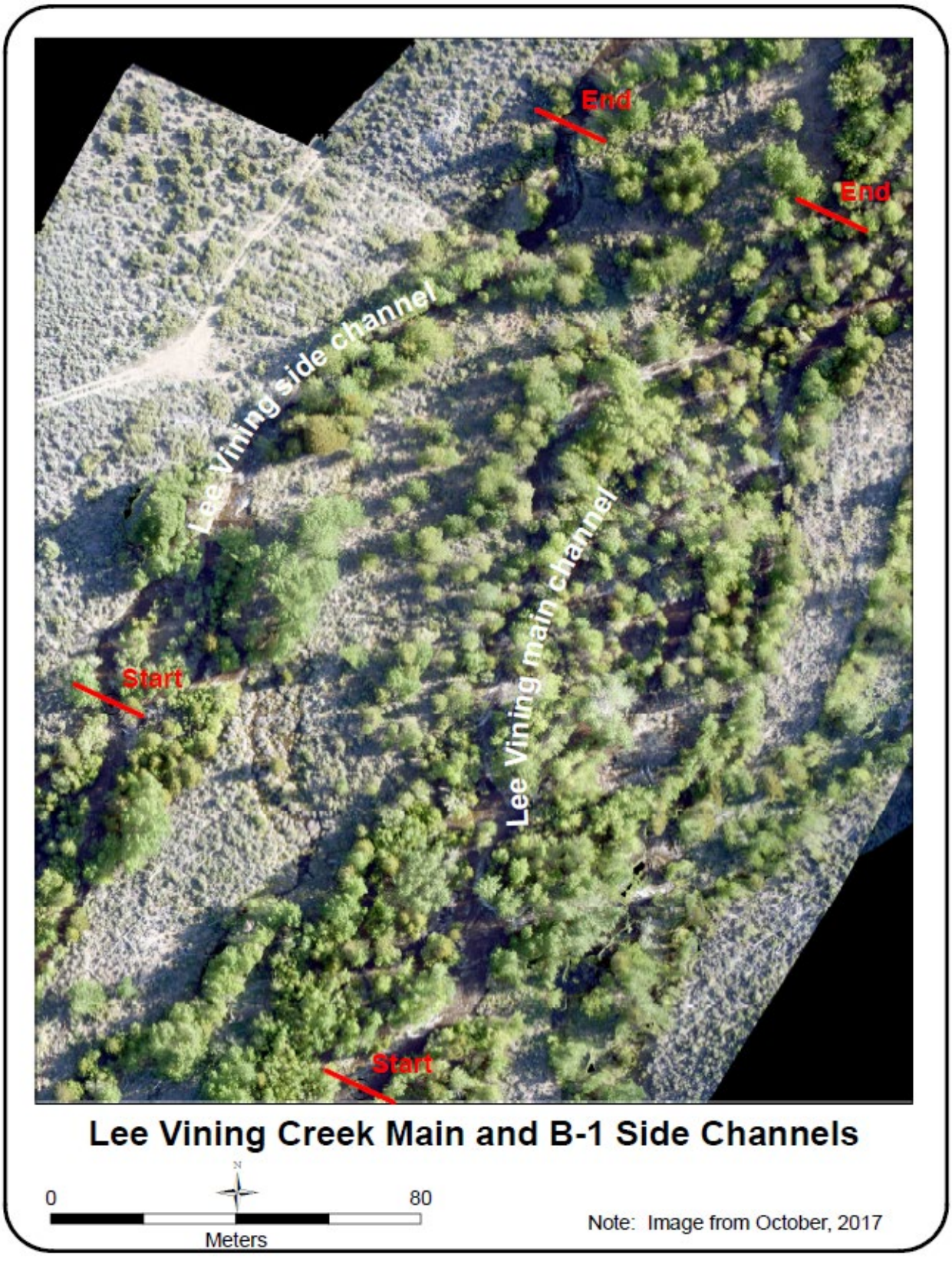
End
End
Lee Vining side channel
Lee Vining main channel
Start
Start
Lee Vining Creek Main and B-1 Side Channels
0
80
Meters
Note: Image from October, 2017

Appendix B: Tables of Numbers of Brown Trout and Rainbow Trout Implanted with PIT Tags (by sampling section) between 2009 and 2023 (Note: no tags implanted in 2013)

Table B-1. Total numbers of trout implanted with PIT tags during the 2009 sampling season, by stream, sample section, age-class and species.

Stream	Sample Section	Number of Age-0 Brown Trout	Number of Age-1 Brown Trout	Number of Age-0 Rainbow Trout	Number of Age-1 Rainbow Trout	Reach Totals
Rush Creek	Upper Rush	256	26	15	1	**298 Trout**
	Bottomlands	164	68	0	0	**232 Trout**
	County Road	108	29	0	0	**137 Trout**
	MGORD	54	642*	0	0	**696 Trout**
Lee Vining Creek	Main Channel	10	45	4	3	**62 Trout**
	Side Channel	5	0	0	1	**6 Trout**
Walker Creek	Above old 395	114	51	0	0	**165 Trout**
Totals:		**711**	**861**	**19**	**5**	**Total Trout: 1,596**

*Many of these MGORD trout were >age-1.

Table B-2. Total numbers of trout implanted with PIT tags during the 2010 sampling season, by stream, sample section, age-class and species.

Stream	Sample Section	Number of Age-0 Brown Trout (<125 mm)	Number of Age-1 and older Brown Trout	Number of Age-0 Rainbow Trout (<125 mm)	Number of Age-1 and older Rainbow Trout	Reach Totals
Rush Creek	Upper Rush	242	11	4	0	**257 Trout**
	Bottomlands	284	3	0	0	**287 Trout**
	County Road	210	7	0	0	**217 Trout**
	MGORD	1	359*	0	12	**372 Trout**
Lee Vining Creek	Main Channel	24	8	0	1	**33 Trout**
	Side Channel	13	0	0	0	**13 Trout**
Walker Creek	Above old 395	81	14	0	0	**95 Trout**
Totals:		**855**	**402**	**4**	**13**	**Total Trout: 1,274**

*Many of these MGORD trout were >age-1.

Table B-3. Total numbers of trout implanted with PIT tags during the 2011 sampling season, by stream, sample section, age-class and species.

Stream	Sample Section	Number of Age-0 Brown Trout (<125 mm)	Number of Age-1 and older Brown Trout	Number of Age-0 Rainbow Trout (<125 mm)	Number of Age-1 and older Rainbow Trout	Reach Totals
Rush Creek	Upper Rush	393	3	30	0	**426 Trout**
	Bottomlands	178	1	11	0	**190 Trout**
	County Road	196	1	6	0	**203 Trout**
	MGORD	8	142*	3	3	**156 Trout**
Lee Vining Creek	Main Channel	24	0	0	0	**24 Trout**
	Side Channel	11	14	0	0	**25 Trout**
Walker Creek	Above old 395	41	0	0	0	**41 Trout**
Totals:		**851**	**161**	**50**	**3**	**Total Trout: 1,065**

*Many of these MGORD trout were >age-1.

Table B-4. Total numbers of trout implanted with PIT tags during the 2012 sampling season, by stream, sample section, age-class and species.

Stream	Sample Section	Number of Age-0 Brown Trout (<125 mm)	Number of Age-1 and older Brown Trout	Number of Age-0 Rainbow Trout (<125 mm)	Number of Age-1 and older Rainbow Trout	Reach Totals
Rush Creek	Upper Rush	117	1	2	0	**120 Trout**
	Bottomlands	110	1	6	0	**117 Trout**
	County Road	0	2	0	0	**2 Trout**
	MGORD	0	0	0	0	**0 Trout**
Lee Vining Creek	Main Channel	125	0	72	0	**197 Trout**
	Side Channel	0	0	0	0	**0 Trout**
Walker Creek	Above old 395	60	0	0	0	**60 Trout**
Age Class Sub-totals:		**412**	**4**	**80**	**0**	**Total Trout: 496**

Table B-5. Total numbers of trout implanted with PIT tags during the 2014 sampling season, by stream, sample section, age-class and species.

Stream	Sample Section	Number of Age-0 Brown Trout (<125 mm)	Number of Age-1 Brown Trout (125-170 mm)	Number of Age-0 Rainbow Trout (<125 mm)	Number of Age-1 Rainbow Trout (125-170 mm)	Section Totals
Rush Creek	Upper Rush	243	86	1	0	**330 Trout**
	Bottomlands	34	43	0	0	**77 Trout**
	MGORD	13	125-199 mm = 60 Brown Trout ≥200 mm = 185 Brown Trout			**258 Trout**
Lee Vining Creek	Main Channel	127	103	5	22	**257 Trout**
	Side Channel	0	0	0	0	**0 Trout**
Walker Creek	Above old 395	42	0	0	0	**42 Trout**
Age Class Sub-totals:		**459**	**232***	**6**	**22**	**Total Trout: 964**

*this sub-total excludes age-1 and older MGORD fish

Table B-6. Total numbers of trout implanted with PIT tags during the 2015 sampling season, by stream, sample section, age-class and species.

Stream	Sample Section	Number of Age-0 Brown Trout (<125 mm)	Number of Age-1 and older Brown Trout	Number of Age-0 Rainbow Trout (<125 mm)	Number of Age-1 and older Rainbow Trout	Section Totals
Rush Creek	Upper Rush	234	2*	7	0	**243 Trout**
	Bottomlands	167	3*	0	0	**170 Trout**
	MGORD	29	125-199 mm = 37 Brown Trout ≥200 mm = 83 Brown Trout (2 shed/new)			**149 Trout**
Lee Vining Creek	Main Channel	195	1*	0	0	**196 Trout**
	Side Channel	0	0	0	0	**0 Trout**
Walker Creek	Above old 395	113	0	0	0	**113 Trout**
Age Class Sub-totals:		**738**	**6****	**7**	**0**	**Total Trout: 871**

*shed tag/new tag implanted **this sub-total excludes age-1 and older MGORD fish

Table B-7. Total numbers of trout implanted with PIT tags during the 2016 sampling season, by stream, sample section, age-class and species.

Stream	Sample Section	Number of Age-0 Brown Trout (<125 mm)	Number of Age-1 and older Brown Trout	Number of Age-0 Rainbow Trout (<125 mm)	Number of Age-1 and older Rainbow Trout	Section Totals
Rush Creek	Upper Rush	36	0	1	0	**37 Trout**
	Bottomlands	79	1*	0	0	**80 Trout**
	MGORD	4 BNT 1 RBT	125-199 mm = 9 BNT ≥200 mm = 154** BNT and 7 RBT			**175 Trout**
Lee Vining Creek	Main Channel	46	1*	0	0	**47 Trout**
	Side Channel	1	0	0	0	**1 Trout**
Walker Creek	Above old 395	228	1*	0	0	**229 Trout**
Age Class Sub-totals:		**394**	**166**	**2**	**7**	**Total Trout: 569**

*shed tag/new tag implanted **two of these BNT = shed tag/new tag implanted

Table B-8. Total numbers of trout implanted with PIT tags during the 2017 sampling season, by stream, sample section, age-class and species.

Stream	Sample Section	Number of Age-0 Brown Trout (<125 mm)	Number of Age-1 and older Brown Trout	Number of Age-0 Rainbow Trout (<125 mm)	Number of Age-1 and older Rainbow Trout	Section Totals
Rush Creek	Upper Rush	192	2*	14	0	**208 Trout**
	Bottomlands	34	0	0	0	**34 Trout**
	MGORD	38	0	2	0	**40 Trout**
Lee Vining Creek	Main Channel	31	0	0	0	**31 Trout**
	Side Channel	5	0	0	0	**5 Trout**
Walker Creek	Above old 395	0	0	0	0	**0 Trout**
Age Class Sub-totals:		**300**	**2**	**16**	**0**	**Total Trout: 318**

*shed tag/new tag implanted

Table B-9. Total numbers of trout implanted with PIT tags during the 2018 sampling season, by stream, sample section, age-class and species.

Stream	Sample Section	Number of Age-0 Brown Trout (<125 mm)	Number of Age-1 and older Brown Trout	Number of Age-0 Rainbow Trout (<125 mm)	Number of Age-1 and older Rainbow Trout	Section Totals
Rush Creek	Upper Rush	314	3*	72	1*	**390 Trout**
	Bottomlands	288	0	0	0	**288 Trout**
	MGORD	25	148**	1	7	**181 Trout**
Lee Vining Creek	Main Channel	87	0	8	0	**95 Trout**
	Side Channel	0	0	0	0	**0 Trout**
Walker Creek	Above old 395	43	2*	0	0	**45 Trout**
Age Class Sub-totals:		**757**	**153**	**81**	**8**	**Total Trout: 999**

*shed tag/new tag implanted **≤250 mm in total length

Table B-10. Total numbers of trout implanted with PIT tags during the 2019 sampling season, by stream, sample section, age-class and species.

Stream	Sample Section	Number of Age-0 Brown Trout (<125 mm)	Number of Age-1 and older Brown Trout	Number of Age-0 Rainbow Trout (<125 mm)	Number of Age-1 and older Rainbow Trout	Section Totals
Rush Creek	Upper Rush	257	3*	28	0	**288 Trout**
	Bottomlands	152	3*	0	0	**155 Trout**
	MGORD	64	167** 8*	1	5	**245 Trout**
Lee Vining Creek	Main Channel	174	0	0	0	**174 Trout**
	Side Channel	0	0	0	0	**0 Trout**
Walker Creek	Above old 395	137	1*	0	0	**138 Trout**
Age Class Sub-totals:		**784**	**182**	**29**	**5**	**Total Trout: 1,000**

*shed tag/new tag implanted **≤250 mm in total length

Table B-11. Total numbers of trout implanted with PIT tags during the 2020 sampling season, by stream, sample section, age-class and species.

Stream	Sample Section	Number of Age-0 Brown Trout (<125 mm)	Number of Age-1 and older Brown Trout	Number of Age-0 Rainbow Trout (<125 mm)	Number of Age-1 and older Rainbow Trout	Section Totals
Rush Creek	Upper Rush	242	1*	27	0	**270 Trout**
	Bottomlands	65	0	0	0	**65 Trout**
	MGORD	80	132** 1*	2	7	**222 Trout**
Lee Vining Creek	Main Channel	102	1*	0	0	**103 Trout**
	Side Channel	0	0	0	0	**0 Trout**
Walker Creek	Above old 395	92	4*	0	0	**96 Trout**
Age Class Sub-totals:		**581**	**139**	**29**	**7**	**Total Trout: 756**

*shed tag/new tag implanted **≤250 mm in total length

Table B-12. Total numbers of trout implanted with PIT tags during the 2021 sampling season, by stream, sample section, age-class and species.

Stream	Sample Section	Number of Age-0 Brown Trout (<125 mm)	Number of Age-1 and older Brown Trout	Number of Age-0 Rainbow Trout (<125 mm)	Number of Age-1 and older Rainbow Trout	Section Totals
Rush Creek	Upper Rush	148	1*	36	0	**185 Trout**
	Bottomlands	106	0	0	0	**106 Trout**
	MGORD	115	259** 1*	0	9	**384 Trout**
Lee Vining Creek	Main Channel	53	0	0	0	**53 Trout**
	Side Channel	17	0	0	0	**17 Trout**
Walker Creek	Above old 395	122	1*	0	0	**123 Trout**
Age Class Sub-totals:		**561**	**262**	**36**	**9**	**Total Trout: 868**

*shed tag/new tag implanted **≤250 mm in total length

Table B-13. Total numbers of trout implanted with PIT tags during the 2022 sampling season, by stream, sample section, age-class and species.

Stream	Sample Section	Number of Age-0 Brown Trout (<125 mm)	Number of Age-1 and older Brown Trout	Number of Age-0 Rainbow Trout (<125 mm)	Number of Age-1 and older Rainbow Trout	Section Totals
Rush Creek	Upper Rush	225	4*	35	0	**264 Trout**
	Bottomlands	225	0	0	0	**225 Trout**
	MGORD	26	49**	1	1	**77 Trout**
Lee Vining Creek	Main Channel	30	1*	1	0	**32 Trout**
	Side Channel	0	0	0	0	**0 Trout**
Walker Creek	Above old 395	104	0	0	0	**104 Trout**
Age Class Sub-totals:		**610**	**54**	**37**	**1**	**Total Trout: 702**

*shed tag/new tag implanted **up to 225 mm in total length

Table B-14. Total numbers of trout implanted with PIT tags during the 2023 sampling season, by stream, sample section, age-class and species.

Stream	Sample Section	Number of Age-0 Brown Trout (<125 mm)	Number of Age-1 and older Brown Trout	Number of Age-0 Rainbow Trout (<125 mm)	Number of Age-1 and older Rainbow Trout	Section Totals
Rush Creek	Upper Rush	53	2*	2	0	**57 Trout**
	Bottomlands	14	0	0	0	**14 Trout**
	MGORD	20	6**	8	0	**34 Trout**
Rush Creek – new sites	Caddis Channel	17	89***	0	11***	**117 Trout**
	Jeffrey Connector	29	14***	0	1***	**44 Trout**
	Old Main Ch.	7	28***	0	0	**35 Trout**
Lee Vining Creek	Main Channel	0	0	0	0	**0 Trout**
	Side Channel	0	0	0	0	**0 Trout**
Walker Creek	Above old 395	1	0	0	0	**1 Trout**
Species/Age Class Sub-totals:		**141**	**139**	**10**	**12**	**Total Trout: 302**

*shed tag/new tag implanted **up to 225 mm in total length ***all fish tagged in new sample sections

Appendix C: Table of PIT-tagged Fish Recaptured during September 2024 Sampling

Date of Recapture	Species	Length (mm)	Weight (g)	PIT Tag Number	Location of 2024 Recapture	Location of Initial Capture and Tagging	Comments
9/15/2024	BNT	304	259	989001039661460	Upper Rush	Upper Rush	
9/15/2024	BNT	282	231	989001039661816	Upper Rush	Upper Rush	
9/15/2024	**RBT**	308	256	989001039661828	Upper Rush	Upper Rush	
9/15/2024	BNT	257	172	989001042091116	Upper Rush	Upper Rush	
9/15/2024	BNT	329	309	989001042091176	Upper Rush	Upper Rush	
9/15/2024	BNT	280	201	989001042091194	Upper Rush	Upper Rush	
9/15/2024	BNT	267	180	989001042091200	Upper Rush	Upper Rush	
9/15/2024	BNT	189	65	989001045526432	Upper Rush	Upper Rush	
9/15/2024	BNT	187	58	989001045526449	Upper Rush	Upper Rush	
9/22/2024	BNT	262	190	989001042091154	Upper Rush	Upper Rush	
9/22/2024	BNT	287	198	989001042091240	Upper Rush	Upper Rush	
9/22/2024	BNT	194	63	989001045526450	Upper Rush	Upper Rush	
9/22/2024	BNT	180	51	989001045526500	Upper Rush	Upper Rush	
9/22/2024	BNT	203	64	989001045526507	Upper Rush	Upper Rush	
9/16/2024	BNT	247	122	989001039661954	Bottomlands	Bottomlands	
9/16/2024	BNT	235	107	989001042091378	Bottomlands	Bottomlands	
9/16/2024	BNT	259	161	989001042091452	Bottomlands	Bottomlands	
9/16/2024	BNT	168	39	989001045526455	Bottomlands	Bottomlands	
9/23/2024	BNT	235	133	989001042091409	Bottomlands	Bottomlands	
9/23/2024	BNT	185	57	989001045526425	Bottomlands	Bottomlands	
9/18/2024	BNT	354	426	989001039661599	MGORD	MGORD	
9/18/2024	BNT	323	392	989001042091196	MGORD	**Upper Rush**	
9/18/2024	BNT	346	400	989001042091257	MGORD	**Upper Rush**	
9/18/2024	BNT	290	271	989001042091269	MGORD	**Upper Rush**	
9/18/2024	BNT	219	95	989001045526471	MGORD	MGORD	
9/24/2024	BNT	313	293	989001039661698	MGORD	**Upper Rush**	
9/24/2024	BNT	290	262	989001042091188	MGORD	**Upper Rush**	
9/24/2024	BNT	289	264	989001042091220	MGORD	**Upper Rush**	
9/24/2024	BNT	210	94	989001045526415	MGORD	MGORD	

Date of Recapture	Species	Length (mm)	Weight (g)	PIT Tag Number	Location of 2024 Recapture	Location of Initial Capture and Tagging	Comments
9/17/2024	BNT	257	169	989001031372382	Walker Ck	Walker Creek	
9/17/2024	BNT	250	151	989001038117355	Walker Ck	Walker Creek	
9/17/2024	BNT	227	116	989001039661169	Walker Ck	Walker Creek	
9/17/2024	BNT	226	111	989001039661174	Walker Ck	Walker Creek	
9/17/2024	BNT	205	72	989001039661189	Walker Ck	Walker Creek	
9/17/2024	BNT	236	117	989001039661217	Walker Ck	Walker Creek	
9/17/2024	BNT	220	116	989001039661219	Walker Ck	Walker Creek	
9/17/2024	BNT	220	107	989001039661322	Walker Ck	Walker Creek	
9/17/2024	BNT	210	82	989001039661760	Walker Ck	Walker Creek	
9/17/2024	BNT	215	100	989001042091434	Walker Ck	Walker Creek	
9/17/2024	BNT	219	95	989001042091436	Walker Ck	Walker Creek	
9/17/2024	BNT	225	114	989001042091484	Walker Ck	Walker Creek	
9/19/2024	BNT	233	133	989001039661683	LV Main	Lee Vining Ck	
9/19/2024	BNT	232	105	989001039661690	LV Main	Lee Vining Ck	
9/19/2024	BNT	232	120	989001042091084	LV Main	Lee Vining Ck	
9/25/2024	BNT	218	93	989001042091057	LV Main	Lee Vining Ck	
9/20/2024	BNT	279	183	989001045526527	8-Channel	8-Channel	
9/20/2024	BNT	276	213	989001039661040	8-Channel	8-Channel	
9/20/2024	BNT	251	157	989001045526516	8-Channel	8-Channel	
9/20/2024	BNT	232	127	989001045526531	Jeffrey Connector	8-Channel	
9/20/2024	BNT	261	161	989001045526536	8-Channel	8-Channel	
9/20/2024	BNT	255	158	989001045526550	8-Channel	8-Channel	
9/20/2024	BNT	264	192	989001045526553	8-Channel	8-Channel	
9/20/2024	BNT	264	176	989001045526610	8-Channel	8-Channel	
9/20/2024	BNT	181	56	989001045526613	Jeffrey Connector	8-Channel	
9/20/2024	BNT	183	51	989001045526623	Jeffrey Connector	8-Channel	
9/20/2024	BNT	200	75	989001045526634	Jeffrey Connector	8-Channel	

Section II. Annual Monitoring Report 2024 Results of Geomorphic and Vegetation Monitoring

Prepared by Jim Graham and Jes Suoja

Annual Monitoring Report 2024
Results of Geomorphic and Vegetation Monitoring

Prepared by California Polytechnic University
For The State Water Resources Control Board, the Los Angeles Department of Water and Power, and the Mono Basin Monitoring Administration Team

Authors:
Jim Graham, Professor
Jes Suoja, Graduate Research Assistant

5/12/2025, Draft

Table of Contents

Definitions

Below are definitions used throughout this document.

- Aerial Photos - For our purposes, this refers to visual and infrared aerial photographs obtained using a drone or other aerial vehicle.
- CHM - Canopy height model. A raster where each pixel contains the height of the canopy above the ground.
- DEM - Digital Elevation Model. A raster where each pixel contains the elevation of the ground.
- Drone - Unmanned / Unoccupied Aerial Vehicle, also known as a UAV.
- DTM - Digital Terrain Model. Another name for a DEM.
- DSM - Digital Surface Model. A raster where each pixel contains the elevation of the top-most feature on the landscape (i.e. top of trees, roofs of houses, ground if there is no cover).
- LADWP - Los Angeles Department of Water and Power.
- LiDAR - Light Detection and Ranging refers to using laser pulses to determine the distance to an object. For our purposes, this refers to scanning the surface of the earth from a drone to determine the height of objects and elevation of the ground.
- LWD - Large woody debris
- NAD83 - North American Datum, 1983. Used to reference geographic coordinates (a latitude and a longitude) to North America.
- RCT - Rifle Crest Thalweg
- RCT-Q: Relationship between the riffle crest thalweg and stream flow typically presented as a chart with RCT on one axis and Q on the other.
- UAV - Unmanned / Unoccupied Aerial Vehicle, also known as a drone.
- WGS84 - World Geodetic System, 1984. Used to reference geographic coordinates (a latitude and a longitude) to the earth.

Executive Summary

This report focuses on the Geomorphic and Vegetation monitoring within the riparian areas of the tributaries that flow into Mono Lake. The goal of this phase of the project is to determine effective monitoring methods for the geomorphic and land cover (specifically vegetation) aspects of the riparian area. The project focuses on developing methods within the Rush Creek riparian area from the Ford to the Narrows with the expectation that the area of study will expand to other riparian systems around the lake when the methods are refined.

The timeframe for this report is from fall of 2023 through spring of 2025. The primary change to the project has been the addition of a Co-PI, Jim Graham, and an increase in the remote sensing aspects of the project.

This study shows that aerial photos with Drones/UAVs can be used to determine vegetation structure to an extent and where there is water that is not hidden by dense canopy. LiDAR based drones can be used to create high resolution, at least 6”, elevation models. These models can then be used to obtain profiles of the watershed at any location, identify nick points, analyze change in geomorphology, and study the hydrology of the area. The data can also be used to identify land cover including the general types of vegetation on the land. LiDAR data also opens up new possibilities for analysis including estimating the amount of soil erosion and sediment deposition.

We also show that on the ground surveying is still required in areas that remote sensing methods cannot penetrate. This includes detecting the extent of water below the canopy and measuring the depth of water anywhere in the study area. Additional work is also needed to improve the classification of vegetation classes. This includes, acquisition of infrared aerial images, surveying for land cover below dense canopy, and additional land cover classification research.

Introduction

Riparian vegetation is considered a keystone habitat in desert riparian ecosystems, meaning that the loss of vegetation can have cascading effects on ecosystem services and functions (Johnson and Jones, 1977; Knight and Bottorff, 1984; Colvin et al., 2019). There is evidence that desert riparian ecosystems are sensitive to human alteration or disturbance (Johnson and Jones, 1977). Because of this, increasing efforts to mitigate the effects of degradation is crucial to restoring essential ecosystems.

Loss of habitats can decrease structural heterogeneity, which is important for the resilience of an ecosystem (Cardinale et al., 2006; Virah-Sawmy, 2009). Shifts or losses in riparian vegetation, and thus fish and waterfowl habitat, may have even larger-scale effects (Naiman et al., 2010; Kominoski et al., 2013). Classification of the vegetation and land cover types can provide insight into the biodiversity and heterogeneity of an ecosystem, both of which can be

indicators of ecosystem health (Virah-Sawmy, 2009). In doing so, researchers can begin to determine the health of the ecosystem and isolate areas that need the most improvement.

The Mono Basin feeds a hypersaline lake with no outlets, known as Mono Lake, and its freshwater tributaries (Mono Basin Research Group, 1977; National Research Council, 1987). Mono Lake is within the rain shadow of the Sierra Nevada, and ranges between 1,800 and 4,000 meters elevation (National Research Council, 1987). Due to diversion of water to Los Angeles since 1941, the water level in Mono Lake has experienced a precipitous decline from historic values (Taylor, 1982). This diversion has led to a myriad of issues, including increased salinity of the lake, loss of riparian and waterfowl habitat, decline in trout populations, increased soil erosion, and channel narrowing along the lake's tributaries (Taylor, 1982; Stine et al., 1984; Colvin et al., 2019).

Rush Creek is the largest of the tributary streams located on the lower southwest side of Mono Lake. The streambed of Rush Creek is "derived from granitic and metamorphic rock moved downstream from the Sierra Nevada by glaciation and bedload transport during high stream flows" (LADWP, 1996). Riparian areas such as Rush Creek provide a favorable microclimate due its ability to moderate evapotranspiration along the riparian corridor. This area experiences large seasonal and annual variability in precipitation (National Research Council, 1987). The majority of precipitation comes in the form of snow in the winter. Annual precipitation varies greatly, from 100 mm per year to 1,000 mm per year (Taylor, 1982). This area also has prolonged periods of drought, as well as periods of heavy precipitation (National Research Council, 1987). The creek has a highly seasonal flow pattern, with flow being highest in the summer when snow melt occurs (Taylor, 1982; National Research Council, 1987). Historically, snowmelt floods were common, but water diversion by the Los Angeles Department of Water and Power (LADWP) has decreased the frequency of flooding (McBain & Trush, Inc. et al., 2010). Prior to restoration efforts the creek had dried up, resulting in near total loss of riparian vegetation, as well as fish and waterfowl habitat (State Water Resources Control Board, 1994).

Utilizing remote sensing techniques, particularly through unoccupied aerial vehicles (UAVs), can increase data collection efficiency and reduce the amount of disturbance to sensitive habitats (Cruzan et al., 2016). Because of this, the use of remote sensing for monitoring restoration has grown in popularity (Bertacchi et al., 2019; Huylenbroeck et al., 2020). In particular, this has been the case in desert riparian ecosystems (Norman et al., 2014; Song et al., 2024). Remote sensing can be used to produce high-resolution imagery for the purpose of classifying vegetation and land cover as part of riparian restoration and monitoring projects (Howland, 1980; Cruzan et al., 2016).

Aside from high-resolution visible spectrum (RGB) aerial imagery, UAVs can also be used with sensors to collect different types of data. One type of data that can be collected with UAVs for the purpose of monitoring changes in vegetation and land cover over time is Light detection and ranging (LiDAR). LiDAR is a product of laser technology and photodetection technology where a high frequency of laser pulses are sent out and the time it takes for the pulse to be reflected back is recorded (Wang et al., 2024). This can be used in restoration efforts to create extremely

detailed models, such as digital surface and elevation models (DSM and DEM) as well as canopy height models (CHMs). Near infrared sensors can also be used with UAVs. Near infrared data can be used to calculate several vegetation indices, which are mathematical equations that calculate plant traits, such as plant vigor and stress, among others (Bannari et al., 1995). For example, the Normalized Difference Vegetation Index can be calculated using red and near infrared imagery to determine greenness (Wilson and Norman, 2018; Gomez-Sapiens et al., 2021). Research has shown that this can be an effective tool when determining vegetation change over time (Wilson and Norman, 2018; Gomez-Sapiens et al., 2021).

The State Water Resources Control Board (SWRCB) required LADWP to establish multiple monitoring teams to address degradation of the Mono Basin waterways. One monitoring team, the Stream Monitoring Team, was tasked with hydrology and geomorphic monitoring, assessing channel roughness, and mapping riparian vegetation and land cover. The main objective of the Stream Monitoring Team for 2024 was to determine effective monitoring methods in accordance with the licensing agreement including developing a protocol to increase monitoring efficiency, accuracy, and reproducibility.

Methods

Study Area

Mono Lake is located on the eastern edge of the eastern Sierra Mountains in California. The closest town is Lee Vining (Figure 1). There are a series of streams that flow into the lake including Lee Vining and Rush Creek.

The study area is Lower Rush Creek from an area known as “the Ford” (37° 54’ 48.7’’ N, 119° 04’ 48.9” W) to “the Narrows” (37° 56’ 50.4” N, 119° 03’ 29.6” W) where Walker Creek joins Rush Creek near Lee Vining, CA (LADWP, 1996; Figure 2). This area of Rush Creek contains herbaceous riparian vegetation, woody riparian vegetation, desert vegetation, and some exotic vegetation (McBain & Trush, 2005). The Mono Basin vegetation consists of large deciduous shrubs or deciduous trees as well as larger conifers which contrast sharply with the surroundings (Taylor, 1982). Primary vegetation along Rush Creek is black cottonwood (Populus balsamifera subsp. trichocarpa), willow (Salix spp.), cattails (Typha latifolia), and various brush species, such as big sagebrush (Artemisia tridentata ssp. tridentata) and rubber rabbitbrush (Ericameria nauseosa) (National Research Council, 1987; Stine, 1991).

Figure 3 provides the names of locations within the Rush Creek study area that are used in this report.

During 2023, aerial photos of the riparian area to the east and north of Lee Vining, including Lee Vining creek (Figure 4). Other riparian areas may be monitored in the future as the monitoring protocol is refined.

Figure 1. Map of California showing the location of Lee Vining, which neighbors Mono Lake.

Figure 2. Aerial Image showing the two main features that bound the study area, the ford and the narrows.

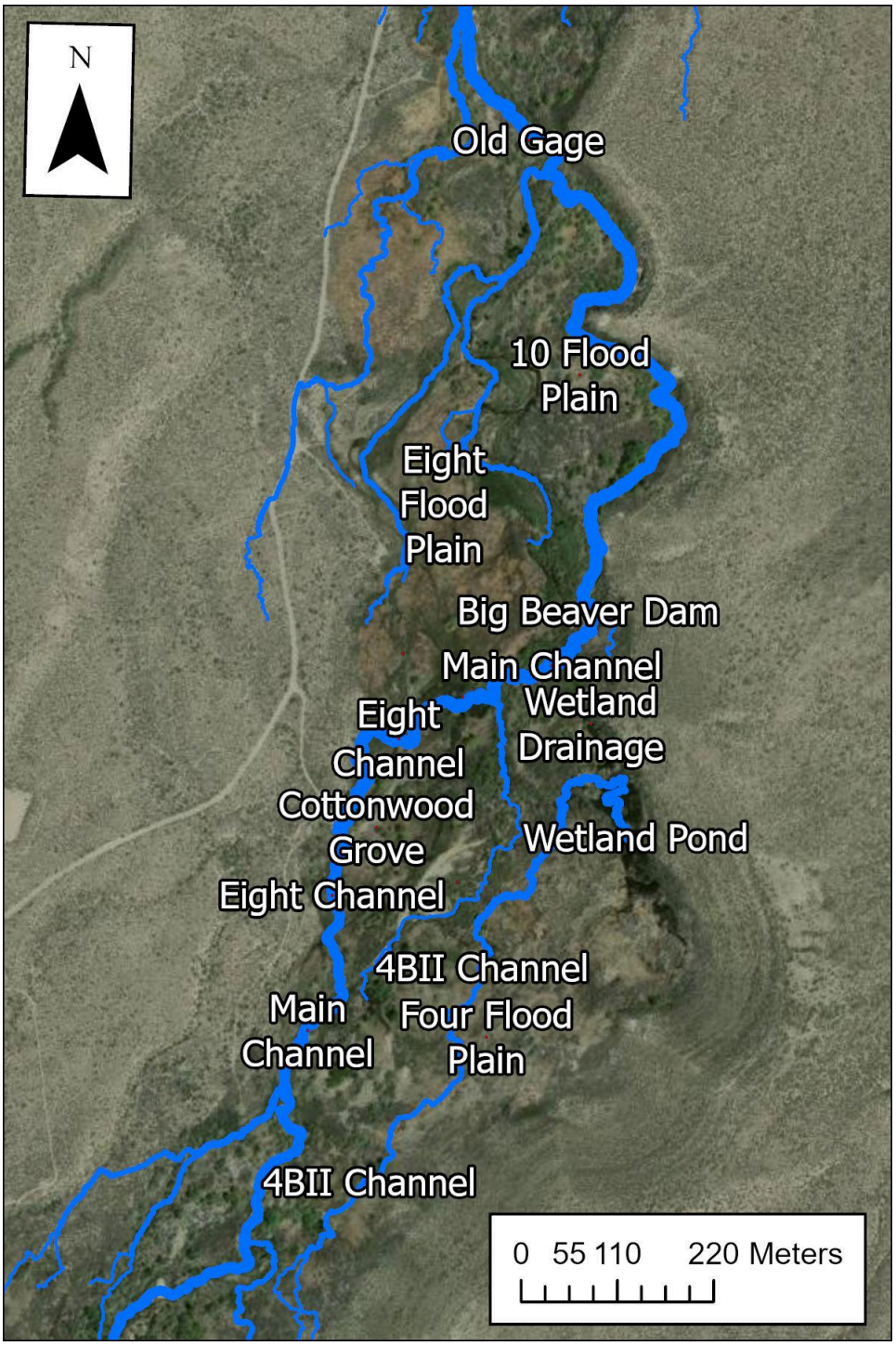

Figure 3. Map of the central area of the study area with labels for features that are mentioned in the text.

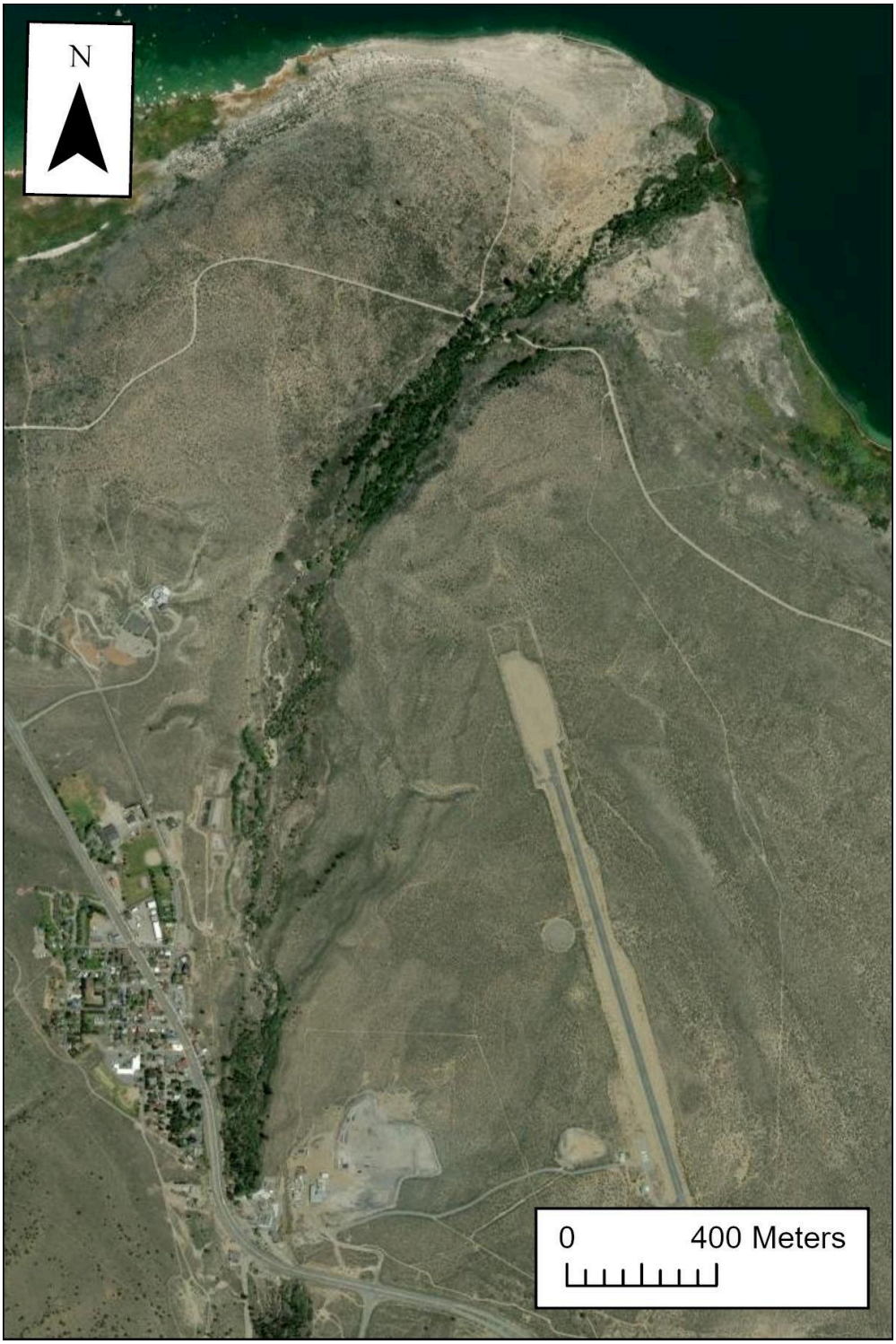

Figure 4. Riparian area to the east and north of the town of Lee Vining.

Data Collection And Processing

Where possible, data was collected in the WGS 84, Universal Transverse Mercator, Zone 11 North (UTM Zone 11 North). Datasets in other spatial references were projected into WGS84, UTM Zone 11 North as soon as possible to keep all working data in the same spatial reference. Standard file formats were used through with LASer (LAS) files for point clouds from LiDAR flights, Shapefiles (shp) being used for vector data, and Tagged Image FIle Format (TIFF) files used for rasters.

2017 Aerial Data

LiDAR data and associated photographic images were provided to us by Robbie Di Paolo. This included LiDAR point clouds and processed LiDAR. The processed LiDAR data appear to have been converted to a Triangulated Irregular Network (TIN) and then to a raster. Investigation into the data showed that we could obtain about 6” (½ foot) resolution.

The data was processed in Cloud Compare version 2, ArcGIS Pro version 3.4.0, BlueSpray B55. The data was defined to be in the spatial reference NAD83, 2011 StatePlane California III, US Feet. For final analysis, the data was projected into WGS84, UTM Zone 11 North.

The LiDAR data for Rush Creek was in a folder labeled Phase 3 with a subfolder for Rush Creek from the highway to Mono Lake was labeled LB and numbered from LB1, at the highway, to LB13, at the lake. Since the focus of this study was from the ford to the narrows, LB8 through LB 5 were used.

Each LB folder contained a large number of LAS files that overlapped without a recognizable pattern but appeared to only have one flight line. The contents of each folder were merged together in CloudCompare into a single point cloud for each LB folder. This created very large files which were then segmented into files of about 2500 x 800 pixels to keep CloudCompare from locking up. The data included flight lines and some pixels that were well above the tree line. These were manually removed.

Experiments showed that the best ground and off-ground (first return) data was obtained by not applying any additional filters to the data and using a Cloth Simulation Filter (CSF) with a resolution of 0.5 feet, 500 maximum iterations, and a classification threshold of 0.02. The classification threshold is much lower than for other LiDAR tasks but did the best job at separating the ground and off-ground points. We believe the low value was required because of the relatively dense point cloud in the dataset which was generated by a drone flying at lower altitudes than typically for an aerial LiDAR survey..

Rasters were then created for each segment of ground and off ground point clouds. Rasters were at 6” per pixel, the average point elevation was used for each pixel with Kriging used to interpolate pixels for pixels that did not overlap with a point from the cloud.

The ground and off-ground rasters were merged together in ArcGIS Pro to create a Digital Survey Model (DSM) and a Digital Terrain Model (DTM, DEM, or ground model). The mean value of overlapping pixels was used in the mosaic operation. The rasters were then manually cropped to remove the artifact from Kriging. The DTM was subtracted from the DSM to create a Canopy Height Model (CHM). The final result was a DTM/DEM and a CHM for each LB area.

Hillshades of the DTM/DEMs were produced to allow visualization of the terrain.

2023 Aerial Data

In July of 2023, photographic images were collected for Rush Creek and Lee Vining creek using a DJI Mavic Pro 3. These images were processed in AgiSoft's MetaShape into orthomosaics.

The surveys were completed by Dr. Jim Graham, a certificated FAA remote pilot and Julia Avina, a Cal Poly Humboldt student. The equipment used was a DJI Mavic Pro Unmanned Aerial Vehicle (UAV) or drone.

Lee Vining Creek was surveyed from just below the town of Lee Vining to where it drains into Mono Lake. Rush Creek was surveyed from the narrows to just past the ford.

2024 Aerial Data

In late July and early August of 2024, photographic images were collected for Rush Creek using a DJI Mavic Pro 3. Visual (RGB) surveys of Rush Creek from the narrows to the ford were completed. These images were processed in AgiSoft's MetaShape into orthomosaics.

In November of 2024, LiDAR data was collected for Rush Creek using a DJI Matrice 300 RTK UAV/drone with a Zenmuse L2 LiDAR sensor. The point clouds were processed in CloudCompare to extract points that were classified as "First Return" and "Ground" datasets. These were then "rasterized" in CloudCompare to create a DSM (surface) and a DTM/DEM (ground). The DEM was then extracted from the DSM to create the CHM (canopy). These flights also provided a high resolution photo dataset for the area.

Stream Network

Stream networks and other hydrological features and analysis can be completed from a DSM. A stream network was completed in BlueSpray using the Water toolset. Profiles of the streams with their elevations can then be extracted in ArcGIS Pro.

Stream Profiles

The availability of high resolution DSMs/DEMs allows stream profiles and profiles of the entire riparian area to be extracted at any area within the study site. Profiles were extracted using the Profile Tool in ArcGIS Pro.

Geomorphological Changes from 2017 to 2024

Once high resolution elevation models were available for 2017 and 2024, the 2024 model could be subtracted from the 2017 model to show the change in elevation over the 7 years. The changes can then be colorized to show areas that have eroded vs. areas of deposition. This work was completed in ArcGIS Pro.

Land Cover

Historical riparian vegetation data for Lower Rush Creek was compiled in order to determine the change in riparian vegetation over time (McBain & Thrush, 2005). Historical data is being digitized in ArcGIS Pro to allow for ease of analysis in the future.

Ground Photography

Old photographs of Rush Creek have been compiled and will become established photo points for routine monitoring. We will add recent photographs to this collection. These will be used to establish photo points during the 2025/2026 season. New photo points will also be established along all benchmarks.

Gauge Data

Gage data has been provided by LADWP. This will be used for future analysis.

Results

Data Collection and Processing

2017 LiDAR Data

We were able to process the LiDAR point clouds from 2017 to create a DEM/DTM and CHM at approximately 6” (15cm) per pixel resolution (Figures 7 and 8). These were created for Rush Creek and the other 5 locations where point clouds were provided.

Examination of the cross-sectional profiles of the LiDAR point clouds showed that the canopy was almost completely represented but that it blocked some areas of the ground which can impact the quality of the final DEMs (Figures 5 and 6).

This dataset contained a very large number of datasets including multiple flights in the same area. This slowed down processing of the data but did not appear to impact the quality of the final product. The overall process was automated with a Python script to reduce the human time required for processing.

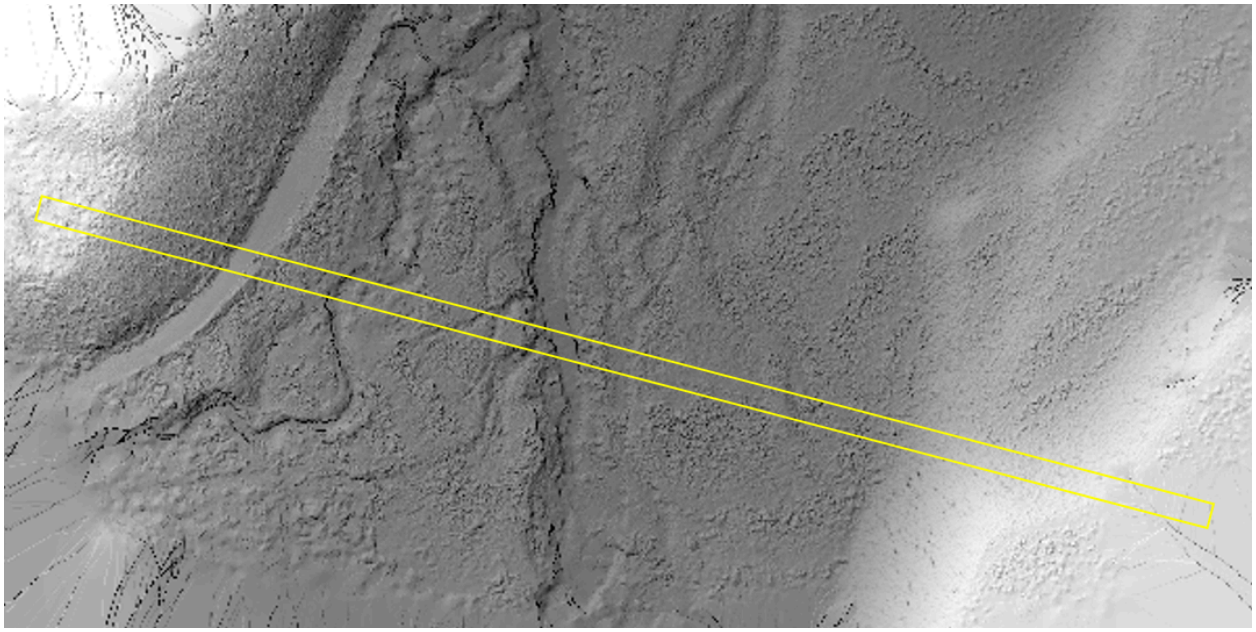

Figure 5. A hillshade of a section of the DEM created from 2017 LiDAR data. The yellow box shows the area for the profiles in the next figure.

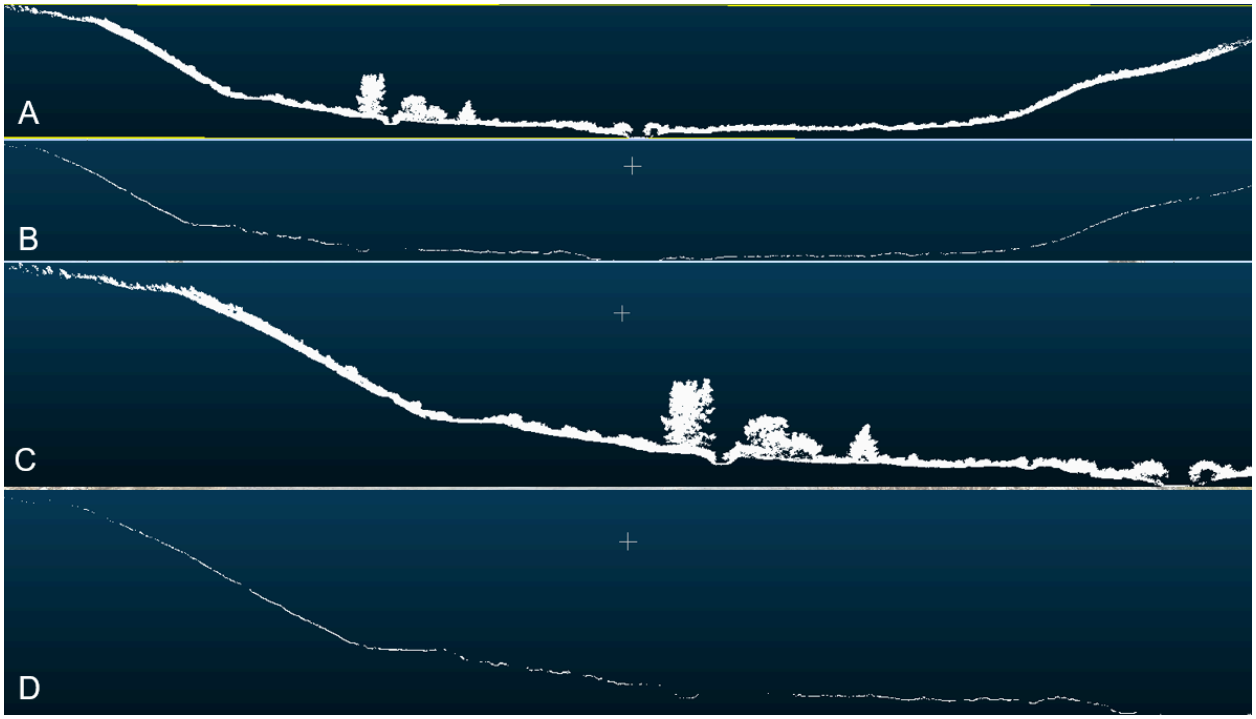

Figure 6. Cross sections of the area shown in Figure 5. A) full cross section showing the entire point cloud. B) Cross section showing just the points that are classified as ground. C) Cross section from the left side of A showing the main stream channel in the middle which is above the older channel at the center of the riparian area. D) Cross section of the ground points from the left side of B showing the lack of ground points below the dense canopy.

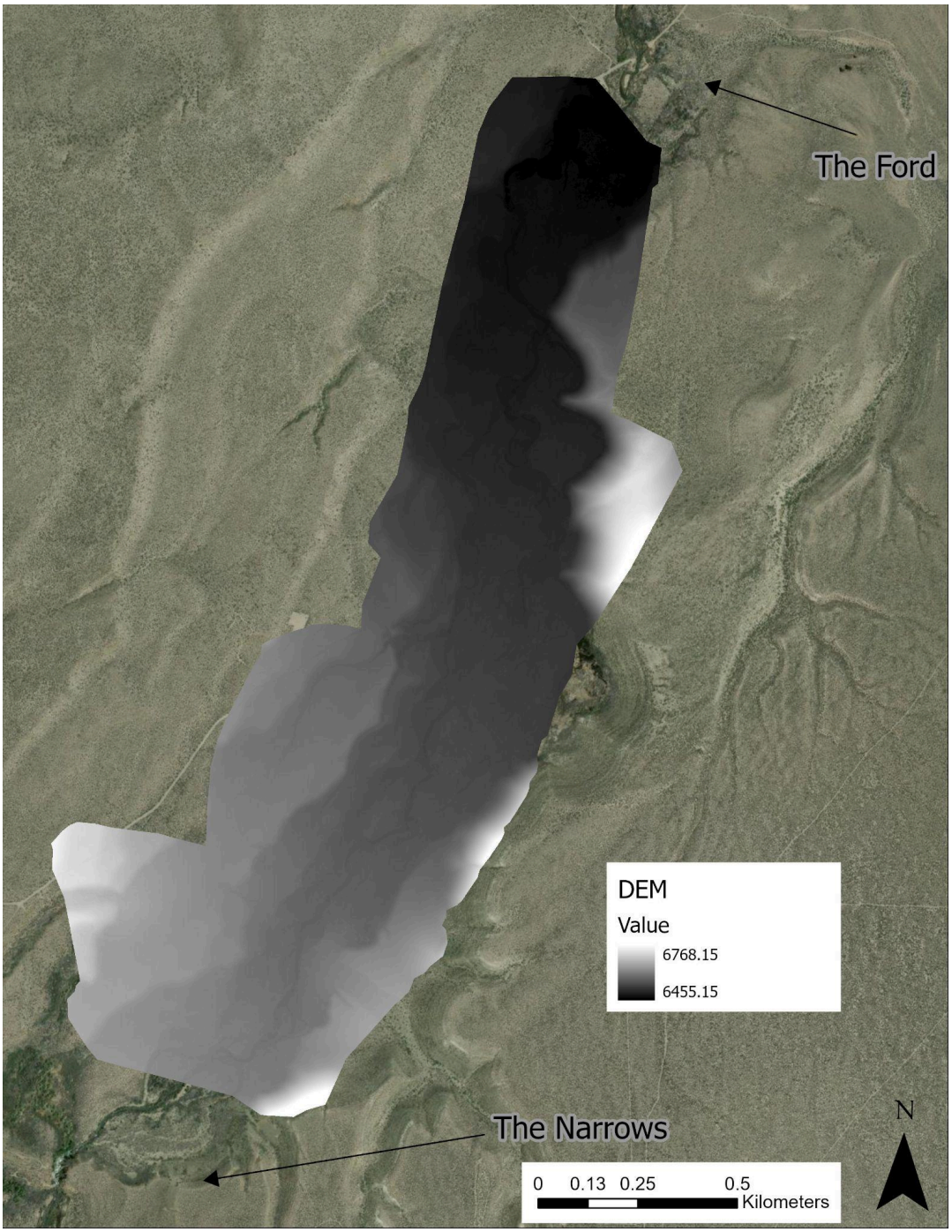

Figure 7. Map showing the DTM/DEM.

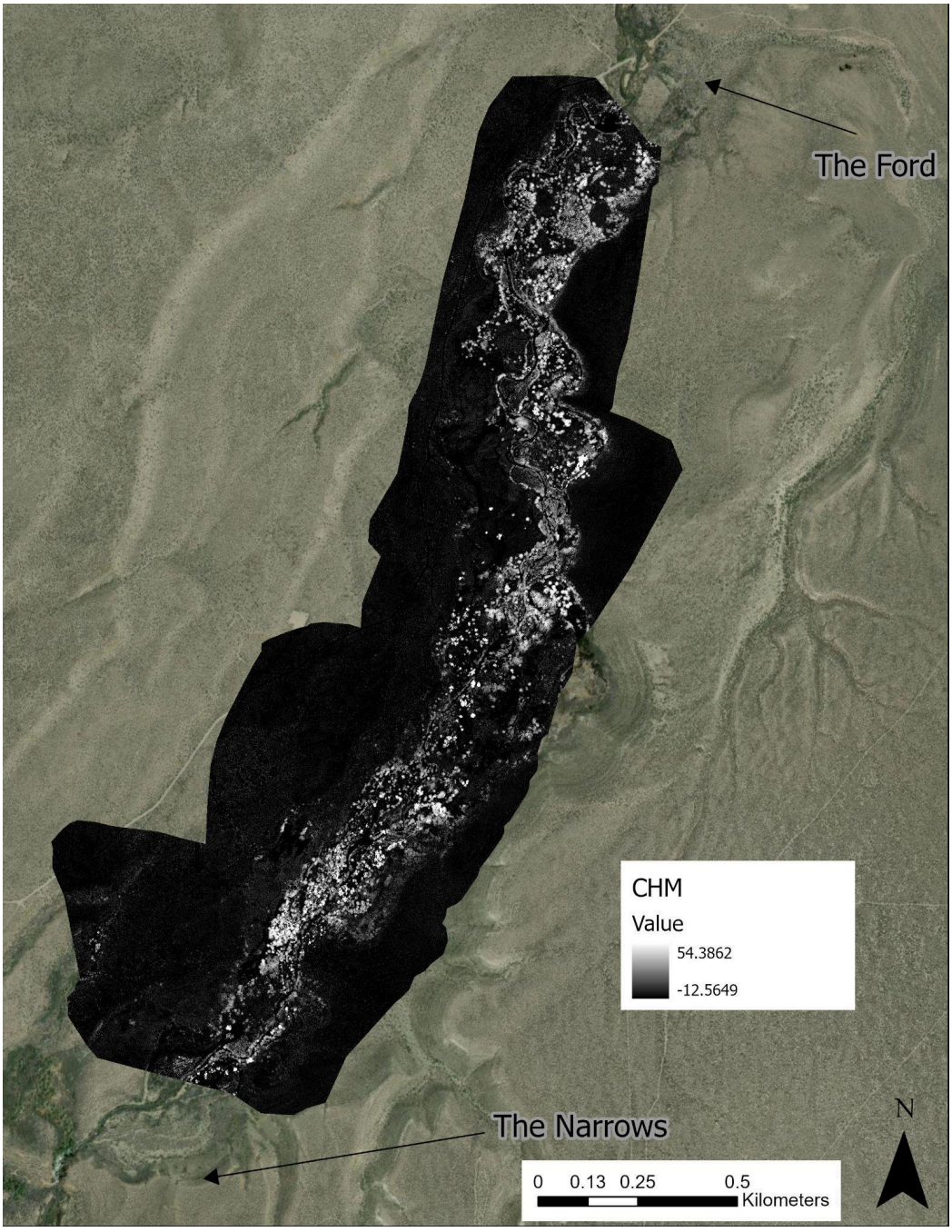

Figure 8. Map showing the CHM

2023 Aerial Photos

A portion of the results for Lee Vining Creek during 2023 are shown in figure 9.

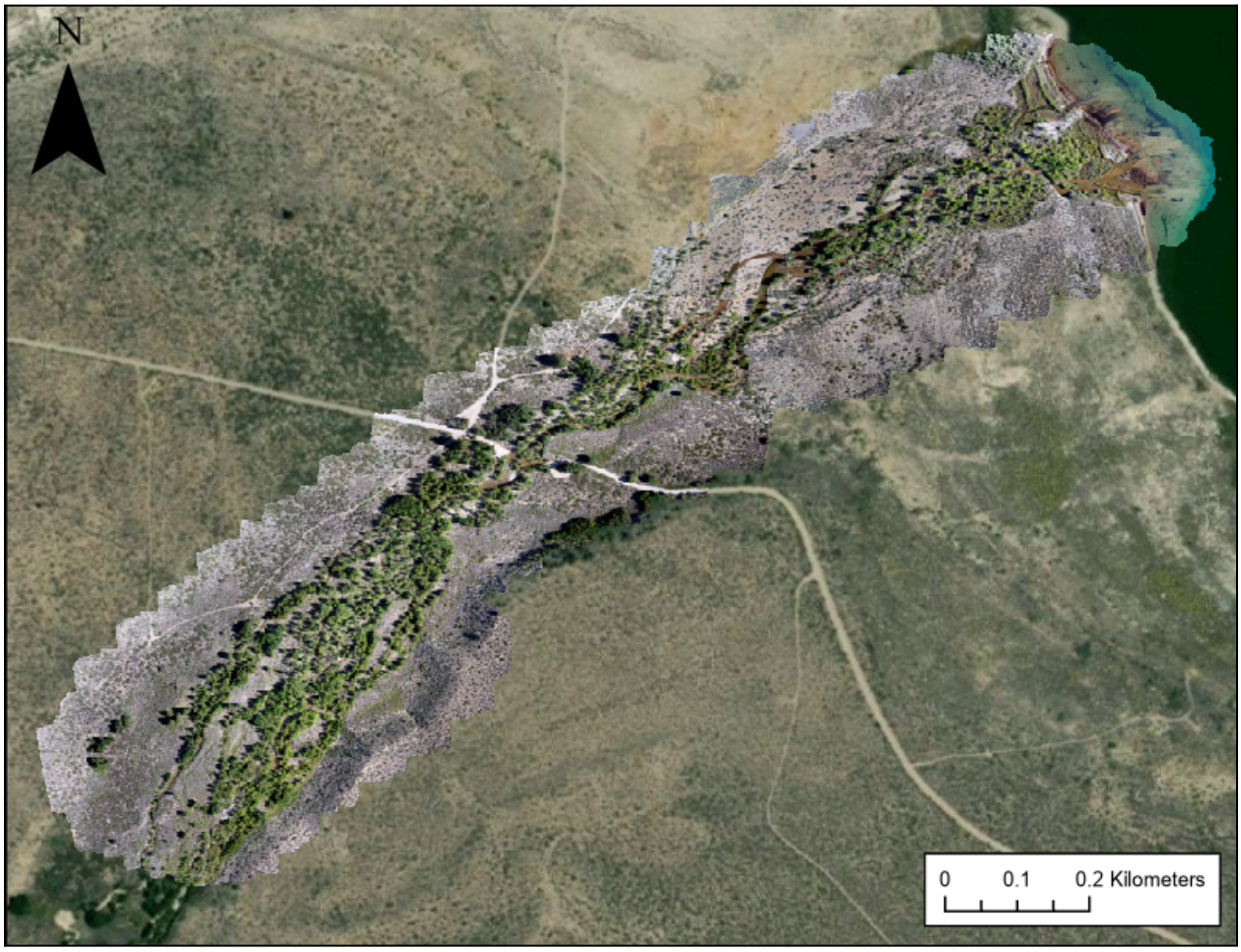

Figure 9. Image of a portion of the survey for Lee Vining Creek.

July 2024 Aerial Photos

The aerial photos captured in July of 2024 were also of very high resolution, less than 3 cm and of high quality (Figure 10). There were issues that appeared along the edges of the images for each flight. Having the flights overlap and then cropping the resulting images should remove this.

Figure 10. Aerial photos from the 2024 flights conducted in July.

November 2024 Aerial Photos

The aerial photos that accompanied the LiDAR taken with the Matrice 300 were of very high quality (Figure 11). The one issue is banding that we believe is a result of the angle of the field of view as the photos are collected. We typically try to fly with the sun directly overhead to reduce capturing the shadows. However, the shadowing could not be avoided in November with the sun low on the horizon throughout the day. We believe the banding is then from the camera seeing one side of the plants (e.g. the northside) to the left of the camera when flying in one direction and then the other side of the plants (e.g. the southside) when flying in the other direction. This would be reversed for the right side of the camera. We have yet to determine how this will impact the land cover classification. However, we also will have data from the summer which does not show the banding (Figure 10).

Figure 11. Aerial Photos taken with the LIDAR data using the Matrice 300.

November 2024 LiDAR Data

The 2024 flights produced 8 point cloud datasets between the ford and the narrows. These showed excellent representation of the canopy and ground (Figures 12 and 13).

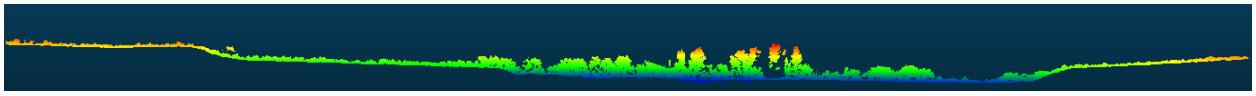

Figure 12. A cross section of the Rush Creek riparian area near the pond.

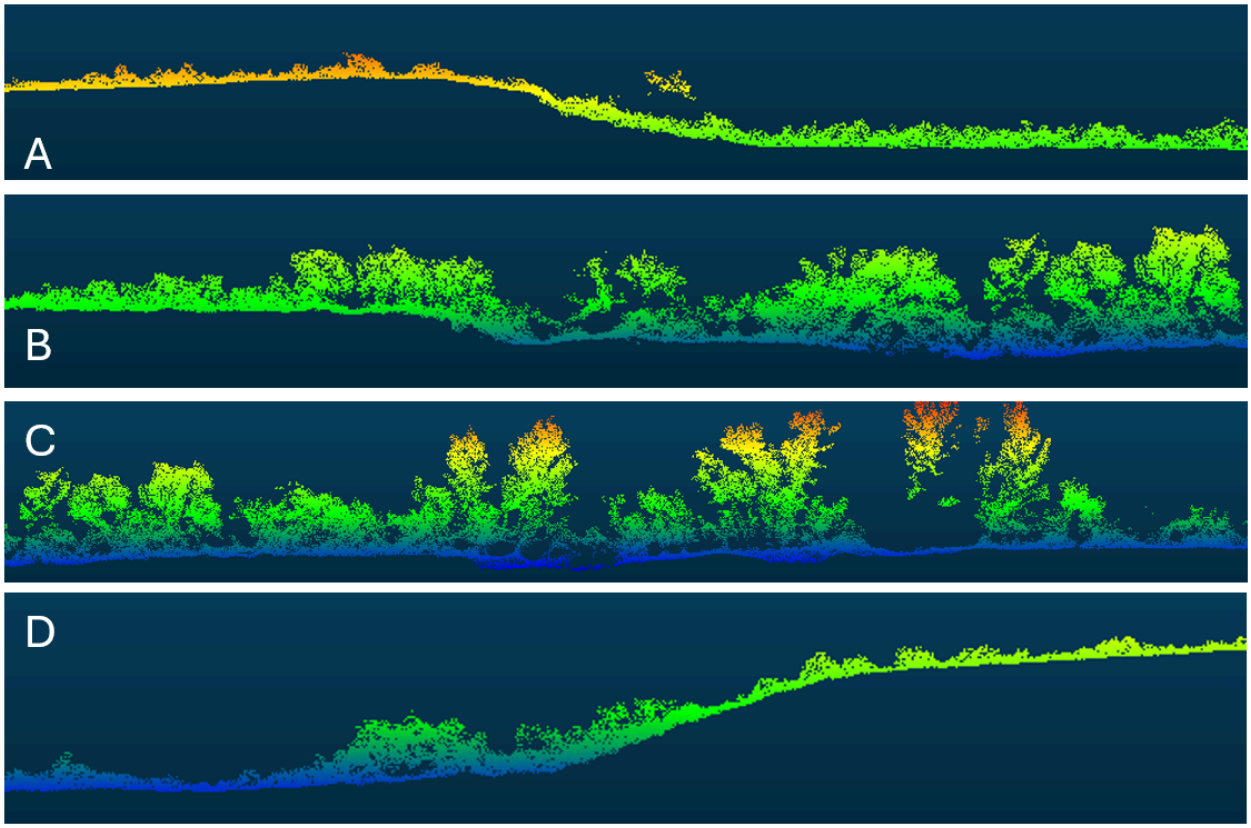

Figure 13. Images from a cross section of the Rush Creek riparian area going from the western (A) to the eastern (D) side of the area.

Two of the LiDAR flights showed a vertical offset of up to 1.4 meters. This was addressed by using common reference points between rasters and then shifting the vertical position of the two rasters to match the vertical position of the points in adjacent rasters. We believe this was caused by moving the ground station and not allowing it adequate time to obtain an accurate vertical fix.

There were two gaps between the final rasters (Figure 14). We believe this was caused by insufficient overlap between the flights and will be addressed in future flights.

Figure 14. Hillshade of the 6” elevation dataset that was created from the 2024 LiDAR point cloud. The two gaps can be seen toward the middle of the map. These prevented the data from being used for stream network creation but the data could be used for other analyses.

Stream Network

The LiDAR data collected in November of 2024 had two slivers between flight areas which prevented us from creating a stream network from the most recent data. Because of this, we created a stream network based on the 2017 data. The stream network was complete except for one area near the wetland pond which was not captured in the LiDAR dataset (Figure 15).

This caused an error in creating the stream network where one of the major streams flowed to a pour point at the eastern edge of the network instead of back into the main stem. This can be addressed by having LiDAR covering the entire riparian area and the surrounding up slopes.

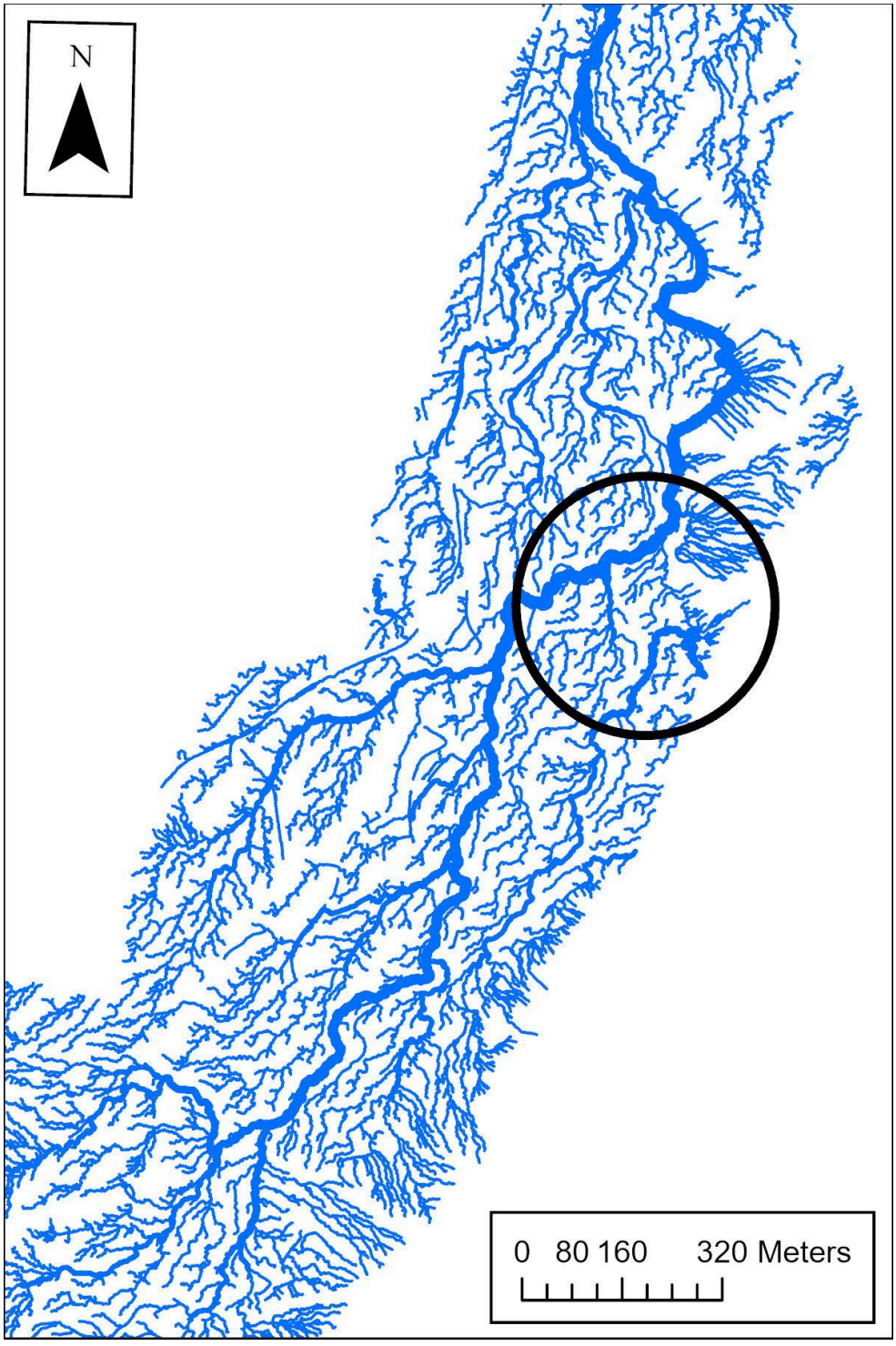

Figure 15. Stream network created from the DEM. The only major issue found is shown in the black circle where the water flows off the data instead of back into the main channel.

Stream Profiles

Examining a cross section of the elevations of the various stream channels near the wetland pond showed that the Eight Channel is actually above the Main Channel and the Wetland Pond even though the Eight Channel was observed carrying all the water through the system in November of 2024 (Figure 16).

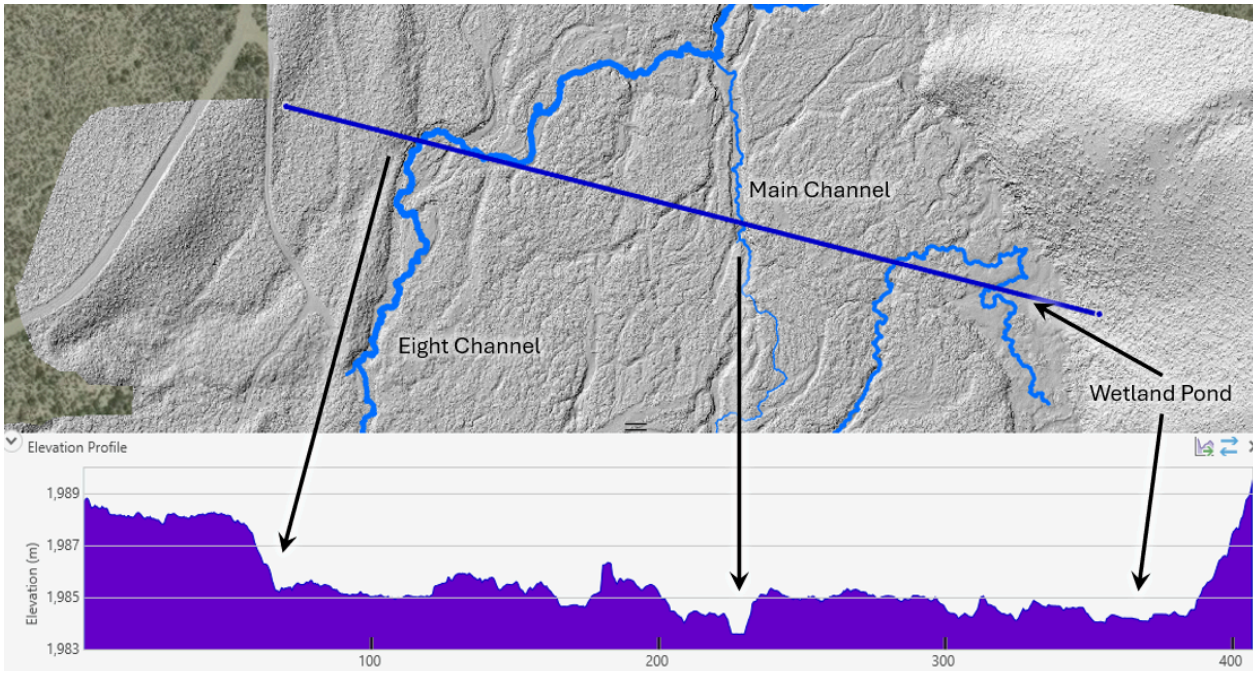

Figure 16. Cross sectional image of the elevation showing how the Eight Channel is actually above the main channel and the wetland pond in elevation.

Geomorphological Changes 2017 to 2024

Large geomorphic changes were visible in the difference between the 2017 and the 2024 DEMs. These were seen throughout the watershed but especially at the area just south of the ford (Figure 17 through 19). Bank erosion and sedimentation were observed in the field at this location between 2017 and 2024 (Figure 20). We believe the changes outside the stream channel are partially due to differences in the LiDAR sensor and processing used between the two studies. These differences should be reduced by using consistent hardware and software for capturing and processing the LiDAR data.

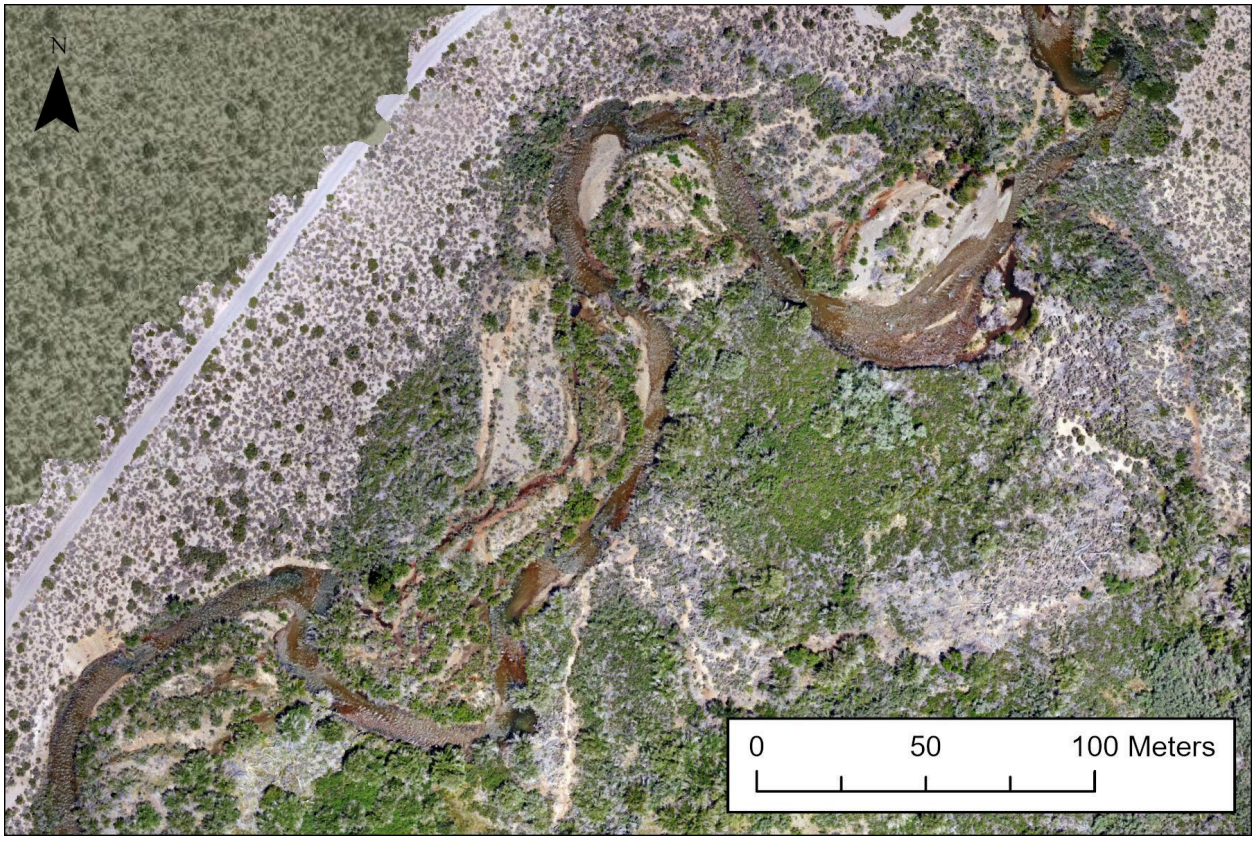

Figure 17. Photo from an aerial flight from 2024 just south of the ford.

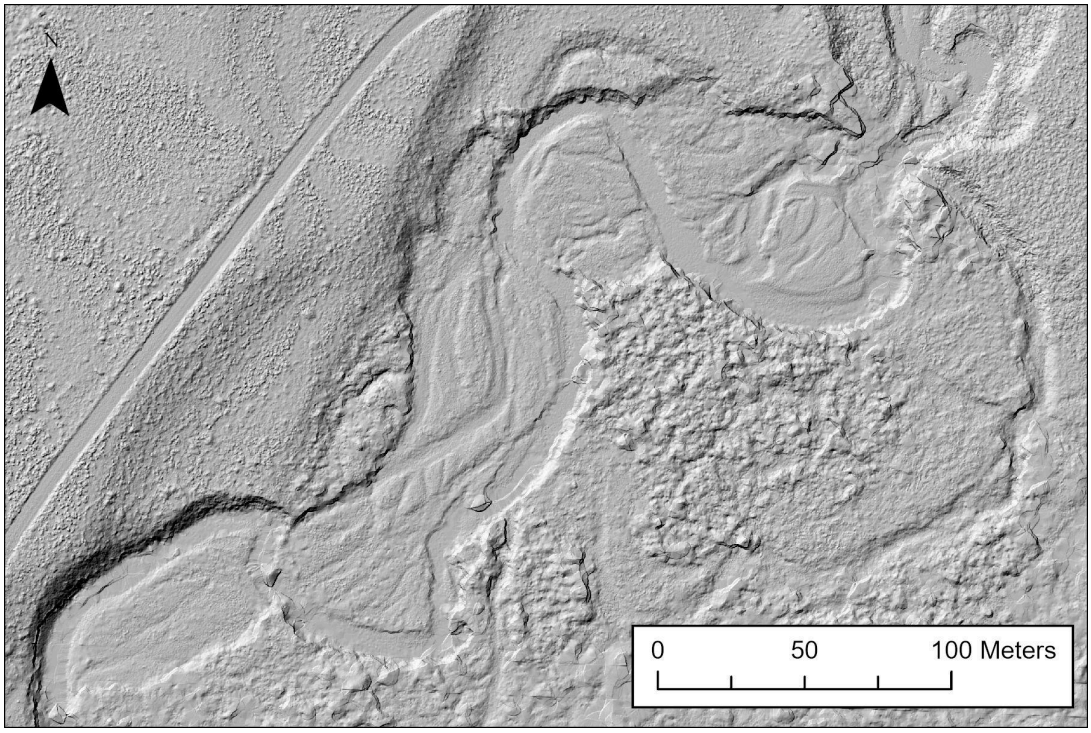

Figure 18. Hillshade of the DEM created from the 2017 LiDAR data.

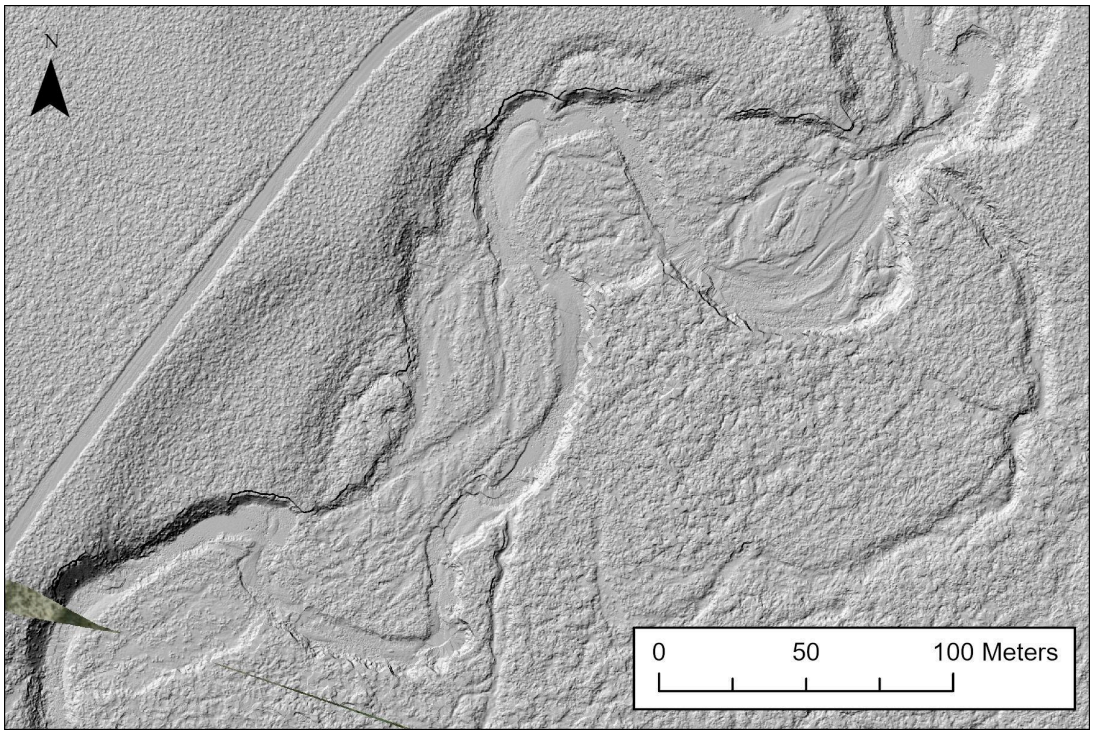

Figure 19. A hillshade of the DEM for 2024 showing the area just south of the ford. Changes from 2017 can be seen in the oxbow forming in the top center of the map.

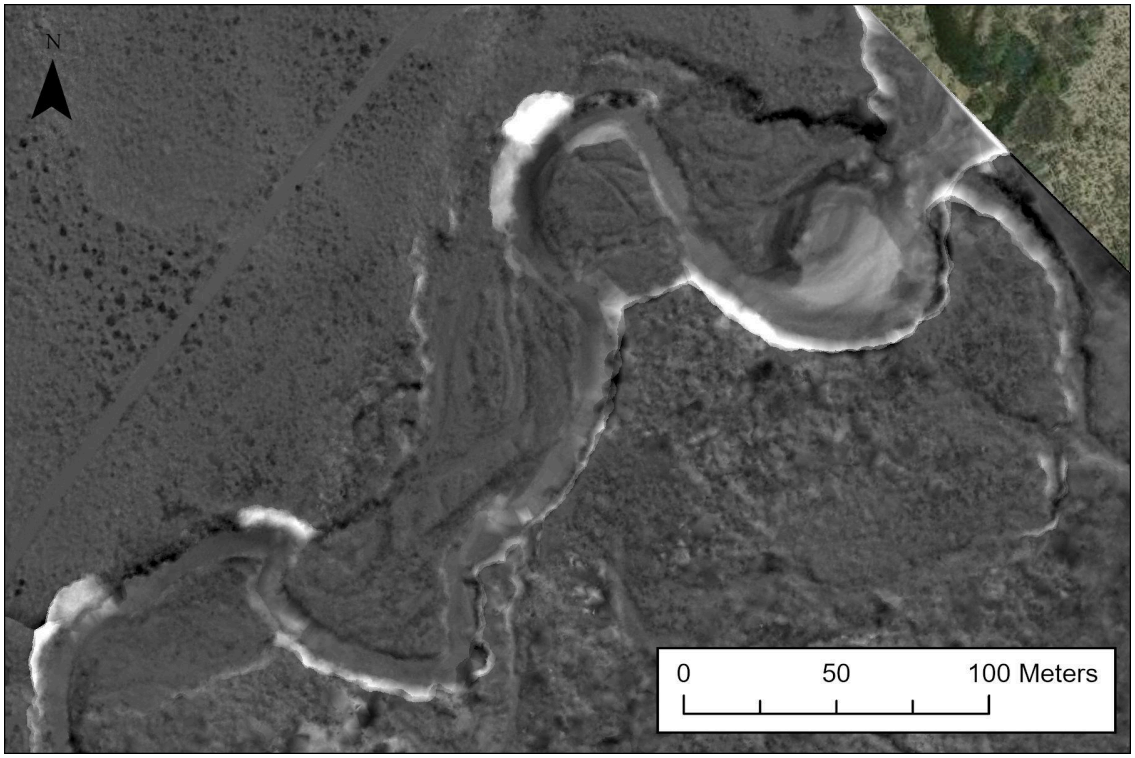

Figure 20. A map showing the change in elevation from the 2017 DEM to the 2024 DEM. The bright white areas represent a reduction in elevation of about 3 meters. However, some of this was created by dense vegetation being removed from the bank as it eroded away. Mid to dark gray areas represent sediment deposition including the light area in the upper left of the image.

Aerial Data, November 2024

During the LiDAR flight, the drone also collects aerial photos. This resulted in a high quality set of aerial photos captured near low flow. Taking aerial photos during the low flow may be valuable for detecting which pools are active throughout the dry season (Figures 21, 22).

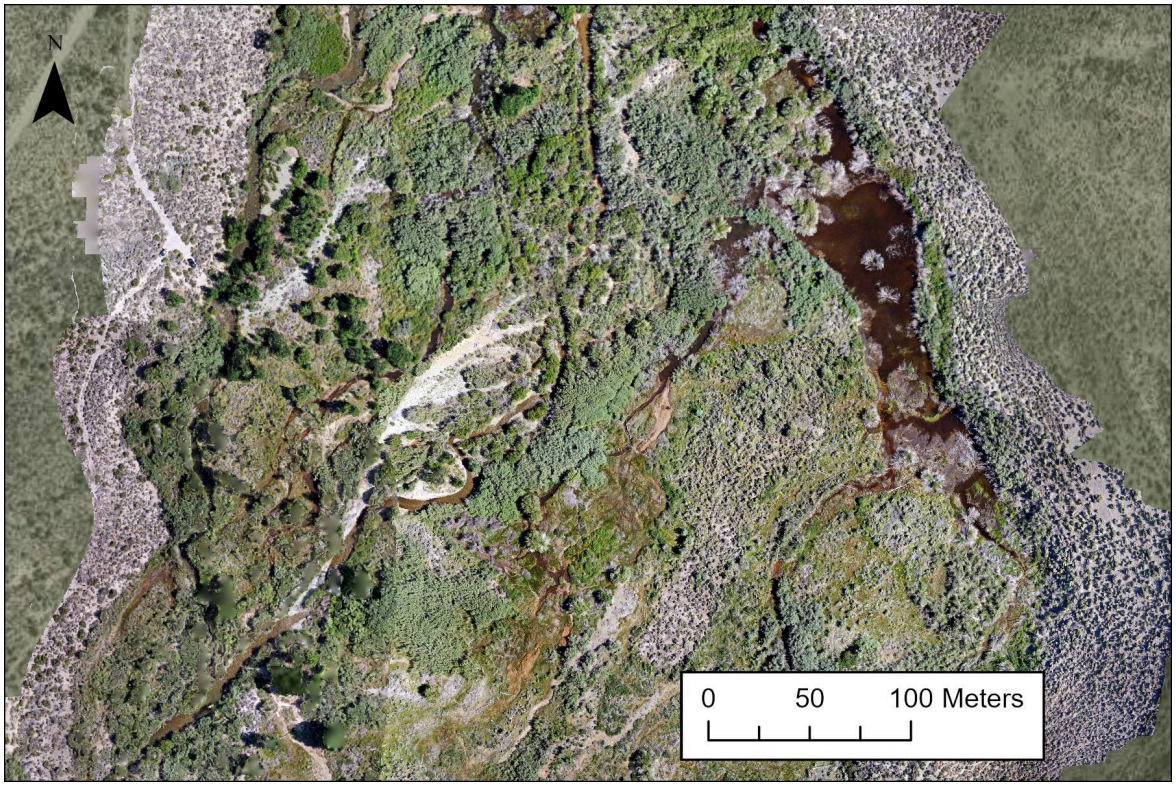

Figure 21. Large pond when full in late July of 2024

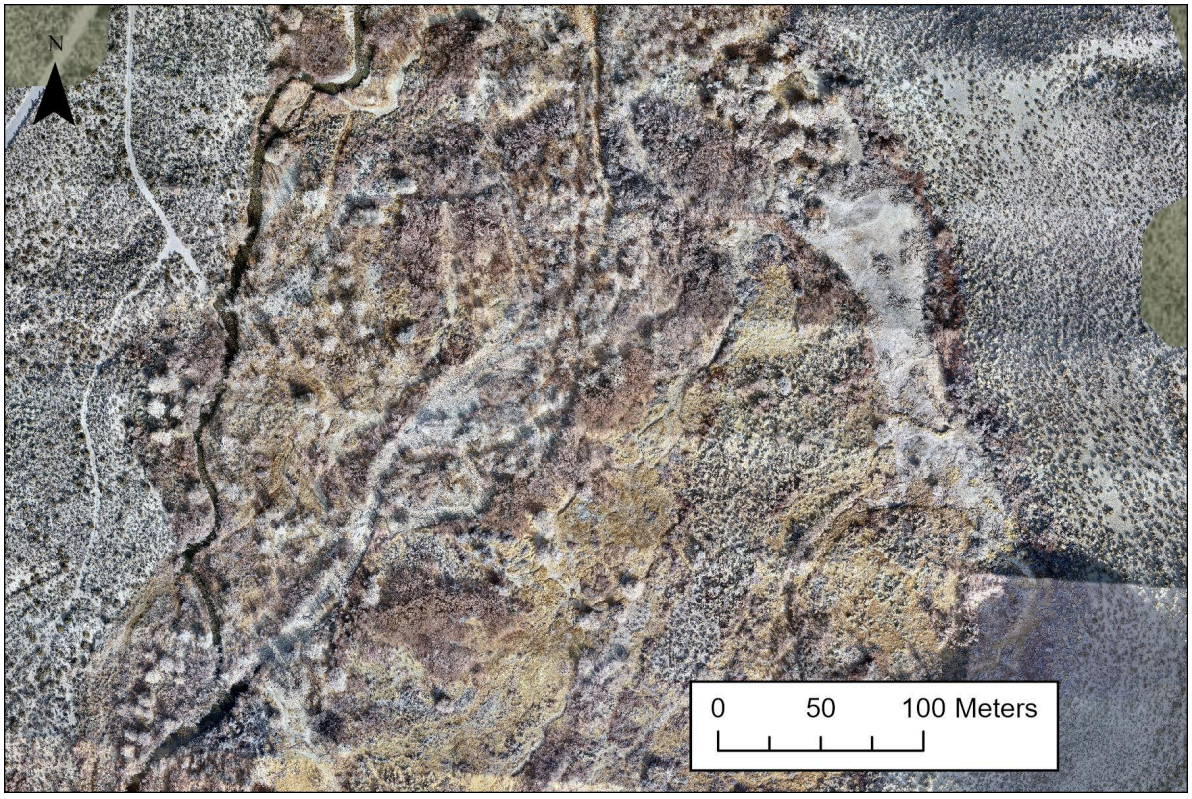

Figure 22. This photo is the same area as Figure 21 during November of 2024.

Land Cover

Digitizing for the 2004 Riparian Atlas images of the study area on Rush Creek has been completed (Figures 23, 24) and 1999 and 1929 images are in process.

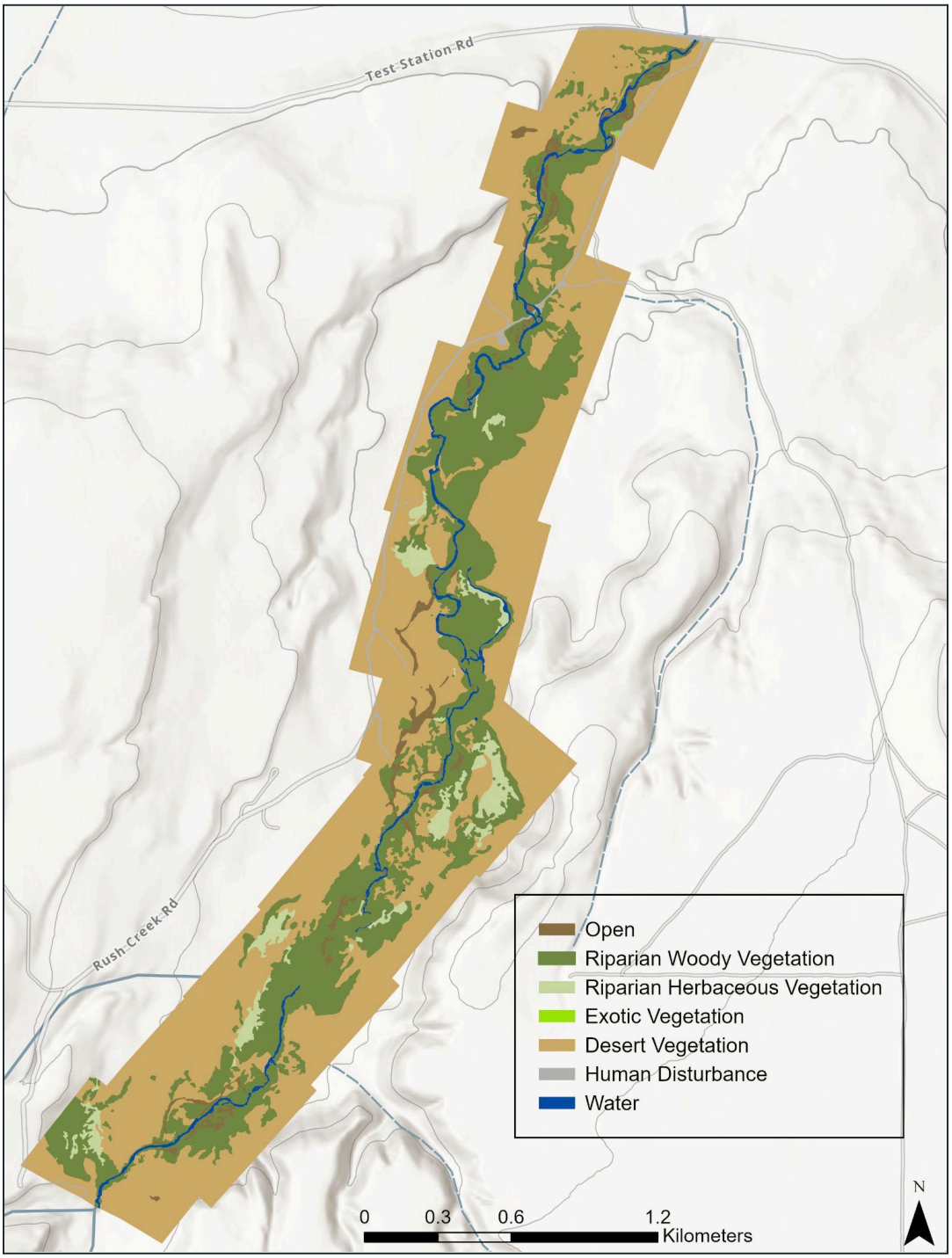

Figure 23. Digitized 2004 Rush Creek imagery from the intersection of Test Station road to the Narrows.

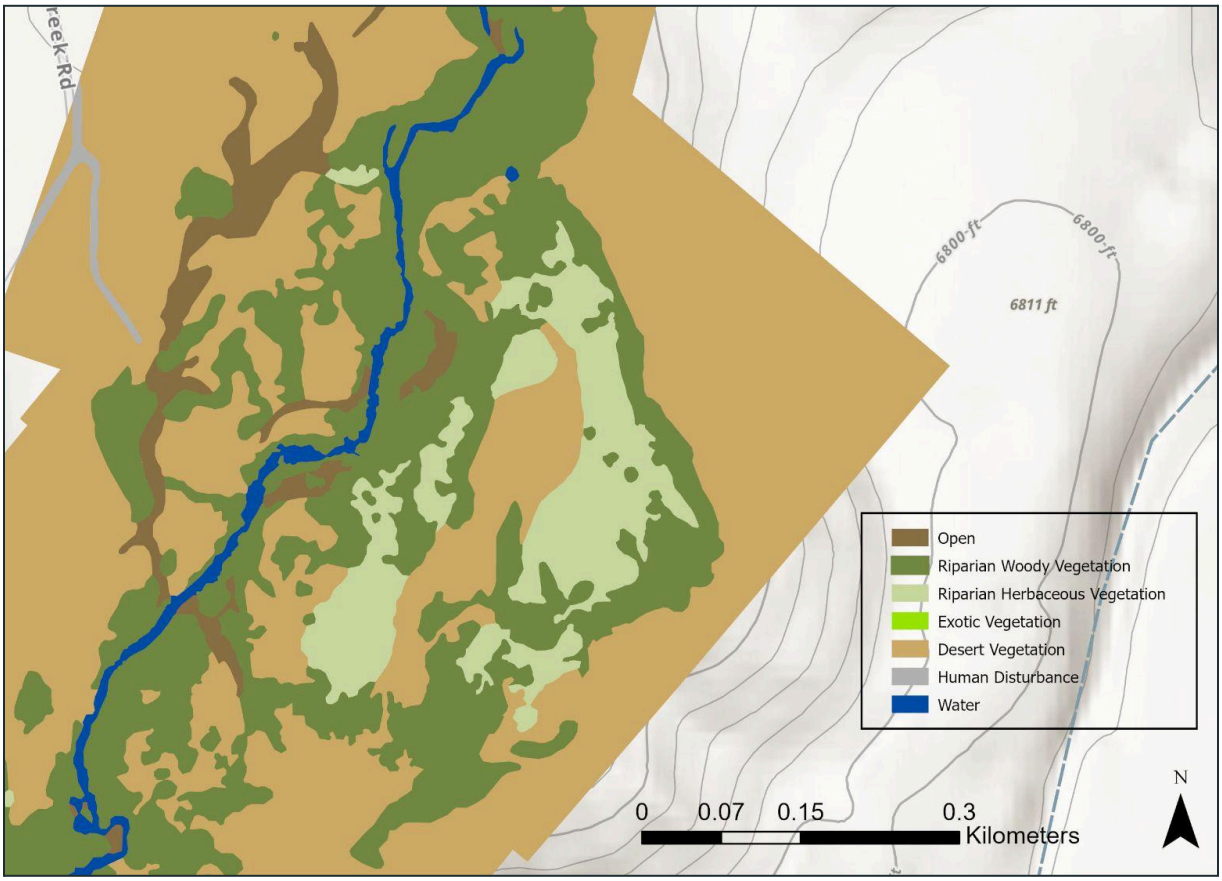

Figure 24. Section of the digitized 2004 Rush Creek imagery to show detail.

Ground Photography

Below are a few sample photos that were taken during the July 2024 trip. We plan to establish photo points for photo monitoring during the 2025 field season.

Figure 25. Photo of the main beaver dam from August, 2024.

Figure 26. This is a photo of one of the last remaining pine trees in this section of Rush Creek. Photos taken in August, 2024.

Discussion

Photogrammetry

The aerial photo data collected shows promise for land cover classification. Acquisition of infrared data should improve the classification. The best classification technique for the current high-resolution RGB aerial imagery is still being determined. Multiple classification techniques are being tested to determine which is the best for the study area and the high-resolution data collected, including Classification and Regression Trees (CART), object-based image analysis, traditional pixel-based image analysis, and machine learning algorithms. Preliminary CART model analysis has been performed, but model variables need to be adjusted in order to improve the accuracy of the classification.

Currently, we are surveying with a visible spectrum UAV (RGB or Red/Green/Blue) and with LiDAR. We have flown with an infrared sensor in the past which allows us to create indexes to analyze the health of vegetation including the Normalized Difference Vegetation Index (NDVI). These models can be used in riparian systems to determine the amount of erosion and deposition and movement of the stream channels over time.

For future flights, we will increase the overlap between the flights so we can remove distortions along the edges of the resulting images. This should allow for consistently high quality aerial photos of effectively any area.

LiDAR

The 2017 data missed a section of the riparian area near the wetland pond while the 2024 data had two gaps because the LiDAR flights did not have enough overlap. This needs to be addressed by having predefined polygons for each flight that covers the entire area and includes adequate overlap. Investigation is underway to remove the overall difference in elevation of the LiDAR datasets and we plan to test a new method in May of 2025.

Change Detection

The elevation models appear to be accurate to within 6” with some artifacts near vertical stream bed changes and where there is dense overstory. The change detection seems to be effective and we feel this can replace cross sectional surveys and can provide data on flood plain gain and loss. If LiDAR is flown at least once a year, the change in stream morphology could be directly related to annual stream flow.

Ground Surveys

Drone surveys were able to detect the land cover types except in those areas where dense canopy covered the land cover. LWD will also block the LiDAR pulses so it will appear as

ground. Some bushes were also so dense as to have the ground within the bush appear higher than actual. We may pursue on the ground surveying through the LWD and below dense canopies. Bushes within areas that become flooded may also be surveyed in the future if needed.

Ground surveys will also be required to determine the area of water, pool depths, RCT elevations, and water depth at RCT. Ground surveys will be needed to detect the width of the stream in areas where the canopy blocks visualizing the water from aerial photos.

Riparian Mapping

The invasive species along Rush Creek are minimal, making it difficult to identify in the high-resolution aerial imagery. During the 2024 flights, we identified a species of thistle growing within the main wetland area along Rush Creek. From the ford to the narrows, quantification of the invasive species will need to be determined by locating pockets of invasives during field work.

Remaining Questions

Below are the questions we feel will determine the type of monitoring that will be required in the future. This is largely based on what we can determine with aerial photography and LiDAR vs. on the ground surveying.

- Can we detect the water surface accurately? We believe this can be done in areas where the stream channels are visible from above but not under the canopy. We expect some level of surveying will be required to determine the location of residual ponds and the width of the stream channel.
- Can we detect the depth of water during dry periods? There are drones available now that use green lasers to penetrate the water surface. However, their depth is limited so surveying the depth of residual pools may be required long term.

Plans for the 2025/2026 Season

The next season will continue to focus on the Rush Creek riparian area from the ford to the narrows.

Goals for the next field season are to:

- Establish a series of benchmarks at high resolution for validation of drone data and to increase the efficiency of on the ground surveys.
- Collect ground truth data for land cover (inc. vegetation).
- Obtain a complete high resolution LiDAR dataset with enough overlap between flights to seamlessly combine the dataset and create complete DEMs and CHMs for additional analysis.

- Test the effectiveness of adding infrared data for land cover classification.
- Obtain a complete set of aerial photos of the study area during relatively high flows.
- Survey a sample of the RCT elevations, water depth at RCTs, water depth and wetted width for pools, and LWD below the canopy. This will be used to determine the long-term process for monitoring RCT elevations and residual pool depths.
- A secondary goal is to establish additional photo points.

Monitoring activities to achieve this will include:

- Flying drone surveys with photo sensors (RGB and IR) and LiDAR during the spring (high flow) and fall (low flow)
- Ground surveys with Emlid professional grade surveying equipment to include:
    - To geolocate existing benchmarks and establish new long-term benchmarks
    - Vegetation cover for modeling
    - RCT surveys for elevations and water depth at low flow
    - Wetted width below the canopy
    - LWD below the canopy
    - Pool depths at low flow
- Establishing photo points for repeat photography

We plan to perform field sampling in the spring during a high flow period and again in the fall during a low-flow period. We do not expect the equipment or methods to change significantly except as described to address issues pointed out in this report except that we plan to collect aerial data with a Mavic 3M. This will provide Near Infrared images which we believe will improve land cover classification.

Conclusion

This study has improved our knowledge of what can be active with modern technology to determine the dynamics of geomorphology and land cover for a section of Rush Creek. We have also continued to add to a growing archive of data on the area. The next two years will provide the results needed to determine the monitoring that is required for the riparian areas adjacent to Mono Lake.

Data Management

All data collected is maintained by the Institute for Spatial Analysis, Modeling and Monitoring at Cal Poly Humboldt (http://gis.humboldt.edu/isamm/). Dr. Jim Graham is the director of the institute. The data is stored on a secure Google Drive shared drive.

A website is in development to allow visualization of the spatial data at:

http://gis.humboldt.edu/websites/monolake/

Archives of the data are made periodically and backups are maintained by Cal Poly Humboldt's Information and Technology Services department.

References

Bannari, A., et al. "A Review of Vegetation Indices." Remote Sensing Reviews, vol. 13, no. 1–2, Aug. 1995, pp. 95–120. Taylor and Francis+NEJM, https://doi.org/10.1080/02757259509532298.

Bertacchi, Andrea, et al. "Using Unmanned Aerial Vehicles for Vegetation Mapping and Identification of Botanical Species in Wetlands." *Landscape and Ecological Engineering*, vol. 15, no. 2, Apr. 2019, pp. 231–40. *Springer Link*, https://doi.org/10.1007/s11355-018-00368-1.

Cardinale, Bradley J., et al. "Effects of Biodiversity on the Functioning of Trophic Groups and Ecosystems." *Nature*, vol. 443, no. 7114, Oct. 2006, pp. 989–92. *EBSCOhost*, https://doi.org/10.1038/nature05202.

Colvin, Susan A. R., et al. "Headwater Streams and Wetlands Are Critical for Sustaining Fish, Fisheries, and Ecosystem Services." *Fisheries*, vol. 44, no. 2, 2019, pp. 73–91. *Wiley Online Library*, https://doi.org/10.1002/fsh.10229.

Cruzan, Mitchell B., et al. "Small Unmanned Aerial Vehicles (Micro-UAVs, Drones) in Plant Ecology." *Applications in Plant Sciences*, vol. 4, no. 9, 2016, p. 1600041. *Wiley Online Library*, https://doi.org/10.3732/apps.1600041.

De Groot, Rudolf S., et al. "A Typology for the Classification, Description and Valuation of Ecosystem Functions, Goods and Services." *Ecological Economics*, vol. 41, no. 3, June 2002, pp. 393–408. *DOI.org (Crossref)*, https://doi.org/10.1016/S0921-8009(02)00089-7.

Gómez-Sapiens, Martha, et al. "Improving the Efficiency and Accuracy of Evaluating Aridland Riparian Habitat Restoration Using Unmanned Aerial Vehicles." Remote Sensing in

Ecology and Conservation, vol. 7, no. 3, 2021, pp. 488–503. Wiley Online Library, https://doi.org/10.1002/rse2.204.

Howland, William G. “Multispectral Aerial Photography for Wetland Vegetation Mapping.” *Photogrammetric Engineering and Remote Sensing*, vol. 46, no. 1, 1980, pp. 87–99.

Huylenbroeck, Leo, et al. “Using Remote Sensing to Characterize Riparian Vegetation: A Review of Available Tools and Perspectives for Managers.” *Journal of Environmental Management*, vol. 267, Aug. 2020, p. 110652. *DOI.org (Crossref)*, https://doi.org/10.1016/j.jenvman.2020.110652.

Johnson, R. Roy, and Dale A. Jones. *Importance, Preservation and Management of Riparian Habitat: A Symposium; Tucson, Arizona; July 9, 1977*. General Technical Report, RM-43, USDA Forest Service, 1977.

Knight, Allen W., and Richard L. Bottorff. “The Importance of Riparian Vegetation to Stream Ecosystems.” *California Riparian Systems*, edited by Richard E. Warner and Kathleen M. Hendrix, DGO-Digital original, 1, University of California Press, 1984, pp. 160–67. *JSTOR*, https://doi.org/10.2307/jj.8501409.25.

Kominoski, John S., et al. “Forecasting Functional Implications of Global Changes in Riparian Plant Communities.” *Frontiers in Ecology and the Environment*, vol. 11, no. 8, 2013, pp. 423–32.

Los Angeles Department of Water and Power. *Mono Basin Stream & Stream Channel Restoration Plan*. 29 Feb. 1996, https://www.monobasinresearch.org/legal/1996streamplan.pdf.

McBain & Trush, Inc. and Ross Taylor and Associates. Synthesis of Instream Flow Recommendationsto the State Water Resources Control Board and the Los Angeles Department of Water and Power. 30 Apr. 2010, https://citeseerx.ist.psu.edu/document?repid=rep1&type=pdf&doi=fa3c7813090c346911ca34dc92ba5063b94db7ea.

Mono Basin Research Group. “Ecological Study of Mono Lake.” *12*, vol. Institute of Ecology, June 1977, https://monobasinresearch.org/onlinereports/1976study/ecologicalstudyofmonolake.pdf.

Moyle, Peter B., and Paul J. Randall. “Evaluating the Biotic Integrity of Watersheds in the Sierra Nevada, California.” *Conservation Biology*, vol. 12, no. 6, 1998, pp. 1318–26.

Naiman, Robert J., et al. *Riparia: Ecology, Conservation, and Management of Streamside Communities*. Elsevier, 2010. *Google Scholar*, https://books.google.com/books?hl=en&lr=&id=n6i_2G2f2KAC&oi=fnd&pg=PR11&dq=Riparia:+ecology,++conservation,+and+management+of+streamside+commun&ots=PkM37PAisl&sig=5luKnm23C537YM9OxxGA-8wvTVA.

National Research Council. *The Mono Basin Ecosystem: Effects of Changing Lake Level*. National Academies Press, 1987, p. 1007. *DOI.org (Crossref)*, https://doi.org/10.17226/1007.

Norman, Laura, et al. “Remote Sensing Analysis of Riparian Vegetation Response to Desert Marsh Restoration in the Mexican Highlands.” *Ecological Engineering*, vol. 70, Sept. 2014, pp. 241–54. *DOI.org (Crossref)*, https://doi.org/10.1016/j.ecoleng.2014.05.012.

Smith, Stanley D., et al. “Functional Responses of Riparian Vegetation to Streamflow Diversion in the Eastern Sierra Nevada.” *Ecological Applications*, vol. 1, no. 1, 1991, pp. 89–97. *JSTOR*, https://doi.org/10.2307/1941850.

Song, Fei, et al. “UAV Quantitative Remote Sensing of Riparian Zone Vegetation for River and Lake Health Assessment: A Review.” *Remote Sensing*, vol. 16, no. 19, Sept. 2024, p. 3560. *DOI.org (Crossref)*, https://doi.org/10.3390/rs16193560.

Srivastava, Diane S., and Mark Vellend. “Biodiversity-Ecosystem Function Research: Is It Relevant to Conservation?” *Annual Review of Ecology, Evolution, and Systematics*, vol. 36, no. 1, Dec. 2005, pp. 267–94. *DOI.org (Crossref)*, https://doi.org/10.1146/annurev.ecolsys.36.102003.152636.

State Water Resources Control Board. *Mono Lake Basin Water Right Decision 1631*. 28 Sept. 1994.

Stine, Scott, et al. “Destruction of Riparian Systems Due to Water Development in the Mono Lake Watershed.” *California Riparian Systems*, edited by Richard E. Warner and Kathleen M. Hendrix, DGO-Digital original, 1, University of California Press, 1984, pp. 528–33. *JSTOR*, https://doi.org/10.2307/jj.8501409.73.

Taylor, Dean William. *Riparian Vegetation of the Eastern Sierra: Ecological Effects of Stream Diversions*. Mono Basin Research Group, 1982.

Ullah, Hameed, et al. “Vegetation Assessments under the Influence of Environmental Variables from the Yakhtangay Hill of the Hindu-Himalayan Range, North Western Pakistan.” *Scientific Reports*, vol. 12, no. 1, Dec. 2022, p. 20973. *www.nature.com*, https://doi.org/10.1038/s41598-022-21097-4.

Uyeda, Kellie A., et al. “Vegetation Mapping Using Hierarchical Object-based Image Analysis Applied to Aerial Imagery and Lidar Data.” *Applied Vegetation Science*, vol. 23, no. 1, Jan. 2020, pp. 80–93. *EBSCOhost*, https://doi.org/10.1111/avsc.12467.

Virah-Sawmy, Malika, et al. “How Does Spatial Heterogeneity Influence Resilience to Climatic Changes? Ecological Dynamics in Southeast Madagascar.” *Ecological Monographs*, vol. 79, no. 4, 2009, pp. 557–74. *Wiley Online Library*, https://doi.org/10.1890/08-1210.1.

Wang, Cheng, et al. *Introduction to LiDAR Remote Sensing*. CRC Press, 2024.

Wilson, Natalie R., and Laura M. and Norman. “Analysis of Vegetation Recovery Surrounding a Restored Wetland Using the Normalized Difference Infrared Index (NDII) and Normalized Difference Vegetation Index (NDVI).” International Journal of Remote Sensing, vol. 39, no. 10, May 2018, pp. 3243–74. Taylor and Francis+NEJM, https://doi.org/10.1080/01431161.2018.1437297.

Wilson, Lucy, et al. “Mapping Restoration Activities on Dirk Hartog Island Using Remotely Piloted Aircraft Imagery.” *Remote Sensing*, vol. 14, no. 6, 6, Jan. 2022, p. 1402. *www.mdpi.com*, https://doi.org/10.3390/rs14061402.

Section III. Mono Lake Limnological Monitoring 2024 Annual Report

Prepared by Robert Jellison, Caroline Vignardi, and John M. Melack

2024 Annual Report

Mono Lake Limnological Monitoring

Robert Jellison, Caroline Vignardi, and John M. Melack

Earth Research Institute

University of California

Santa Barbara, CA 93106

Submitted to:

Los Angeles Department of Water and Power

<date>

TABLE OF CONTENTS

LIST OF TABLES

LIST OF FIGURES

CHAPTER 1
INTRODUCTION

Saline lakes are widely recognized as productive aquatic habitats, that harbor distinctive assemblages of species and often support large populations of resident or migratory birds. Saline lakes throughout the world are threatened by decreasing size and increasing salinity due to climate changes and diversions of freshwater inflows for irrigation and other human uses. At Mono Lake, California, diversions of freshwater streams out of the basin beginning in 1941 led to a decline in surface elevation and an increase of the lake's salinity. In 1994, the State Water Resources Control Board (SWRCB) of California issued a decision to amend Los Angeles' water rights (Decision 1631) by restricting water diversions until the surface elevation of the lake reached 1,948 m (6392 ft).

Long-term monitoring of the plankton and their physical, chemical, and biological environment is essential to understanding the effects of changing lake levels and salinities and has been mandated by the SWRCB. Measurements of the vertical distribution of temperature, dissolved oxygen, conductivity, and nutrients are requisite for interpreting how variations in these variables affect the plankton populations. The limnological monitoring program at Mono Lake includes the collection and interpretation of limnological data.

This report fulfills the requirements for limnological monitoring of Mono Lake set forth in State Water Resources Control Board Order Nos. 98-05 and 98-07. The limnological monitoring program consists of four components: meteorological, physical and chemical, phytoplankton, and brine shrimp populations. Meteorological data are collected with sensors on Paoha Island, while the other three components are assessed during monthly surveys (except when the lake is inaccessible in winter). The methodology employed is detailed in Chapter 2, and results obtained during 2024 are presented in Chapter 3. In Chapter 4 we use measurements made with sensors suspended in Mono Lake to provide further analyses of stratification and mixing, and related variations in dissolved oxygen and chlorophyll fluorescence. We also present results from a series of experiments done to develop a method for estimates of primary production by phytoplankton using changes in dissolved oxygen.

This work was supported by a contract from the National Fish and Wildlife Foundation with funds from the Los Angeles Department of Water and Power (LADWP) to J. M. Melack at the Earth Research Institute, University of California, Santa Barbara. Laboratory work was performed at the Sierra Nevada Aquatic Research Laboratory, University of California.

CHAPTER 2
METHODS

Meteorology

Meteorological measurements are recorded at a station located on the southwestern shore of Paoha Island at 1948 m elevation (Fig. 1**Error! Reference source not found.**), approximately 2 meters above the current elevation of the lake. Samples are collected at 1-minute intervals, with data logged every 5 minutes and stored on an Onset RX3004 logger; data are uploaded to HOBOlink web-based software at cellular connection intervals of 1 hour. The meteorological station was installed on 30 May 2023.

Wind speed and direction are measured at a height of 3 m above the surface of the island with an R.M. Young wind monitor (model 5103 with threshold of 1 m s^{-1} for propeller and 1.1 m s^{-1} for vane and accuracy of ±0.3 m s^{-1} or 1% of reading, and ±3° for wind direction). Mean wind speed and direction and maximum wind speed during each five-minute interval are recorded. Additional measurements include photosynthetically available radiation (PAR, spectral range 400 to 700 nm, Onset sensor S-LIA-M003 with a resolution of 2.5 µmol m^{-2} s^{-1} and accuracy of ±5 µmol m^{-2} s^{-1}), solar radiation (spectral range 300 to 1100 nm, Onset sensor S-LIB-M003 with resolution of 1.25 W m^{-2} and accuracy of ±10 W m^{-2} or ±5%, if greater), barometric pressure (Onset sensor S-BPM-CM50 with resolution of 0.01 mbar and accuracy of ±3.0 mbar), and relative humidity (RH) and air temperature (Onset sensor S-THC with a resolution of 0.02 °C and of 0.01% for RH, and accuracy of ±0.25 °C and ±2.5% from 10% to 90% RH or ±5% below 10% and above 90% RH). Rainfall rates and cumulative amounts are obtained with an unheated tipping bucket gauge (Onset sensor S-RGB-M002 with a resolution of 0.2 mm, and 1% accuracy for rainfall rates up to 12.7 cm h^{-1}).

Sampling Regime

The limnological monitoring program in 2024 included monthly surveys from March through December; the boat launch site was not accessible in February. Surveys include sampling at 12 stations (Fig. 1) over one or two days depending on the weather conditions. When conducted over two days, lakewide surveys and Station 6 profiles are conducted on consecutive days, when possible.

Fig. 1. Sampling stations on Mono Lake. Red points and numbers indicate permanently moored buoys, + sign indicates location of Paoha Island meteorological Station. Depth contours are in meters.

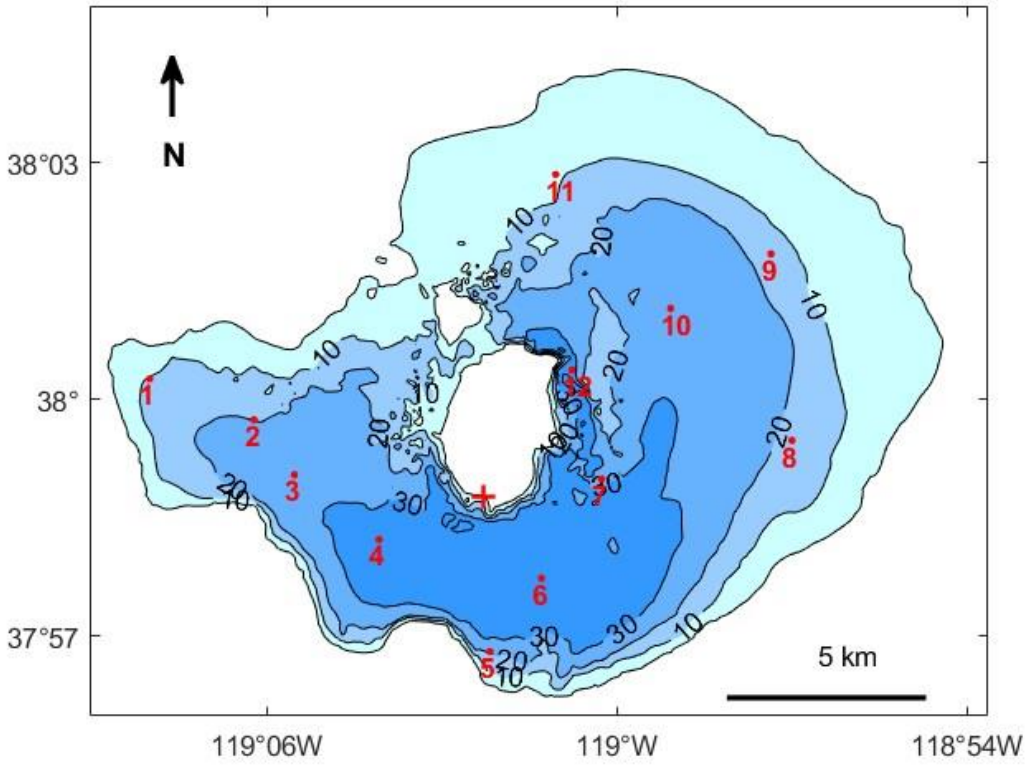

Field Procedures

In Situ Profiles

Depth, water temperature, conductivity, dissolved oxygen, fluorescence and turbidity are measured at twelve buoyed stations with a free-falling profiler (Rinko profiler model ASTD 102 with extended conductivity range): depth, resolution 0.02 m and accuracy ±0.3%; temperature, resolution 0.001 °C and accuracy ±0.01 °C; conductivity, resolution 0.001 mS cm^{-1} and accuracy ±0.01 mS cm^{-1}; dissolved oxygen, resolution 0.01 mg L^{-1} and accuracy ±2%. The Rinko oxygen probe is calibrated against Miller titrations (Walker et al. 1970) of Mono Lake water at a range of salinities. Fluorescence outputs require calibration for conditions in Mono Lake to correct readings for chlorophyll.

The profiler is lowered at a rate of ~0.2 m s^{-1} and sampled at 100-ms intervals or approximately every 2 cm. Pressure readings are converted to depth using ambient air pressure at

the time of readings and the density profile based on in-situ temperature and salinity. Relationships between conductivity, temperature, salinity, and density for the chemical composition of Mono Lake are given by Jellison et al. (1999a, b). Conductivity readings at in-situ temperatures (C_t) are converted to specific conductance at 25 °C (C_{25}) using:

$$C_{25} = \frac{C_t}{1 + 0.02124(t-25) + 9.16\times10^{-5}(t-25)^2}$$

where t is the in-situ temperature. The density of Mono Lake water is given by:

$$\rho(t, C_{25}) = 1.0034 + 1.335\times10^{-5}t - 6.20\times10^{-6}t^2 + 4.897\times10^{-4}C_{25} + 4.23\times10^{-6}C_{25}^2 - 1.35\times10^{-6}tC_{25}$$

Total dissolved solids derived from conductivity for Mono Lake water is given by:

$$TDS(g\ kg^{-1}) = 3.386 + 0.564\times C_{25} + 0.00427\times C_{25}^2.$$

To obtain TDS in grams per liter, the above expression was multiplied by the density at 25 °C for a given standardized conductivity given by:

$$\rho_{25}(C) = 0.99986 + 5.2345\times10^{-4}C + 4.23\times10^{-6}C^2$$

Mono Lake often has strong vertical temperature and salinity gradients. A mismatch in sensor time constants or water parcel sampled by the thermistor and conductivity electrode will result in spiking. While the time constants for the Rinko thermistor and conductivity electrodes are both listed by the manufacturer as 0.2 s, laboratory experiments indicated thermistor and conductivity electrode time constants of 0.14 s and 0.05 s, respectively. Conductivity spiking was examined after shifting the temperature readings by 0, 0.1, 0.2, 0.3, 0.4, and 0.5 s relative to conductivity in profiles over the course of the year, with a 0.2 s shift providing the least amount of spiking. Therefore, temperature readings were shifted by 0.2 s when calculating standardized (25 °C) conductivity. Depending on the details of each profile spiking may still occur after accounting for the difference in sensor response times; spikes were removed by visually inspecting each profile and then conductivity readings were further smoothed by a 6-point (~0.12 m) moving average.

Time-series measurements of water temperature are obtained with RBR Solo® thermistors (accuracy 0.002 °C) sampling every ten seconds and deployed on moorings at Stations 3 and 6. Uppermost thermistors were suspended below and shaded by a surface float,

and deeper ones were on a taut-line mooring suspended from a float ~0.5 to 1 m below the water surface. Moored RBR Concerto^3 conductivity-temperature-depth sensors, PME MiniDOT optical dissolved oxygen sensors with wipers to remove biofouling, and Turner C-Fluor chlorophyll sensors with wipers to remove biofouling are deployed on the mooring lines at several depths.

Transparency is estimated as the depth a white Secchi disc, 20 cm in diameter, is visible, viewed on the shaded side of the boat to avoid glare, and, under calm conditions, if possible.

Vertical profiles of photosynthetically active radiation (400 to 700 nm, PAR) were obtained using a Licor LI-192 SB underwater sensor, and the attenuation coefficient of PAR was computed from the profiles.

Water Samples

Samples for chlorophyll and ammonium analyses are collected from nine discrete depths (0.2, 2, 8, 12, 16, 20, 24, 28, and 35 m) at Station 6, and with a 0 to 9 m integrating tube sampler at seven Stations (1, 2, 5, 6, 7, 8, and 11). Samples for ammonium analyses are filtered immediately upon collection through Gelman A/E glass-fiber filters and kept chilled and dark until returned to the laboratory. Water samples used for analysis of chlorophyll are filtered through a 120-µm sieve to remove all stages of *Artemia* and kept chilled and dark until filtered in the laboratory.

Artemia Samples

Artemia are sampled by one net tow at each of the twelve, buoyed stations. Samples are taken with a plankton net (1 m x 0.30 m diameter, 120-µm Nitex mesh) towed vertically through the water column. Samples are preserved with 5% formalin in lake water. When adults are present, an additional net tow is taken from Stations 1, 2, 5, 6, 7, 8, and 11 to collect adult females for brood size and length analysis. A net efficiency factor of 70% was used (Lenz 1984).

Laboratory Procedures

Water Samples

Samples are returned to the laboratory and within 7 hours of collection are analyzed for ammonium and filtered for subsequent chlorophyll determinations. Chlorophyll samples are filtered onto 47 mm Whatman GF/F filters and kept frozen until the pigments are analyzed within one to two weeks.

Filters for chlorophyll *a* analyses are homogenized in 90% acetone and extracted at room temperature in the dark. Following clarification by centrifugation, absorption is measured at 750 and 663 nm on a spectrophotometer (Abbott Corporation, model SV1100D spectrophotometer). The sample is then acidified in the cuvette, and absorption again determined at the same wavelengths to correct for phaeopigments. Absorptions were converted to phaeophytin-corrected chlorophyll *a* concentrations with the formula (Golterman & Clymo, 1969):

$$Chl_s = 27.46[(A663_0 - A750_0) - 1.054(A663_a - A750_a)]1000v/V$$

where:

Chl_S = chlorophyll *a* concentration of sample (µg L^{-1})
$A663_0$ = absorption at 663 nm before acidification
$A750_0$ = absorption at 750 nm before acidification
$A663_a$ = absorption at 663 nm after acidification
$A750_a$ = absorption at 750 nm after acidification
v = Volume of extract (mL)
V = Volume of filtered water (mL)
1.054 = volume correction after addition of 200 µL acid

During periods of low phytoplankton concentrations (<5 µg chl *a* L^{-1}), fluorescence of extracted pigments is measured on a fluorometer (Turner Designs, model TD-700) calibrated using dilutions of samples measured spectrophotometrically. Fluorometric determination of chlorophyll *a* is obtained with the formula:

$$Chl_s = [(\tau/\tau - 1)(R_0 - R_a)]/(v/V)$$

where:

Chl_s = Chlorophyll *a* concentration of the sample (µg L^{-1})
τ = ratio of standard R_b/R_a
R_0 = before acid fluorometer reading (µg L^{-1})
R_a= after acid fluorometer reading of sample (µg L^{-1})
v = volume extracted (mL)
V = volume filtered (mL)

Ammonium concentrations are measured using the indophenol blue method (Strickland & Parsons 1972). Internal standards are used to account for matrix effects in Mono Lake water.

Artemia Samples

Artemia are counted under a stereomicroscope (6x or 12x power). Depending on the number of shrimp, counts are made of the entire sample or of subsamples made with a Folsom plankton splitter. Samples are split such that a count of >100 animals are obtained. Shrimp are classified into adults (instars > 12), juveniles (instars 8–11), and nauplii (instars 1–7) according to Heath's classification (Heath 1924). Adults are sexed and adult females divided into ovigerous and non-ovigerous. Adult ovigerous females are further classified according to their reproductive mode, ovoviviparous or oviparous. A small percentage of ovigerous females are unclassifiable if eggs are in an early developmental stage. Nauplii at seven stations (Stations 1, 2, 5, 6, 7, 8, and 11) are further classified into distinct instars 1–7.

Live females collected for brood size and length analysis are kept cool and in low densities during transport to the laboratory. Immediately on return to the laboratory, females are randomly selected, isolated in individual vials, and preserved. Brood size is determined by counting the number of eggs in the ovisac including those dropped in the vial, and egg type and shape are noted. Female length (mm) is measured from the tip of the head to the end of the caudal furca (setae not included).

Artemia biomass (dry weight) is obtained from the whole sample or first split of counted samples by drying at 60 °C for 48 h.

CHAPTER 3
RESULTS AND DISCUSSION

Surface Elevation

Snowmelt runoff, climatic conditions and diversion policies in 2024 resulted in ~1 ft surface elevation rise from 6383.15 ft on 1 January 2024 to 6384.1 ft on 1 July 2024 (Fig. 2, Mono Lake Committee, pers. comm.). This was followed by a steady decline from 1 August to 6382.9–6383.0 ft in December. This contrasts sharply with 2023 when exceptional runoff led to a 4.6 ft (1.4 m) rise in surface elevation and the onset of a period of meromixis (persistent salinity stratification).

Fig. 2. Mono Lake surface elevation, 2024 (ft asl, USGS datum)

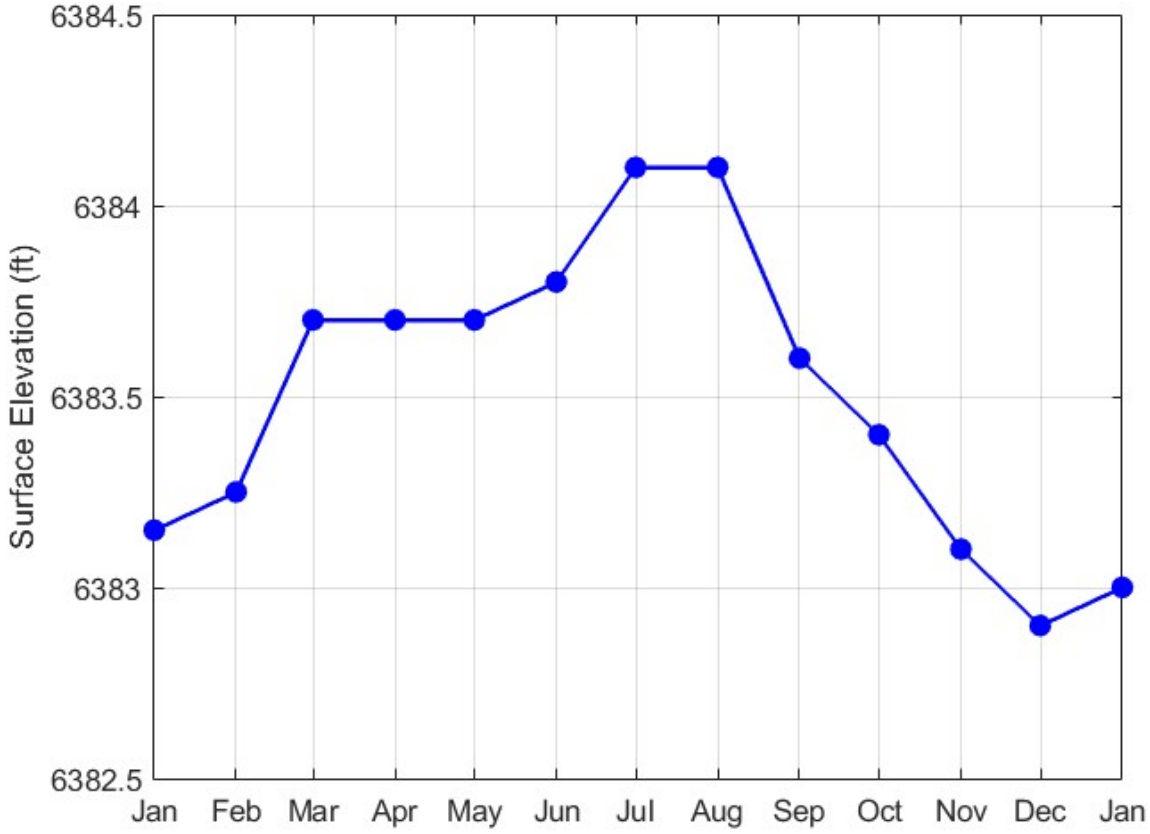

Meteorological Data

Wind Speed and Direction

Wind has strong diel variation in the Mono Basin with WSW winds increasing in the afternoon. Daily minimum wind speed only exceeded 1 m s^{-1} on 7 days. Exceptionally high hourly mean wind speeds of 17.7 m s^{-1} were observed on 3 March when gusts up to 23.7 m s^{-1} were recorded (Fig. 3). There were several other periods of sustained high winds, most notably in November and December. Winds were predominately from the west southwest (Fig. 4).

Fig. 3. Hourly mean wind speed (m s^{-1}), 2024.

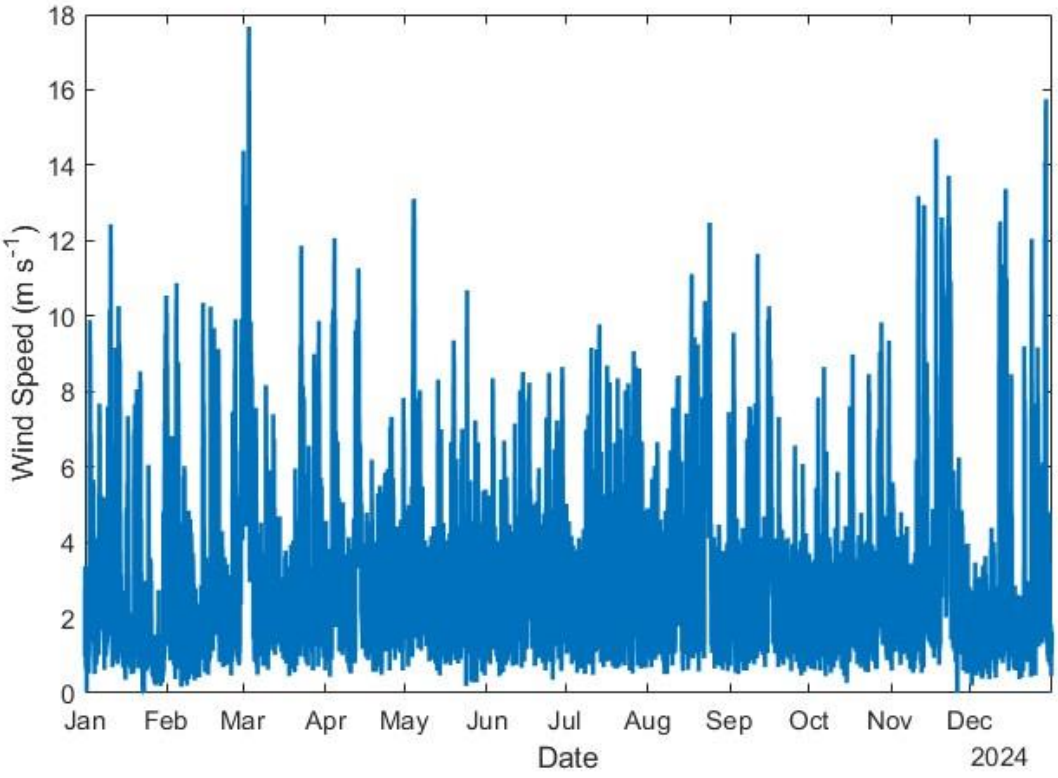

Fig. 4. Wind rose of hourly mean direction and speed, 2024.
Colors denote wind speeds in m s^{-1}. Percentages refer to the proportion of time spent in each 10-degree wind direction sector.

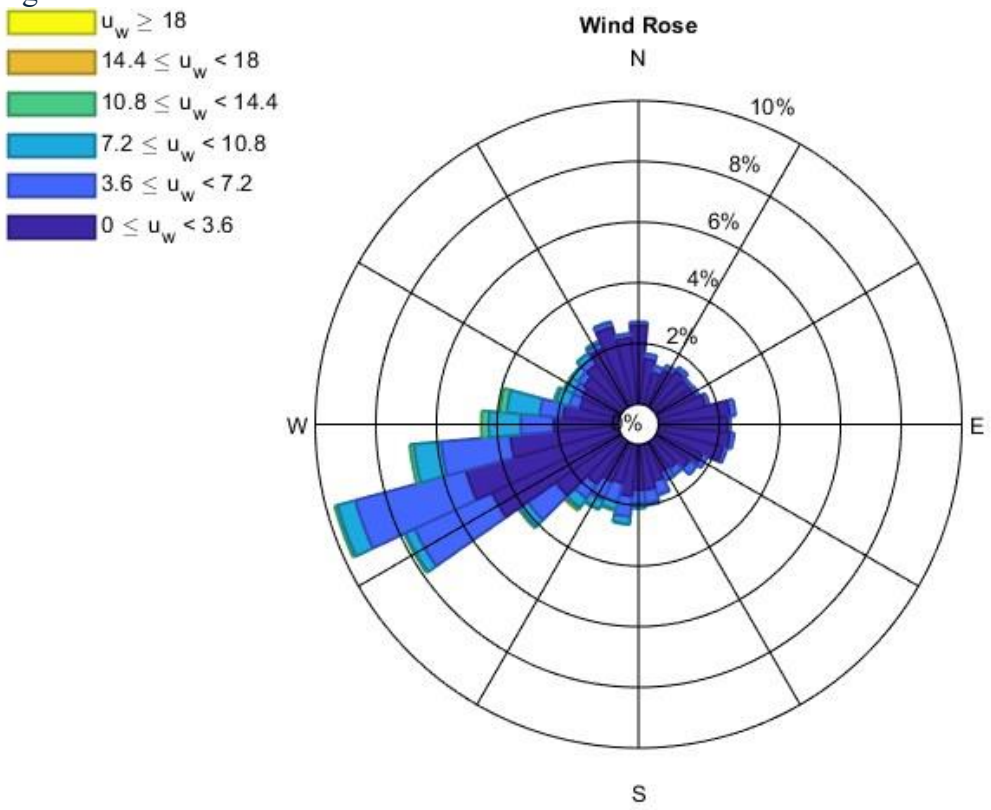

Air Temperature

Hourly mean air temperatures generally ranged from ~10 to 30 °C in summer with several periods with highs of 30 to 34 °C in midsummer (Fig. 5). Winter hourly temperatures were typically ~-5 to 10 °C, with exceptionally cold temperatures (-5 to -10 °C) occurring briefly in each of January, February, and December.

Fig. 5. Hourly mean air temperatures (°C) at Paoha Island, 2024.

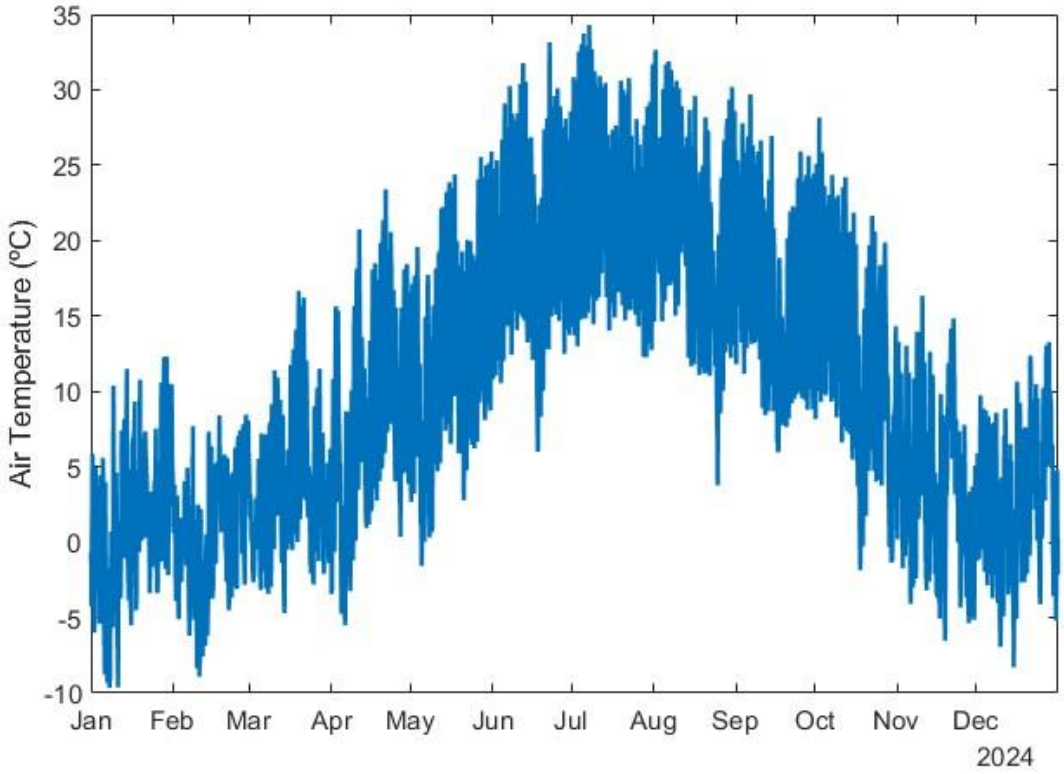

Incident Photosynthetically Available Radiation (PAR)

Daily values of photosynthetically available radiation under clear skies range from about ~19 Einsteins m^{-2} day^{-1} at the winter solstice to ~64 Einsteins m^{-2} day^{-1} mid-June (Fig. 6). However, daily values are reduced during cloudy periods. During 2024, the annual mean was 38.7 Einsteins m^{-2} day^{-1}, with daily values ranging from 2.5 Einsteins m^{-2} day^{-1} on 4 February to 65.0 Einsteins m^{-2} day^{-1} on 14 June.

Fig. 6. Daily photosynthetically available radiation, 2024.

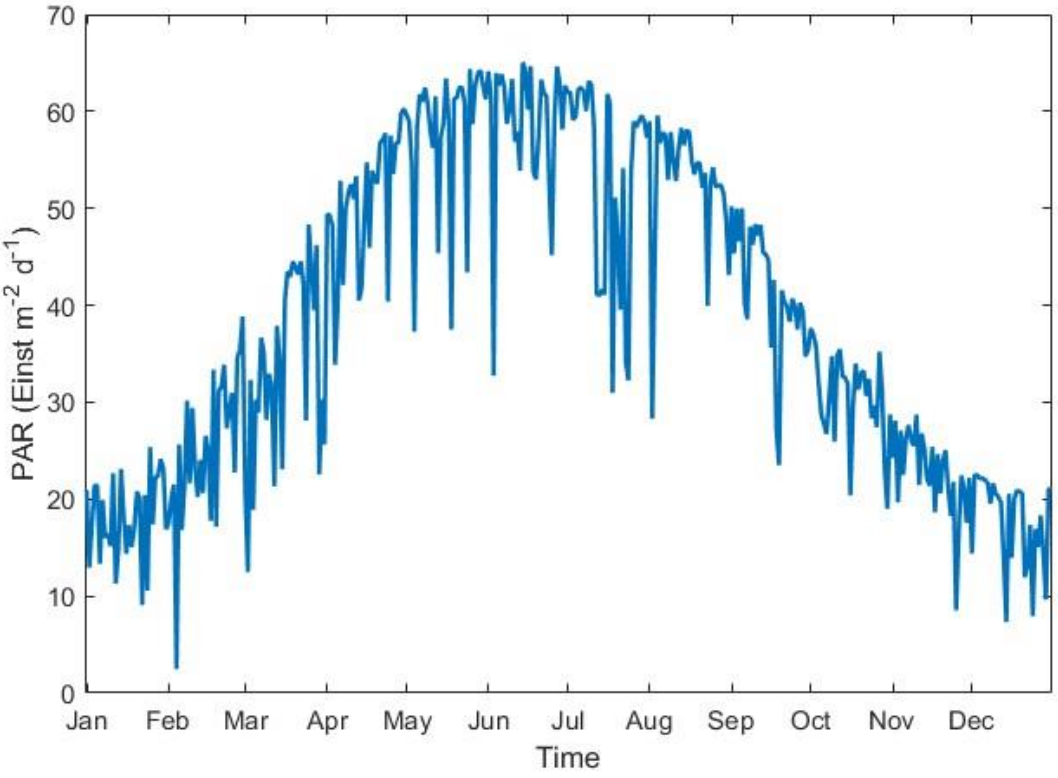

Relative Humidity and Precipitation

A general pattern in relative humidity of mostly 30–60% in summer and mostly 60–80% in winter was observed (Fig. 7). Mean daily relative humidity values ranged from 28% on 17 June to 98% on 4 February.

Fig. 7. Mean daily relative humidity (%), 2024.

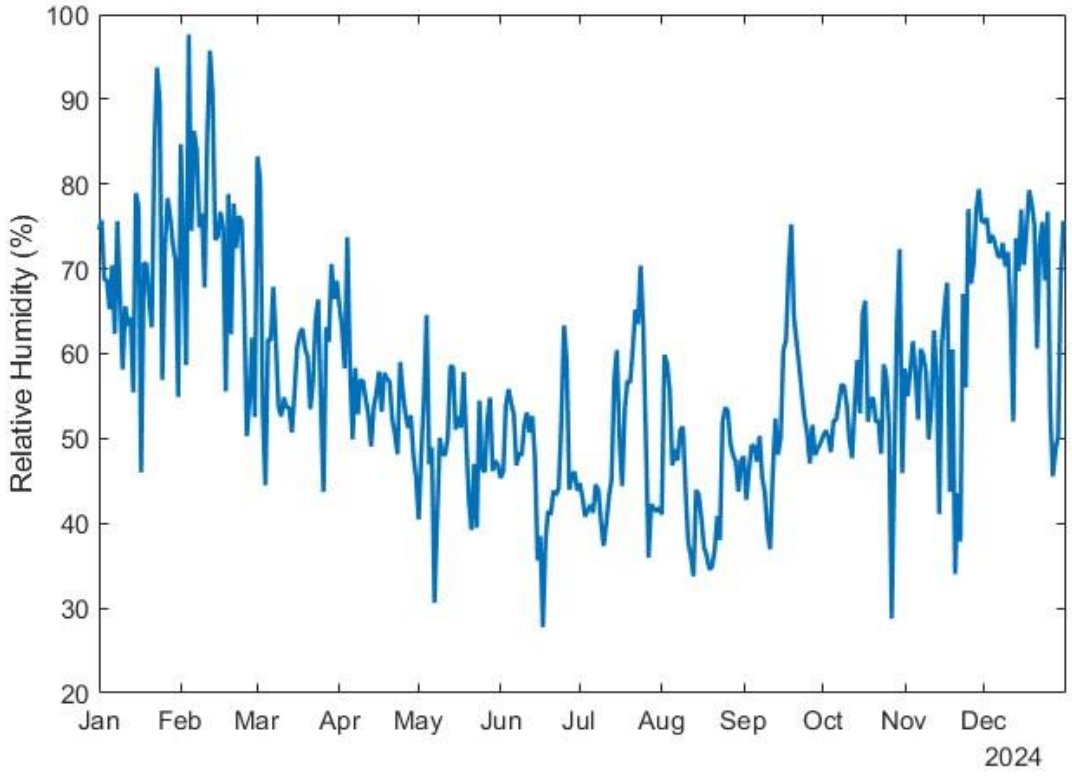

Paoha Island, located in the Sierra Nevada rain shadow, received 113 mm (4.45 in) of rain in 2024. A storm on 22 July brought 38.6 mm, while events on 19 February (23.4 mm) and 26 November (9.4 mm) added another third of the annual total (Fig. 8).

Fig. 8. Daily precipitation (mm) at Paoha Island, 2024.

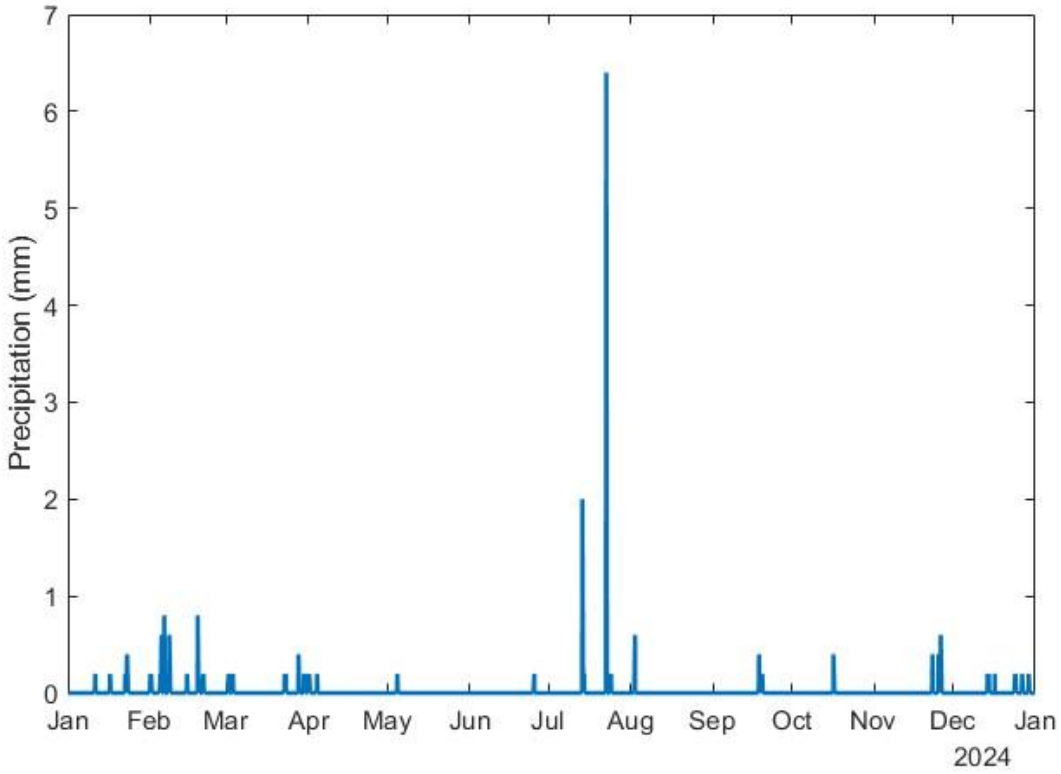

Water temperatures

Seasonal thermal stratification

The annual pattern of thermal stratification in Mono Lake results from seasonal variations in climatic factors (e.g., air temperature, solar radiation, wind speed, humidity) and their interaction with density stratification arising from the timing and magnitude of freshwater inputs. The typical annual pattern observed for large temperate lakes differs from that in hypersaline Mono Lake due to the absence of ice cover, unique temperature-density properties, and variations in salinity. In Mono Lake, a winter period of circulation, which varies in depth, typically extends from late November to early February after which seasonal thermal and salinity stratification are altered due to increased insolation and increased freshwater inflows. Six episodes of persistent stratification (meromixis) have occurred since 1982 (1983–1988, 1994–2003, 2005–2007, 2010–2012, 2017–2020, 2023–present) when vertical salinity gradients arose from above average snowmelt runoff and increased freshwater inflows. During 2021 through 2022 winter holomixis (full water column circulation) occurred. In late 2022, partial mixing of

upper waters into the hypolimnion occurred between November and December but a period of complete mixing did not occur and a 6th episode of meromixis has been initiated in 2023.

At centrally-located Station 6, water temperatures within the mixolimnion varied from approximately 4.4 °C on 13 March to approximately 22.3 °C on 18 July, before decreasing to approximately 4.4 °C on 19 December 2024 (Table 1, Fig. 9). Temperatures within the deep monimolimnion increased slightly from approximately 2.7 °C on 13 March to approximately 3.4 °C on 19 December 2024, indicating some vertical mixing or the possibility of deep spring inputs. Temperatures in the upper mixed layer increased ~4 °C between the March and April surveys. The depth of the thermocline (> 1 °C m^{-1}) increased from 9 m in mid-May to 12 m by mid-October. Cooling between October and November surveys resulted in further deepening of the top of the thermocline ~15 m. On the 19 December survey, the thermocline was at 15–16 m and coincided with the chemocline.

Fig. 9. Seasonal water temperatures (°C) at Station 6, 2024 (white triangles indicate thermistor chain data, red triangles indicate CTD surveys). Daily averaged temperature data from a permanently moored thermistor chain (see Chapter 4) were used to determine temperature change early in the year before the 1st survey conducted on 13 March 2024.

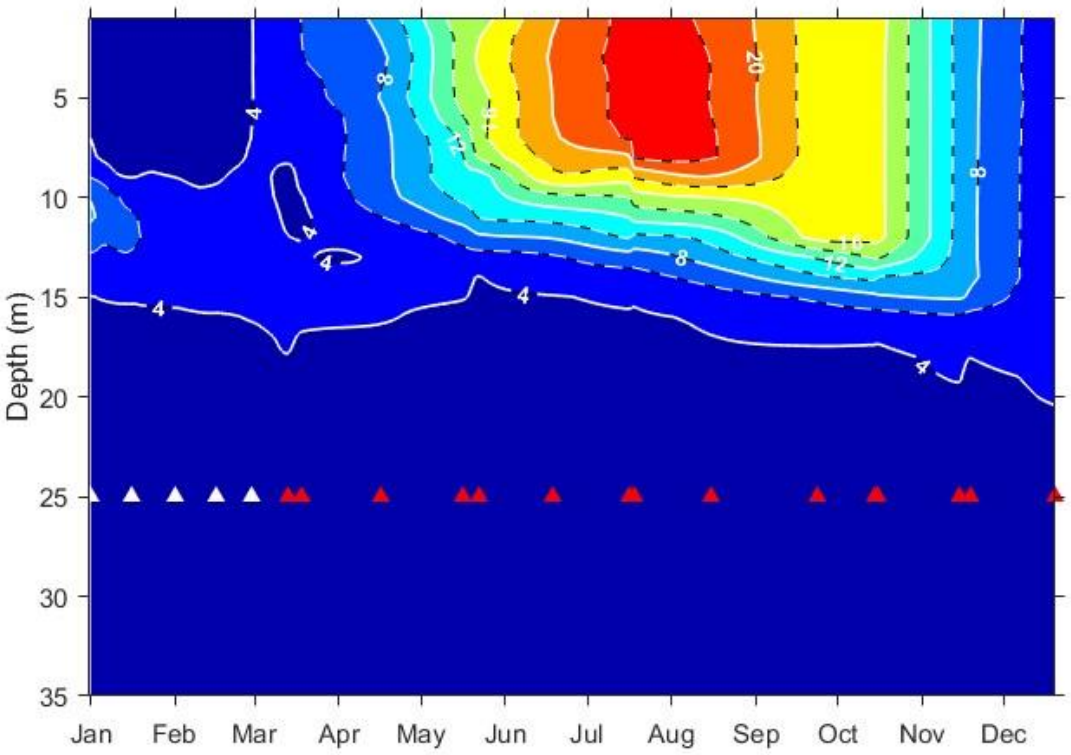

Table 1. Temperature (°C) at Station 6, March–December, 2024.

Depth (m)	3/13	4/16	5/16	6/18	7/18	8/15	9/23	10/14	11/18	12/19
1	4.5	8.7	15.3	19.7	22.3	21.7	17.2	16.6	8.5	4.5
2	4.4	8.1	14.7	20.0	22.3	21.8	17.2	16.5	8.5	4.4
3	4.4	7.6	14.8	20.2	22.3	22.0	17.2	16.5	8.5	4.4
4	4.4	7.8	14.9	20.1	22.4	22.0	17.2	16.5	8.4	4.5
5	4.4	8.1	14.6	20.0	22.4	21.9	17.2	16.5	8.4	4.6
6	4.4	7.6	13.9	20.0	22.3	22.0	17.2	16.6	8.4	4.5
7	4.4	7.5	12.4	19.7	22.4	22.2	17.2	16.7	8.4	4.5
8	4.3	7.5	11.9	18.7	22.2	22.2	17.2	16.7	8.4	4.4
9	3.5	7.4	11.6	17.5	18.2	19.9	17.1	16.7	8.4	4.4
10	3.6	7.2	10.5	13.3	15.0	16.1	17.0	16.7	8.4	4.4
11	3.8	6.0	8.9	10.7	12.7	13.6	17.0	16.7	8.3	4.4
12	4.0	4.4	6.6	8.2	9.6	10.7	16.7	16.7	8.3	4.4
13	4.4	4.1	5.3	5.8	6.9	9.0	12.3	14.3	8.3	4.4
14	4.7	4.1	4.3	4.9	5.2	6.8	9.7	10.6	8.4	4.3
15	4.6	4.1	4.1	3.9	4.2	5.0	6.4	7.5	7.7	4.3
16	4.4	4.1	3.7	3.7	3.8	4.2	4.9	5.1	5.3	5.2
17	4.2	3.9	3.9	3.6	3.6	4.0	4.1	4.2	4.3	5.4
18	4.0	3.7	3.8	3.5	3.5	3.8	3.8	3.8	4.0	4.9
19	3.8	3.6	3.5	3.5	3.5	3.7	3.7	3.7	3.7	4.2
20	3.7	3.4	3.4	3.4	3.5	3.6	3.6	3.6	3.7	4.1
21	3.6	3.4	3.4	3.3	3.5	3.5	3.6	3.6	3.6	3.9
22	3.4	3.3	3.3	3.3	3.5	3.5	3.6	3.6	3.5	3.8
23	3.3	3.2	3.3	3.3	3.4	3.4	3.5	3.5	3.5	3.8
24	3.3	3.2	3.3	3.3	3.4	3.4	3.5	3.5	3.5	3.7
25	3.1	3.1	3.2	3.3	3.3	3.4	3.4	3.4	3.5	3.7
26	3.0	3.1	3.2	3.3	3.3	3.4	3.4	3.4	3.5	3.6
27	3.0	3.0	3.1	3.2	3.3	3.3	3.4	3.4	3.4	3.6
28	2.9	3.0	3.1	3.2	3.3	3.3	3.4	3.4	3.4	3.5
29	2.9	3.0	3.1	3.2	3.2	3.3	3.4	3.4	3.4	3.5
30	2.8	2.9	3.1	3.1	3.2	3.3	3.4	3.4	3.4	3.5
31	2.7	2.9	3.0	3.1	3.2	3.3	3.3	3.3	3.4	3.5
32	2.7	2.8	3.0		3.2	3.2	3.3	3.3	3.4	3.5
33	2.7	2.8	3.0		3.2	3.2	3.3	3.3	3.4	3.4
34	2.7	2.8	3.0		3.1	3.2	3.3	3.3	3.4	3.4
35	2.7	2.8	2.9		3.1	3.2	3.3	3.3	3.4	3.4
36	2.7	2.8			3.1	3.2	3.3	3.3		3.4
37	2.7	2.8			3.1		3.3	3.3		3.4
38	2.6						3.3	3.3		
39	2.6						3.3	3.3		

Vertical temperature profiles at central, deep Station 6 show slight deepening of the mixed layer during the summer, followed by marked deepening between the August and September surveys as the mixolimnion cooled. By the 19 December survey the mixolimnion had cooled to almost 4.4 °C, only a degree warmer than monimolimnetic temperatures. However, a small region of slightly warmer temperature persisted at the 16–18 m chemocline (Fig. 10).

Fig. 10. High-resolution (~3–5 cm) water temperature profiles, Station 6, 2024.

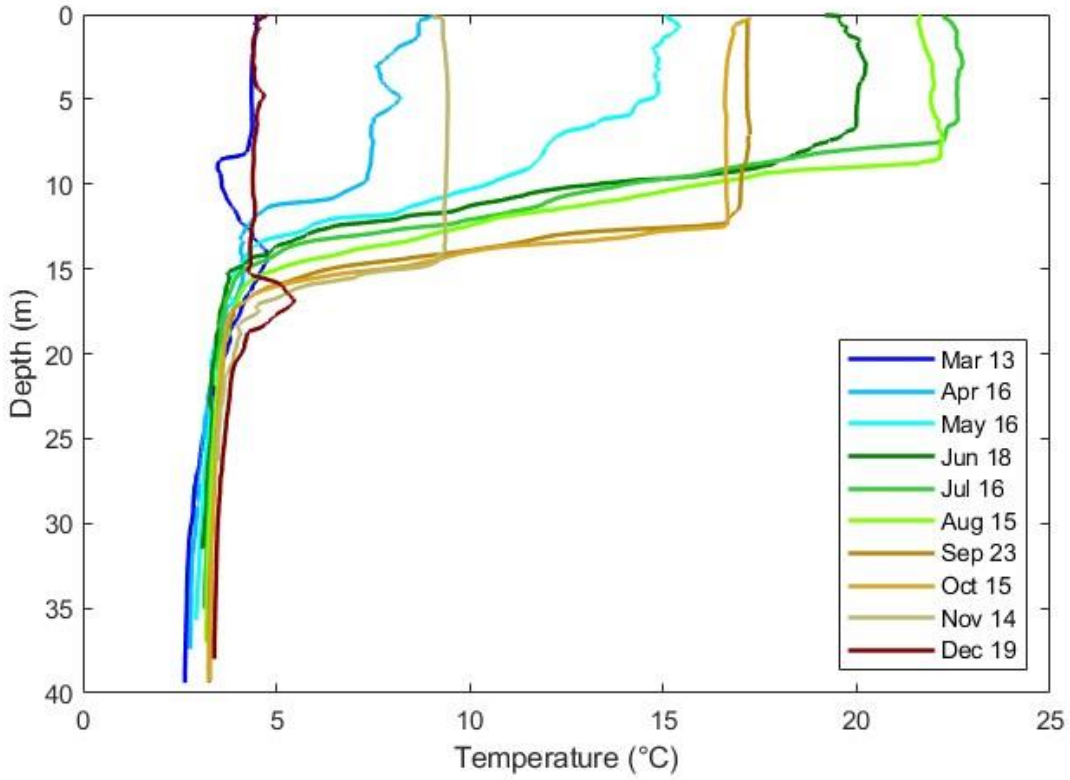

Spatial variability

The complex morphometry of Mono Lake (steep-sided western basins, shallow sloping eastern basin, two large islands and several small islets in the center), prevailing southwesterly winds, and freshwater inflows predominantly into the western basins result in spatial heterogeneity of physical, chemical, and biological features in the lake. Profiles of temperature, conductivity, fluorescence, and dissolved oxygen are taken at 12 stations to assess spatial variability and enable more accurate assessment of long-term trends. Here, we present temperature data from all 12 stations to illustrate some major spatial patterns.

On 16 April 2024, water temperature in the upper 10 m were significantly higher in the eastern half of the lake (Stations 7-12) compared to the western portion of the lake, Stations 1-5 (Fig. 11). At 5 m depth, the temperature ranged from 7.1 °C at Station 4 to 9.1 °C at Station 12. The thermocline depth was similar varying between 11 and 12 m among stations. Beneath the thermocline at ~15 m depth, an area of slightly warmer (4.3 vs 3.7 °C) water was present at the eastern stations, while temperatures in the deep monimolimnion were similar.

Fig. 11. Lakewide temperature profiles on 16 April 2024.

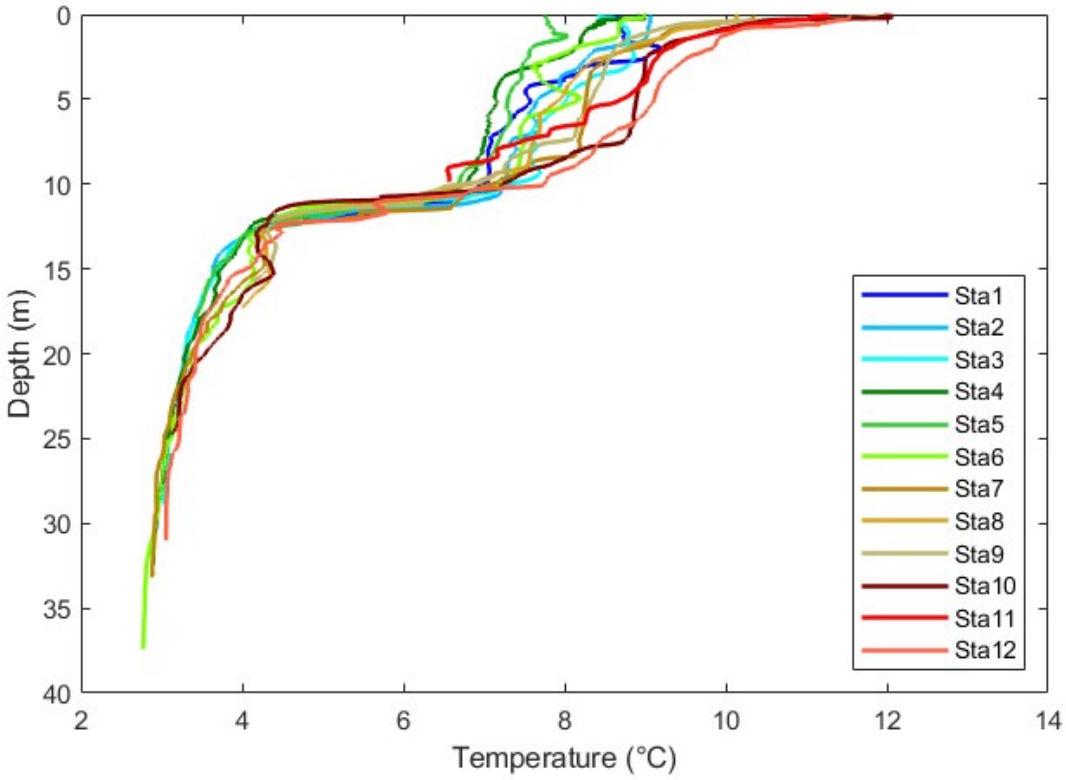

The noticeably warmer near-surface temperatures (<1 m depth) at the eastern stations may be partially explained by diurnal heating and sampling later in the day. Stations are visited in numeric order on lakewide surveys and typically span 5–7 hours on the lake. Data from a permanently moored thermistor chain at Station 6 provides an estimate of diurnal heating.

Continuously recorded thermistor data at Station 6 during mid-April show diurnal heating of 1–2 °C at 1 m depth, somewhat less at 1.9 m, and little to none at 3.4 m depth (Fig. 12). The diurnal water temperatures peaked in late afternoon. The 16 April survey was conducted between 8 am and 1 pm, when temperature increased only 0.5 °C at 1 m depth and less than 0.1 °C at 1.9 m depth and below. We conclude the warmer water temperatures observed on 16 April below 2 m depth cannot be explained by diurnal heating and represent lakewide differences. Shallower, gently sloping eastern basin and inflowing snowmelt waters in the western basin likely account for the difference.

Fig. 12. Diurnal water temperature variation at Station 5, 14–18 April 2024.

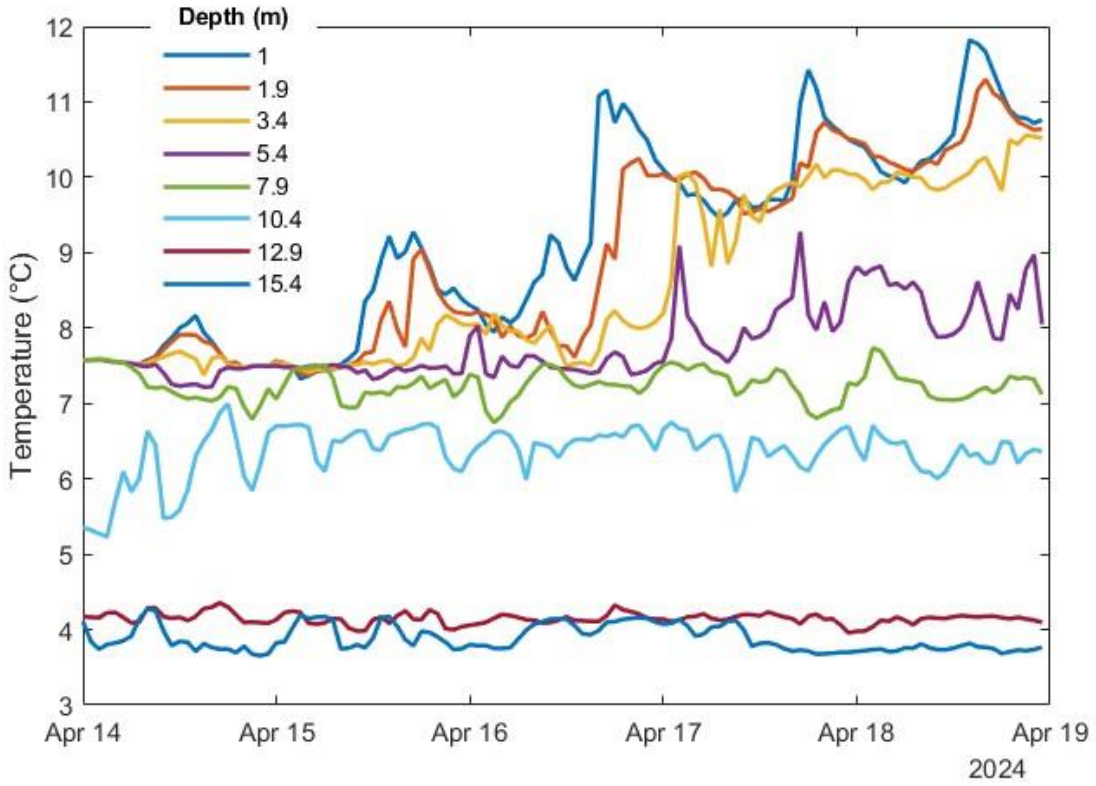

In contrast, the inter-basin differences in temperature were smaller by midsummer and a large portion of the slightly warmer mixolimnetic water temperatures in the eastern basin during summer can be explained by diurnal heating and the time of sampling (Fig. 13). At Stations 1–4 in the west, temperature between 1 and 7 m varied between 21.4–21.8 °C, while temperature was 22.1–22.5 °C at the eastern station (7–12) with Station 5 & 6 intermediate. Diurnal warming measured by the thermistor chain at Station 6, indicated a warming of ~0.6 °C at 1.5 m and above, decreasing to no warming at 8 m.

Fig. 13. Lakewide temperature profiles on 15 August 2024.

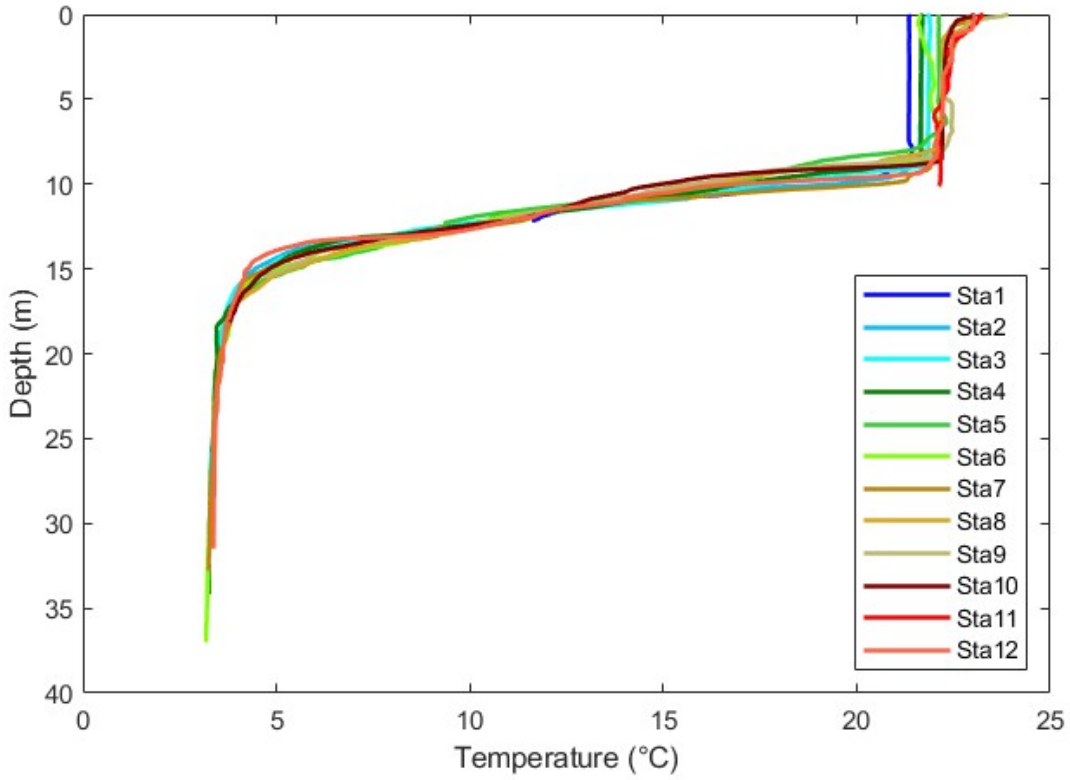

While these inter-basin water temperatures are small and likely of little significance to the biota, they would be important in heat budget and long-term warming analyses.

The November lakewide survey highlights temporal variability (Fig. 14). The survey was halted on 14 November after sampling Stations 1-7 due to weather and completed on 18 November, with Station 6 resampled. There were marked differences in both the thermocline depth and mixolimnetic temperatures. The eastern Stations 8–12 were >1 °C cooler than the western ones. Station 6 sampled on both days was also ~1 °C cooler. While the thermocline depth at Station 6 was at nearly the same depth on both days, it was more than a meter deeper at the eastern Stations 8, 10, and 12. Station 9 and 11 are shallow and their bottoms above the thermocline. Without continuous thermistor chain measurements, it is not possible to tell whether this was a deepening event in the eastern basin which would entrain nutrient-rich water or due to large internal seiches. Our two thermistor chains are deployed for 6 months intervals and were retrieved and re-deployed in October 2024. An analysis of their data following retrieval in May 2025 will allow analysis of this event.

Fig. 14. Lakewide temperature profiles on 14 & 18 November 2024.

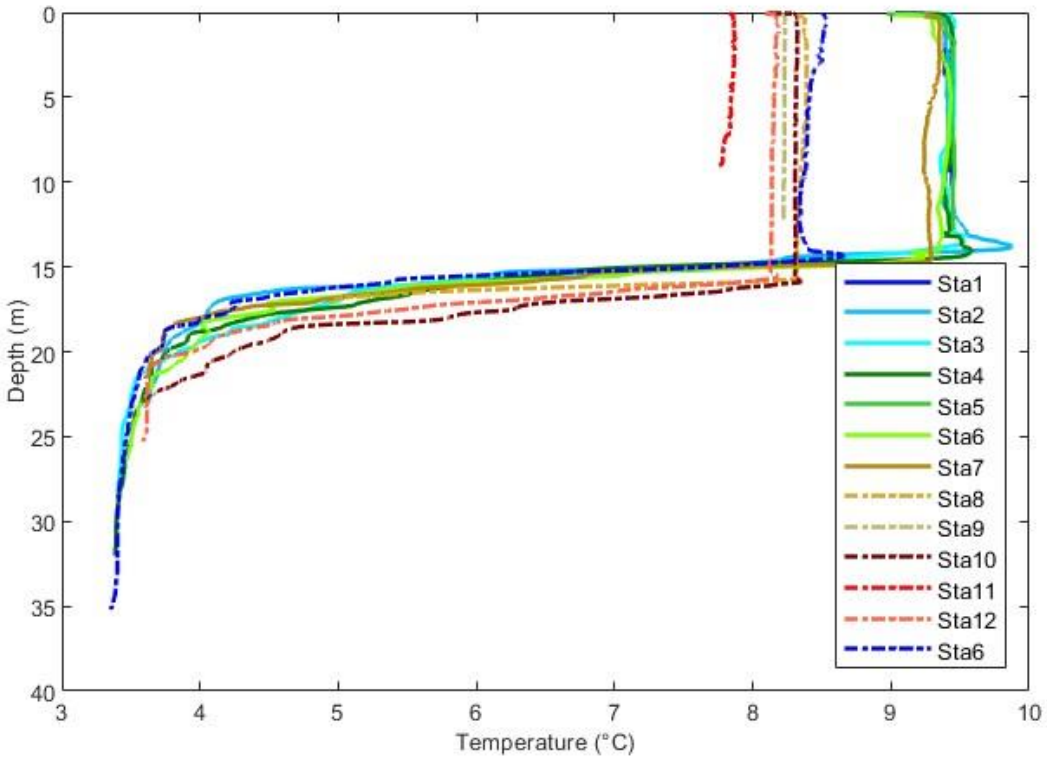

Specific Conductance and Salinity

On the first lakewide survey (13 March 2024), specific conductance (and salinity) at central Station 6 was 76.0 mS cm^{-1} (70.9 g kg^{-1}) in the mixed upper 7 m of the water column and 84.1 mS cm^{-1} (81 g kg^{-1}) in the deep monimolimnion (Table 2). At western stations values were slightly lower in the upper 2 m due to proximity to inflowing streams and surface runoff (Fig. 15). By mid-summer mixolimnetic specific conductance had decreased slightly to 75.0 mS cm^{-1} (69.7 g kg^{-1}). Although the 2024 runoff was much lower than in 2023, slightly lower conductivities were observed at the western stations (Fig. 16). Decreased runoff and increased evaporation led to declining lake levels in August, and mixolimnetic specific conductance gradually increased to 78.8–79.0 mS cm^{-1} (~74.5 g kg^{-1}). Near-surface salinities were slightly lower at the western stations in December as lake levels rose slightly (Fig. 17).

Little mixing between the mixolimnion and lower waters beneath the chemocline (monimolimnion) occurred, as indicated by only a slight decrease in specific conductance from 84.1 to 83.8 mS cm^{-1} between 18 March and 19 December in the deeper water.

Table 2. Specific conductance (mS cm^{-1} at 25ºC) at Station 6, March–December, 2024.

Depth (m)	3/13	4/16	5/16	6/18	7/18	8/15	9/23	10/14	11/18	12/19
1	76.0	76.2	75.8	74.6	75.0	75.6	77.2	77.4	78.5	78.8
2	76.0	76.2	76.0	74.9	75.0	75.7	77.3	77.5	78.5	78.8
3	76.0	76.2	76.1	75.1	75.0	75.7	77.3	77.5	78.6	78.8
4	76.0	76.2	76.3	75.1	75.0	75.8	77.3	77.5	78.6	78.9
5	76.0	76.4	76.5	75.2	75.0	75.8	77.3	77.5	78.6	78.9
6	76.0	76.3	76.7	75.2	75.1	75.9	77.3	77.5	78.6	79.0
7	76.0	76.3	76.8	75.6	75.1	75.9	77.4	77.5	78.6	79.0
8	76.1	76.4	76.7	75.9	75.4	75.9	77.4	77.6	78.6	79.0
9	76.8	76.4	76.7	76.3	76.3	76.1	77.4	77.6	78.6	79.0
10	77.6	76.4	76.7	77.7	77.0	77.5	77.4	77.6	78.6	79.0
11	79.3	77.8	77.1	78.5	77.5	78.1	77.4	77.6	78.6	79.0
12	81.1	80.8	79.9	80.0	79.6	79.8	77.5	77.6	78.6	79.0
13	82.4	82.0	81.7	82.4	81.8	81.1	80.7	80.1	78.6	79.0
14	83.0	82.9	83.0	83.1	82.9	82.4	82.0	82.1	78.6	79.0
15	83.5	83.4	83.3	83.6	83.6	83.3	83.3	83.2	82.9	79.1
16	83.7	83.7	83.5	83.7	83.7	83.6	83.6	83.6	83.5	81.7
17	83.8	83.8	83.7	83.7	83.8	83.7	83.7	83.7	83.6	83.0
18	83.8	83.8	83.8	83.8	83.8	83.7	83.8	83.8	83.7	83.4
19	83.8	83.9	83.8	83.8	83.8	83.7	83.8	83.8	83.8	83.5
20	83.9	83.9	83.9	83.8	83.8	83.8	83.8	83.8	83.8	83.6
21	83.9	83.9	83.9	83.9	83.8	83.8	83.8	83.8	83.8	83.6
22	83.9	83.9	83.9	83.9	83.9	83.8	83.8	83.8	83.8	83.7
23	84.0	83.9	83.9	83.9	83.9	83.8	83.8	83.8	83.8	83.7
24	84.0	84.0	83.9	83.9	83.9	83.9	83.8	83.8	83.8	83.7
25	84.0	84.0	83.9	83.9	83.9	83.8	83.8	83.8	83.8	83.7
26	84.0	84.0	84.0	83.9	83.9	83.9	83.8	83.8	83.8	83.7
27	84.0	84.0	84.0	83.9	83.9	83.9	83.8	83.8	83.8	83.7
28	84.0	84.0	84.0	83.9	83.9	83.9	83.8	83.9	83.8	83.7
29	84.0	84.0	84.0	83.9	83.9	83.9	83.9	83.9	83.8	83.8
30	84.0	84.0	84.0	84.0	83.9	83.9	83.9	83.9	83.8	83.8
31	84.1	84.0	84.0	84.0	83.9	83.9	83.9	83.9	83.8	83.8
32	84.1	84.0	84.0		83.9	83.9	83.9	83.9	83.8	83.8
33	84.1	84.0	84.0		84.0	83.9	83.9	83.9	83.8	83.8
34	84.1	84.1	84.0		84.0	83.9	83.9	83.9	83.8	83.8
35	84.1	84.1	84.0		84.0	83.9	83.9	83.9	83.9	83.8
36	84.1	84.1			84.0	83.9	83.9	83.9		83.8
37	84.1	84.1			84.0		83.9	83.9		83.8
38	84.1						83.9	83.9		
39	84.1						83.9	83.9		

Fig. 15. Specific conductance (mS cm^{-1}), 18 March 2024.

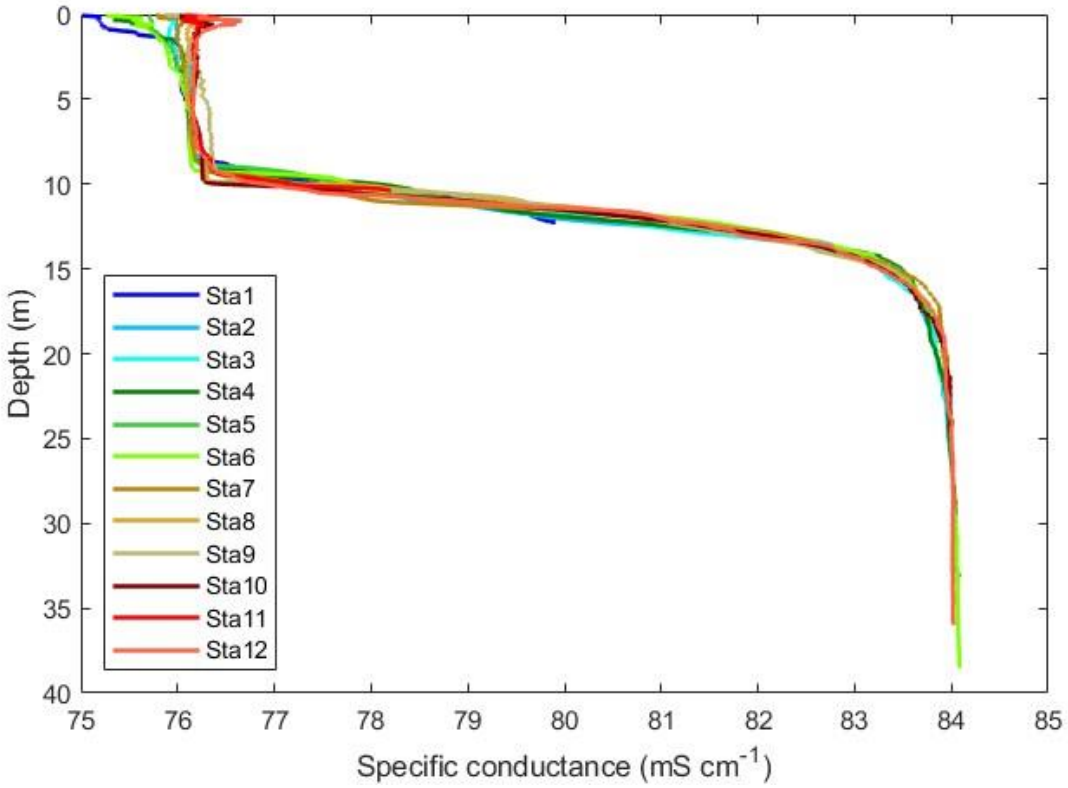

Persistent chemical stratification continued through 2024, and a chemocline existed throughout the year. However, the depth of the mixolimnion continued to increase with the depth of the 82 mS isocline increasing from 12.7 m on 18 March to 16.2 m on 19 December (Fig. 18, Fig. 19). On 19 December a sharp chemocline existed where specific conductance increased by 3.9 mS cm^{-1} (5.7 g kg^{-1}) between 15 and 17 m depth.

Fig. 16. Specific conductance (mS cm^{-1}), 18 July 2024.

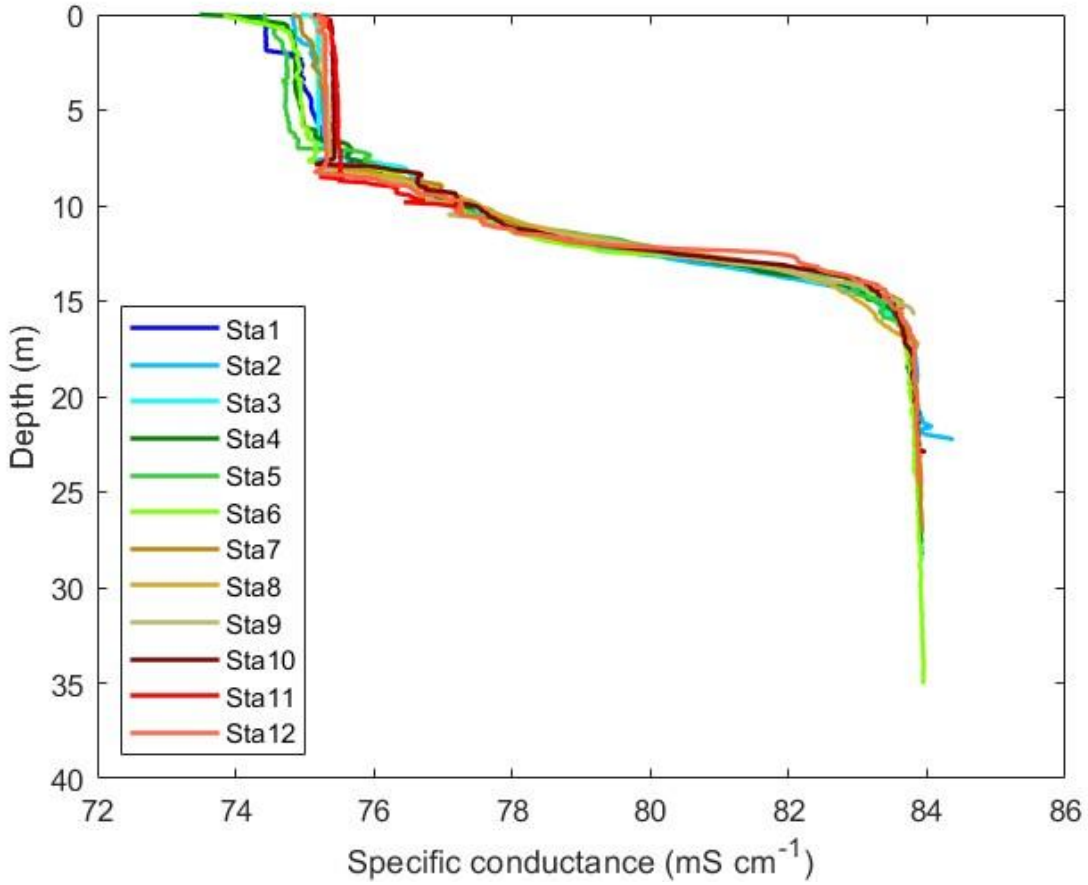

Fig. 17. Specific conductance (mS cm^{-1}), 19 December 2024

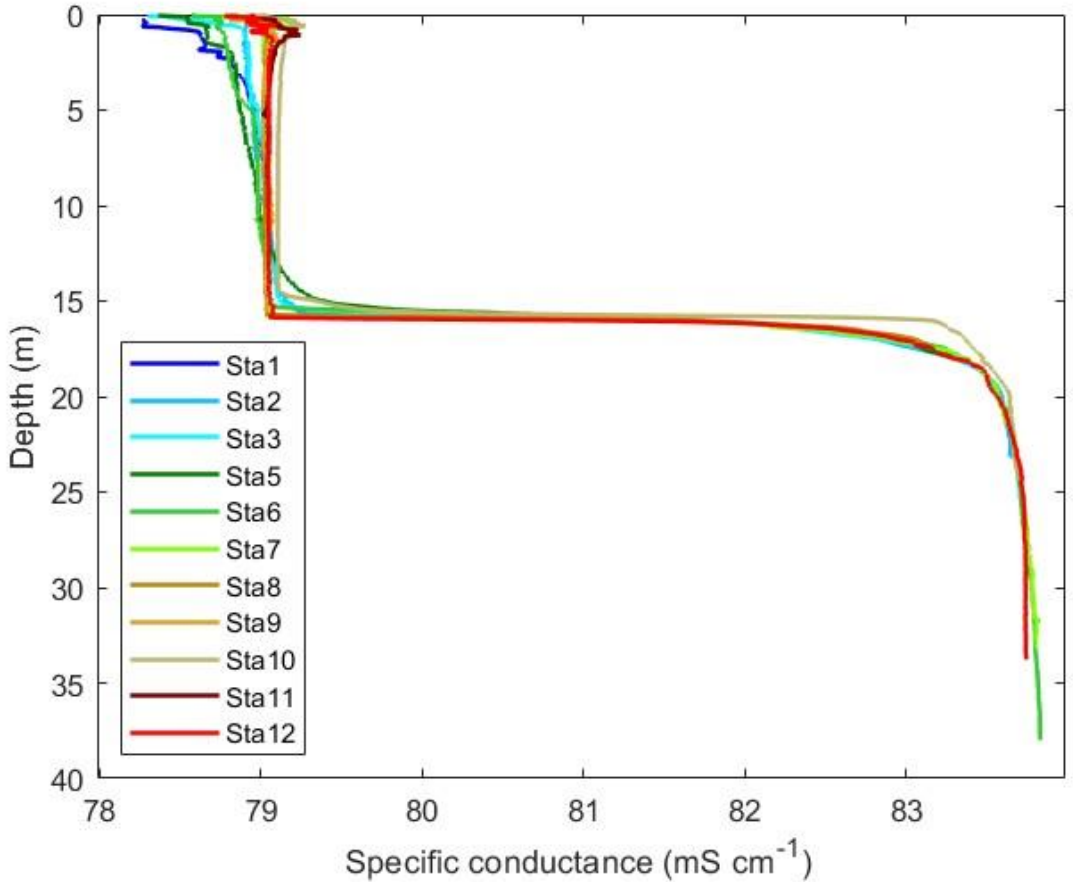

The seasonal pattern of salinity stratification is well-described by specific conductance at the centrally located deep Station 6 (Fig. 18 & 19). A strong (~4 mS cm^{-1}) mid-depth chemocline remained present throughout the year. There was a slight freshening of the mixolimnion in June and July due to inflowing freshwater streams followed by a gradual increase through December due to evaporative concentration and decreased freshwater inputs. The depth of the chemocline slowly descended through the year, with the 80 mS cm^{-1} isocline lowering 4.2 m from 11.4 m on 13 March to 15.6 m on 19 December.

Fig. 18. Seasonal specific conductance at Station 6, 2024.

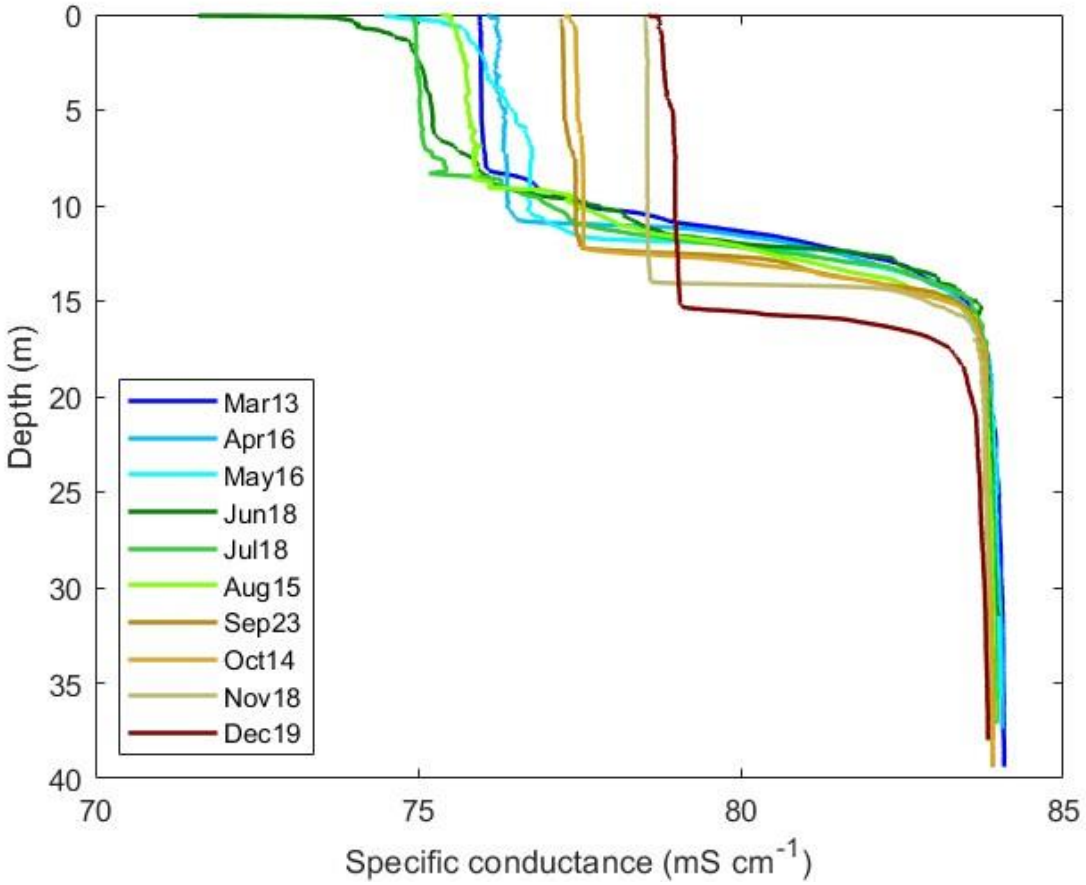

Fig. 19. Specific conductance (mS cm^{-1} at 25 ºC) at Station 6, 2024 (red triangles indicate sampling dates). Contours before 13 March 2024 sampling were interpolated from sampling on 12 December 2023.

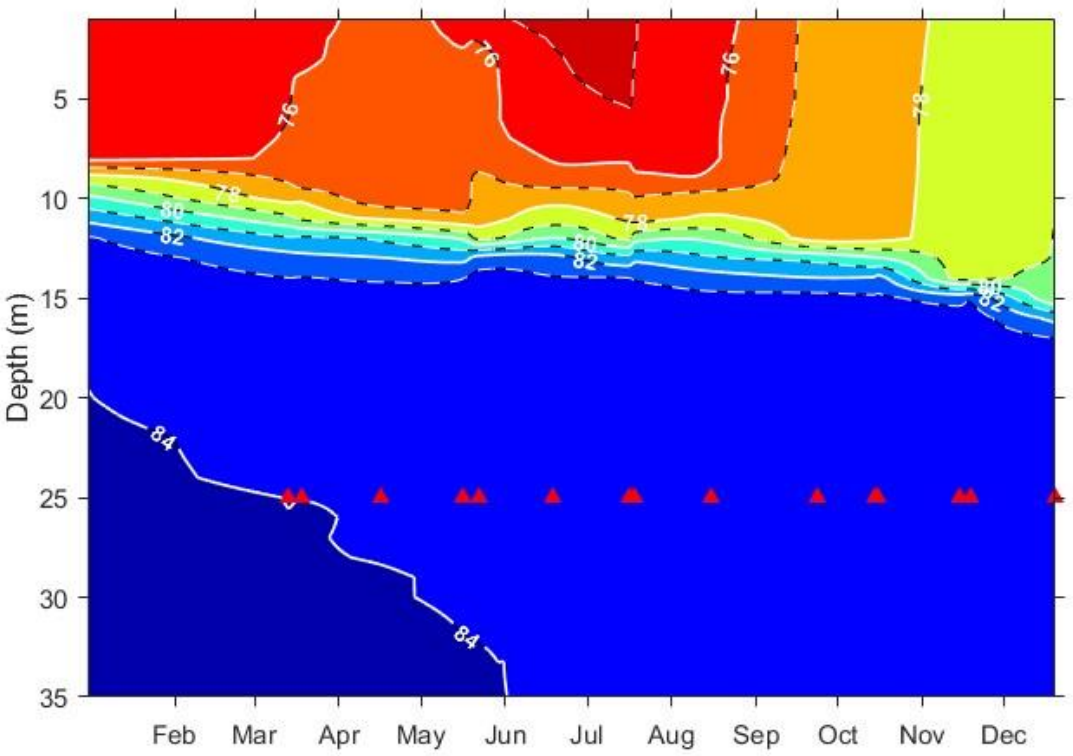

Density Stratification: Thermal and Chemical

The large seasonal variation in freshwater inflows observed in the eastern Sierra Nevada and year-to-year climatic variation has led to complex patterns of seasonal density stratification. Much of the year-to-year variation in the plankton dynamics observed at Mono Lake can be attributed to marked differences in chemical stratification resulting from variation in freshwater inflows and its effect on nutrient supply. The density difference between 2 and 32 m was 9.6 kg m^{-3} on 13 March, increased to 15.2 kg m^{-3} on 16 July due to both increased salinity and thermal stratification, before decreasing to 6 kg m^{-3} on 19 December (Fig. 20).

Seasonal density stratification reflects contributions from both thermal and salinity stratification (Fig. 20). At the peak density stratification on 16 July, salinity stratification contributed twice as much to overall density stratification (10.3 kg m^{-3}) as thermal stratification (4.9 kg m^{-3}). The peak salinity stratification decreased from 20.3 kg m^{-3} in August 2023 to 15.2 kg m^{-3} in July 2024. The density stratification observed during the previous five episodes of

meromixis suggest the current episode will continue through 2025 and possibly beyond depending on climate and water diversion policies (Fig. 21). The recurring multi-year episodes of meromixis have introduced large variations in mixing and nutrient supply which complicate analysis of the effects of changing salinity associated with lake level management (Fig. 22). Prior to 1982, continuously declining lake levels due to large annual diversions prevented recurring meromictic episodes (Jellison et al., 2024).

Fig. 20. Density stratification between 2 and 32 m, 2023–2024.

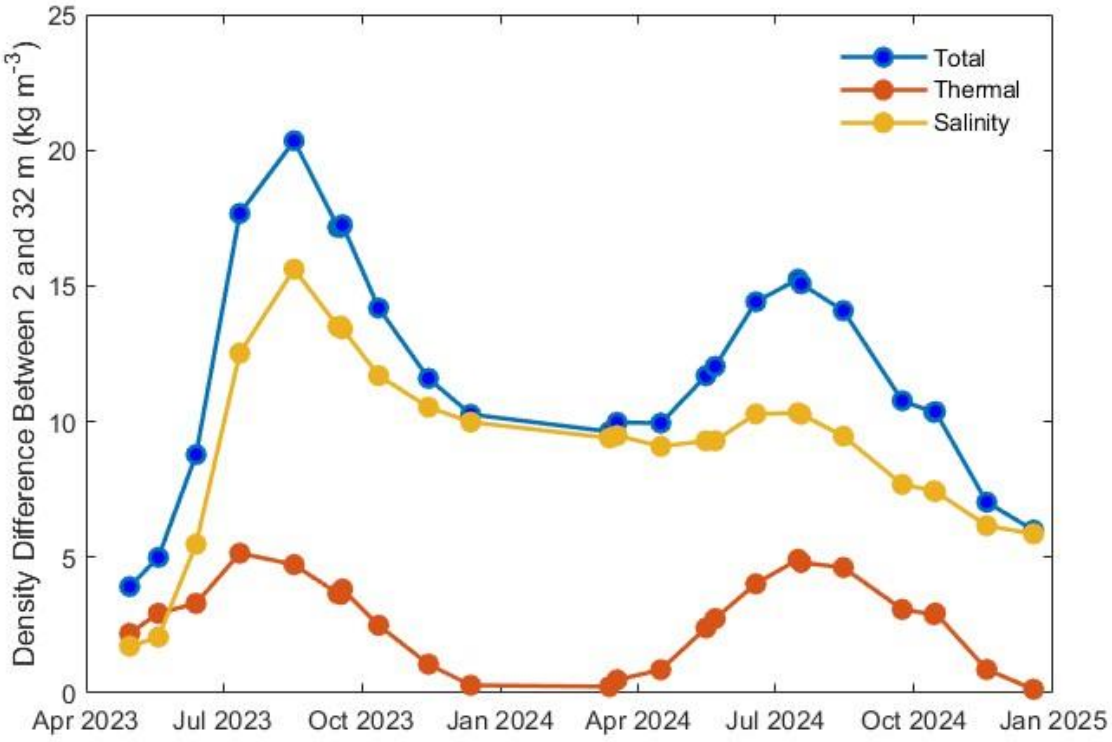

Fig. 21. Density stratification due to temperature and salinity, 1983–2024.

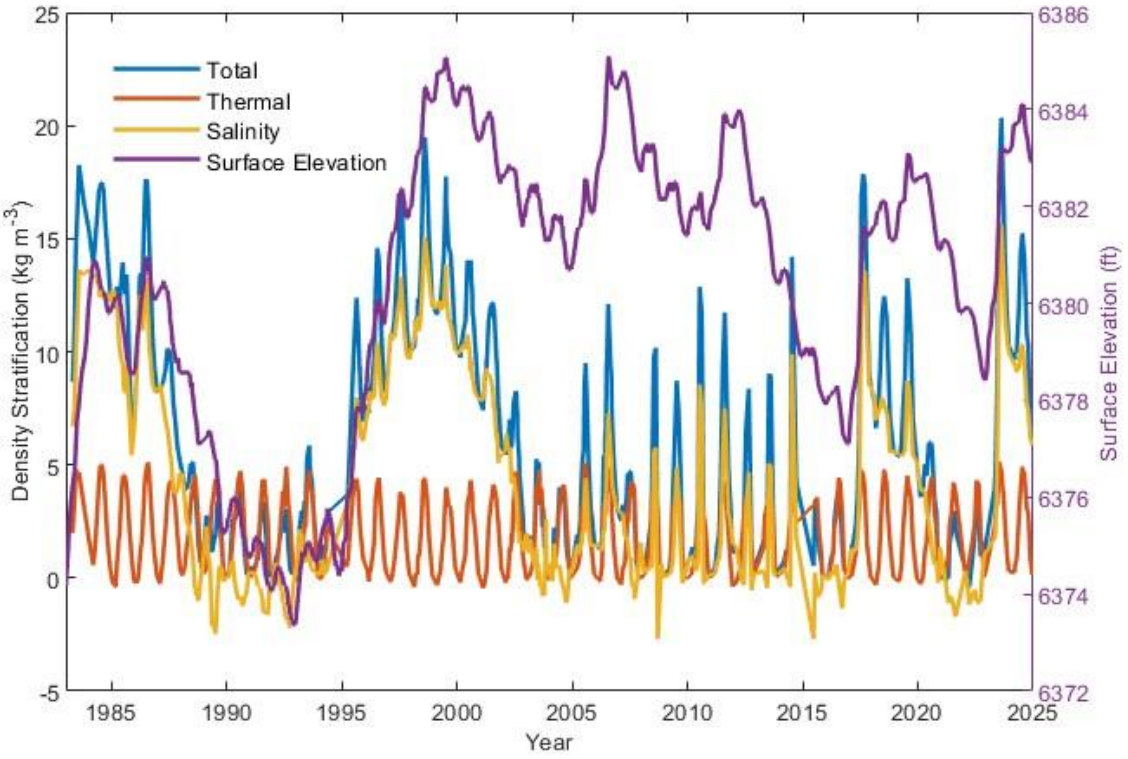

Fig. 22. Meromictic Episodes

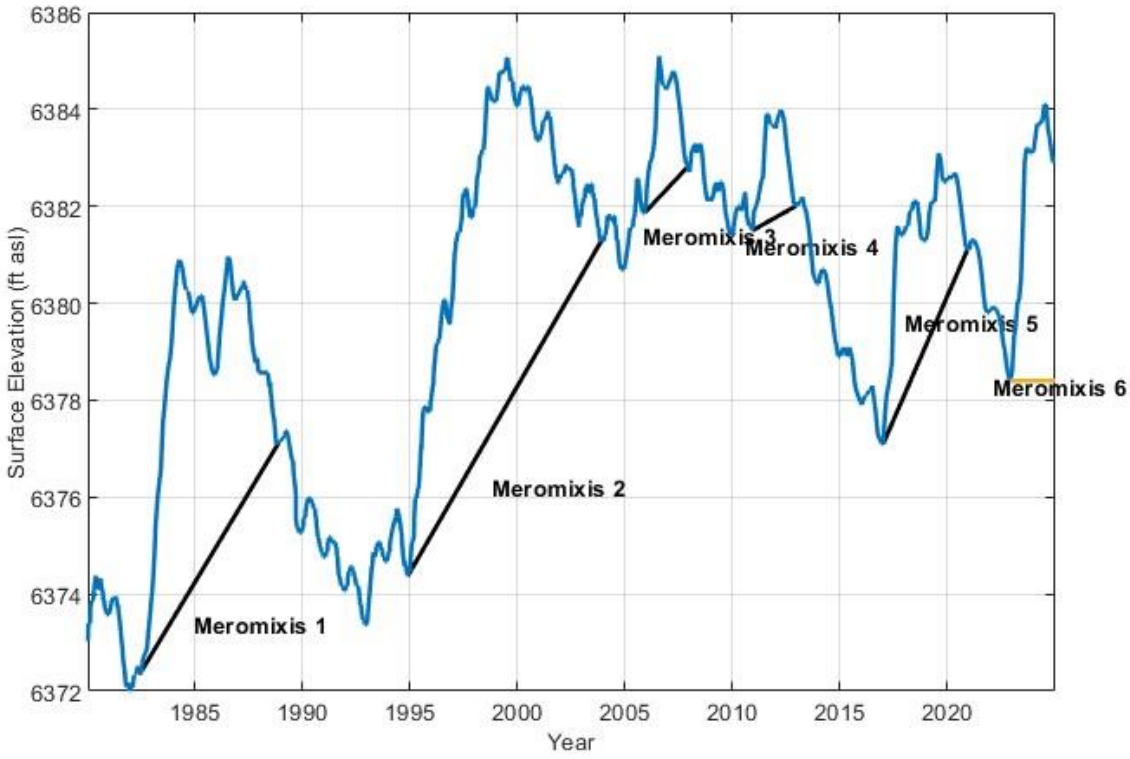

Transparency and Light Attenuation

In Mono Lake, variation in transparency is largely driven by changes in algal biomass, which is influenced by the balance between primary production and loss processes such as grazing by *Artemia*. Secchi depth serves as a useful proxy for lake clarity, reflecting seasonal shifts in phytoplankton abundance, *Artemia* density, and nutrient availability.

The lakewide mean Secchi transparency was 1.02 ± 0.04 m in March and 0.85 ± 0.04 m in April (Table 3), indicating relatively low transparency in early spring, likely corresponding to increased algal growth and suspended particulate matter. As the season progressed, transparency steadily increased, peaking at 10.39 ± 0.16 m in mid-August and remaining high during September and October (9.96 ± 0.14 and 8.06 ± 0.37 m, respectively) reflecting a period of maximum water clarity. This period coincides with both a seasonal decline in phytoplankton biomass in summer and peak grazing activity by *Artemia*, which exerts strong top-down control on algal populations.

Following the period of maximum water clarity, Secchi depth declined, dropping to 3.53 ± 0.07 m in November and further to 1.26 ± 0.05 m in December (Table 3), coinciding with an increase in chlorophyll (10.2 ± 0.2 μg L^{-1} and 22.2 ± 0.9 μg L^{-1}, respectively). This suggests a fall bloom of phytoplankton, likely resulting from reduced grazing pressure as *Artemia* populations decline seasonally, along with possible nutrient supply from increased mixing. Additionally, increased wind-induced resuspension of sediments and organic matter in the fall months may contribute to reduced water clarity.

Wind and gust speeds recorded at Paoha Island in November (15.8 and 21.2 m s^{-1}, respectively) and December (18.3 and 24.4 m s^{-1}, respectively) (Fig. 3) were above yearly average wind speed and gust speed of 14.8 and 20.75 m s^{-1}, respectively. While the seasonal dynamics of phytoplankton growth and grazing in Mono Lake are evident, it is important to note that the lake is meromictic, meaning deep water layers remain isolated from surface mixing for extended periods. This limits full nutrient redistribution from deep anoxic waters but it allows for localized mixing effects in the upper water column, especially during periods of strong winds.

The western sector had slightly higher transparency than the eastern sector throughout the year, with peak values reaching 10.82 ± 0.20 m in August compared to 9.97 ± 0.06 m in the eastern sector (Table 3). This difference may reflect variations in nutrient availability, localized upwelling, or differential grazing pressure across lake sectors. Additionally, notable seasonal differences in phytoplankton abundance between the sectors were observed. During the summer, the eastern sector typically experiences slightly higher phytoplankton biomass, which reduces transparency compared to the western sector. By the end of the year, this pattern can reverse, with reduced transparency in the western sector due to a buildup of phytoplankton, potentially linked to seasonal nutrient supply and reduced grazing by *Artemia.* These shifts underline the complex interactions between biological and physical processes regulating Mono Lake's clarity.

Table 3. Secchi depths (m), March–December, 2024. S.E. is standard error. 'n' in last rows refers to number of stations averaged. '*' in '11/18' column indicates stations sampled on 11/18.

	Dates								11/14	
Station	3/18	4/16	5/16	6/18	7/16	8/15	9/23	10/15	11/18*	12/19
Western sector										
1	1.00	0.70	1.90	5.50	9.50	11.00	10.25	9.50	4.10	1.30
2	1.00	0.79	2.10	5.60	8.75	10.70	10.50	9.50	3.50	1.10
3	0.90	0.80	1.70	5.50	8.75	11.50	10.00	9.50	3.60	1.40
4	0.85	0.85	1.70	6.10	8.75	11.00	10.50	9.50	3.50	1.10
5	1.20	0.69	2.15	6.00	8.50	10.70	10.50	8.50	3.70	1.05
6	1.30	0.75	1.70	5.90	7.75	10.00	10.00	8.25	3.60	1.10
Mean	1.04	0.76	1.88	5.77	8.67	10.82	10.29	9.13	3.67	1.18
S.E.	0.07	0.03	0.09	0.11	0.23	0.20	0.10	0.24	0.09	0.06
n	6	6	6	6	6	6	6	6	6	6
Eastern sector										
7	1.00	0.80	1.80	5.50	7.25	9.80	10.00	7.00	3.30	1.20
8	1.10	1.00	2.10	5.20	6.25	10.00	10.00	7.50	3.50*	1.60
9	0.95	0.95	2.10	4.00	7.25	10.20	9.25	7.50	3.50*	1.35
10	1.00	0.90	1.70	4.10	7.25	10.00	9.00	7.50	3.50*	1.30
11	1.00	1.10	1.70	3.40	8.50	10.00	10.00	5.50	3.10*	1.40
12	0.90	0.85	1.70	4.60	7.25	9.80	9.50	7.00	3.40*	1.20
Mean	0.99	0.93	1.85	4.47	7.29	9.97	9.63	7.00	3.38	1.34
SE	0.03	0.04	0.08	0.32	0.29	0.06	0.18	0.32	0.07	0.06
n	6	6	6	6	6	6	6	6	6	6
Lakewide										
Mean	1.02	0.85	1.86	5.12	7.98	10.39	9.96	8.06	3.53	1.26
S.E.	0.04	0.04	0.06	0.25	0.27	0.16	0.14	0.37	0.07	0.05
n	12	12	12	12	12	12	12	12	12	12

The highest transparency observed in August 2024 (10.4 m) was higher than observed in 2023 (7.1 m) and much higher than the two 3-yr periods of low summer transparency observed in 2014–2016 and 2020–2022 during declining lake levels (Fig. 23). Summer transparency in 2024 was the 10th highest among the past 43 years (1982–2024).

Fig. 23. Long-term changes in transparency (Secchi depth) and surface elevation.

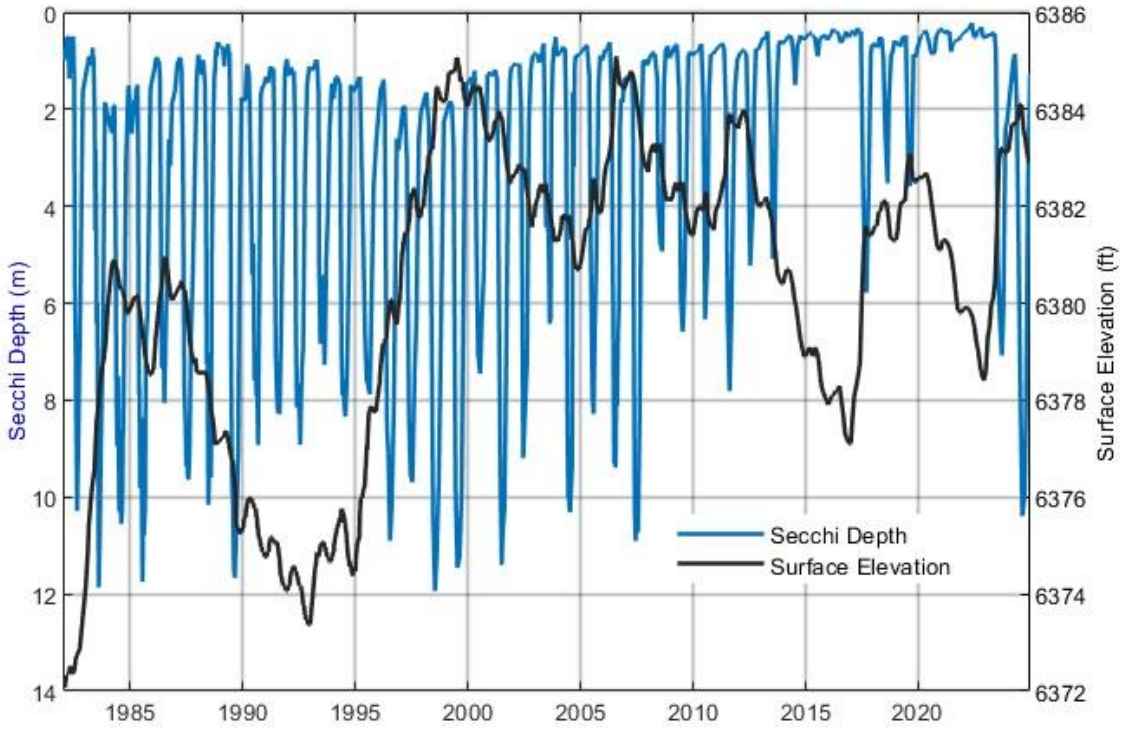

The attenuation of photosynthetically active radiation within Mono Lake's water column varies seasonally and is driven primarily by changes in algal biomass (Fig. 24). PAR attenuation ranged from ~ 0.5 to 0.7 in March and April, reflecting the increased algal growth and suspended particulate matter. PAR attenuation decreased during the summer months, corresponding to periods of decreased chlorophyll *a* levels near the surface. As the season progressed, PAR attenuation decreased until October. As the season transitioned into autumn, PAR attenuation increased, indicating increased chlorophyll *a* levels near the surface. PAR attenuation increased until late December (Fig. 24), correlating with the Secchi depth decline. The observed patterns in PAR attenuation highlight the dynamic relationship between light availability, phytoplankton abundance, and ecosystem processes in Mono Lake.

Fig. 24. PAR light attenuation (fraction of surface) at Station 6, 2024.

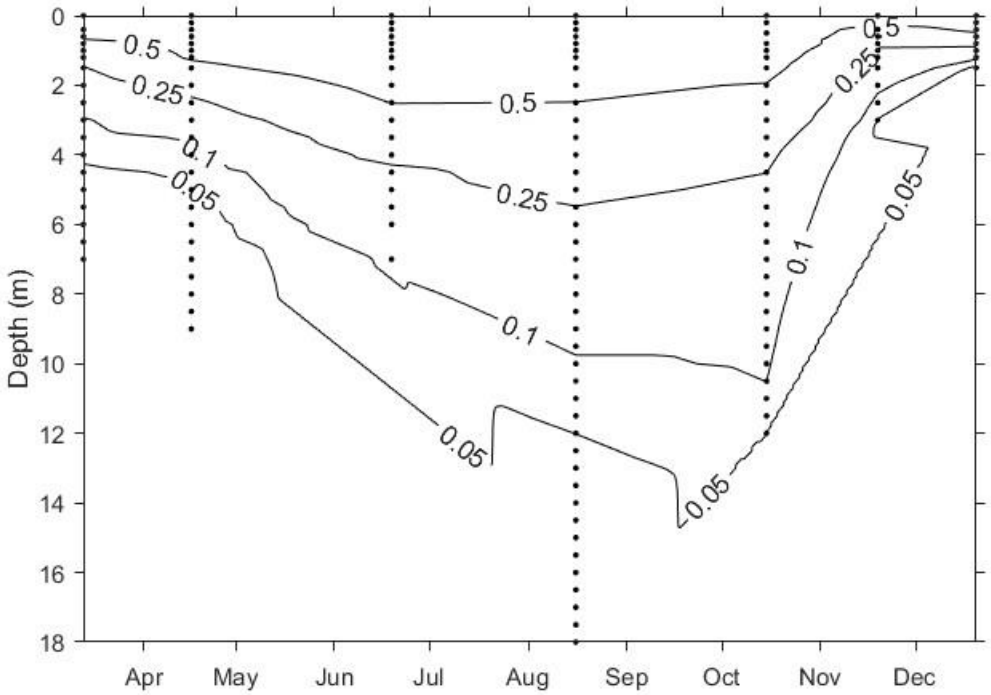

Dissolved Oxygen

Dissolved oxygen concentrations are a function of salinity, temperature, and the balance between photosynthesis and community respiration. In the euphotic zone of Mono Lake, dissolved oxygen concentrations are typically highest during the spring. As the water temperature and *Artemia* population increase through the spring, dissolved oxygen concentrations decrease. Beneath the euphotic zone, bacterial and chemical processes deplete the oxygen once the lake stratifies. During meromictic periods, the monimolimnion remains anoxic throughout the year.

In 2024, dissolved oxygen concentrations in the upper water (≤12 m) ranged from 1.4 to 7.1 mg L^{-1} (Fig. 25, Fig. 26, Table 4). Dissolved oxygen concentrations declined gradually in water above 12 m from 1.4 to 5.1 mg L^{-1} (March), 2.2 to 5.5 mg L^{-1} (April), and 3.8 to 4.7 mg L^{-1} (May). Summer values in water above 12 m gradually increased, ranging from 3.4 to 4.6 mg L^{-1}in June, from 3.4 to 7.1 mg L^{-1} in July and from 3.6 to 5.5 mg L^{-1} in August.

In September, October, and November, dissolved oxygen concentrations were 3.5, 4.2, and 4.5 mg L^{-1}, respectively, with low variation (>0.1 mg L^{-1}) from depths of 1 m to 11 m. On

19 December, dissolved oxygen concentrations were 5.0 mg L^{-1} at 2 m depth and 3.4 mg L^{-1} at 16 m depth. The water below 14 m was anoxic (<0.5 mg L^{-1}) throughout the year, and depth of anoxia decreased gradually to 18 m by December.

Fig. 25. Seasonal dissolved oxygen at Station 6.

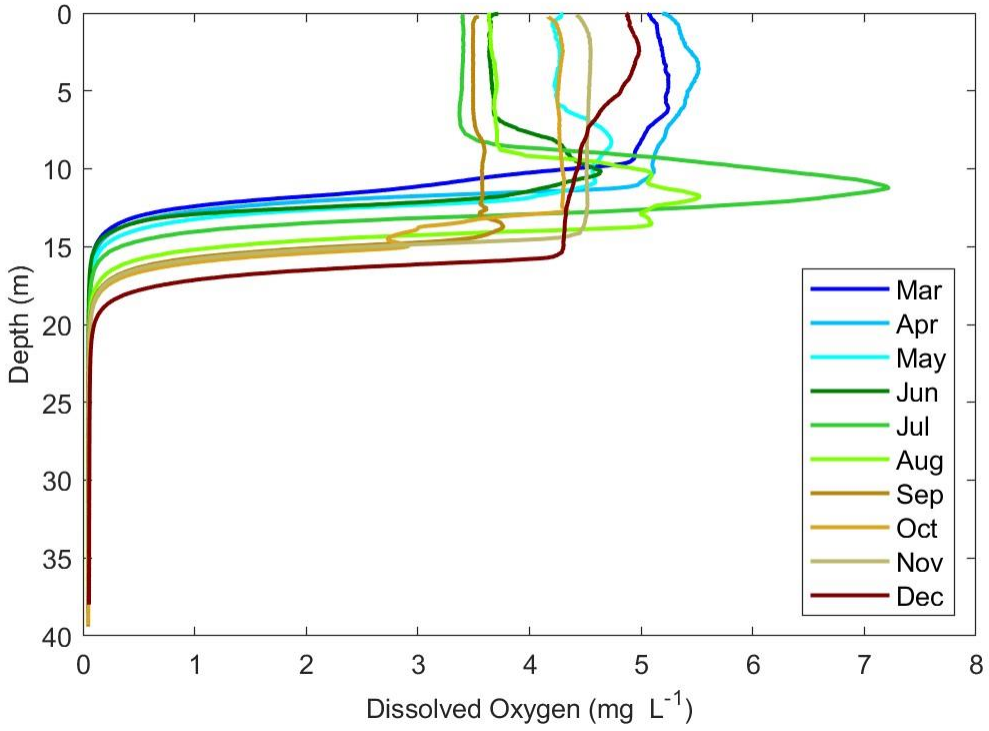

Fig. 26. Dissolved oxygen (mg L^{-1}) at Station 6, 2024.

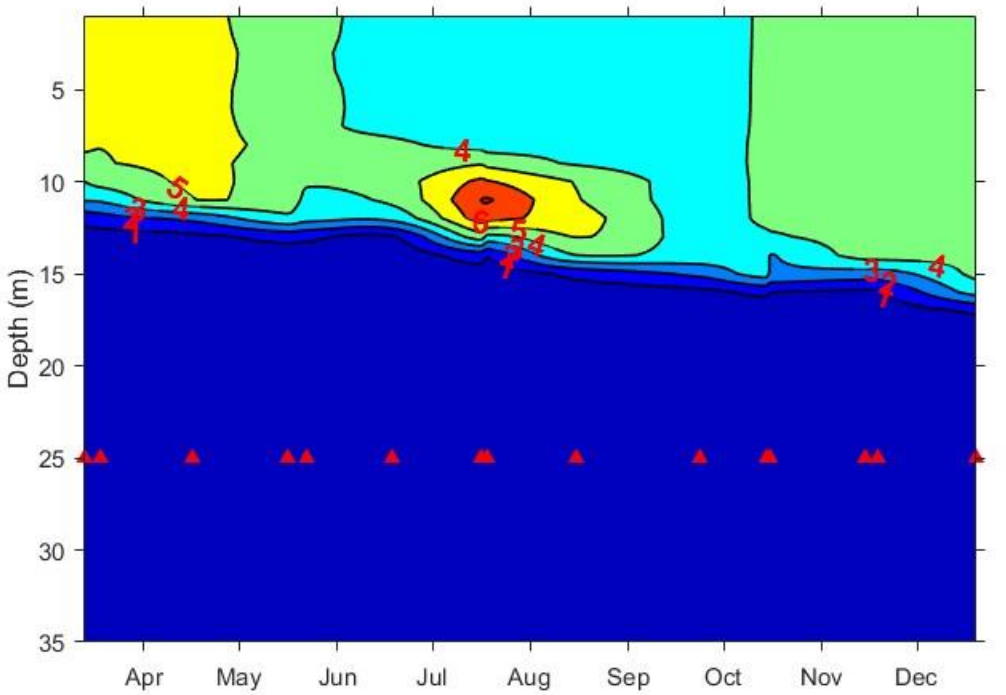

Table 4. Dissolved oxygen (mg L^{-1}) at Station 6, March–December, 2024.

Depth (m)	3/13	4/16	5/16	6/18	7/18	8/15	9/23	10/14	11/18	12/19
1	5.0	5.3	4.2	3.7	3.4	3.6	3.5	4.2	4.5	4.9
2	5.0	5.4	4.3	3.6	3.4	3.7	3.5	4.2	4.5	5.0
3	5.1	5.5	4.3	3.6	3.4	3.7	3.5	4.2	4.5	5.0
4	5.1	5.5	4.2	3.7	3.4	3.7	3.5	4.2	4.6	4.9
5	5.1	5.4	4.2	3.7	3.4	3.7	3.5	4.2	4.6	4.8
6	5.1	5.4	4.3	3.7	3.4	3.7	3.5	4.2	4.5	4.7
7	5.1	5.3	4.5	3.8	3.4	3.7	3.5	4.2	4.5	4.6
8	5.1	5.2	4.7	4.2	3.5	3.7	3.6	4.2	4.5	4.5
9	4.9	5.1	4.7	4.3	4.7	3.9	3.6	4.2	4.5	4.5
10	4.0	5.1	4.6	4.6	6.1	4.9	3.6	4.2	4.5	4.4
11	3.1	5.0	4.6	4.3	7.1	5.1	3.6	4.2	4.5	4.4
12	1.4	2.2	3.8	3.4	6.4	5.5	3.6	4.2	4.5	4.3
13	0.5	0.7	1.3	0.9	3.7	5.0	3.6	3.8	4.5	4.3
14	0.3	0.3	0.5	0.3	1.1	4.0	3.7	3.5	4.5	4.3
15	0.1	0.1	0.2	0.1	0.3	1.3	2.3	3.5	2.5	4.3
16	0.1	0.1	0.1	0.1	0.1	0.4	0.7	1.2	0.8	3.4
17	0.1	0.1	0.1	0.1	0.1	0.2	0.3	0.4	0.3	1.2
18	0.1	0.1	0.1	0.1	0.1	0.1	0.1	0.2	0.2	0.4
19	0.1	0.1	0.1	0.1	0.1	0.1	0.1	0.1	0.1	0.2
20	0.1	0.1	0.1	0.0	0.1	0.1	0.1	0.1	0.1	0.1
21	0.1	0.1	0.0	0.0	0.1	0.1	0.1	0.1	0.1	0.1
22	0.1	0.1	0.0	0.0	0.1	0.1	0.1	0.1	0.1	0.1
23	0.1	0.0	0.0	0.0	0.1	0.0	0.1	0.1	0.1	0.1
24	0.1	0.0	0.0	0.0	0.1	0.0	0.1	0.1	0.1	0.1
25	0.1	0.0	0.0	0.0	0.1	0.0	0.0	0.1	0.1	0.1
26	0.1	0.0	0.0	0.0	0.0	0.0	0.0	0.1	0.1	0.1
27	0.1	0.0	0.0	0.0	0.0	0.0	0.0	0.1	0.1	0.1
28	0.1	0.0	0.0	0.0	0.0	0.0	0.0	0.1	0.1	0.1
29	0.1	0.0	0.0	0.0	0.0	0.0	0.0	0.0	0.1	0.1
30	0.1	0.0	0.0	0.0	0.0	0.0	0.0	0.0	0.1	0.1
31	0.1	0.0	0.0	0.0	0.0	0.0	0.0	0.0	0.1	0.1
32	0.1	0.0	0.0		0.0	0.0	0.0	0.0	0.1	0.1
33	0.1	0.0	0.0		0.0	0.0	0.0	0.0	0.1	0.1
34	0.1	0.0	0.0		0.0	0.0	0.0	0.0	0.1	0.1
35	0.1	0.0	0.0		0.0	0.0	0.0	0.0	0.1	0.1
36	0.1	0.0			0.0	0.0	0.0	0.0		0.1
37	0.1	0.0			0.0		0.0	0.0		0.1
38	0.1						0.0	0.0		
39	0.1						0.0	0.0		

Fluorescence

Fluorescence measurements are directly related to phytoplankton chlorophyll but are influenced by variations in species composition, physiological state, and environmental conditions. Hence, the fluorescence profiles are used to indicate patterns and are not converted to chlorophyll concentrations.

At Station 6 (Fig. 26), a seasonal pattern in fluorescence values was observed. In the upper water column values were relatively high from March to May, peaking in April before declining in June and remaining low through October. From July onwards, values increased at depths below 7 m. In August, values peaked at 13 m, while in September and October maximum values were recorded at 15 m. By December, values were stable in the upper 15 m but increased at 16 m and deeper.

Fig. 27. Seasonal fluorescence profiles at Station 6.

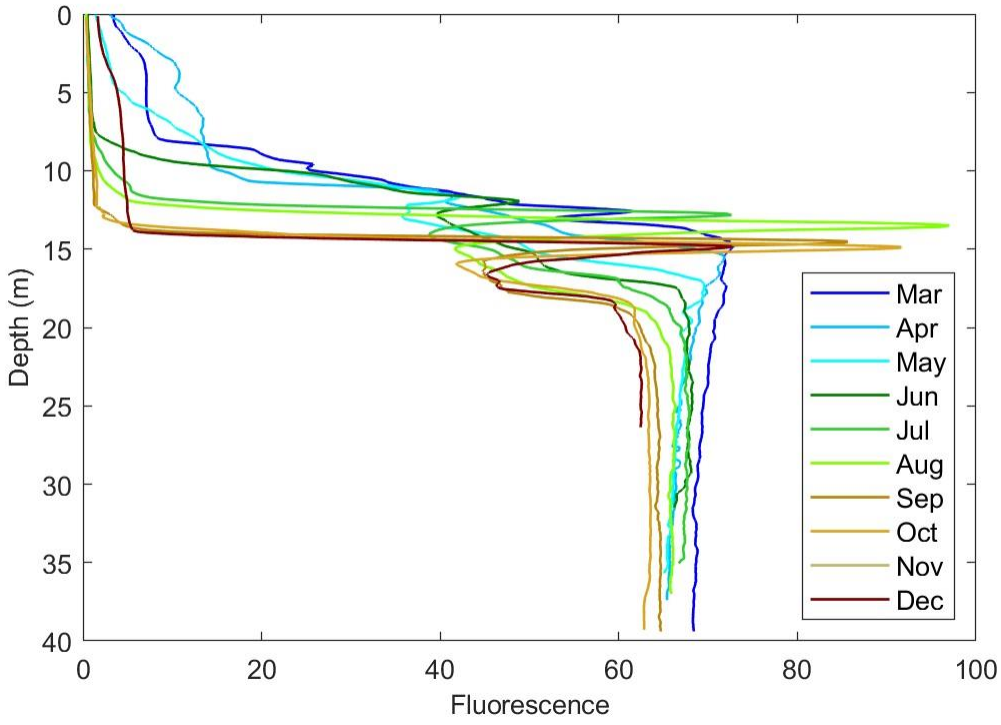

Vertical Distributions of Temperature, Turbidity, Dissolved Oxygen, and Fluorescence (Station 6): Summer and Autumn

Beginning in July, a conspicuous peak in dissolved oxygen and fluorescence occurred in the pycnocline (Fig. 28). A likely reason for the elevated dissolved oxygen is photosynthetic oxygen production by abundant phytoplankton, as indicated by the peak in fluorescence intensity and turbidity. Within the pycnocline vertical mixing would be reduced and confine the oxygen production to this zone. *Artemia* could preferentially graze this zone of elevated phytoplankton. Discrete-depth sampling of *Artemia* would be required to examine this possibility.

Fig. 28. Temperature, turbidity, dissolved oxygen, and fluorescence at Station 6, 16 July 2024.

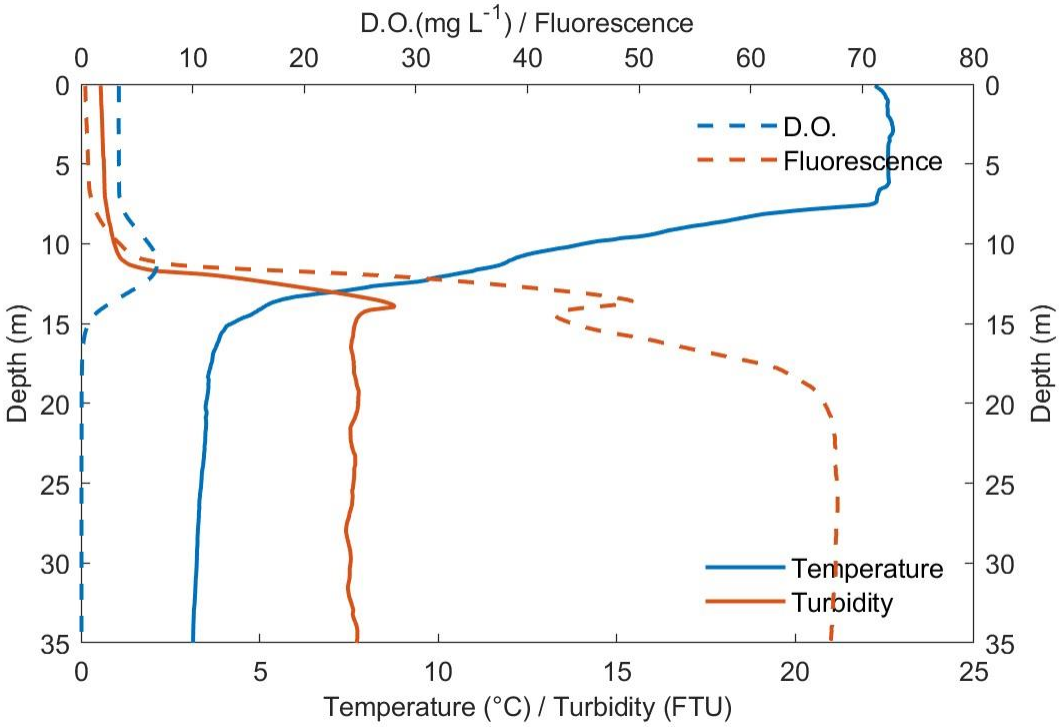

Stratification through August further intensified this pattern (Fig. 28), with the fluorescence peak and associated dissolved oxygen (DO) peak becoming more pronounced. The pycnocline restricted vertical mixing at ~10–15 m, where light was sufficient for photosynthesis. This resulted in increased turbidity, likely from phytoplankton biomass and organic particle accumulation. By October, fluorescence and turbidity had declined at ~10–15 m (Fig. 30). Strong and sustained winds in November and December partially mixed the surface and mid-water layers, redistributing oxygen but not fully disrupting stratification (Fig. 31). Future analyses of vertical *Artemia* distributions and wind-driven mixing dynamics could help clarify the biological and physical drivers of these seasonal patterns.

Fig. 29. Temperature, turbidity, dissolved oxygen, and fluorescence at Station 6, 15 August 2024.

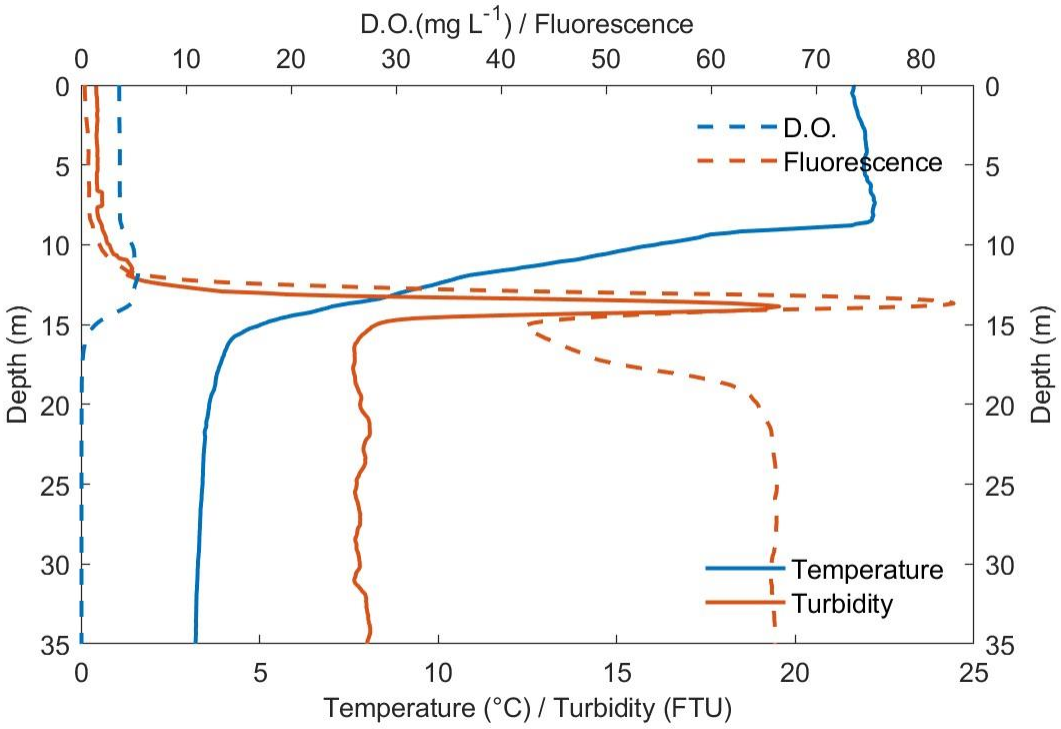

Fig. 30. Temperature, turbidity, dissolved oxygen, and fluorescence at Station 6, 15 October 2024.

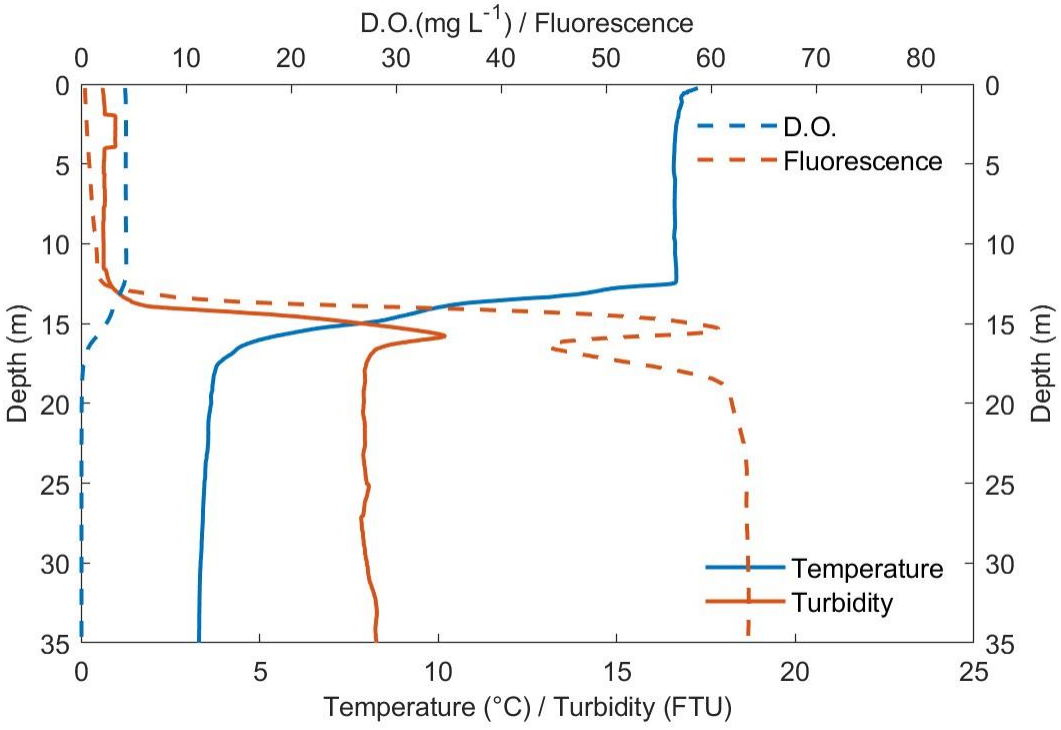

Fig. 31. Temperature, turbidity, dissolved oxygen, and fluorescence at Station 6, 19 December 2024.

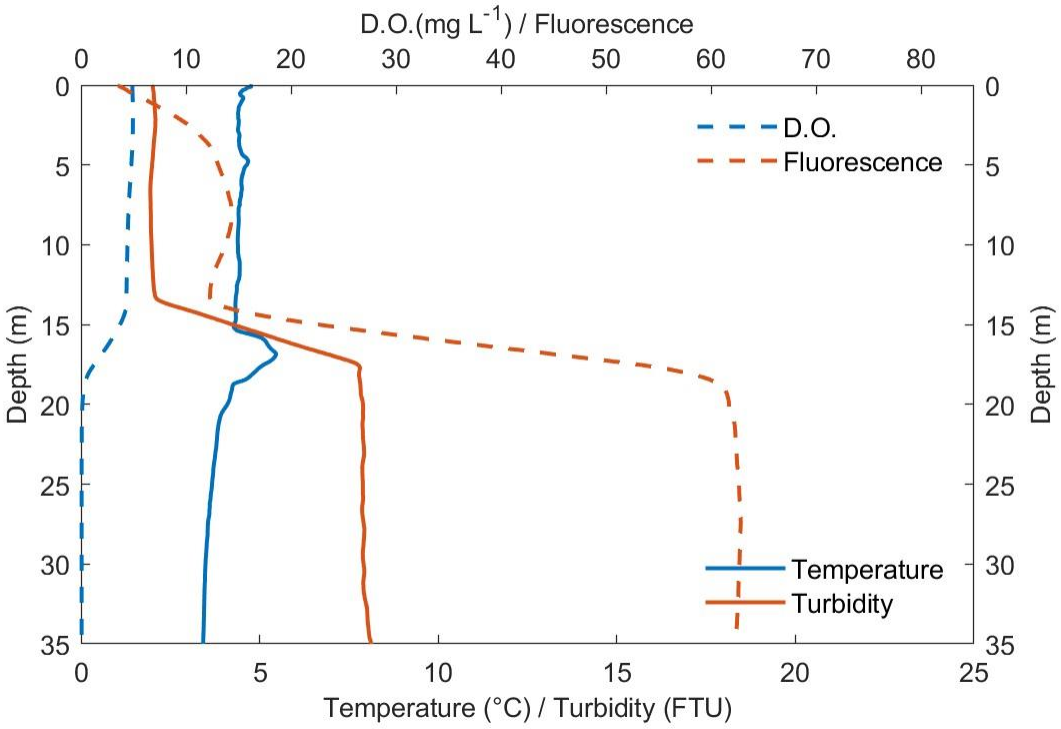

Ammonium

Nitrogen remains the primary limiting macronutrient in Mono Lake, as phosphate is abundant year-round at concentrations between 350 and 450 µM (Melack and Jellison 1998). External nitrogen inputs are low compared to internal recycling fluxes within the lake (Jellison and Melack 1993a, b). Ammonium concentrations in the euphotic zone are influenced by a combination of excretion by *Artemia*, uptake by algae, upward fluxes from deeper layers, release from sediments, volatilization, and minor external inputs. Since a substantial portion of particulate nitrogen, in the form of algal detritus and *Artemia* fecal pellets, sinks and undergoes remineralization in the hypolimnion, vertical mixing plays a critical role in regulating internal nitrogen cycling throughout the year.

In 2024, ammonium concentrations at the deep, central Station 6 followed the expected seasonal trend, with low epilimnetic concentrations in the upper water column and a progressive accumulation of ammonium in the hypolimnion over time (Table 5, Fig. 32). On 13 March, ammonium concentrations were elevated at 12 m (20 µM) and increased at 16 m (82.3 µM). The persistence of deep-water ammonium with limited vertical exchange indicates that the

chemocline restricted the upward transport of nutrients. By 16 May, ammonium concentrations in surface waters (≤8 m) were below 0.3 µM, while hypolimnetic concentrations increased to 57.7 µM at 16 m and 93.6 µM at 35 m.

Ammonium accumulation in deep waters continued throughout the summer, peaking at 105.6 µM at 35 m on 23 September and reaching a maximum of 133.4 µM by 19 December at 35 m. The high ammonium concentrations in October and November (>88 µM) from 20–35 m highlight the ongoing isolation of Mono Lake's monimolimnion, where organic matter remineralization fuels nutrient accumulation in an environment largely decoupled from surface processes.

Ammonium concentrations for August at depths 16, 20, 24, 28, and 35 m are not reported due to anomalies or inconsistencies. Despite these missing values, ammonium trends from other depths and sampling periods remain consistent with expected seasonal patterns.

Table 5. Ammonium (µM) profiles at Station 6, March–December, 2024.

Depth	Dates									
(m)	3/13	4/16	5/16	6/19	7/18	8/15	9/23	10/14	11/18	12/19
0.2	0.5	0.3	0.2	0.4	1.3	0.6	2.3	0.6	0.2	0.4
2	1.3	0.4	0.3	0.5	1.1	0.4	2.2	0.7	0.3	0.3
8	1.8	0.2	0.2	0.4	0.8	0.5	1.3	0.6	0.3	0.4
12	20.0	0.5	5.1	5.7	5.7	0.4	1.4	0.8	0.3	0.3
16	82.3	51.4	57.7	71.8	64.5		64.2	65.1	30.7	2.5
20	73.1	62.3	97.5	80.6	81.4		91.1	67.8	92.6	105.7
24	80.2	61.3	88.0	84.6	78.8		75.2	64.5	88.4	121.3
28	100.2	64.0	83.8	94.2	77.8		69.3	68.0	91.9	127.5
35	90.3	66.0	93.6	90.1	86.2		105.6	96.7	107.7	133.4

Fig. 32. Ammonium at Station 6, 2024. Isopleths are ammonium concentrations (µM).

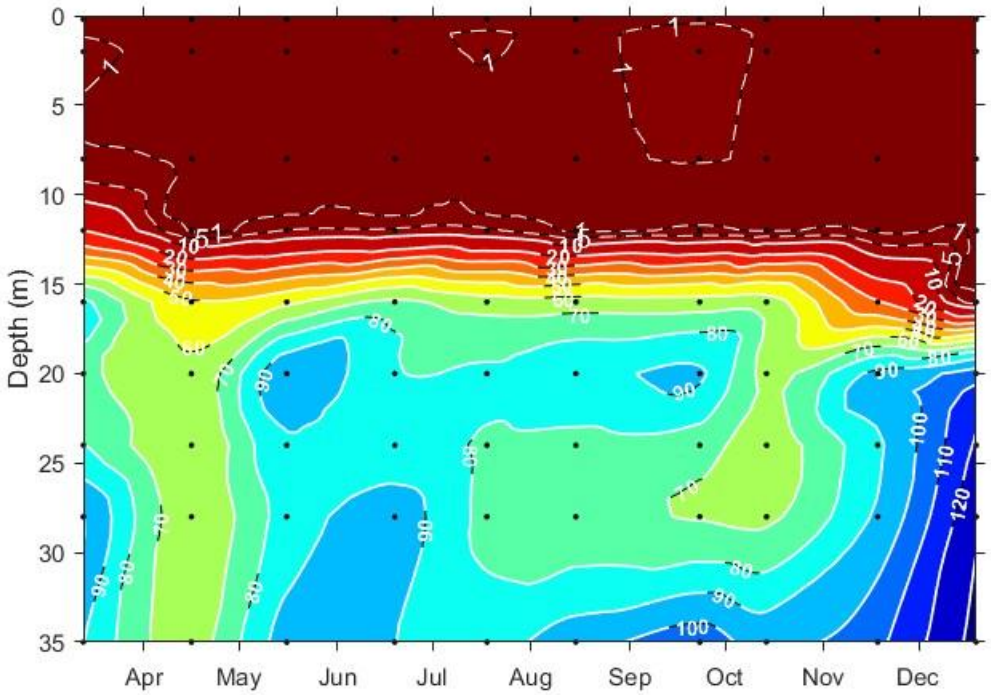

Epilimnetic ammonium concentrations, as indicated by the upper 9-m lakewide integrated samples, were generally below 2 µM throughout most of the year, except for July, August and September, when mean ammonium concentrations ranged from 2.5 to 3.0 µM at Station 1 (Table 6). The lowest ammonium concentrations occurred in April and November, when surface values were as low as 0.3 µM. Spatial variability among stations was also evident, with the highest surface values observed at Station 1 from July to September (Fig. 33).

Table 6. Ammonium (µM) lakewide at 7 stations in upper 9 m of water column, March–December, 2024. S.E. is standard error. '*' in '11/18' column indicates stations sampled on 11/18.

	Dates									
Station	3/18	4/16	5/16	6/18	7/16	8/15	9/23	10/15	11/14 11/18*	12/19
1	0.6	0.5	0.4	1.2	3.0	3.1	2.5	0.5	0.6	1.3
2	0.4	0.2	0.6	0.3	1.2	2.4	2.1	0.8	0.3	0.6
5	1.1	0.4	0.4	0.4	1.4	1.0	2.5	1.4	0.2	0.3
6	0.8	0.2	0.5	0.3	0.4	1.2	2.4	1.7	0.3	0.5
7	0.9	0.3	0.5	0.2	1.0	0.7	1.5	1.8	0.2	0.5
8	0.8	0.2	0.2	0.2	0.4	0.8	1.3	0.5	0.2*	0.5
11	0.8	0.2	0.3	0.2	0.4	1.5	2.5	0.7	0.3*	0.4
Mean	0.77	0.30	0.41	0.39	1.12	1.52	2.11	1.05	0.30	0.57
S.E.	0.09	0.04	0.05	0.14	0.34	0.34	0.20	0.21	0.05	0.13

Fig. 33. Ammonium (µM) in upper 9 m of the water column at 7 stations, 2024.

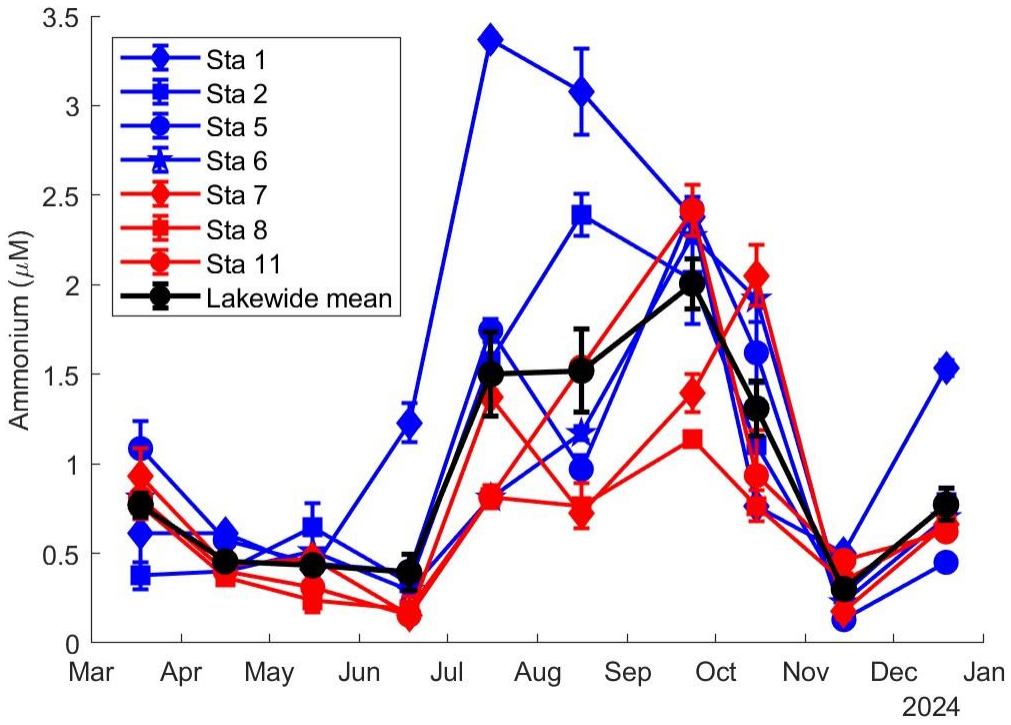

Phytoplankton

Phytoplankton abundance, as characterized by chlorophyll *a* concentration, shows pronounced seasonal variation. High phytoplankton abundance in spring is followed by low phytoplankton biomass during summer due to *Artemia* grazing.

On 18 March 2024, chlorophyll concentrations at Station 6 remained relatively low throughout the water column (above 8 m depth), ranging from 17.5 to 18.4 µg chl L^{-1} (Table 7, Fig. 34). During the 16 April survey, algal biomass had a slight increase, with concentrations ranging from 19.9 to 24.3 µg chl L^{-1}. By May, epilimnetic algal biomass at 8 m depth declined to 15.5 µg chl L^{-1}, and near surface water (< 2 m) concentrations ranged from 4.5 to 6.4 µg chl L^{-1}. This downward trend continued in June, with epilimnetic chlorophyll concentrations (upper 8 m) dropping further to 2.8 µg chl L^{-1}. The July survey recorded the lowest concentrations, ranging between 1.8 and 1.5 µg chl L^{-1}. Between July and October 2024, chlorophyll concentrations in the water column at Station 6 remained consistently low, fluctuating between 2.7 and 3.3 µg chl L^{-1}. Levels gradually increased in late autumn (10.3 to 10.8 µg chl L^{-1}) and continued rising in winter (24.1 to 27.9 µg chl L^{-1}) as the *Artemia* population declined (Table 7, Fig. 34).

At greater depths (12 m and below), chlorophyll concentrations were high during the 13 March survey and remained elevated until 19 June, ranging from 47.9 to 131.4 µg chl L^{-1}. Beginning in July, a pronounced increase in chlorophyll concentration at 16 m was observed, persisting through November before declining in December (Table 7, Fig. 34). This pattern suggests the formation of a deep chlorophyll maximum (DCM) at ~16 m, likely driven by stratification and nutrient availability. The stability of the pycnocline during late summer and autumn would have confined phytoplankton within this depth range, where light levels were still sufficient for photosynthesis and ammonium concentrations were elevated (Table 5).

Consistently high ammonium concentrations at 16 m likely supported sustained phytoplankton growth at this depth. However, by November, ammonium began to decline and in December, had dropped to 2.5 µM, coinciding with a large reduction in chlorophyll *a* (from 245.7 µg L^{-1} in November to 27.9 µg L^{-1} in December). This suggests that the depletion of available ammonium, along with increasing wind-driven turbulence in November and December, contributed to the breakdown of the DCM.

Profiles of fluorescence, turbidity, and extracted chlorophyll data at 16 m support the presence of a DCM, maintained by nutrient retention and stratification until late autumn. The breakdown of this structure in December, along with declining ammonium availability at 16 m, indicates a transition towards a more mixed but still stratified system, with deep nutrient regeneration continuing separately from surface and mid-depth biological processes.

Table 7. Chlorophyll *a* (µg L^{-1}) at Station 6, March–December 2024.

Depth	Dates									
(m)	3/13	4/16	5/16	6/19	7/18	8/15	9/23	10/14	11/18	12/19
0.2	18.4	19.9	4.5	1.3	1.5	3.3	2.7	3.4	10.8	26.2
2	17.8	23.5	6.4	1.5	1.6	3.7	3.0	3.4	11.3	24.1
8	17.5	24.3	15.5	2.8	1.8	3.3	2.8	3.7	10.5	26.7
12	74.6	70.4	47.9	72.5	5.2	5.9	4.7	4.2	10.6	27.6
16	109.9	131.4	109.3	92.2	107.8	117.0	180.4	209.4	245.7	27.9
20	95.8	104.1	112.9	93.6	85.5	108.1	106.4	108.4	99.4	135.5
24	95.9	123.0	109.7	95.5	79.3	116.7	119.9	118.1	98.1	125.0
28	94.7	104.2	107.6	106.2	101.0	129.3	115.0	114.4	90.4	136.4
35	84.8	102.8	86.4	101.5	86.5	130.7	203.5	119.9	96.5	139.8

Fig. 34. Chlorophyll *a* at Station 6, March–December, 2024. Isopleths of chlorophyll concentration (µg L^{-1}).

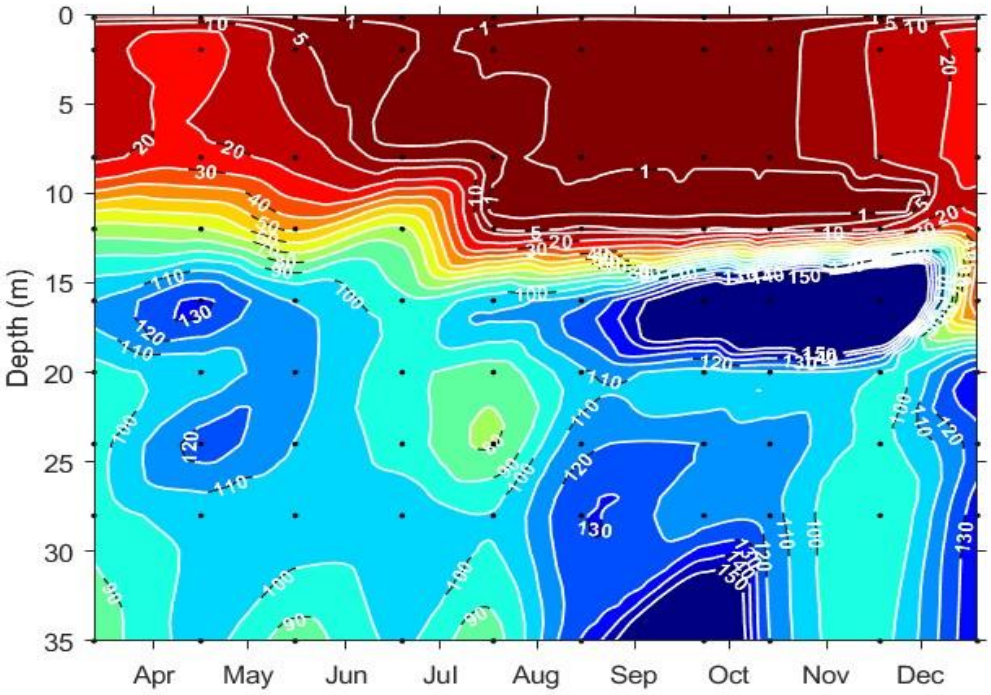

On 18 March, chlorophyll *a* concentrations in upper 9-m integrated samples collected from seven lakewide stations were relatively low and showed little variation, ranging from 18.3 to 15.6 µg chl L^{-1}. By 16 April, concentrations increased slightly, ranging from 26.2 to 19.2 µg chl L^{-1} (Table 8, Fig. 35). A 50% decrease in chlorophyll concentration was observed by 16 May, with a lakewide mean of 8.8 ± 0.5 µg chl L^{-1}. Epilimnetic chlorophyll levels continued to decline, reaching low values by the 18 June survey, with a lakewide mean of 1.9 ± 0.1 µg chl L^{-1}. On 16 July, algal biomass reached its lowest lakewide concentration, with a mean of 1.6 ± 0.1 µg chl L^{-1}. However, concentrations began to rise in late autumn, exceeding 2.3 µg chl L^{-1}. By 14 November, epilimnetic algal biomass in the upper 9 m increased to 10.9–9.4 µg chl L^{-1}, with a lakewide mean of 10.2 ± 0.2 µg chl L^{-1}. This upward trend continued in December, with epilimnetic chlorophyll concentrations rising further to 25.2–17.9 µg chl L^{-1} (Table 8, Fig. 35).

Table 8. Chlorophyll *a* (µg L $^{-1}$) at 7 stations in upper 9 m of water column, March–December 2024. S.E. is standard error. '*' in '11/18' column indicates stations sampled on 11/18.

	Dates									
Station	3/18	4/16	5/16	6/18	7/16	8/15	9/23	10/15	11/14 11/18*	12/19
1	16.7	22.6	10.4	1.3	1.2	0.8	0.9	2.5	10.7	21.1
2	16.8	22.1	9.0	1.8	1.8	1.3	1.5	3.0	10.7	23.8
5	16.2	26.2	6.8	2.0	1.5	2.5	2.8	3.2	9.6	23.0
6	15.6	23.8	8.9	1.8	1.9	2.8	2.9	3.3	9.4	23.8
7	17.3	19.8	7.2	2.1	1.8	4.0	3.2	4.8	9.7	25.2
8	18.3	19.7	9.1	2.1	1.4	3.6	3.0	4.5	10.1*	17.9
11	16.0	19.2	10.1	2.4	1.3	2.0	1.6	6.4	10.9*	20.9
Mean	16.7	21.9	8.8	1.9	1.6	2.4	2.3	4.0	10.2	22.2
S.E.	0.3	1.0	0.5	0.1	0.1	0.4	0.3	0.5	0.2	0.9

Fig. 35. Chlorophyll *a* (µg chl *a* L^{-1}) in upper 9 m of the water column at 7 stations, 2024.

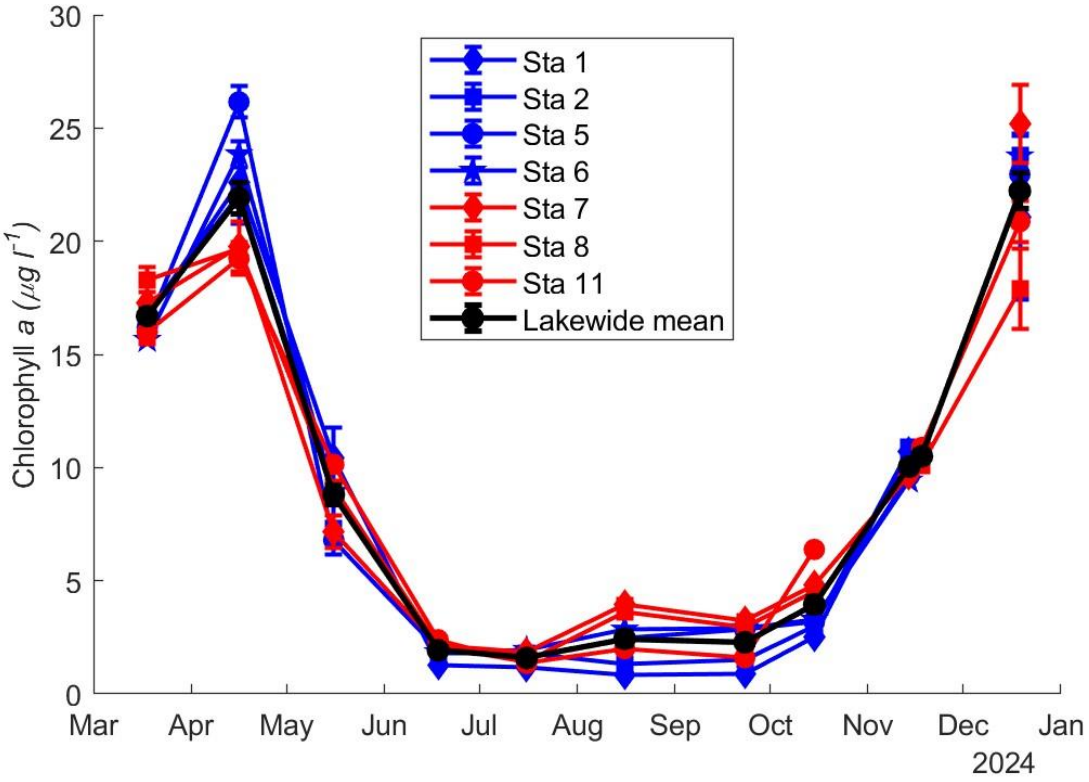

The large seasonal variation in epilimnetic chlorophyll concentrations (integrated over the upper 9 m) masks the significant but less pronounced spatial differences observed throughout the year. Early in the year, phytoplankton abundance is generally lower in the eastern sector of

the lake (Stations 7, 8, and 11) compared to the western sector (Stations 1, 2, 5, and 6), but it increases during the summer. This pattern appears to be inversely related to *Artemia* abundance.

In 2024, while chlorophyll concentrations were relatively evenly distributed across all stations, algal biomass in the eastern sector was slightly higher than in the western sector during the summer months (Fig. 35).

Artemia Population Dynamics

Zooplankton populations in temperate lakes are highly variable across spatial and temporal scales. The Mono Lake monitoring program collects samples from 12 stations distributed across the lake and the relative standard errors of lakewide estimates are typically 10-20%. However, on any given sample date the standard error of a lakewide estimate may be smaller or larger depending on the spatial variability. Local convergences of water masses may concentrate shrimp to well above the overall mean. For these reasons, a single level of significant figures in presenting data (e.g., rounding to 10s, 100s, 1000s or even 10,000s) is inappropriate, and standard errors of each lakewide estimate are included using the ± notation. The reader is cautioned to consider the standard errors when making inferences from the data.

Hatching of Over-wintering Cysts and Maturation of the 1st Generation

Hatching of overwintering cysts is initiated by warming water temperatures and oxic sediment conditions. The peak of hatching usually occurs during March, but significant hatching may occur during February. A small amount of hatching may even occur during January in shallow nearshore regions. The survey conducted on 18 March indicated that the spring *Artemia* hatch was underway, with abundances among 12 stations ranging from 9,000 to 100,000 individuals m^{-2}. The estimated lakewide abundance was 32,000 ± 7,000 m^{-2}, with a mean abundance of naupliar instars at 32,000 ± 7,000 m^{-2} (Table 9, Table 10). The population was primarily composed of instars 1 (23%), 2 (46%), and 3 (24%), with a smaller presence of instars 4 and 5, as well as juveniles (Table 11, Table 12, Table 14). A few adults were present resulting in a lakewide estimate of 155 ± 45 m^{-2}.

Table 9. Mean *Artemia* lakewide and sector abundances (m^{-2}), March–December 2024. Adult females are separated depending on eggs present: und, undifferentiated egg mass; empty, empty ovisac; cyst, cysts in ovisac; nauplii, naupliar eggs in ovisac. Lakewide refers to Stations 1-12, western sector refers to Stations 1-6, and eastern sector refers to Stations 7-12. Note: Before making inferences from this data, it is important to review the standard error associated with *Artemia* counts in Table 10.

		Instars	Adult			Adult female		Adult fem	Adult	
	1-7	8-11	male	und	empty	cyst	nauplii	total	total	Total
Lakewide										
3/18	31,640	47	97	0	54	0	0	54	151	31,838
4/16	73,476	27	0	0	15	0	0	15	15	73,518
5/16	23,997	31,107	1,489	0	6,841	0	0	6,841	8,330	63,434
6/18	6,472	27,116	6,539	134	15,526	27	0	15,687	22,227	55,815
7/16	4,809	12,193	11,268	476	9,980	2,482	248	13,186	24,453	41,455
8/15	5,459	3,280	12,797	94	4,038	7,606	832	12,569	25,366	34,105
9/23	8,159	865	12,746	211	962	6,992	919	9,085	21,831	30,855
10/15	7,611	624	7,772	50	379	5,679	453	6,561	14,333	22,567
11/16	6,849	1,997	3,181	0	647	3,820	444	4,911	8,092	16,938
12/19	1,875	649	101	0	298	65	5	369	469	2,993
Western Sector										
3/18	25,801	27	47	0	40	0	0	40	87	25,915
4/16	39,427	27	0	0	30	0	0	30	30	39,484
5/16	19,182	23,367	1,797	0	5,848	0	0	5,848	7,646	50,195
6/18	6,385	34,017	8,853	161	23,823	54	0	24,038	32,891	73,293
7/16	5,929	15,909	13,843	349	13,038	2,468	134	15,989	29,832	51,670
8/15	5,446	5,017	17,492	107	5,875	8,102	778	14,863	32,354	42,817
9/23	6,211	1,274	16,968	282	1,422	9,323	1,127	12,153	29,121	36,606
10/15	9,423	677	11,569	0	711	8,089	516	9,316	20,885	30,986
11/14	6,076	1,999	4,608	0	1,019	5,848	765	7,632	12,240	20,315
12/19	667	563	121	0	288	80	10	379	500	1,730
Eastern Sector										
3/18	37,478	67	148	0	67	0	0	67	215	37,760
4/16	107,525	27	0	0	0	0	0	0	0	107,552
5/16	28,813	38,846	1,180	0	7,834	0	0	7,834	9,014	76,673
6/18	6,559	20,215	4,225	107	7,230	0	0	7,337	11,563	38,337
7/16	3,689	8,478	8,692	604	6,922	2,495	362	10,382	19,074	31,241
8/15	5,473	1,543	8,102	80	2,200	7,109	885	10,275	18,377	25,392
9/23	10,107	456	8,524	141	503	4,661	711	6,016	14,541	25,104
10/15	5,798	570	3,974	101	47	3,270	389	3,806	7,780	14,148
11/18	7,622	1,995	1,754	0	275	1,791	124	2,190	3,944	13,561
12/19	3,082	734	80	0	309	50	0	359	439	4,256

Table 10. Standard errors of *Artemia* lakewide and sector means (Table 9), March–December 2024. Adult females are separated depending on eggs present: und, undifferentiated egg mass; empty, empty ovisac; cyst, cysts in ovisac; nauplii, naupliar eggs in ovisac. Lakewide refers to Stations 1 -12, western sector refers to Stations 1-6, and eastern sector refers to Stations 7-12.

		Instars	Adult			Adult female		Adult fem	Adult	
	1-7	8-11	male	und	empty	cyst	nauplii	total	total	Total
Lakewide										
3/18	7,031	21	35	0	28	0	0	28	43	7,054
4/16	15,647	18	0	0	13	0	0	13	13	15,642
5/16	2,757	3,885	199	0	780	0	0	780	822	6,703
6/18	1,199	3,828	1,157	74	3,386	27	0	3,366	4,132	7,907
7/16	693	1,666	1,356	137	1,458	480	81	1,836	3,138	5,059
8/15	904	940	2,141	41	1,046	923	125	1,811	3,734	4,591
9/23	1,347	232	2,459	69	255	1,605	164	2,029	4,412	4,841
10/15	1,406	121	1,608	34	227	1,366	59	1,604	3,061	4,274
11/16	1,103	377	792	0	210	1,428	216	1,836	2,600	3,372
12/19	489	114	21	0	74	17	4	85	101	611
Western Sector										
3/18	5,818	27	26	0	25	0	0	25	26	5,851
4/16	17,910	27	0	0	26	0	0	26	26	17,912
5/16	2,801	3,229	344	0	1,162	0	0	1,162	1,300	5,210
6/18	1,474	3,309	1,181	110	4,437	54	0	4,334	4,396	5,892
7/16	1,015	2,201	1,853	205	1,836	462	105	2,396	4,175	6,578
8/15	1,627	1,569	3,083	68	1,797	1,384	158	2,916	5,575	6,956
9/23	1,252	358	4,356	117	397	2,933	273	3,633	7,896	8,999
10/15	2,358	238	2,288	0	425	2,270	57	2,686	4,626	6,616
11/14	776	406	1,272	0	366	2,608	403	3,344	4,586	5,417
12/19	184	109	29	0	63	26	7	77	95	330
Eastern Sector										
3/18	13,040	32	60	0	53	0	0	53	77	13,064
4/16	17,108	27	0	0	0	0	0	0	0	17,101
5/16	4,039	5,658	136	0	965	0	0	965	1,048	10,022
6/18	2,037	5,872	1,535	107	1,797	0	0	1,783	3,209	10,871
7/16	764	1,357	1,414	186	1,497	894	113	2,437	3,785	5,253
8/15	972	469	1,361	51	488	1,317	207	1,955	3,275	3,739
9/23	2,213	204	708	72	209	749	165	1,073	1,430	2,984
10/15	1,350	79	605	64	39	858	102	1,036	1,628	2,877
11/18	2,125	678	569	0	67	726	45	827	1,351	4,016
12/19	659	207	31	0	142	21	0	162	188	948

Table 11. Percentage in different classes for *Artemia* lakewide and sector means (Table 9), March–December 2024. Adult females are separated depending on eggs present: und, undifferentiated egg mass; empty, empty ovisac; cyst, cysts in ovisac; nauplii, naupliar eggs in ovisac. Lakewide refers to Stations 1 -12, western sector refers to Stations 1-6, and eastern sector refers to Stations 7-12. Adult female "und", "cyst", and "nauplii", given as percentage of ovigerous females. Adult female "empty" given as percentage of adult females. “Instars 1-7”, “Instars 8-11”, “Adult male”, “Adult fem total”, “Adult total” given as percentage of total shrimp.

		Instars	Adult			Adult female		Adult fem	Adult	
	1-7	8-11	male	und	empty	cyst	nauplii	total	total	Total
Lakewide										
3/18	99.4	0.1	0.3	0.0	100.0	0.0	0.0	0.2	0.5	100
4/16	99.9	0.0	0.0	0.0	100.0	0.0	0.0	0.0	0.0	100
5/16	37.8	49.0	2.3	0.0	100.0	0.0	0.0	10.8	13.1	100
6/18	11.6	48.6	11.7	83.3	99.0	16.7	0.0	28.1	39.8	100
7/16	11.6	29.4	27.2	14.9	75.7	77.4	7.7	31.8	59.0	100
8/15	16.0	9.6	37.5	1.1	32.1	89.2	9.7	36.9	74.4	100
9/23	26.4	2.8	41.3	2.6	10.6	86.1	11.3	29.4	70.8	100
10/15	33.7	2.8	34.4	0.8	5.8	91.9	7.3	29.1	63.5	100
11/16	40.4	11.8	18.8	0.0	13.2	89.6	10.4	29.0	47.8	100
12/19	62.6	21.7	3.4	0.0	80.9	92.9	7.1	12.3	15.7	100
Western Sector										
3/18	99.6	0.1	0.2	0.0	100.0	0.0	0.0	0.2	0.3	100
4/16	99.9	0.1	0.0	0.0	100.0	0.0	0.0	0.1	0.1	100
5/16	38.2	46.6	3.6	0.0	100.0	0.0	0.0	11.7	15.2	100
6/18	8.7	46.4	12.1	75.0	99.1	25.0	0.0	32.8	44.9	100
7/16	11.5	30.8	26.8	11.8	81.5	83.6	4.5	30.9	57.7	100
8/15	12.7	11.7	40.9	1.2	39.5	90.1	8.7	34.7	75.6	100
9/23	17.0	3.5	46.4	2.6	11.7	86.9	10.5	33.2	79.6	100
10/15	30.4	2.2	37.3	0.0	7.6	94.0	6.0	30.1	67.4	100
11/14	29.9	9.8	22.7	0.0	13.4	88.4	11.6	37.6	60.3	100
12/19	38.6	32.6	7.0	0.0	76.1	88.9	11.1	21.9	28.9	100
Eastern Sector										
3/18	99.3	0.2	0.4	0.0	100.0	0.0	0.0	0.2	0.6	100
4/16	100.0	0.0	0.0	0.0	0.0	0.0	0.0	0.0	0.0	100
5/16	37.6	50.7	1.5	0.0	100.0	0.0	0.0	10.2	11.8	100
6/18	17.1	52.7	11.0	100.0	98.5	0.0	0.0	19.1	30.2	100
7/16	11.8	27.1	27.8	17.4	66.7	72.1	10.5	33.2	61.1	100
8/15	21.6	6.1	31.9	1.0	21.4	88.0	11.0	40.5	72.4	100
9/23	40.3	1.8	34.0	2.6	8.4	84.5	12.9	24.0	57.9	100
10/15	41.0	4.0	28.1	2.7	1.2	87.0	10.3	26.9	55.0	100
11/18	56.2	14.7	12.9	0.0	12.6	93.5	6.5	16.1	29.1	100
12/19	72.4	17.3	1.9	0.0	86.0	100.0	0.0	8.4	10.3	100

Artemia lakewide abundance reached 74,000 ± 16,000 m^{-2} by the mid-April survey as the spring hatch continued (Table 9, Table 10). The population consisted almost entirely of naupliar instars (99.9%) with instars 3-5 constituting 79.5% of the total population (Table 14). Naupliar abundance decreased 16 May 2024 with abundance ranging from 11,000 to 44,000 m^{-2} among the 12 stations, and an overall lakewide mean of 24,000 ± 3,000 m^{-2} (Table 9). The majority of the population was evenly distributed among naupliar instars 7 and juveniles, constituting 83.6% of the total population. Adult *Artemia* constituted 13.1% of the total population on 16 May 2024, when they numbered 8,000 ± 100 m^{-2} (Table 15, Table 16), with adult male and adult female being 2.3% and 10.8%, respectively.

On 18 June, naupliar abundance dropped to 6,000 ± 1,000 m^{-2}, constituting only 11.6% of the total population, with juveniles and adults being 48.6% and 39.8%, respectively (Table 9, Table 10, Table 11). Fecund females were present during the 18 June survey only at Stations 2, 6, and 10, with a lakewide mean of 161 ± 93 m^{-2} (Table 15, Table 16). Lakewide mean naupliar abundance declined further to 5,000 ± 1000 m^{-2} on 16 July, followed by a decline in juveniles and an increase in adults (29% and 59% of the total population, respectively) (Table 9, Table 10, Table 11).

Mean lakewide adult abundance peaked on 15 August at 25,000 ± 4,000 m^{-2} and remained high on 23 September at 22,000 ± 4,000 m^{-2} (Table 9, Table 10). This was followed by a decline in the following months, with abundances of 14,000 ± 3,000 m^{-2} in October and 8,000 ± 3,000 m^{-2} in November. By 19 December, adult numbers had decreased to 500 ± 100 m^{-2}.

The hatching of overwintering cysts was generally higher in the eastern sector of the lake, which has gradually sloping, shallow sediments. During the March, April, and May surveys, naupliar abundance in the east was consistently greater than in the west. In March, the mean naupliar abundance was 37,000 ± 13,000 m^{-2} in the east compared to 26,000 ± 6,000 m^{-2} in the west. This trend continued in April and May, with 108,000 ± 17,000 m^{-2} and 29,000 ± 3,000 m^{-2} in the east, respectively, versus 39,000 ± 18,000 m^{-2} and 19,000 ± 3,000 m^{-2} in the west (Fig. 36).

Juvenile and naupliar abundance remained higher in the eastern sector through June, with 7,000 ± 2,000 m^{-2} naupliar abundance in the east compared to 6,000 ± 1,000 m^{-2} in the west. However, this pattern shifted in July, when naupliar abundance was higher in the western sector

(6,000 ± 1,000 m^{-2}) than in the east (4,689 ± 000 m^{-2}). This difference persisted in subsequent months, with the western sector showing higher total *Artemia* abundance than the eastern sector in August and September, particularly among adult populations (Fig. 36).

By October and November, naupliar abundance had declined in both sectors, but the western sector continued to have slightly higher total *Artemia* abundance. By December, nauplii and juveniles had very low across the lake.

Table 12. Mean *Artemia* lakewide and sector instar analysis, March–December 2024. Lakewide refers to Stations 1, 2, 5, 6, 7, 8, and 11, western sector refers to Stations 1, 2, 5, and 6, and eastern sector refers to Stations 7, 8, and 11. Instars 8-11 refers to juveniles. Note: Before making inferences from this data, it is important to review standard errors associated with *Artemia* counts in Table 13.

	Instars									
	1	2	3	4	5	6	7	8-11	Adults	Total
Lakewide										
3/18	8,347	16,643	8,612	2,162	69	0	0	46	155	36,033
4/16	2,176	6,712	12,636	18,554	28,934	4,996	1,581	0	26	75,614
5/16	2,346	1,242	1,610	2,575	3,403	4,415	8,462	29,572	7,496	61,121
6/18	2,552	3,771	931	184	92	0	414	33,193	21,592	62,731
7/16	1,311	1,886	943	471	161	46	23	12,049	25,594	42,483
8/15	2,070	1,518	977	908	379	92	0	3,794	26,272	36,010
9/23	575	1,035	1,311	1,403	897	333	391	862	16,350	23,156
10/15	354	644	1,204	1,167	1,624	946	601	454	11,095	18,089
11/16	1,319	351	529	693	1,406	1,242	1,725	2,383	10,578	20,224
12/19	319	178	135	152	259	224	356	555	540	2,719
Western Sector										
3/18	6,901	10,292	4,889	1,087	0	0	0	0	91	23,260
4/16	1,273	3,335	6,459	12,269	17,918	2,626	231	0	45	44,155
5/16	2,093	885	1,690	2,575	2,495	3,300	6,117	23,984	6,278	49,416
6/18	2,897	3,622	805	0	0	0	483	37,666	27,284	72,757
7/16	1,771	2,616	1,127	443	241	80	40	16,700	32,596	55,614
8/15	2,495	1,690	1,087	1,127	80	0	0	5,433	31,751	43,662
9/23	664	986	1,368	1,167	765	302	121	946	17,404	23,722
10/15	423	714	1,469	1,328	1,761	895	624	372	14,909	22,495
11/14	1,117	141	342	724	1,127	1,066	1,801	2,193	14,366	22,877
12/19	161	65	35	25	60	91	171	443	508	1,559
Eastern Sector										
3/18	10,275	25,111	13,575	3,595	161	0	0	107	241	53,065
4/16	3,380	11,214	20,872	26,935	43,622	8,156	3,380	0	0	117,559
5/16	2,683	1,717	1,502	2,575	4,614	5,902	11,590	37,022	9,121	76,727
6/18	2,093	3,970	1,100	429	215	0	322	27,230	14,004	49,363
7/16	698	912	698	510	54	0	0	5,848	16,258	24,977
8/15	1,502	1,288	832	617	778	215	0	1,610	18,967	25,808
9/23	456	1,100	1,234	1,717	1,073	376	751	751	14,943	22,401
10/15	262	550	852	952	1,442	1,013	570	563	6,009	12,213
11/18	1,590	630	778	651	1,777	1,476	1,623	2,636	5,526	16,687
12/19	530	329	268	322	523	402	604	704	584	4,266

Table 13. Standard errors of *Artemia* lakewide and sector instar analysis (Table 12), March–December 2024. Lakewide refers to Stations 1, 2, 5, 6, 7, 8, and 11, western sector refers to Stations 1, 2, 5, and 6, and eastern sector refers to Stations 7, 8, and 11. Instars 8-11 refers to juveniles.

	Instars									
	1	2	3	4	5	6	7	8-11	Adults	Total
Lakewide										
3/18	1,679	5,457	3,475	1,223	48	0	0	30	45	11,608
4/16	739	2,271	4,138	5,604	9,688	2,601	1,197	0	23	23,944
5/16	781	293	330	766	706	1,015	1,803	5,798	978	10,703
6/18	646	1,000	230	138	59	0	207	5,036	4,214	10,434
7/16	527	423	229	90	93	46	23	2,859	4,674	8,142
8/15	690	289	250	464	208	59	0	1,529	5,540	6,904
9/23	154	199	359	420	283	100	188	187	1,423	2,660
10/15	124	196	316	290	414	294	141	80	2,466	3,170
11/16	546	198	184	186	409	293	381	534	4,163	5,302
12/19	111	80	69	88	129	95	131	149	162	894
Western Sector										
3/18	763	4,256	2,834	798	0	0	0	0	25	8,000
4/16	283	1,930	3,747	7,100	14,066	1,651	142	0	39	27,510
5/16	1,369	357	532	1,076	942	835	1,138	5,067	934	8,027
6/18	975	1,063	161	0	0	0	308	3,729	4,054	9,255
7/16	877	428	341	121	154	80	40	3,365	5,934	9,542
8/15	1,126	423	391	815	80	0	0	2,388	8,361	10,409
9/23	133	268	528	452	324	125	77	238	2,078	3,711
10/15	221	315	481	443	621	314	224	100	2,940	3,423
11/14	518	141	116	257	237	231	467	362	6,826	7,937
12/19	99	46	24	19	22	29	33	74	135	345
Eastern Sector										
3/18	3,914	10,464	6,850	2,720	93	0	0	54	80	23,692
4/16	1,547	3,302	5,694	7,585	8,518	5,760	2,676	0	0	30,985
5/16	653	387	429	1,340	653	1,970	3,407	11,636	1,624	21,444
6/18	915	2,170	543	284	107	0	322	10,890	6,407	20,841
7/16	284	234	284	163	54	0	0	967	2,501	3,709
8/15	722	426	336	316	390	107	0	887	5,322	5,085
9/23	343	361	581	858	568	193	349	349	1,948	4,636
10/15	42	248	356	397	632	637	198	121	1,623	4,085
11/18	1,219	409	395	330	969	667	754	1,297	2,404	7,736
12/19	169	145	131	168	235	183	252	354	382	1,806

Table 14. Lakewide and sector percentage (given as percentage of total shrimp) in different classes for *Artemia* instar analysis (Table 12), March–December 2024. Lakewide refers to Stations 1, 2, 5, 6, 7, 8, and 11, the western sector refers to Stations 1, 2, 5, and 6, and eastern sector refers to Stations 7, 8, and 11. Instars 8-11 refers to juveniles. Instars 1 – 7 given as percentage of total instars, "Instars 8-11", and "Adults" given as percentage of total shrimp.

	Instars									
	1	2	3	4	5	6	7	8-11	Adults	Total
Lakewide										
3/18	23.3	46.4	24.0	6.0	0.2	0.0	0.0	0.1	0.4	100
4/16	2.9	8.9	16.7	24.5	38.3	6.6	2.1	0.0	0.0	100
5/16	9.8	5.2	6.7	10.7	14.1	18.4	35.2	48.4	12.3	100
6/18	32.1	47.5	11.7	2.3	1.2	0.0	5.2	52.9	34.4	100
7/16	27.1	39.0	19.5	9.7	3.3	1.0	0.5	28.4	60.2	100
8/15	34.8	25.5	16.4	15.3	6.4	1.5	0.0	10.5	73.0	100
9/23	9.7	17.4	22.1	23.6	15.1	5.6	6.6	3.7	70.6	100
10/15	5.4	9.8	18.4	17.8	24.8	14.5	9.2	2.5	61.3	100
11/16	18.2	4.8	7.3	9.5	19.4	17.1	23.7	11.8	52.3	100
12/19	19.6	11.0	8.3	9.4	15.9	13.8	21.9	20.4	19.9	100
Western Sector										
3/18	29.8	44.4	21.1	4.7	0.0	0.0	0.0	0.0	0.4	100
4/16	2.9	7.6	14.6	27.8	40.6	6.0	0.5	0.0	0.1	100
5/16	10.9	4.6	8.8	13.4	13.0	17.2	31.9	48.5	12.7	100
6/18	37.1	46.4	10.3	0.0	0.0	0.0	6.2	51.8	37.5	100
7/16	28.0	41.4	17.8	7.0	3.8	1.3	0.6	30.0	58.6	100
8/15	38.5	26.1	16.8	17.4	1.2	0.0	0.0	12.4	72.7	100
9/23	12.4	18.4	25.5	21.7	14.2	5.6	2.2	4.0	73.4	100
10/15	5.9	9.9	20.4	18.4	24.4	12.4	8.6	1.7	66.3	100
11/14	17.7	2.2	5.4	11.5	17.8	16.9	28.5	9.6	62.8	100
12/19	26.4	10.7	5.8	4.1	9.9	14.9	28.1	28.4	32.6	100
Eastern Sector										
3/18	19.5	47.6	25.8	6.8	0.3	0.0	0.0	0.2	0.5	100
4/16	2.9	9.5	17.8	22.9	37.1	6.9	2.9	0.0	0.0	100
5/16	8.8	5.6	4.9	8.4	15.1	19.3	37.9	48.3	11.9	100
6/18	25.7	48.8	13.5	5.3	2.6	0.0	4.0	55.2	28.4	100
7/16	24.3	31.8	24.3	17.8	1.9	0.0	0.0	23.4	65.1	100
8/15	28.7	24.6	15.9	11.8	14.9	4.1	0.0	6.2	73.5	100
9/23	6.8	16.4	18.4	25.6	16.0	5.6	11.2	3.4	66.7	100
10/15	4.6	9.8	15.1	16.9	25.6	18.0	10.1	4.6	49.2	100
11/18	18.6	7.4	9.1	7.6	20.8	17.3	19.0	15.8	33.1	100
12/19	17.8	11.0	9.0	10.8	17.6	13.5	20.3	16.5	13.7	100

Fig. 36. Lakewide *Artemia* abundance during 2024: nauplii (instars 1-7), juveniles (instars 8-11), and adults (instars 12+).

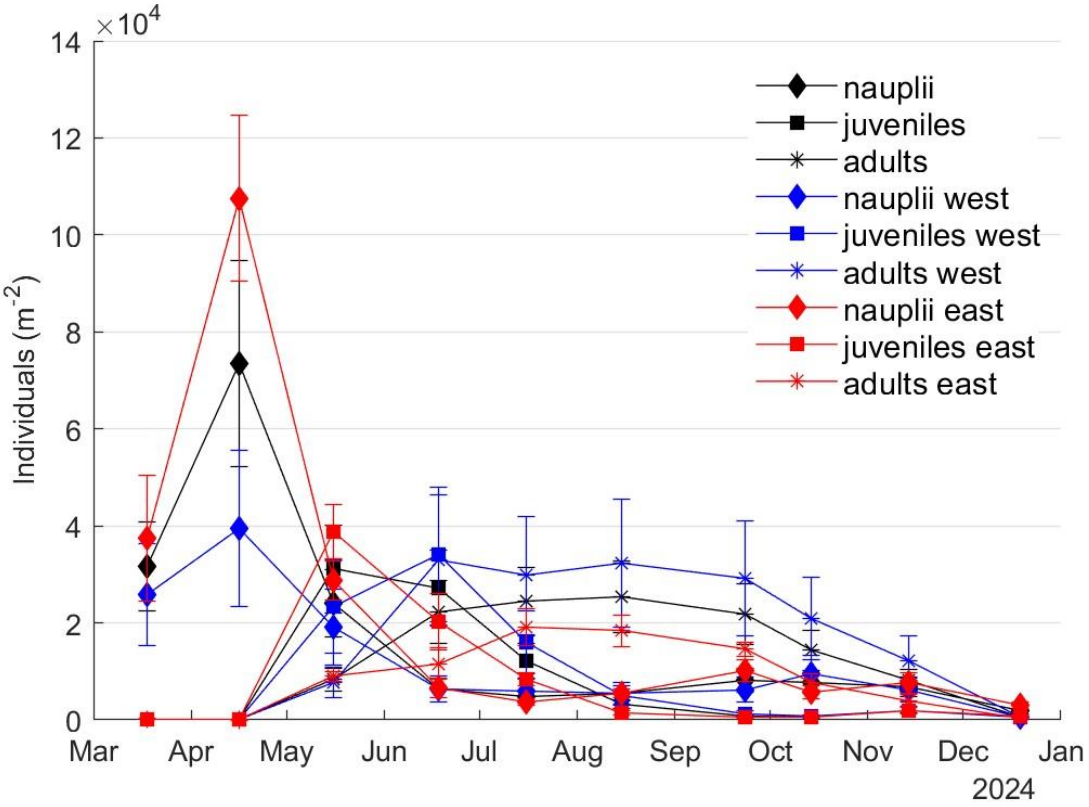

Ovoviviparous Reproduction and the Second Generation

Ovoviviparous reproduction depends on ambient food levels and age. *Artemia* produce multiple broods and ovoviviparous reproduction occurs primarily with the first brood, rarely occurring in second and subsequent broods.

During the early part of the reproductive season (March and April), the population included a small number of non-ovigerous females (54 ± 28 m^{-2} in March and 15 ± 13 m^{-2} in April). By the surveys on 16 May and 18 June, non-ovigerous females made up 10.8% and 28.1% of the total population, respectively. On 18 June, ovigerous females numbered 161 ± 93 m^{-2} and accounted for only 1% of the 3,000 total adult females, with the majority (99%) having empty ovisacs. By 16 July, ovigerous females increased to 25% of the population, totaling 13,000 ± 2,000 m^{-2} individuals, while females with empty ovisacs decreased to 76% (Table 15, Table 16, Table 17, Fig. 37).

Ovigerous females continued to increase through the summer, reaching 68% of 13,000 ± 1,811 m^{-2} females on August, 89% of 9,000 ± 2,000 m^{-2} on 23 September, and peaking at 94% of 7,000 ± 2,000 m^{-2} on 15 October. The percentage of ovigerous females declined to 87% of 5,000 ± 2,000m^{-2} on 16 November and further dropped to 19% of 400 ± 100 m^{-2} by 19 December. Cyst production remained consistently high, ranging from 88% to 93% of adult females between mid-July and mid-November (Table 15, Table 16, Table 17). The high abundance of later naupliar instars during July–September (Table 14) and the emergence of a secondary peak in adult population abundance suggest that a significant number of ovoviviparously produced individuals were successfully recruited into the adult population.

Table 15. Mean *Artemia* lakewide and sector reproductive summary, March–December 2024. Lakewide refers to Stations 1, 2, 5, 6, 7, 8, and 11, western sector refers to Stations 1, 2, 5, and 6, and eastern sector refers to Stations 7, 8, and 11. Adult female are separated depending on eggs present: und, undifferentiated egg mass; empty, empty ovisac; cyst, cysts in ovisac; nauplii, naupliar eggs in ovisac. Before making inferences from these data, review standard errors associated with *Artemia* counts in Table 16.

			Adult females			
	Total	Ovigery	empty	und	cyst	nauplii
Lakewide						
3/18	54	0	54	0	0	0
4/16	15	0	15	0	0	0
5/16	6,841	0	6,841	0	0	0
6/18	15,687	161	15,526	134	27	0
7/16	13,186	3,206	9,980	476	2,482	248
8/15	12,569	8,531	4,038	94	7,606	832
9/23	9,085	8,122	962	211	6,992	919
10/15	6,561	6,182	379	50	5,679	453
11/16	4,911	4,264	647	0	3,820	444
12/19	369	70	298	0	65	5
Western Sector						
3/18	40	0	40	0	0	0
4/16	30	0	30	0	0	0
5/16	5,848	0	5,848	0	0	0
6/18	24,038	215	23,823	161	54	0
7/16	15,989	2,951	13,038	349	2,468	134
8/15	14,863	8,987	5,875	107	8,102	778
9/23	12,153	10,731	1,422	282	9,323	1,127
10/15	9,316	8,605	711	0	8,089	516
11/14	7,632	6,613	1,019	0	5,848	765
12/19	379	91	288	0	80	10
Eastern Sector						
3/18	67	0	67	0	0	0
4/16	0	0	0	0	0	0
5/16	7,834	0	7,834	0	0	0
6/18	7,337	107	7,230	107	0	0
7/16	10,382	3,461	6,922	604	2,495	362
8/15	10,275	8,075	2,200	80	7,109	885
9/23	6,016	5,513	503	141	4,661	711
10/15	3,806	3,759	47	101	3,270	389
11/18	2,190	1,915	275	0	1,791	124
12/19	359	50	309	0	50	0

Table 16. Standard errors of *Artemia* lakewide and sector reproductive summary (Table 15), March–December 2024. Lakewide refers to Stations 1, 2, 5, 6, 7, 8, and 11, western sector refers to Stations 1, 2, 5, and 6, and eastern sector refers to Stations 7, 8, and 11. Adult females are separated depending on eggs present: und, undifferentiated egg mass; empty, empty ovisac; cyst, cysts in ovisac; nauplii, naupliar eggs in ovisac.

			Adult females			
	Total	Ovigery	empty	und	cyst	nauplii
Lakewide						
3/18	28	0	28	0	0	0
4/16	13	0	13	0	0	0
5/16	780	0	780	0	0	0
6/18	3,366	93	3,386	74	27	0
7/16	1,836	621	1,458	137	480	81
8/15	1,811	1,017	1,046	41	923	125
9/23	2,029	1,792	255	69	1,605	164
10/15	1,604	1,390	227	34	1,366	59
11/16	1,836	1,641	210	0	1,428	216
12/19	85	19	74	0	17	4
Western Sector						
3/18	25	0	25	0	0	0
4/16	26	0	26	0	0	0
5/16	1,162	0	1,162	0	0	0
6/18	4,334	159	4,437	110	54	0
7/16	2,396	624	1,836	205	462	105
8/15	2,916	1,502	1,797	68	1,384	158
9/23	3,633	3,256	397	117	2,933	273
10/15	2,686	2,269	425	0	2,270	57
11/14	3,344	3,010	366	0	2,608	403
12/19	77	31	63	0	26	7
Eastern Sector						
3/18	53	0	53	0	0	0
4/16	0	0	0	0	0	0
5/16	965	0	965	0	0	0
6/18	1,783	107	1,797	107	0	0
7/16	2,437	1,131	1,497	186	894	113
8/15	1,955	1,486	488	51	1,317	207
9/23	1,073	900	209	72	749	165
10/15	1,036	1,000	39	64	858	102
11/18	827	766	67	0	726	45
12/19	162	21	142	0	21	0

Table 17. *Artemia* lakewide and sector reproductive summary percentages (Table 15), March–December 2024. Lakewide refers to Stations 1, 2, 5, 6, 7, 8, and 11, western sector refers to Stations 1, 2, 5, and 6, and eastern sector refers to Stations 7, 8, and 11. Adult females are separated depending on eggs present: und, undifferentiated egg mass; empty, empty ovisac; cyst, cysts in ovisac; nauplii, naupliar eggs in ovisac. "Ovigery" and "empty" are given as percentages of total number of females. "und" is given as percentage of ovigerous females. Cyst and nauplii are given as percentage of individuals with differentiated egg masses.

		Adult females				
	Total	Ovigery	empty	und	cyst	nauplii
Lakewide						
3/18	100	0	100	0	0	0
4/16	100	0	100	0	0	0
5/16	100	0	100	0	0	0
6/18	100	1	99	83	100	0
7/16	100	24	76	15	91	9
8/15	100	68	32	1	90	10
9/23	100	89	11	3	88	12
10/15	100	94	6	1	93	7
11/16	100	87	13	0	90	10
12/19	100	19	81	0	93	7
Western Sector						
3/18	100	0	100	0	0	0
4/16	100	0	100	0	0	0
5/16	100	0	100	0	0	0
6/18	100	1	99	75	100	0
7/16	100	18	82	12	95	5
8/15	100	60	40	1	91	9
9/23	100	88	12	3	89	11
10/15	100	92	8	0	94	6
11/14	100	87	13	0	88	12
12/19	100	24	76	0	89	11
Eastern Sector						
3/18	100	0	100	0	0	0
4/16	0	0	0	0	0	0
5/16	100	0	100	0	0	0
6/18	100	1	99	100	0	0
7/16	100	33	67	17	87	13
8/15	100	79	21	1	89	11
9/23	100	92	8	3	87	13
10/15	100	99	1	3	89	11
11/18	100	87	13	0	94	6
12/19	100	14	86	0	100	0

Fig. 37. Reproductive characteristics of *Artemia* during 2024: lakewide mean abundance of total females and ovigerous females (top), brood size (middle), and percent of females ovoviviparous and ovigerous (bottom). Vertical lines are the standard errors of the estimates.

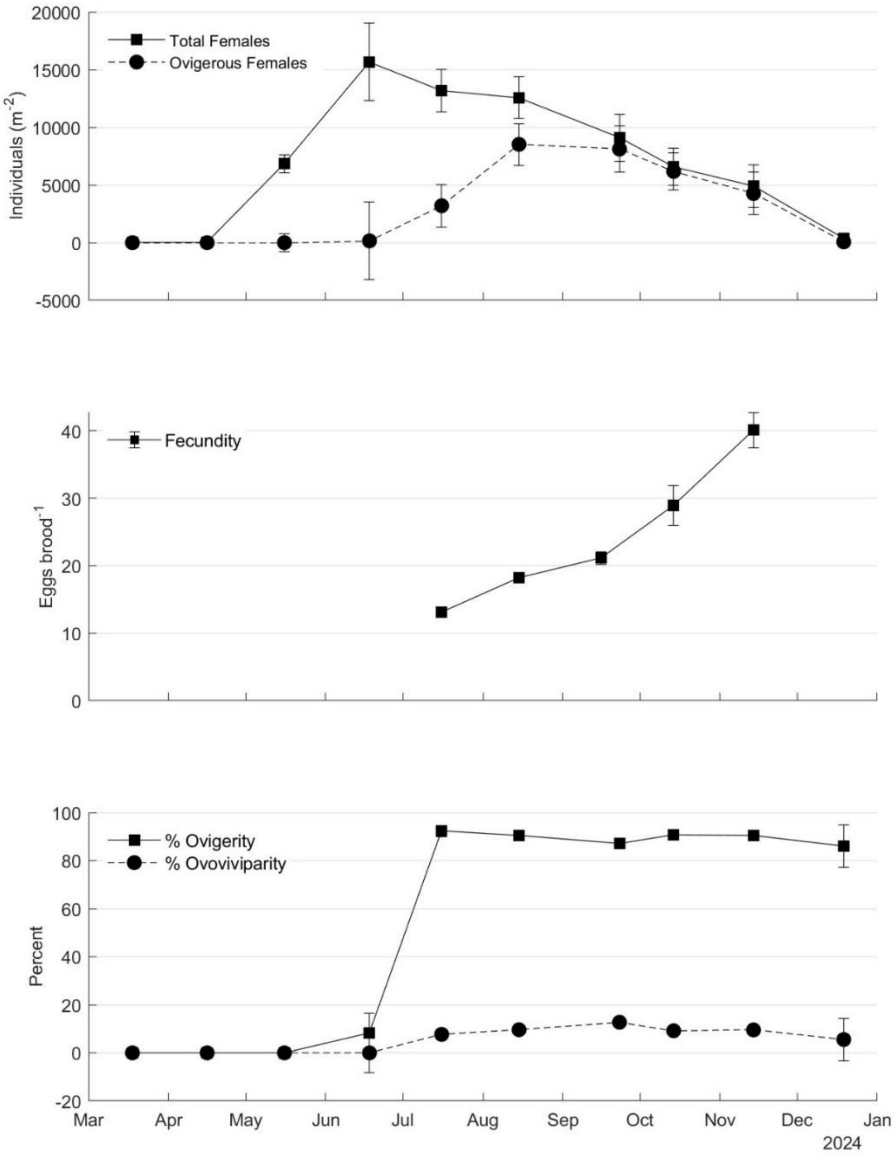

Lakewide mean fecundity ranged from 13 to 21 eggs brood^{-1} from June to September (Table 18, Fig. 37). Lakewide mean individual fecundity increased in October, November, and December (29, 41, and 37 eggs brood^{-1}, respectively) as food became abundant but total

reproduction was minimal by mid-December as adult numbers were very low. The mean length of adult females varied from 8.3 to 10.1 mm during the year.

Table 18. *Artemia* fecundity summary, June–December 2024. "%cyst" and "%indented" refers to the percentage of the type (cyst or naupliar) and shape (indented or round) of the eggs, respectively. S.E. is standard error. 'n' refers to number of stations averaged. '#fem' refers to number of females averaged.

	#eggs/brood				Female length (mm)			
	Mean	S.E.	%cyst	%indented	Mean	S.E.	n	#fem
Lakewide								
6/18	19	3.6	91	64	8.5	0.4	2	11
7/16	13	0.6	91	63	8.3	0.1	7	70
8/15	18	0.8	93	49	8.7	0.1	7	70
9/23	21	1.2	84	76	8.9	0.1	7	70
10/15	29	1.7	94	54	9.3	0.1	7	70
11/16	41	2.8	88	48	10.1	0.1	7	65
12/19	37	3.9	91	45	9.8	0.2	6	11
Western Sector								
6/18	19		100	100	8.0		1	1
7/16	13	0.8	88	48	8.3	0.1	4	40
8/15	18	1.0	100	53	8.6	0.1	4	40
9/23	22	1.8	88	75	8.9	0.1	4	40
10/15	24	2.1	93	53	9.1	0.2	4	40
11/14	42	3.4	82	44	10.2	0.1	4	39
12/19	36	3.5	100	67	10.0	0.3	4	6
Eastern Sector								
6/18	19	4.0	90	60	8.6	0.4	1	10
7/16	13	1.0	97	83	8.3	0.2	3	30
8/15	19	1.2	83	43	8.8	0.1	3	30
9/23	20	1.6	80	77	9.0	0.1	3	30
10/15	35	2.2	97	57	9.6	0.2	3	30
11/18	40	5.1	96	54	9.9	0.2	3	26
12/19	37	8.1	80	20	9.6	0.2	2	5

Artemia Biomass

In 2024, mean lakewide *Artemia* biomass peaked in July at 7.8 ± 1.0 g dry weight m^{-2}, followed by a steady decline in August (4.3 ± 0.5 g dry weight m^{-2}), September (4.4 ± 0.6 g dry weight m^{-2}), October (4.9 ± 0.8 g dry weight m^{-2}), and November (4.5 ± 0.9 g dry weight m^{-2}) before dropping to 0.4 ± 0.1 g dry weight m^{-2} in December (Table 19). Biomass was slightly

higher in the eastern sector during the early months (March to May), but thereafter, *Artemia* biomass had marked spatial variability among stations. By July, the western sector reached a maximum of 9.0 ± 1.4 g dry weight m^{-2}, compared to 6.6 ± 1.3 g dry weight m^{-2} in the eastern sector. The seasonal increase from March (0.3 ± 0.1 g dry weight m^{-2}) to July, followed by a gradual decline through late fall, aligns with the typical annual life cycle of *Artemia* in Mono Lake.

Table 19. *Artemia* biomass (g dry weight m^{-2}) summary, March–December 2024. S.E. is standard error. 'n' in last column refers to number of stations averaged.

	Date	Mean	S.E.	n
Lakewide				
	3/18	0.3	0.1	12
	4/16	0.8	0.2	12
	5/16	4.2	0.3	12
	6/18	7.1	0.8	12
	7/16	7.8	1.0	12
	8/15	4.3	0.5	12
	9/23	4.4	0.6	12
	10/15	4.9	0.8	12
	11/16	4.5	0.9	12
	12/19	0.4	0.1	12
Western Sector				
	3/18	0.2	0.1	6
	4/16	0.5	0.2	6
	5/16	4.0	0.3	6
	6/18	8.9	0.5	6
	7/16	9.0	1.4	6
	8/15	4.5	0.9	6
	9/23	5.4	1.1	6
	10/15	6.7	0.9	6
	11/14	6.1	1.3	6
	12/19	0.4	0.0	6
Eastern Sector				
	3/18	0.3	0.1	6
	4/16	1.0	0.1	6
	5/16	4.3	0.4	6
	6/18	5.2	1.0	6
	7/16	6.6	1.3	6
	8/15	4.1	0.5	6
	9/23	3.5	0.2	6
	10/15	3.2	0.7	6
	11/18	2.9	1.0	6
	12/19	0.5	0.1	6

Long-term Trends in *Artemia*

Artemia Mean Seasonal Abundance, 1979–2024

The seasonal (1 May–30 November) mean abundance of adult *Artemia* has varied over 4.5-fold, ranging from 8,000 to 37,000 m^{-2}, with an overall mean of 19,000 m^{-2} (Table 20). The 2024 mean seasonal abundance of 18,000 m^{-2} was in the middle of the observed 46 years (1979–2024). However, 2024 was unusual in that a pronounced peak was not found based on monthly sampling, as had been observed in nearly all other years, but rather had a broad distribution extending well into autumn (Fig. 38). The summer peak abundance has fluctuated more than 5-fold, from 20,000 to 105,000 m^{-2}, with a long-term average of 42,000 m^{-2}. The 2024 peak abundances was the 7th lowest observed while the broad distribution led to a higher median value (11th highest). The centroid of distribution, representing the center of seasonal abundance, has ranged from day 174 to day 260, with an overall mean of day 210, indicating high variability in the seasonal timing of *Artemia* abundance. In 2024, the centroid of the Artemia abundance distribution was 224, the 9th latest in the past 45 years.

Table 20. Mean seasonal adult *Artemia* abundance (1 May –30 November) and centroid of distribution, 1979–2024. The centroid of *Artemia* distribution is the average of time weighted by adult abundance.

Year	Mean (m^{-2})	Median (m^{-2})	Peak (m^{-2})	Centroid (day of year)
1979	14,100	12,300	31,700	216
1980	14,600	10,200	40,400	236
1981	32,000	21,100	101,700	238
1982	37,000	31,700	105,200	260
1983	18,100	16,500	39,900	230
1984	17,000	19,300	40,200	203
1985	18,500	20,300	33,100	220
1986	14,700	17,400	33,000	192
1987	23,800	22,700	54,300	232
1988	27,600	25,800	71,600	206
1989	36,100	29,100	92,500	256
1990	20,200	17,600	34,900	230
1991	18,100	19,500	34,600	227
1992	18,900	19,500	34,600	220
1993	15,000	16,700	26,900	215
1994	16,600	18,800	29,400	213
1995	15,600	17,200	24,400	203
1996	17,700	17,900	34,600	215
1997	14,400	16,400	27,300	203
1998	19,400	21,400	34,000	227
1999	20,200	21,500	38,400	225
2000	10,600	9,100	22,400	210
2001	20,000	20,000	38,000	209
2002	11,600	10,000	25,500	199
2003	13,100	13,800	29,500	203
2004	32,200	36,900	75,500	174
2005	20,000	19,800	45,400	192
2006	21,500	20,300	55,700	185
2007	18,800	17,500	41,800	186
2008	12,000	12,700	27,600	189
2009	26,000	17,900	72,100	179
2010	14,900	7,400	46,200	191
2011	21,300	16,900	48,900	193
2012	16,700	12,000	53,800	178
2013	27,700	33,300	57,800	195
2014	14,300	8,100	45,000	194
2015	8,200	6,200	19,900	183
2016	11,400	11,000	19,700	221
2017	16,200	16,600	27,700	223
2018	12,900	12,800	23,200	215
2019	14,400	13,400	28,200	220
2020	13,800	14,300	25,900	208
2021	22,600	23,100	50,700	198
2022	16,200	15,400	32,700	222
2023	19,800	20,000	45,300	219
2024	17,600	20,100	25,400	224
Mean	**18,800**	**17,900**	**42,300**	**210**
Min	**8,200**	**6,200**	**19,700**	**174**
Max	**37,000**	**36,900**	**105,200**	**260**

Fig. 38. Adult *Artemia* abundance, 1982–2024. Red lines show years when May–June abundance exceeded 40,000 m^{-2}. Blue lines indicate years of exceptionally high autumn abundance.

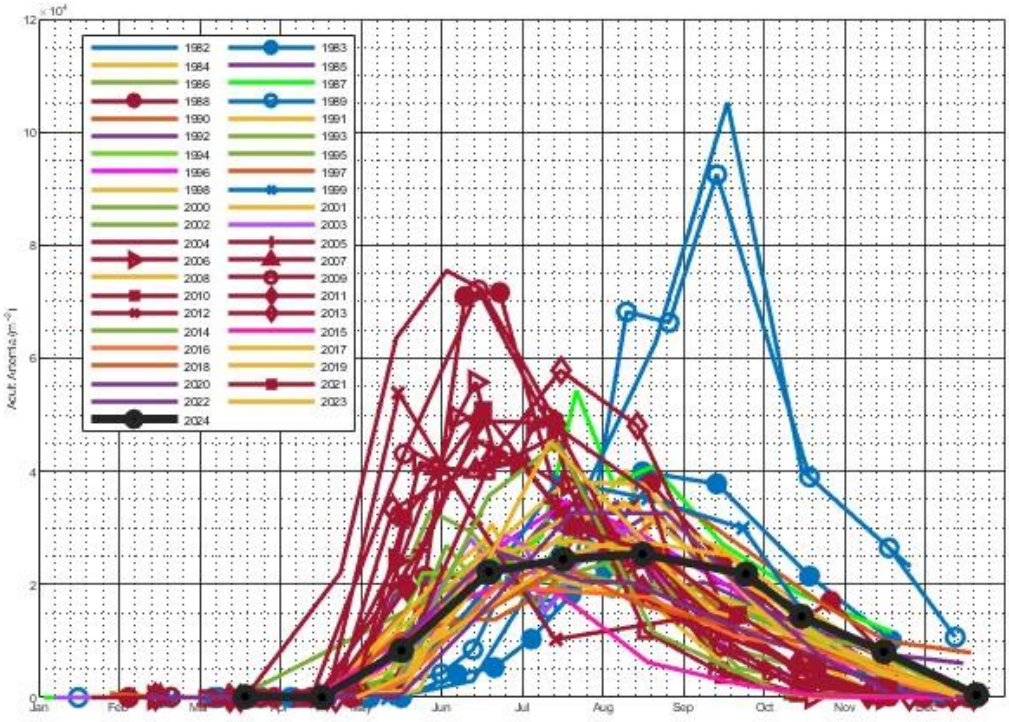

Fig. 39. Abundance-weighted centroid of adult *Artemia,* 1982–2024.

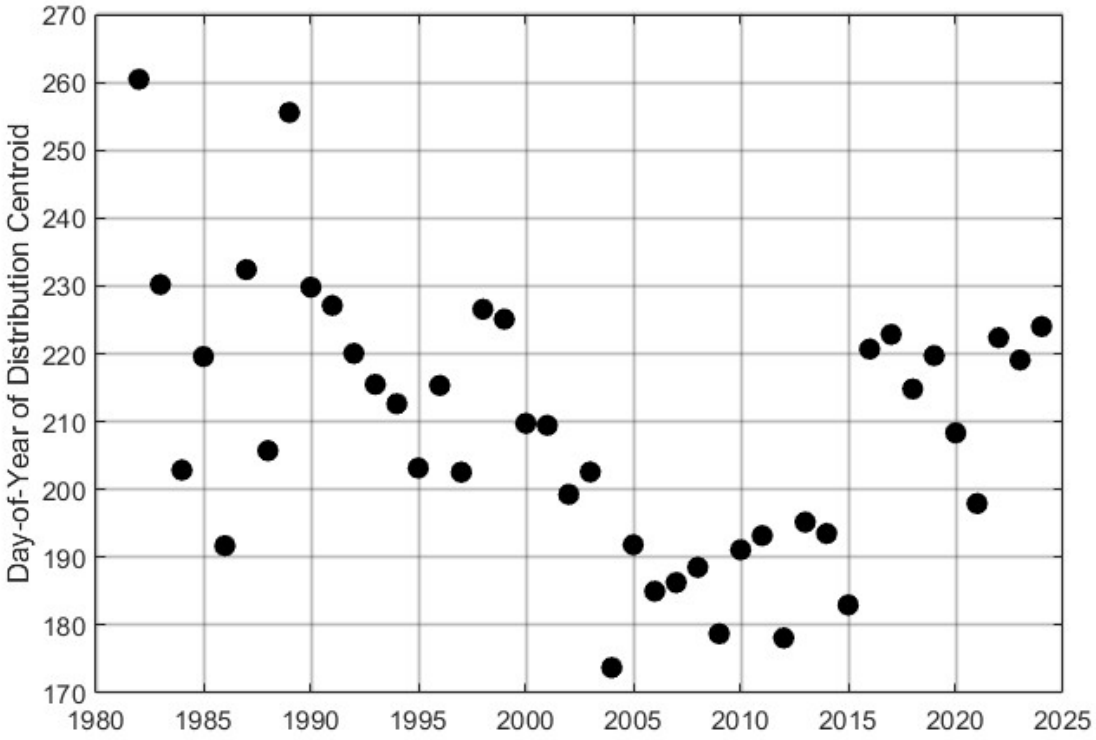

Artemia Mean Annual Nauplii and Cyst Production, 1983–2024

In 2024, estimated annual naupliar production (197,000 m^{-2}) was near the long-term mean of 184,000 m^{-2}. However, annual cyst production (1.6 x 10^6 m^{-2}) was the lowest observed; less than half the long-term average of 3.7 x 10^6 m^{-2} (Table 21). Although there is large year-to-year variation, the linear fit to data from 1983 to 2024 would suggests a decrease of 50,000 cysts yr^{-1} (Fig. Fig. 40).

Table 21. Annual nauplii and cyst production, 1983–2024.

Year	Nauplii (x 10^3 m^{-2})	Cyst (x 10^6 m^{-2})
1983	70	5.2
1984	67	3.7
1985	104	4.4
1986	197	3.5
1987	183	5.2
1988	132	4.8
1989	47	4.7
1990	398	4.7
1991	634	5.2
1992	60	4.7
1993	247	5.7
1994	86	5.7
1995	123	4.0
1996	27	3.5
1997	5	3.0
1998	40	3.2
1999	42	3.8
2000	64	3.3
2001	128	3.0
2002	92	2.7
2003	460	4.5
2004	51	2.2
2005	252	3.9
2006	311	5.4
2007	219	3.0
2008	155	3.0
2009	140	3.1
2010	79	1.9
2011	79	2.4
2012	100	4.3
2013	526	4.8
2014	464	2.8
2015	252	1.9
2016	232	2.5
2017	344	3.7
2018	124	2.5
2019	177	3.0
2020	114	2.9
2021	78	3.2
2022	79	4.4
2023	552	3.4
2024	197	1.6
Mean	184	3.7
Minimum	5	1.6
Maximum	634	5.7

Fig. 40. Annual nauplii and cyst production, 1983–2024.

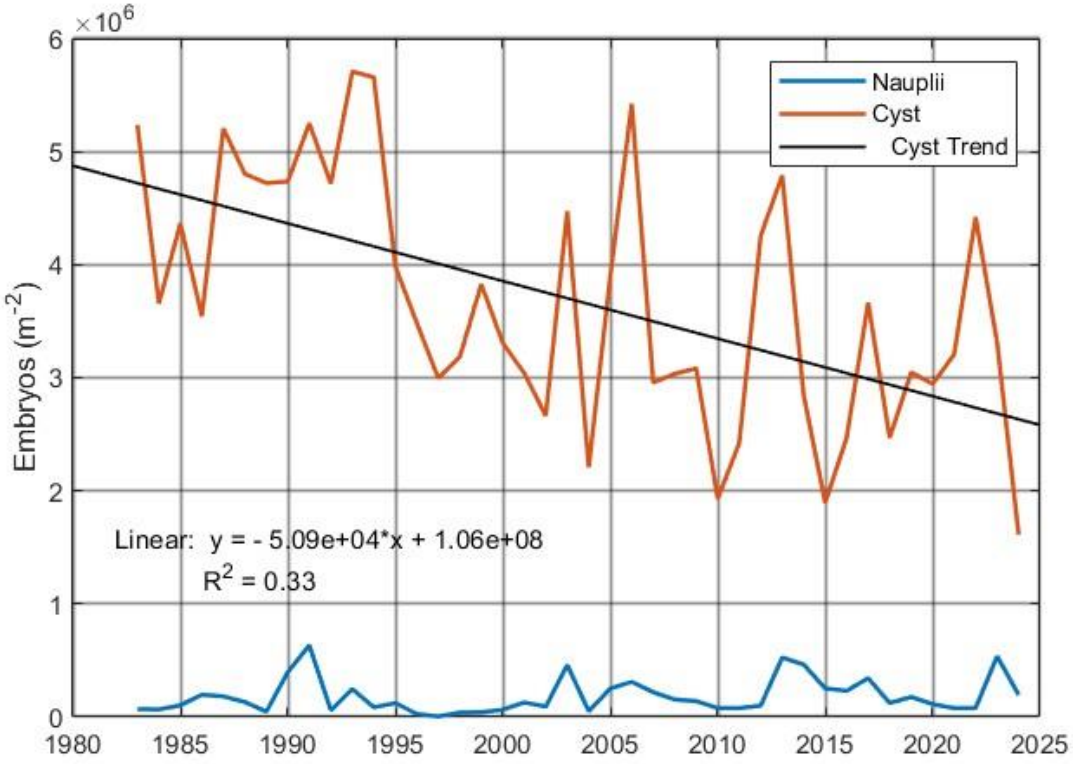

Both naupliar and cyst production were markedly lower in 2024, the second year of a strong meromictic event, compared to 2023 during the onset of meromixis (Fig. 41). Annual naupliar and cyst production are calculated from the number of ovoviviparous (nauplii-producing) or oviparous (cyst-producing) females, their fecundity (#eggs in brood sac), and a temperature dependent brood interval. Because both estimates of naupliar and cyst production were different from 2023, several factors that may contribute to these differences were examined.

Both the mixed-layer temperatures (2-m depth) and fecundity were similar between the two years (Fig. 42). However, the numbers of ovoviviparous and oviparous females were markedly less in 2024 (Fig. 43) and this accounts for the lower estimates of both nauplii and cyst production in 2024.

Fig. 41. Naupliar and cyst production, 2023–2024.

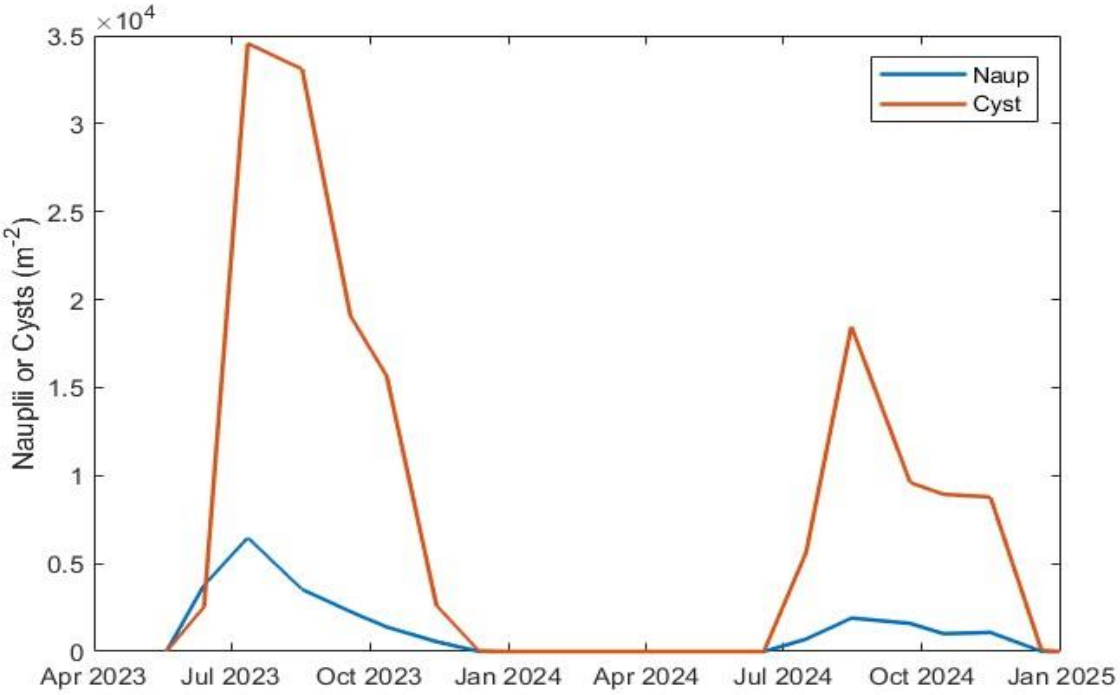

Fig. 42. Temperature and Fecundity, 2023–2024.

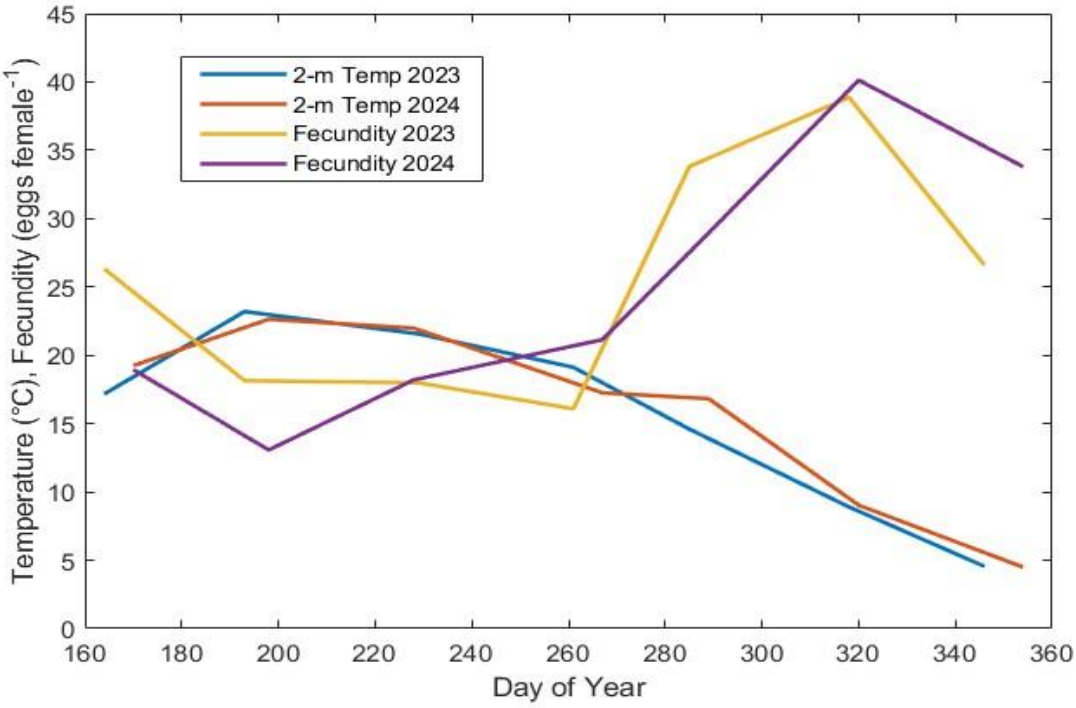

Fig. 43. Ovoviviparous and oviparous female abundance, 2023–2024.

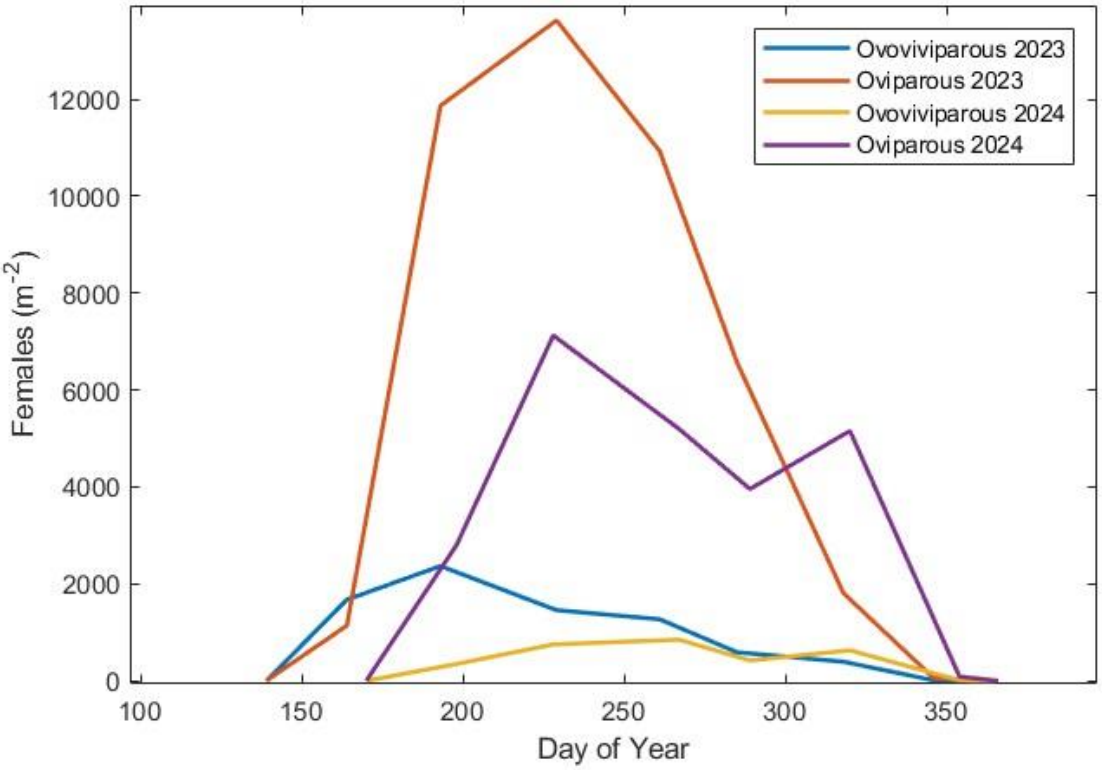

While the lower numbers of reproducing females accounts for the large differences in reproductive output between 2023 and 2024, the long-term trend of decreasing female length and fecundity continues. A linear fit to abundance-weighted reproductive female length suggests slightly more than a 1 mm decrease in length (~10%) over the 42 years (1983–2024) (Fig. 45). However, much of this decrease is driven by the current and previous two episodes of meromixis. A somewhat larger decrease in fecundity has occurred with a linear fit decreasing from ~50 in 1983 to ~29 eggs female^{-1} in 2024 (Fig. 45).

Fig. 44. Mean abundance-weighted fecundity of ovigerous females, 1983–2024.

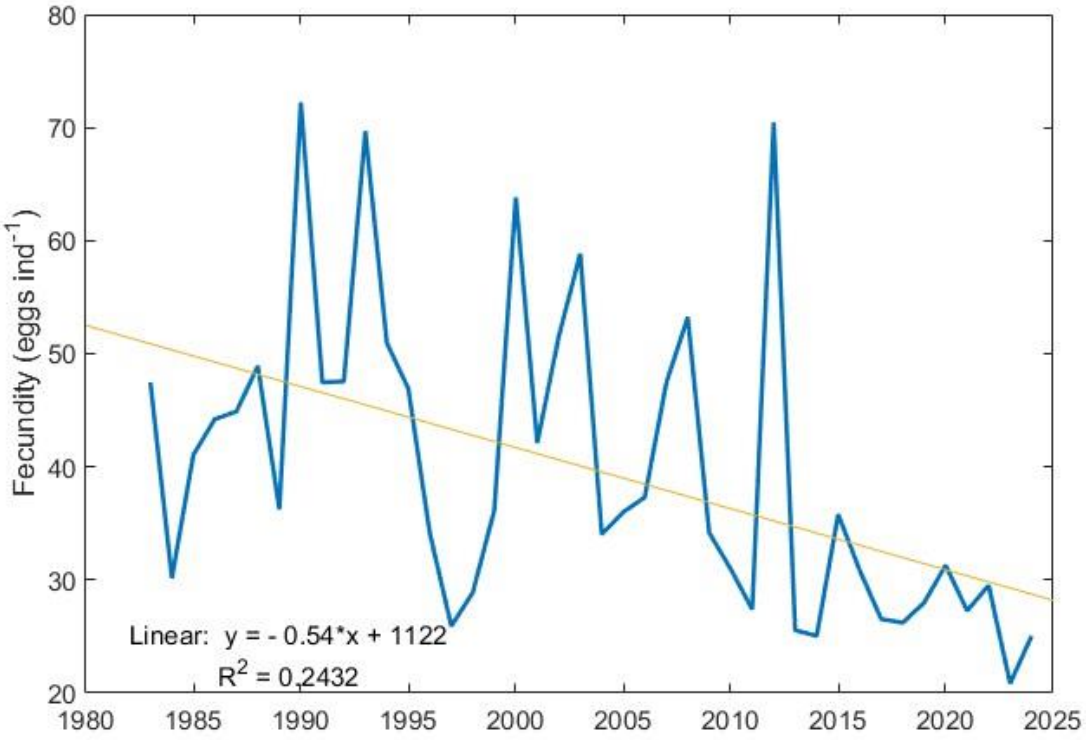

.

Fig. 45. Annual mean abundance-weight reproductive female length, 1983–2024.

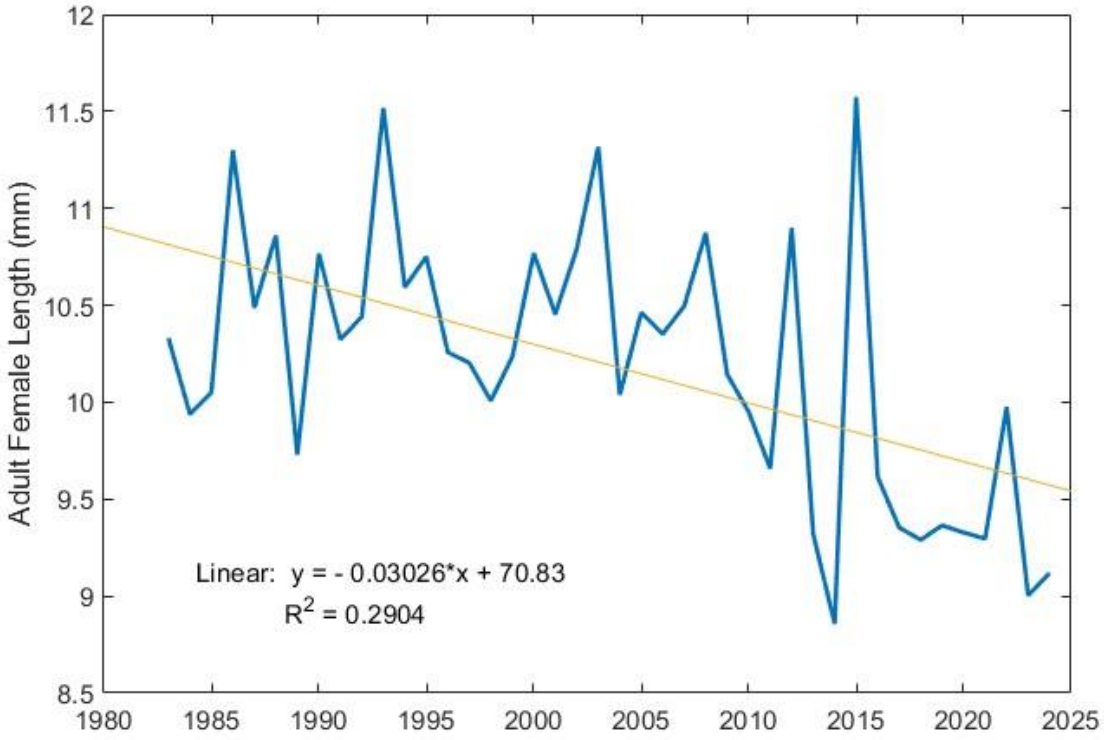

In summary, strong persistent salinity stratification persisted through 2024 following the onset of meromixis due to high runoff in spring 2023. While the upper mixed-layer deepened to 15 m in 2024, a period of winter holomixis was prevented and this sixth period of meromixis will continue through 2025. The vertical structure of ammonium, chlorophyll, dissoved oxygen, and fluorescence reflect the effects of strong temperature and salinity gradients. The impact of meromixis on reducing the upward flux of ammonium, the limiting nutrient for phytoplankton productivity has been documented (Jellison et al. 1993b), and low levels of chlorophyll and high transparency occurred throughout the summer. While similar to observations in 2023, these conditions contrast with those in 2020–2022 prior to the onset of the current episode of meromixis. The seasonal (1 May to 30 November) lakewide abundance of adult *Artemia* in 2024 (20,100 m^{-2}) was similar to the 45-yr mean of (17,900 m^{-2}), a large peak observed during most years was absent. The center of the *Artemia* distribution was shifted later in the year (224 day of year), two weeks later than the long-term mean but within the previously observed range. The annual production of over-winter cysts (1.6 million m^{-2}) was the lowest observed since calculations began in 1983 and less than half the long-term mean of 3.7 million m^{-2}. The

calculated decrease in cyst production resulted from both fewer ovigerous (egg-carrying) females and lower fecudity (i.e. brood size).

CHAPTER 4
FURTHER ANALYSES

Thermal Structure, Conductivity, Dissolved Oxygen and Fluorescence

Methods

Time-series measurements of water temperature were obtained with thermistors deployed on vertical arrays. Thermistor arrays had the upper-most loggers suspended below and shaded by a surface float, and deeper ones were on taut-line moorings with a float ~1 to 1.5 m below the water surface (Fig. 46). The thermistors were RBR Solo® thermistors, individually calibrated by the vendor (accuracy $\pm$0.002 ºC), sampled at 0.1 Hz at depths shown in figures below. Conductivity was measured with RBR Concerto^3 conductivity-temperature-depth (CTD) sensors, individually calibrated by vendor (conductivity with extended range, accuracy $\pm$ 0.003 mS cm^{-1}; temperature accuracy $\pm$0.002 ºC; depth (pressure) accuracy $\pm$0.05% full range). Dissolved oxygen was measured with optical sensors (PME MiniDOT loggers; accuracy of 5% of measurement or 0.3 mg L^{-1}, whichever is larger, and resolution of 0.01 mg L^{-1}) recording every 10 minutes. In comparison to dissolved oxygen concentrations near 100% saturation with atmospheric air measured by Miller titration, values produced by the PME algorithm for the same elevation and salinity were about 10% higher. Fluorescence was measured with a Turner C-FLUOR sensor for chlorophyll with red excitation connected to a PME C-FLUOR data logger. DO and fluorescence sensors had PME wipers attached that eliminated biofouling. The voltage output of the C-FLUOR sensors was converted to chlorophyll based on a regressed against measurements of chlorophyll in samples (see Chapter 3) from approximately the same depths as the sensors.

Fig. 46. Surface float (tan wooden square) with sensors suspended below and connected to subsurface buoys (orange round) at about 1 m below lake surface with additional sensors below on taut line with weight on bottom.

Results

Thermal structure

Results from moored thermistors deployed at Stations 3 and 6 from October 2023 through May 2024 are illustrated in Fig. 47 and Fig. 48. At both stations water above 15 m gradually cooled through autumn and winter, eventually mixing around DOY 440 (mid-March). A region of elevated temperature between 8 and 12 m persisted well into the winter. The monimolimnion warmed very slightly over the whole record but remained below ~4 ^{o}C. By April, the near-surface waters were beginning to warm and exceeded 16 ^{o}C with a strong thermal gradient by mid-May (DOY 500), though episodes of mixing are evident in the upper water column. Up and down oscillations of isotherms are indicative of internal wave activity and mixing processes.

Results from moored thermistors deployed at Stations 3 and 6 from May through October 2024 are illustrated in Fig. 49 and Fig. 50. At both stations, a 3 to 4 m thick, steep thermal gradient was present persisting until DOY 240 at Station 6 and DOY 260 at Station 3, after which mixing deepened and narrowed the gradient. Over the period of record, the thermocline gradually descended as the upper water cooled. Within the upper water column, intermittent

periods with diel or several day stratification appear which will influence vertical mixing of phytoplankton and their exposure to light.

Fig. 47. Temperature contours (as 2 h averages) October 2023 through May 2024 at Station 6. Days of year in 2024 are added to DOY of 365 at the end of 2023. Red dots indicate depths of thermistors.

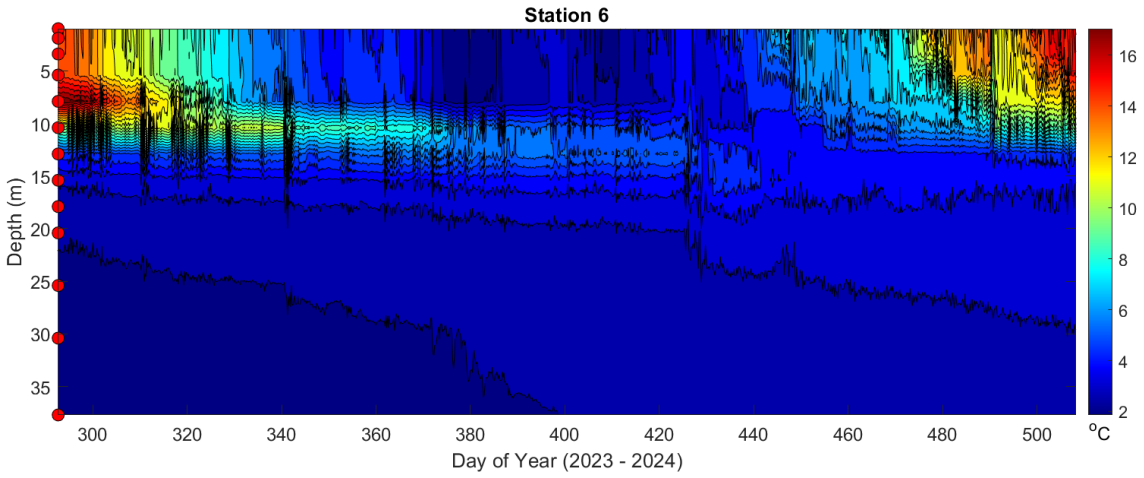

Fig. 48. Temperature contours (as 2 h averages) October 2023 through May 2024 at Station 3. Days of year in 2024 are added to DOY of 365 at the end of 2023. Red dots indicate the depths of thermistors.

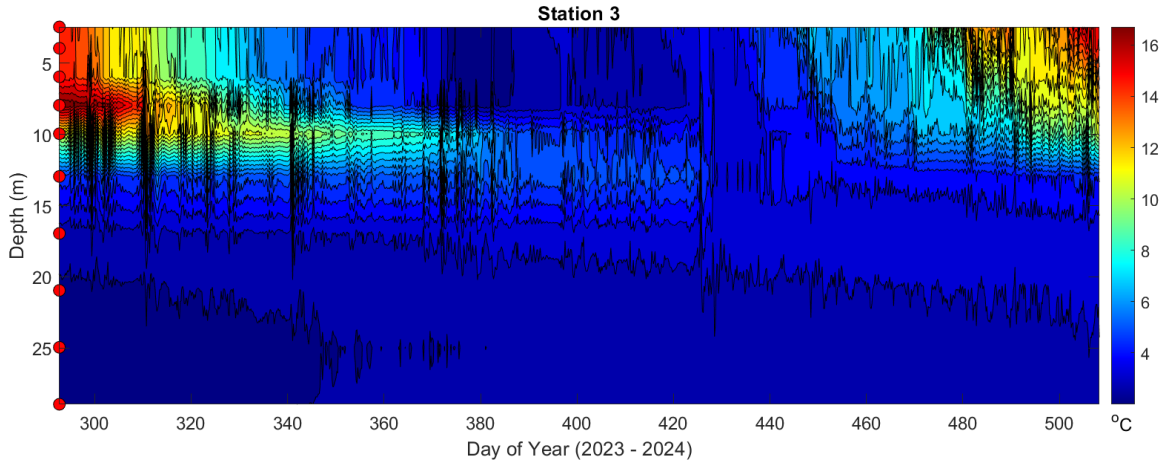

Fig. 49. Temperature contours (as 2 h averages) May through October 2024 at Station 6. Red dots indicate the depths of thermistors. Days of year in 2024 start with DOY of 0 in January.

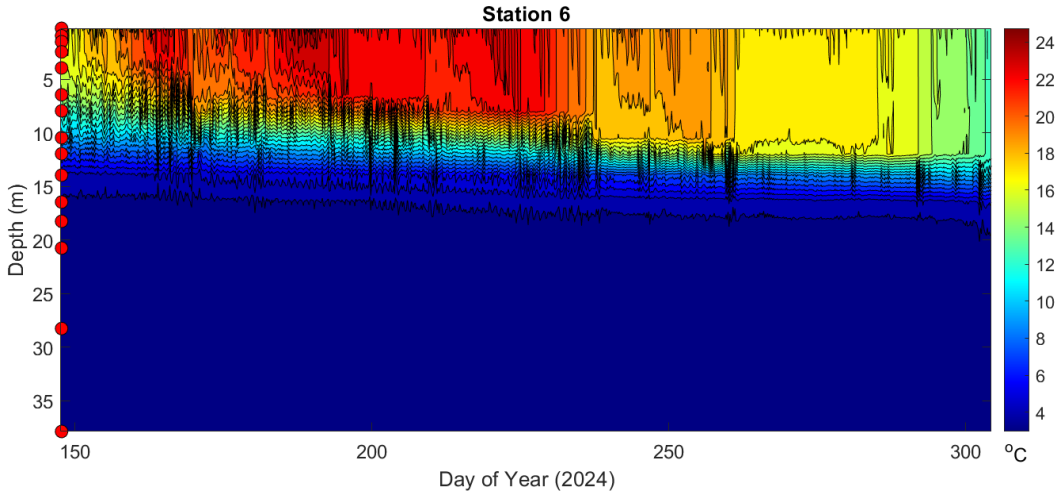

Fig. 50. Temperature contours (as 2-h averages) May through October 2024 at Station 3. Red dots indicate the depths of thermistors. Days of year in 2024 start with DOY of 0 in January.

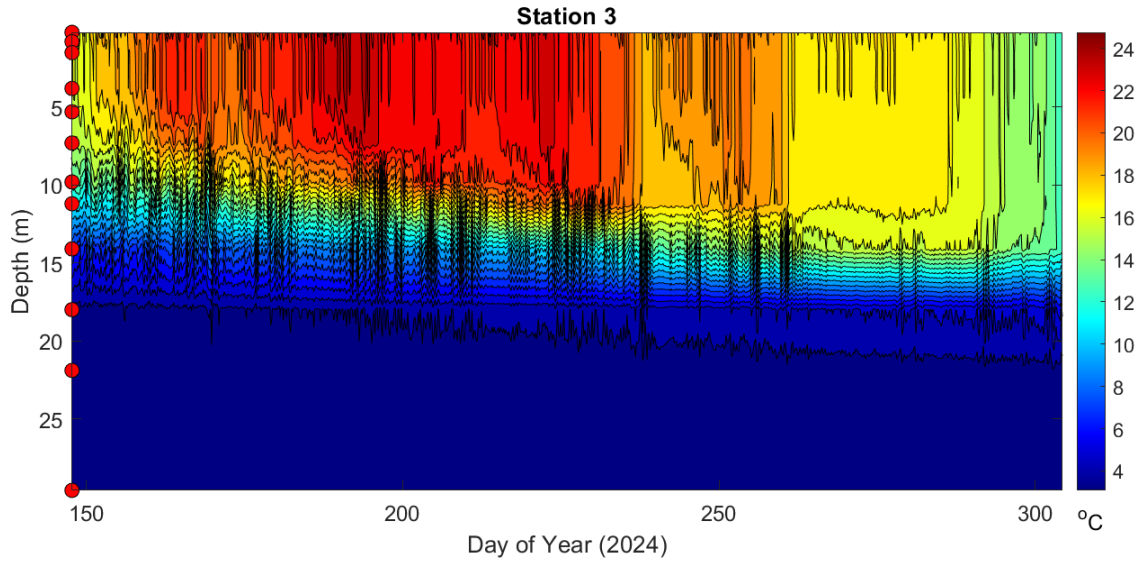

The section below on eddy diffusivity uses the thermistor data in the calculation of vertical exchange, a way to quantify consequences of meromixis and rates of supply of nutrients to the upper water column.

Conductivities

Specific conductivities (conductivities normalized to 25 ºC) recorded within the mixolimnion in the summer of 2023 at Station 3, and from November 2023 through May 2024 at Stations 3 and 6 illustrate considerable, high frequency variability (Fig. 51, Fig. 52, Fig. 53). The variations and intermittent spikes are indicative of mixing as stream inflows mix with the water below, as internal waves occur, and as other mixing processes operate. In contrast, during the

summer of 2023, specific conductivities at 14.4 m at Station 3 remained quite stable at 84 ± 0.5 mS cm^{-1} (Fig. 54). Specific conductivities recorded at a series of depths from May through October 2024 at Station 6 illustrate the stable chemical stratification with quite small variations at each depth: 5.5 m, 75–76 mS cm^{-1}; 8.5 m, 76–77 mS cm^{-1}; 12.5 m, 82 mS cm^{-1}; 15.5 m, 83 mS cm^{-1}.

Fig. 51. Specific conductance (mS cm^{-1}) at 3.4 m, Station 3.

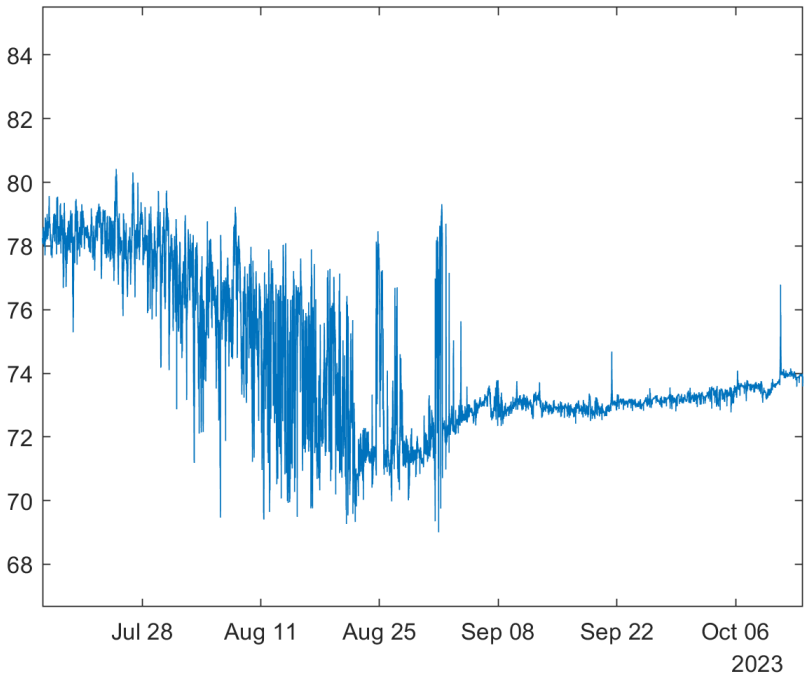

Fig. 52. Specific conductance (mS cm^{-1}) at 8.95 m, Station 3.

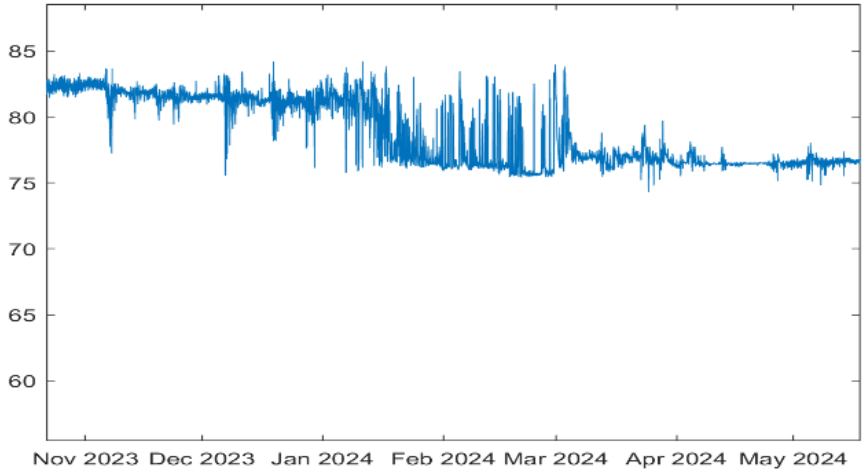

Fig. 53. Specific conductance (mS cm^{-1}) at 6.9 m, Station 6.

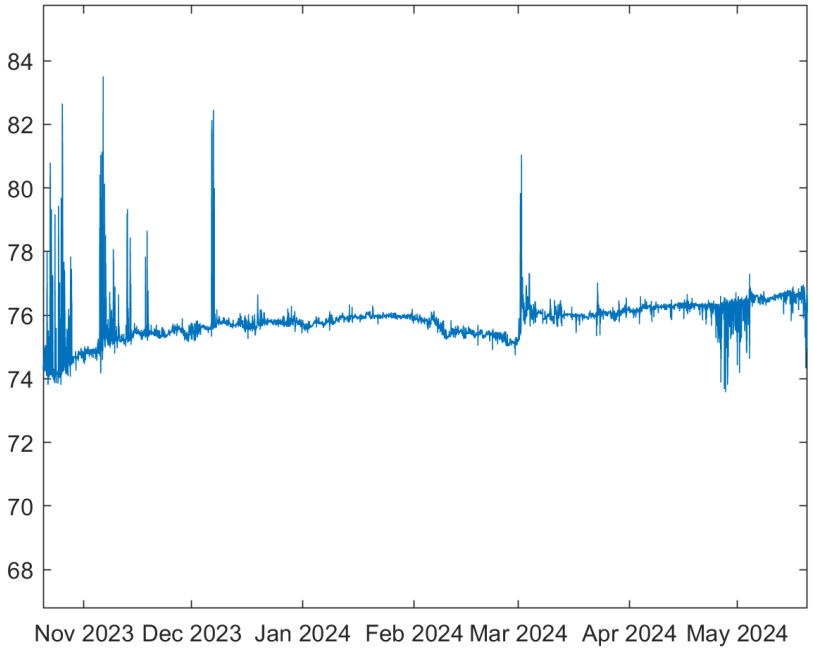

Fig. 54. Specific conductance (mS cm^{-1}) at 14.4 m, Station 3.

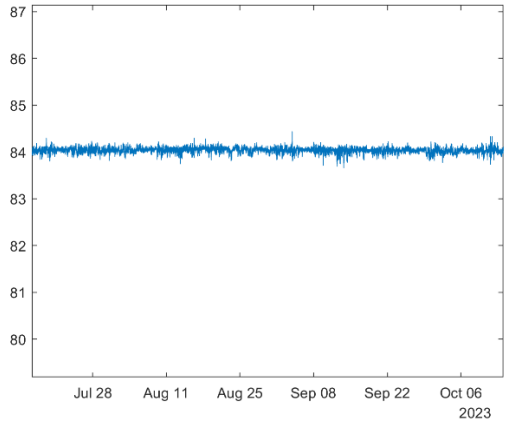

Dissolved Oxygen and Fluorescence

Dissolved oxygen at 1.5 m varied from about 5.5 to 7.5 mg L^{-1} from October 2023 through May 2024 at Station 6 (Fig. 55). Values had muted changes during autumn and winter compared to increased variability in spring, as the water warmed. Furthermore, variations in chlorophyll levels were muted in the winter and increased in the spring (Fig. 56). Dissolved oxygen and water temperature variations at 5 m from October 2023 through May 2024 at Station 3 were similar to those at Station 6 (Fig. 57).

Dissolved oxygen concentrations from May through October 2024 at Station 6 at 1.3 m and at Station 3 at 6.3 m were similar and ranged from about 4.4 to 6 mg L^{-1} (Fig. 58, Fig. 59). The higher dissolved oxygen concentrations early and late in the period and lower values in much of the summer correspond with phytoplankton chlorophyll variations (Fig. 60), except for a mid-summer increase in dissolved oxygen. Overall, the sensor data supplement the monthly survey data to indicate that sufficient dissolved oxygen is present in the mixolimnion for *Artemia* metabolism.

Fig. 55. Dissolved oxygen (blue line; mg L^{-1}) and water temperature (red line; °C) from October 2023 through May 2024 at Station 6 at 1.5 m.

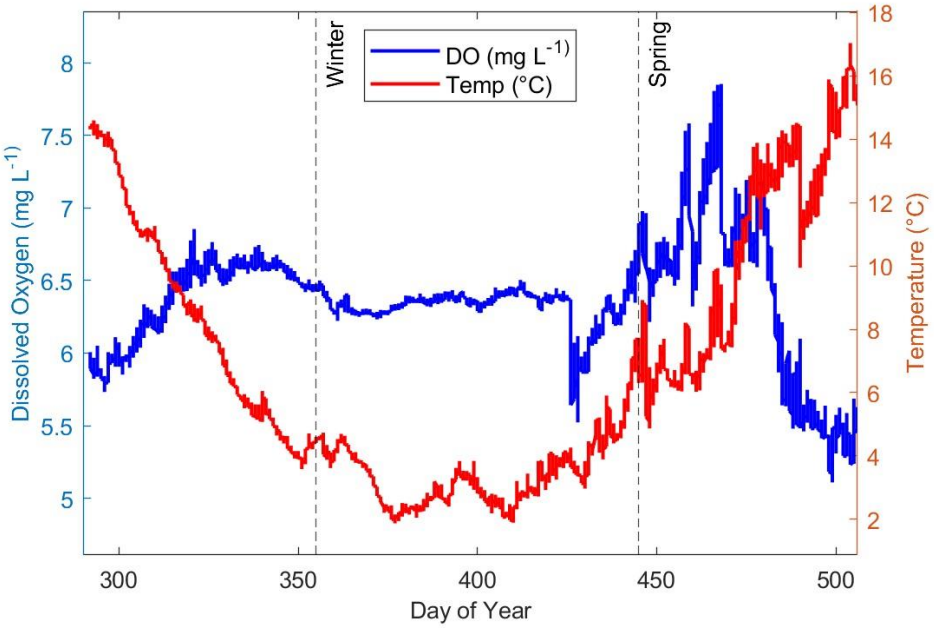

Fig. 56. Chlorophyll derived from fluorescence from October 2023 through May 2024 at Station 6 at 4.4 m.

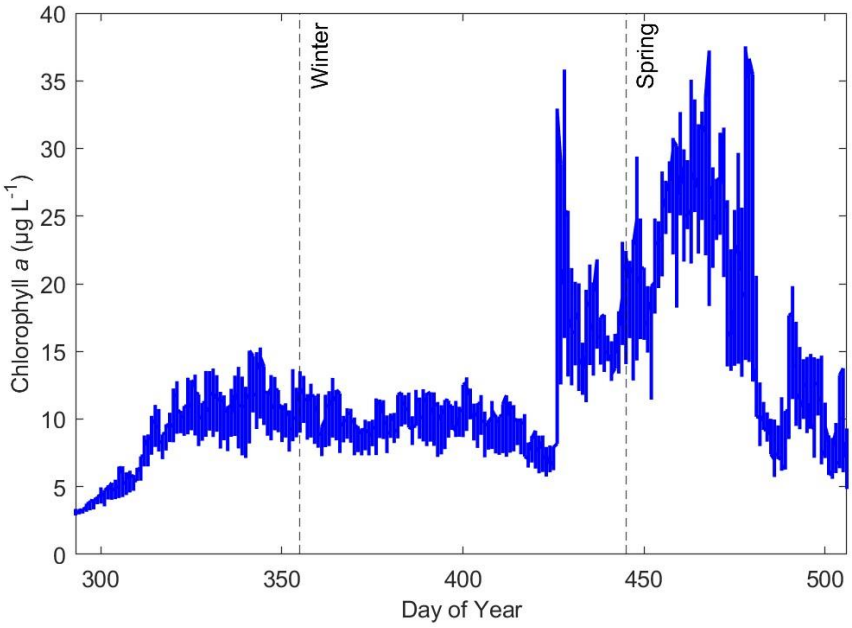

Fig. 57. Dissolved oxygen (blue line; mg L^{-1}) and water temperature (red line; °C) from October 2023 through May 2024 at Station 3 at 5 m.

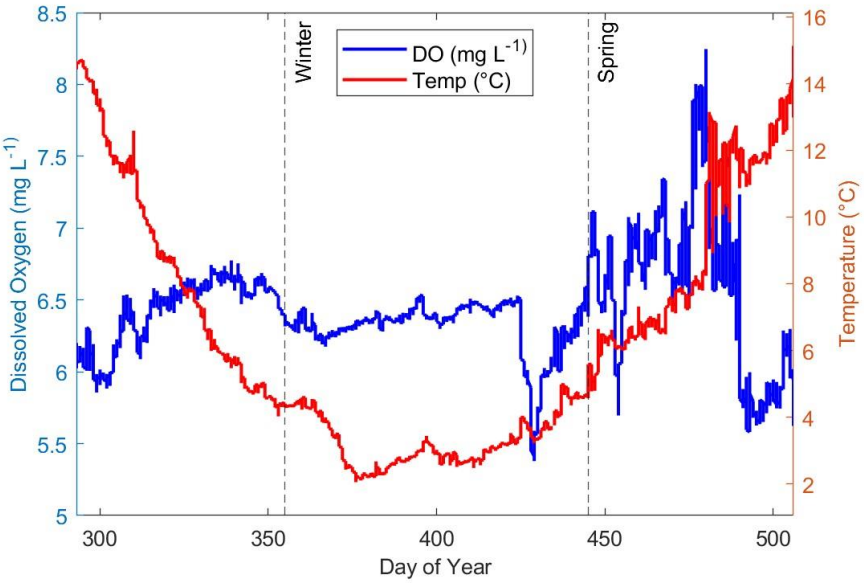

Fig. 58. Dissolved oxygen (blue line; mg L^{-1}) and water temperature (red line; °C) from May through October 2024 at Station 6 at 1.3 m.

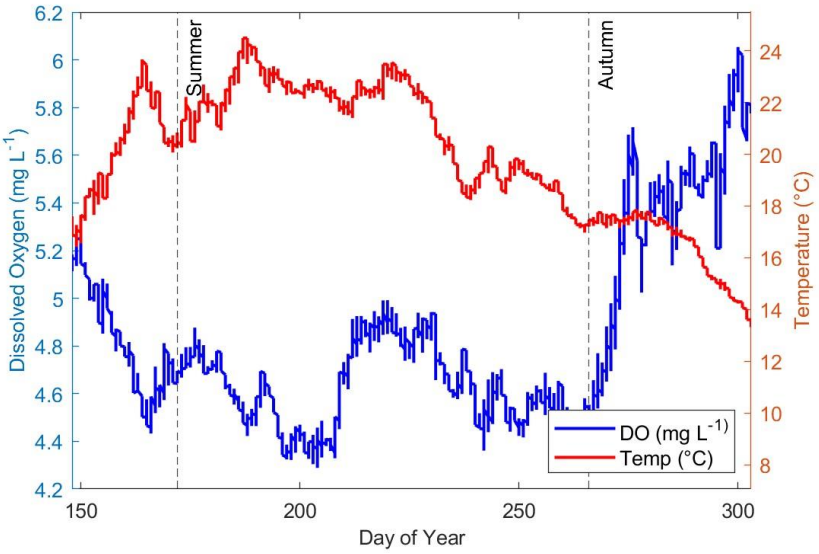

Fig. 59. Dissolved oxygen (blue line; mg L^{-1}) and water temperature (red line; °C) from from May through October 2024 at Station 3 at 6.3 m.

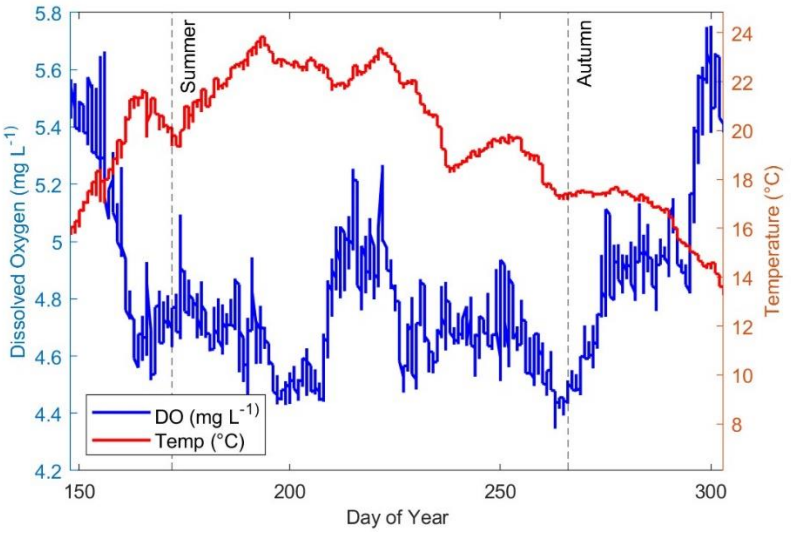

Fig. 60. Chlorophyll derived from fluorescence from May through October 2024 at Station 6 at 5 m.

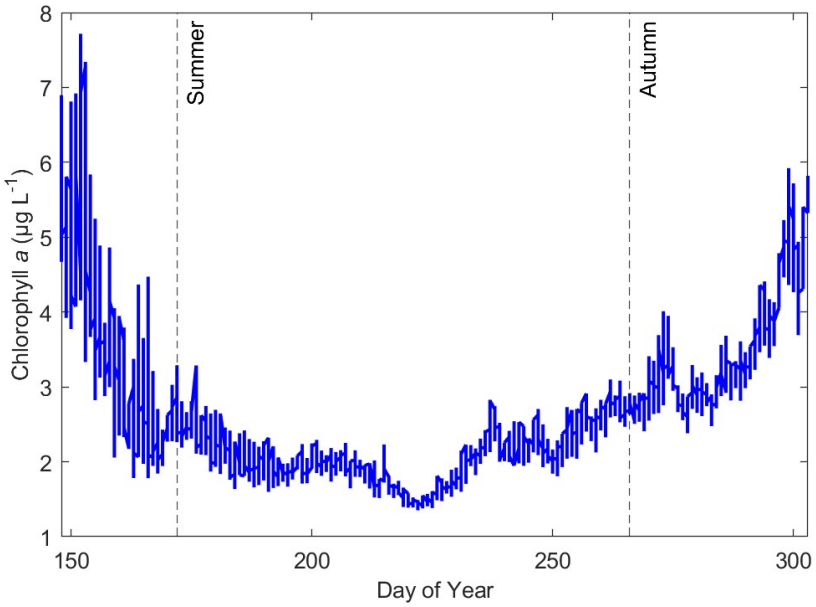

Eddy Diffusivity

Vertical mixing redistributes heat, solutes, and particles, and can be represented by the coefficient of eddy diffusivity (K_z) that can be assessed from changes in heat content as described by Jassby and Powell (1975). This approach provides K_z within the thermocline and deeper water if advection or heating by sediments are negligible. Prior work in Mono Lake

illustrated changes in K_z during contrasting periods of meromixis and holomixis. For example, Jellison and Melack (1993a) reported mean summer diffusivities (June through September) were lowest during periods with strong chemical stratification in 1984 and 1986, increased from 1986 to 1989 as chemical stratification decreased. Jellison et al. (1993b) and MacIntyre and Jellison (2001) combined K_z values with vertical gradients in ammonium concentrations to calculate vertical fluxes of ammonium.

Eddy diffusivity (K_z) was calculated with data collected in 2023 and 2024, following Jassby and Powell (1975), with terms re-organized, as follows:

$$K_z = -\frac{1}{\rho_0 c A_z \frac{\partial \theta}{\partial z}} \left(\rho_0 c \frac{d}{dt} \int_z^{z_m} A_z \theta_z dz - R_z \right) \qquad (1)$$

where ρ_0 is the mean density of Lake Mono water (approximately $1070\ kg/m^3$); $c = 0.99 \times 4.184 \times 10^6/\rho_0$ the thermal capacity of water in the lake; $R_z = A_z SW_z$ is the accumulative incoming shortwave radiation across the horizontal area (A_z) at depth z (SW_z) during each time interval. K_z is not reported if heat flux indicates cooling or the vertical temperature gradient is less than 0.005 $^oC\ m^{-1}$. The heat flux into the sediments and the radiation absorbed by the sediments are not included.

Incoming shortwave radiation measured at the Lee Vining Station (5-minute data), light attenuation, water level, and the hypsographic curve are included in the analyses (Fig. 61). Light attenuation coefficient for May 2024 was based on Secchi depth, others were obtained from light profiles (see Chapter 2); water level data are monthly. Vertical profiles of temperature were obtained from moored thermistors (see section above) and from monthly CTD casts (see Chapter 2).

Fig. 61. a – incoming shortwave radiation (SWin) measured at Lee Vining Station; b – light attenuation coefficient (K_d); c – water level; d – hypsographic curve of Lake Mono.

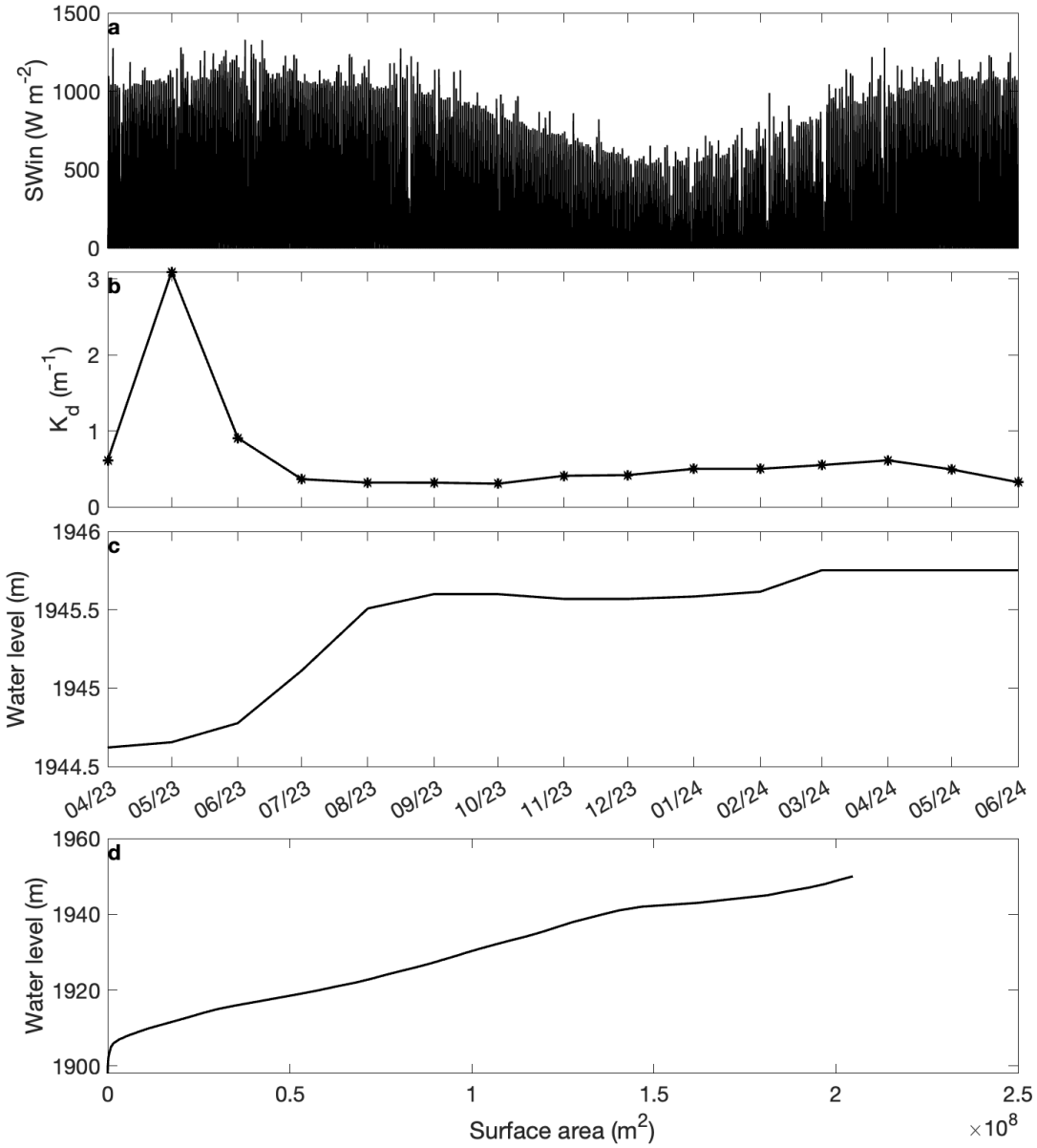

K_z calculated with moored thermistor data

K_z was calculated with thermistor data collected at Stations 3 and 6 for two periods: 14 July 2023 to 14 October 2023 and from 19 October 2023 to 22 May 2024. The 10-second temperature data was bin-averaged with a 5-minute bin width, and the 5-minute temperature data was filtered during the calculation of K_z with 7-day, 14-day and 30-day filters. Similarly, R_z was

calculated with the 5-minute SW_z, corrected for albedo and refraction angle, and filtered with the same temporal filters as temperature. K_z was calculated with the filtered data following Eq. 1.

Results from Station 6 are provided as examples. K_z between 5 and 20 m from 19 October 2023 to 22 May 2024 (*on order of* 10^{-4} m^2 s^{-1}, Fig. 62) was on average about 2 orders higher than that from 14 July 2023 to 14 October 2023 (*on order of* 10^{-6} m^2 s^{-1}, Fig. 63).

Fig. 62. Period from 19 October 2023 to 22 May 2024. a – 5-min temperature (color) and filtered temperature (black, 7-day filter) at Station 6; b – heat content; c – change of heat content; d – solar heat; e – heat flux with solar heat subtracted; f – K_z in logarithmic scale.

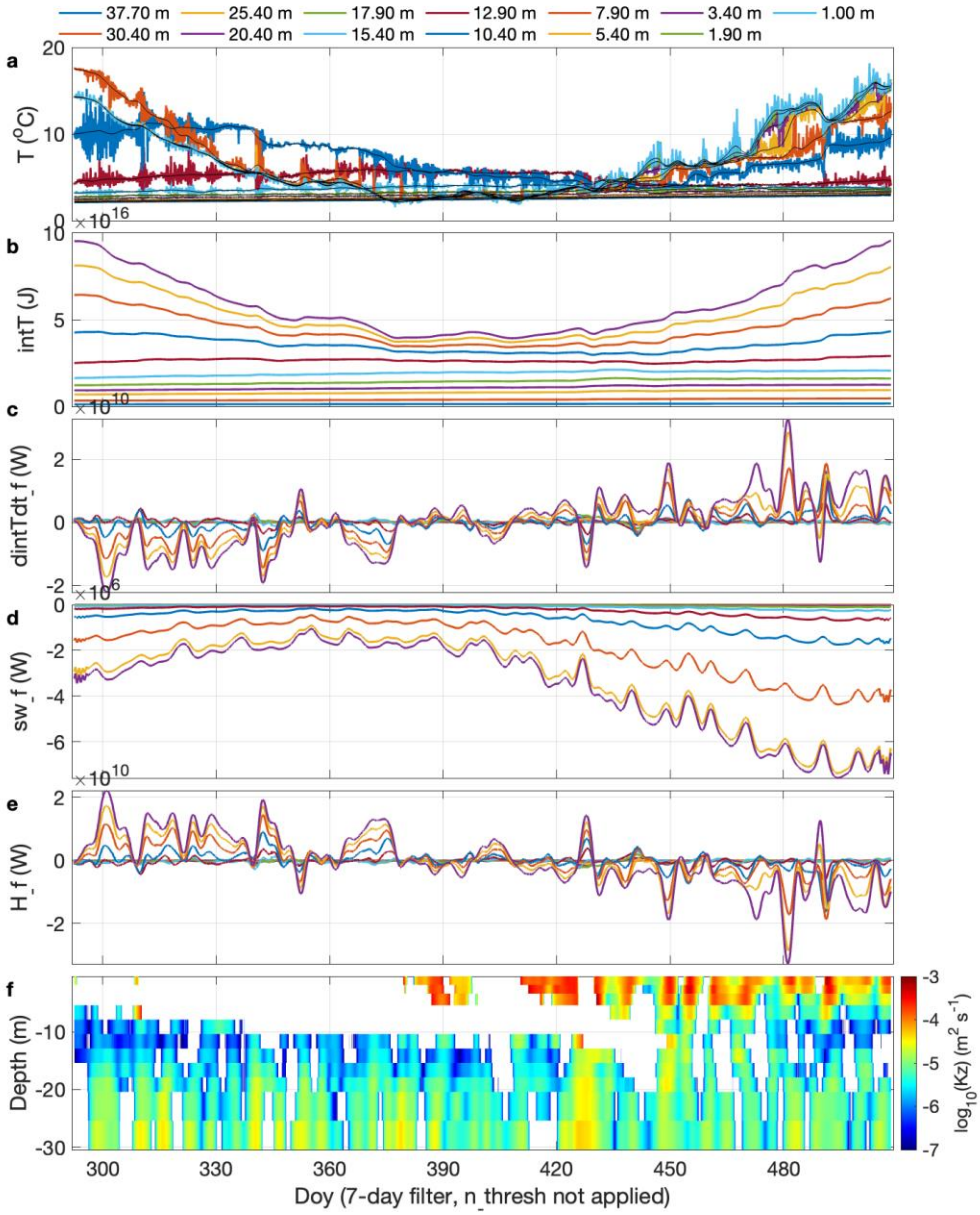

Fig. 63. Period 14 July 2023 to 14 October 2023. a – 5-min temperature (color) and filtered temperature (black, 7-day filter) at Station 6; b – heat content; c – change of heat content; d – solar heat; e – heat flux with solar heat subtracted; f – Kz in logarithmic scale.

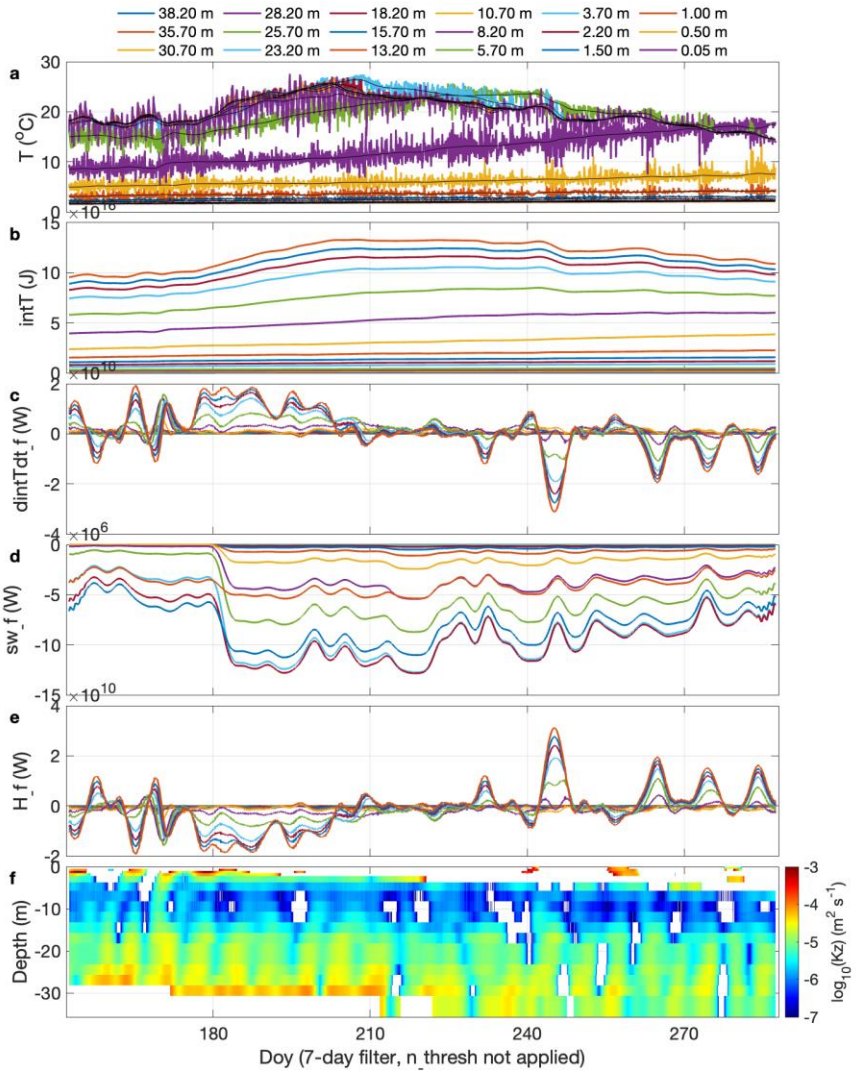

K_z calculated with data from CTD profiles

K_Z was also calculated with the CTD profiler data collected during surveys from April 2023 to May 2024, in two ways: 1) Calculations using data from Stations 3, 4, 6, 7, 10, 12 with Sweer correction. 2) Calculation using data from Station 3 or 6.

The Sweer correction is done to account for differences among stations owed to internal wave motions or other hydrodynamic processes not associated with K_z, as follows: 1) Set the minimum and maximum temperature as 0 and 30 °C, respectively, for all CTD profiles from the chosen stations. 2) For each profile, find the depth from bottom to surface by linear interpolation of temperature at 0.1 °C increments. In this step, temperature above the depth where the

maximum temperature was below surface was excluded. 3) Average the depths of isotherms across all the stations to create a lakewide average temperature profile for the campaign date.

Averaged temperature profiles from all lakewide surveys conducted between April 2023 and May 2024 were organized into a time-depth matrix and used with the same MATLAB code as for thermistor chain data to calculate K_z without being filtered. Similarly, calculations at single stations were done with temperature profiles of all surveys re-organized into a time-depth matrix of uniform depths without being filtered.

As an example, K_z calculated with data from the 6 chosen stations with Sweer correction is similar to those calculated at single stations, averaging around 10^{-6} m^2 s^{-1} (Fig. 64, Fig. 65, Fig. 66), and lower than the K_z calculated with thermistor chain data during both periods.

Fig. 64. a – CTD temperature with Sweer correction for Stations 3, 4, 6, 7, 10 and 12 from April 2023 to May 2024; b – heat content; c – change of heat content; d – solar heat; e – heat flux with solar heat subtracted; f – K_z with logarithmic scale.

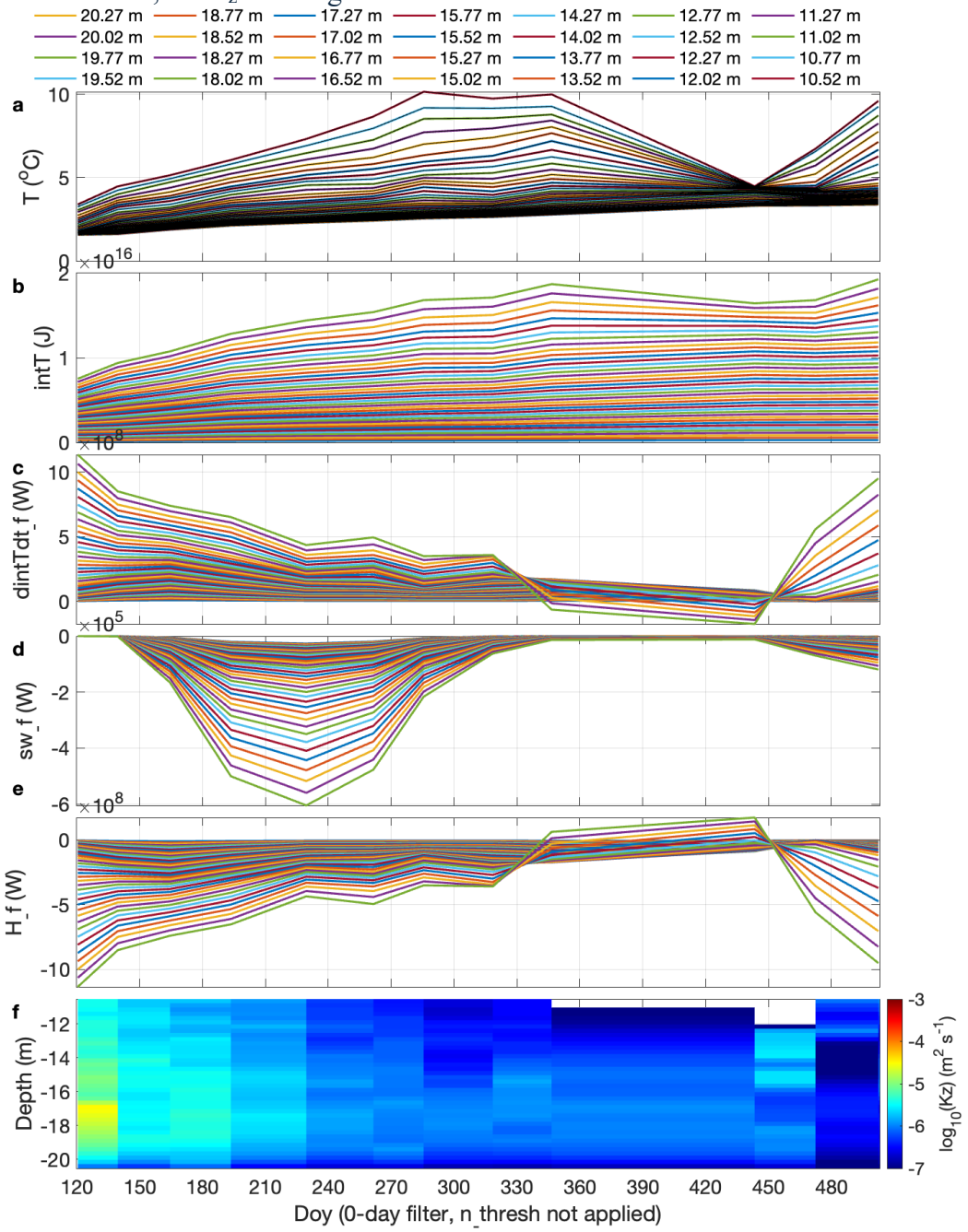

Fig. 65. a – CTD temperature Station 3 from April 2023 to May 2024; b – heat content; c – change of heat content; d – solar heat; e – heat flux with solar heat subtracted; f – Kz with logarithmic scale.

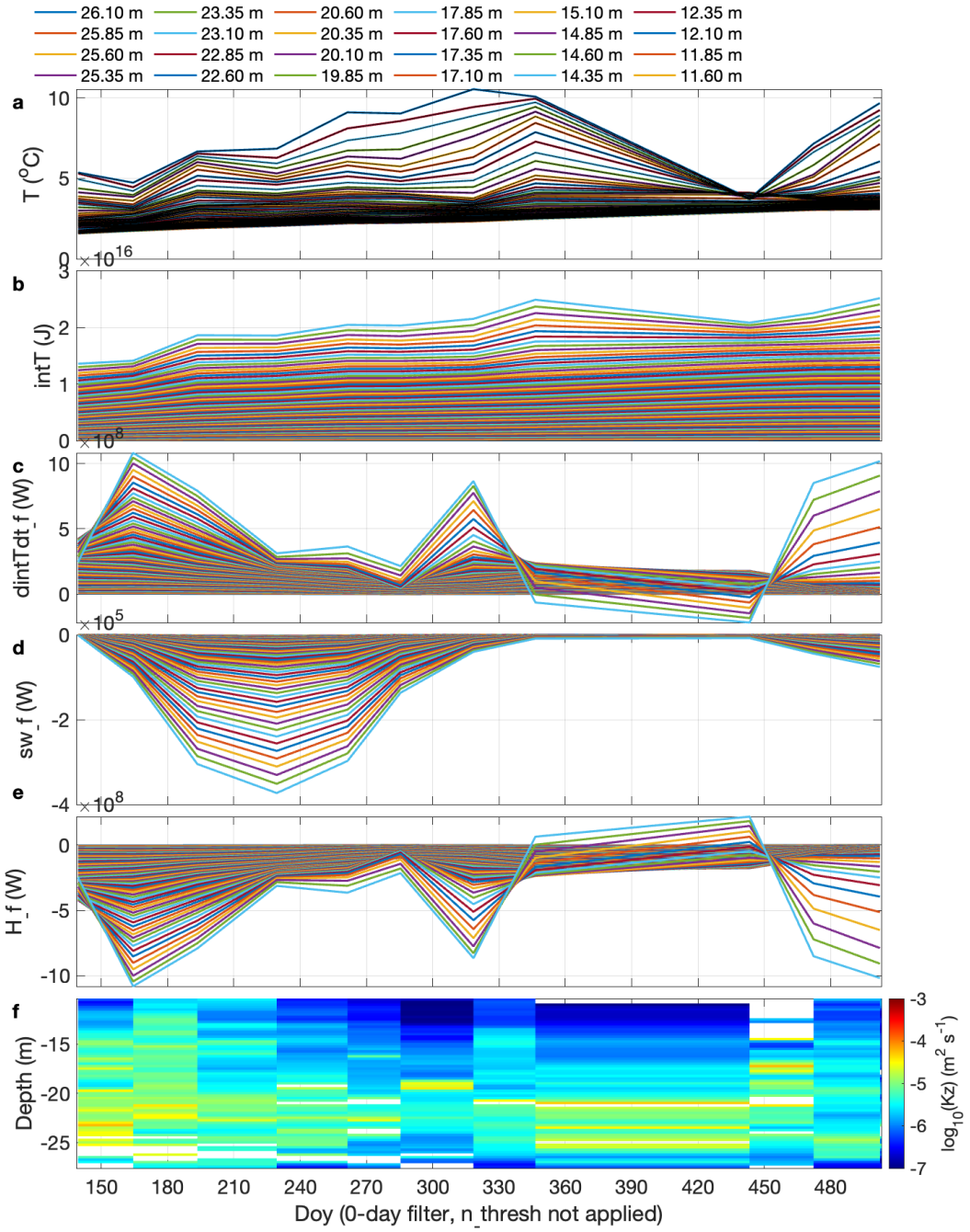

Fig. 66. a – CTD temperature Station 6 from April 2023 to May 2024; b – heat content; c – change of heat content; d – solar heat; e – heat flux with solar heat subtracted; f – Kz with logarithmic scale.

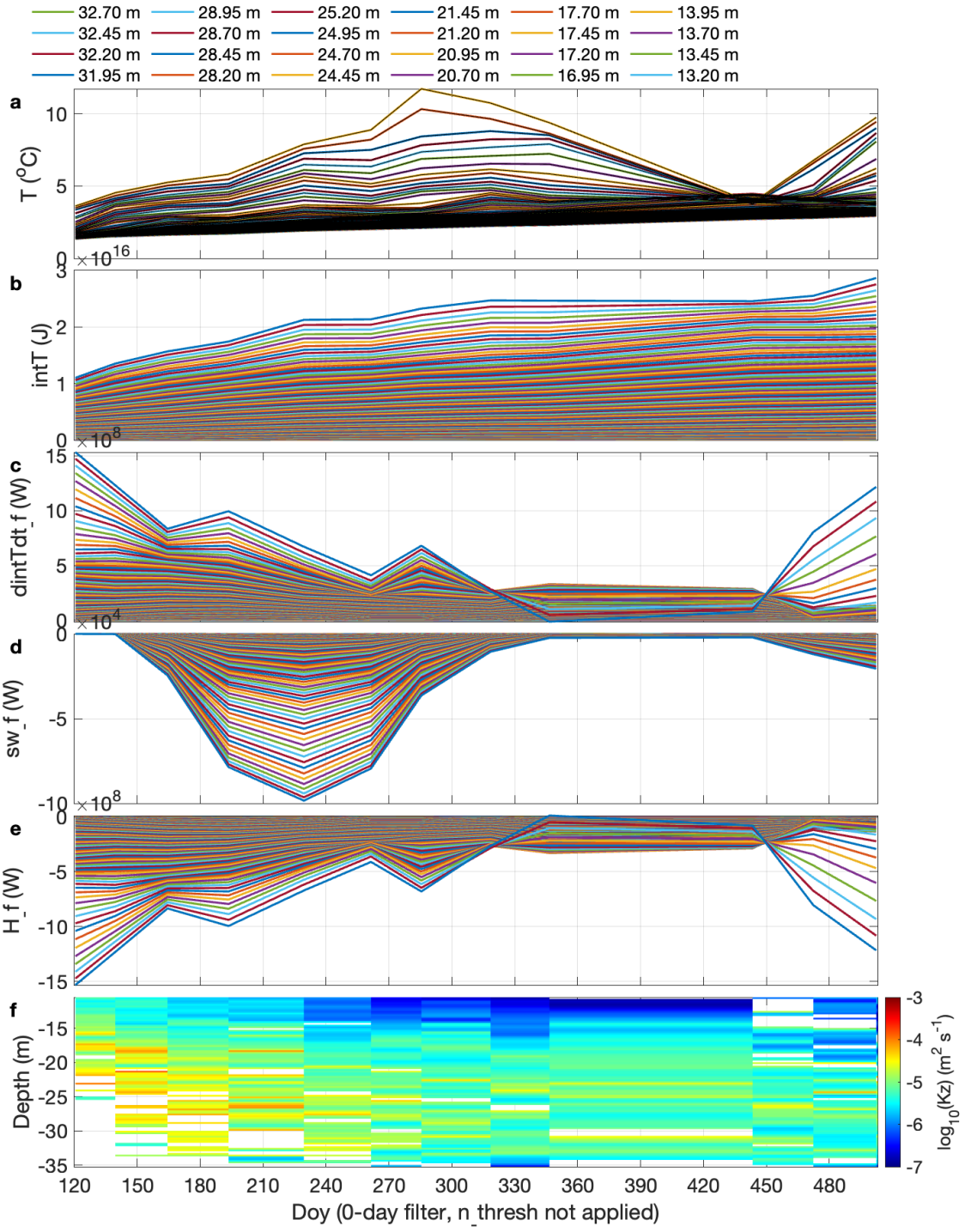

Photosynthesis and Respiration

Photosynthesis by phytoplankton is a key component of primary production in Mono Lake and supports higher trophic levels including *Artemia* and nesting and migratory birds. Planktonic primary production is the net result of photosynthesis and respiration, which is determined by the abundance and physiological condition of the phytoplankton, temperature, nutrient, and light environments. Phytoplankton abundance is the balance of growth and loss processes where losses include Artemia grazing, sinking, and cell senescence. The complex, non-linear interactions of these processes are challenging to unravel and require further analyses of the on-going monitoring measurements.

Prior studies of phytoplankton photosynthesis in Mono Lake were based on uptake of ^{14}C-bicarbonate and examined seasonal and inter-annual variations and relations with environmental factors. Jellison and Melack (1988) reported that phytoplankton primary production was two to three times higher during the spring of 1983 than in the springs of 1984 and 1985, following the development of strong chemical stratification which limited the upward supply of ammonium. Sixty-eight percent of the seasonal variation in the chlorophyll-specific rate of carbon uptake was explained by a regression on temperature (53%), chlorophyll *a* (12%), and the carbon:chlorophyll *a* ratio (3%). Jellison and Melack (1993c) measured photosynthetic activity in Mono Lake during a period spanning the onset (1983), persistence (1984-l987), and breakdown of meromixis (1988). A gradual increase in photosynthetic production occurred before meromixis ended, and annual production was greatest in 1988. Most of the variation in rates of light-saturated carbon uptake normalized to chlorophyll a was explained by temperature (60%) and indices of the light and nutrient environments accounted for an additional 8%.

In 2024, an approach to estimate both photosynthesis and respiration by phytoplankton by changes in dissolved oxygen was developed. Continuous, high-frequency DO measurements were made in containers with lake water incubated in the laboratory under different light levels. Changes in DO concentration in the light represent net ecosystem production, and changes in the dark record respiration.

Methods

Laboratory procedures

Mono Lake water was collected at Station 6 from 0.2 m and 12 m using a peristaltic pump. *Artemia* were removed from sampled water using a funnel equipped with a 120-µm mesh

screen. Upon arrival at the laboratory, sampled water was maintained at 10 °C in dark conditions until the experiment began the following day. Prior to the start of the experiment, water samples from each depth were mixed and filtered again through a 120-µm sieve. Duplicate bottles (1-gallon PET bottles, Uline S-15711) were filled, one DO sensor (PME MiniDOT) was placed in each bottle, and DO concentrations and temperatures were recorded every 10 min. DO concentration was adjusted for salinity of Mono Lake, with values of 70 ppt at 0.2 m and 80 ppt at 12 m, and for the local elevation at SNARL of 2160 m.

Bottles were incubated in a water bath and illuminated by full-spectrum (blue 420–470 nm, green 500–570 nm, and red 610–680 nm wavelengths) LED lamps under a 12h:12 h dark:light cycle at two light levels and in the dark. Light intensities were measured in the water bath with a submersible cosine-corrected PAR quantum sensor at multiple depths and positions. Different light levels were obtained by enclosing bottles in neutral density screens. Dark bottles were incubated in a separate dark water bath.

Water samples were taken at the beginning of the experiment for both depth samples and at the end of the experiment from each replicate sample bottle, for measurements of chlorophyll *a* concentration (µg L^{-1}) obtained with GF/F filter extraction analyses (see methods in Chapter 2).

Calculations of metabolic rates

Net Ecosystem Production (NEP) is determined from daytime changes in DO and include photosynthesis and respiration. DO changes per hour were averaged over the 12-hour illuminated periods. Rates are reported per hour.

Respiration rate is calculated from the decline in DO during nighttime in containers illuminated during the day (RL) and in containers incubated only in the dark (RD). Changes per hour were averaged over the 12-hour dark periods. Rates are reported per hour.

Results

Three sets of measurements were made as the methodology was developed (Table 22Table 22. Photosynthesis and Respiration Experiments.), and calculated values for NEP, RL and RD are summarized in Table 23, Table 24,Table 25. Metabolic rates had highly significant differences between 0.2 m and 12 m or 16 m (One-way ANOVA, $p < 0.001$).

Table 22. Photosynthesis and Respiration Experiments.

Incubation Dates	Temperature Range (°C)	Sample Water Depth (m)	PAR (E m^{-2} d^{-1})	PAR (µmol m^{-2} s^{-1})	Chla Start (µg L^{-1})	Chla End (µg L^{-1})
6/6–10/2024	18.3 – 20.7					
		0.2	19	436		14.9
		0.2	11	266		16.2
		0.2	3	65		15.5
		0.2	Dark	Dark		14.6
6/21–30/2024	16.9 – 21.1					
		0.2	10	224	0.23	0.21
		0.2	4	101	0.23	0.45
		0.2	0	0	0.23	0.13
		12	10	224	85	61
		12	4	101	85	70
		12	Dark	Dark	85	64
8/20–22/2024	18.9 – 20.9					
		0.2	8	184	2.3	1.6
		0.2	4	83	2.3	3.1
		0.2	0	0	2.3	1.8
		16	8	184	117	119
		16	4	83	117	219
		16	Dark	Dark	117	104

Based on the results of these trials, the changes in DO are sufficient to allow calculation of photosynthetic rates of the phytoplankton and of respiration rates of phytoplankton and other uncharacterized microbes and the lighting system is sufficient to characterize the photosynthesis versus light relationship.

Table 23. Mean hourly estimates of NEP and RL incubated from 6–10 June 2024 with samples from depth 0.2 m under different light intensities. DO changes expressed as µg O_2 L^{-1} h^{-1}.

Dates	6/6	6/7	6/8	6/9	6/10
			0.2 m		
PAR = 19 E m^{-2} d^{-1}					
NEP	47	29	33	31	33
RL	17	22	26	29	34
PAR = 11 E m^{-2} d^{-1}					
NEP	41	10	16	15	17
RL	11	6	9	11	19
PAR = 3 E m^{-2} d^{-1}					
NEP	19	8	16	23	23
RL	8	6	17	18	25

Table 24. Mean hourly estimates of NEP, RL, and RD incubated from 21–30 June 2024 with samples from two depths (0.2 m and 12 m) under different light intensities. DO changes expressed as µg O_2 L^{-1} h^{-1}.

Dates	6/21	6/22	6/23	6/24	6/25	6/26	6/27	6/28	6/29	6/30
				0.2 m						
PAR = 10 E m^{-2} d^{-1}										
NEP	16	19	20	26	26	22	18	16	15	15
RL	4	13	18	24	25	24	24	23	23	23
PAR = 4 E m^{-2} d^{-1}										
NEP	7	10	12	16	17	19	21	22	20	17
RL	7	6	12	14	17	18	21	23	23	22
Dark										
RD	5	5	17	11	15	19	20	32	30	46
				12 m						
PAR = 10 E m^{-2} d^{-1}										
NEP	293	241	222	201	204	212	207	221	224	212
RL	37	93	131	156	136	166	172	188	198	200
PAR = 4 E m^{-2} d^{-1}										
NEP	241	230	249	229	221	207	190	171	161	172
RL	26	81	125	173	165	177	168	159	134	144
Dark										
RD	21	14	39	26	22	14	0	0	0	0

Table 25. Mean hourly estimates of NEP and RL incubated from 20–22 August 2024 with samples from two depths (0.2 m and 16 m) under different light intensities. DO changes expressed as µg O_2 L^{-1} h^{-1}.

Dates	8/20	8/21	8/22
		0.2 m	
PAR = 8 E m^{-2} d^{-1}			
NEP	40	63	57
RL	45	48	56
PAR = 4 E m^{-2} d^{-1}			
NEP	15	68	69
RL	42	67	71
Dark			
RD	20	9	13
		16 m	
PAR = 8 E m^{-2} d^{-1}			
NEP	338	868	706
RL	201	314	317
PAR = 4 E m^{-2} d^{-1}			
NEP	90	533	690
RL	77	180	329

REFERENCES

Golterman, H. L., and R. S. Clymo. Methods for chemical analysis of fresh waters. IBP Handbook No. 8.

Heath, H. The external development of certain phyllopods. J. Morphology 38: 453–483.

Jassby, A. and T. Powell. 1975. Vertical patterns of eddy diffusion during stratification in Castle Lake, California. Limnol. Oceanogr. 20: 530–543.

Jellison, R., and J. Melack. 1988. Photosynthetic activity of phytoplankton and its relation to environmental factors in hypersaline Mono Lake, California. Hydrobiologia 158: 69–88.

Jellison, R., and J. Melack. 1993a. Meromixis in hypersaline Mono Lake, California. 1. Stratification and vertical mixing during the onset, persistence, and breakdown of meromixis. Limnology and Oceanography 38: 1008–1019.

Jellison, R., L. Miller, J. Melack, and G. Dana. 1993b. Meromixis in hypersaline Mono Lake, California. 1. Nitrogen fluxes. Limnology and Oceanography 38: 1020–1039.

Jellison, R. and J.M. Melack. 1993c. Algal photosynthetic activity and its response to meromixis in hypersaline Mono Lake, California. Limnol. Oceanogr.38: 8 18–837.

Jellison, R., Vignardi, C, and Melack, J. M (Earth Research Institute, UCSB). 2024. Mono Basin Annual Monitoring Reports. Section III. Mono Lake Limnological Monitoring 2023 Annual Report. Submitted to California State Water Resources Control Board by Los Angeles Department of Water and Power.

Jellison, R., S. MacIntyre, and F. J. Millero. 1999a. Density and conductivity properties of Na-CO3-Cl-SO4 brine from Mono Lake, California, USA. Int. J. Salt Lake Research 8: 41–53.

Jellison, R., S. MacIntyre, and F. J. Millero. 1999b. Density and conductivity properties of Na-CO3-Cl-SO4 brine from Mono Lake, California, USA (erratum). Int. J. Salt Lake Research 8:384.

Lenz, P. H. 1984. Life-history analysis of an *Artemia* population in a changing environment. Journal of Plankton Research 6:967–983.

MacIntyre, S. and R. Jellison. 2001. Nutrient fluxes from upwelling and enhanced turbulence at the top of the pycnocline in Mono Lake, California. Hydrobiologia 466:13–29.

Melack, J. M. and Jellison, R. 1998. Limnological conditions in Mono Lake: contrasting monomixis and meromixis in the 1990s. Hydrobiologia 384:21–39.

Strickland, J. D. H., and T. R. Parsons. 1972. A practical handbook of seawater analysis. Bull. Fish. Res. Bd. Canada.

Sweers, H.F. 1968. Two methods of describing the “average” vertical temperature distribution of a lake. J. Fish. Res. Bd. Can. 25:191l–1922.

Walker, K. F., Williams, W. D., and Hammer, U. T. 1970. The Miller Method for oxygen determination applied to saline lakes. Limnol. Oceanogr. 15:815–815.

Section IV. Mono Basin Waterfowl

2024 Monitoring Report

Prepared by Los Angeles Department of Water and Power

Mono Basin Waterfowl
2024 Monitoring Report

Prepared by:
Los Angeles Department of Water and Power
Bishop, CA 93514

Prepared for the State Water Resources Control Board
and Los Angeles Department of Water and Power
May 2025

Contents

Figures

Tables

Abbreviations

LADWP	Los Angeles Department of Water and Power
BLPO	Black Point
BRCR	Bridgeport Creek
CHCL	Chalk Cliffs
COPO	County Ponds
DECR	DeChambeau Creek
DEEM	DeChambeau Embayment
DEPO	DeChambeau Ponds
HIBA	Hilton Bay
LASP	Layton Springs
LVCR	Lee Vining Creek
MCBA	McGee Bay
MICR	Mill Creek
NESH	Northeast Shore
NOLA	North Landing
RACO	Ranch Cove
RUCR	Rush Creek
SAPO	Sandy Point
SASP	Simons Spring
SOTU	South Tufa
SSLA	South Shore Lagoons
SWRCB	State Water Resources Control Board
UPOW	Upper Owens River
WASP	Warm Springs
WESH	West Shore
WICR	Wilson Creek

Introduction

The Mono Lake Water Right Decision 1631 (D1631) adopted by the State Water Resources Control Board (SWRCB) in 1994 modified the City of Los Angeles Department of Water and Power's (LADWP) Water Rights Licenses 10191 and 10192. This modification was in response to the public trust requirements for the Mono Basin and the associated environmental impacts originating from these licenses. A requirement of D1631 and subsequent Restoration Order 98-05 was the preparation of a Waterfowl Habitat Restoration Plan (the Plan) to restore and manage waterfowl habitat at Mono Lake and which prescribed continued monitoring of waterfowl populations, lake limnology, lake fringing wetlands, and hydrology in the Basin. Order 98-05 specified that the waterfowl program be carried out under the direction of a Waterfowl Director approved by the Deputy Director of Water Rights. Ms. Deborah House, LADWP Watershed Resources Specialist, fulfilled the role of Waterfowl Director from 2002 until her retirement in 2024, at which time she vacated her position as SWRCB appointed Mono Basin Waterfowl Director. LADWP's Water Rights Licenses 10191 and 10192 were amended in 2021 (Amended Licenses); Condition 22 in the Amended Licenses describes the process for designating a new Waterfowl Director, which was initiated following Ms. House's retirement. LADWP and the Mono Basin Parties circulated a Request for Proposals for a new Waterfowl Director in spring 2025, but a replacement director has not yet been appointed.

In the absence of a Waterfowl Director in 2024, LADWP wildlife biologists and consultants continued waterfowl population monitoring through summer and fall 2024 per the Plan. This compliance report presents data collected in 2024 but does not contain a thorough analysis or recommendations in the absence of a Waterfowl Director, as has been provided in past years. A future Mono Basin Waterfowl Director will analyze these data once appointed by the SWRCB.

2024 Monitoring

The 2024 Mono Basin Waterfowl program monitoring consisted of the following components: 1) three breeding waterfowl ground counts during June and July, 2) hydrologic spring surveys in September 2024, 3) six fall migratory waterfowl counts using boat and ground surveys with assistance from a consultant, 4) aerial photographs from a helicopter in the fall to document conditions of lake fringing wetland habitats.

Waterfowl Population Surveys

Population surveys were conducted to evaluate the response of waterfowl to the reestablishment of waterfowl habitat at Mono Lake. There is limited historic data for waterfowl use of Mono Lake, however, based on the information available, the SWRCB concluded that Mono Lake was at one time a major concentration area for migratory waterfowl, and supported a much larger waterfowl population prior to out-of-basin water diversions (SWRCB 1994). The SWRCB determined that diversion-induced impacts to waterfowl were more significant than for other waterbird species. For reference to Mono Lake, both Bridgeport and Crowley Reservoirs are also surveyed.

Waterfowl population monitoring in 2024 included summer ground counts at Mono Lake and fall surveys at Mono Lake, Bridgeport Reservoir, and Crowley Reservoir (Figure 1). In 2024, due to absence of a Mono Basin Waterfowl Director, summer and fall surveys were conducted by LADWP Watershed Resources staff and Stantec Consulting Services Inc. (Stantec) under the direction of Watershed Resources staff. Watershed Resources staff received training under the former Mono Basin Waterfowl Director and have considerable experience with the Mono Lake Waterfowl Habitat Restoration Project.

Since 2002, LADWP staff had conducted waterfowl population monitoring annually at Mono Lake, Bridgeport Reservoir, and Crowley Reservoir, which support the greatest number of waterfowl in Mono County. These water bodies provide data on species diversity, abundance, and population trends both at a local and regional scale. Unlike previous years where an aircraft was used, the 2024 fall surveys were conducted entirely from a boat. The shift in sampling protocol was because of safety concerns associated with low-flying aircraft and the loss of the Waterfowl Director, who had considerable experience and skill in conducting such surveys from an aircraft.

Survey Areas

Mono Lake

Mono Lake is centrally located in Mono County and lies just east of the town of Lee Vining (Figure 1). Mono Lake is a highly productive, deep-water saline lake and invertebrate foods predominate. The Mono Lake brine shrimp and alkali flies are virtually the only aquatic invertebrates in the open water. Although the highly saline water, overall depth, and low diversity of food items may limit habitat quality for waterfowl - nearshore and onshore resources for waterfowl include several perennial creeks and their deltas along the west shore, numerous fresh and brackish springs

scattered around the perimeter, and small, temporary and semi-permanent fresh and brackish ponds. The fall migratory waterfowl community at Mono Lake is dominated by species able to exploit these invertebrate resources; and Northern Shoveler and Ruddy Duck, together constitute approximately 90% of all waterfowl between September and mid-November (LADWP 2018).

Shoreline subareas and Cross-lake Transects

The shoreline and open water areas were divided into shoreline subareas and cross-lake transect zones for determining the spatial distribution of waterfowl (Figure 2). The entire Mono Lake shoreline was divided into 15 shoreline subareas, generally following those established by Jehl (2002). A sampling grid established in 2002 to survey open-water areas of Mono Lake consists of eight parallel transects spaced at one-minute (1/60th of a degree, approximately one nautical mile) intervals that were further divided into a total of 25 sub-segments of approximately equal length.

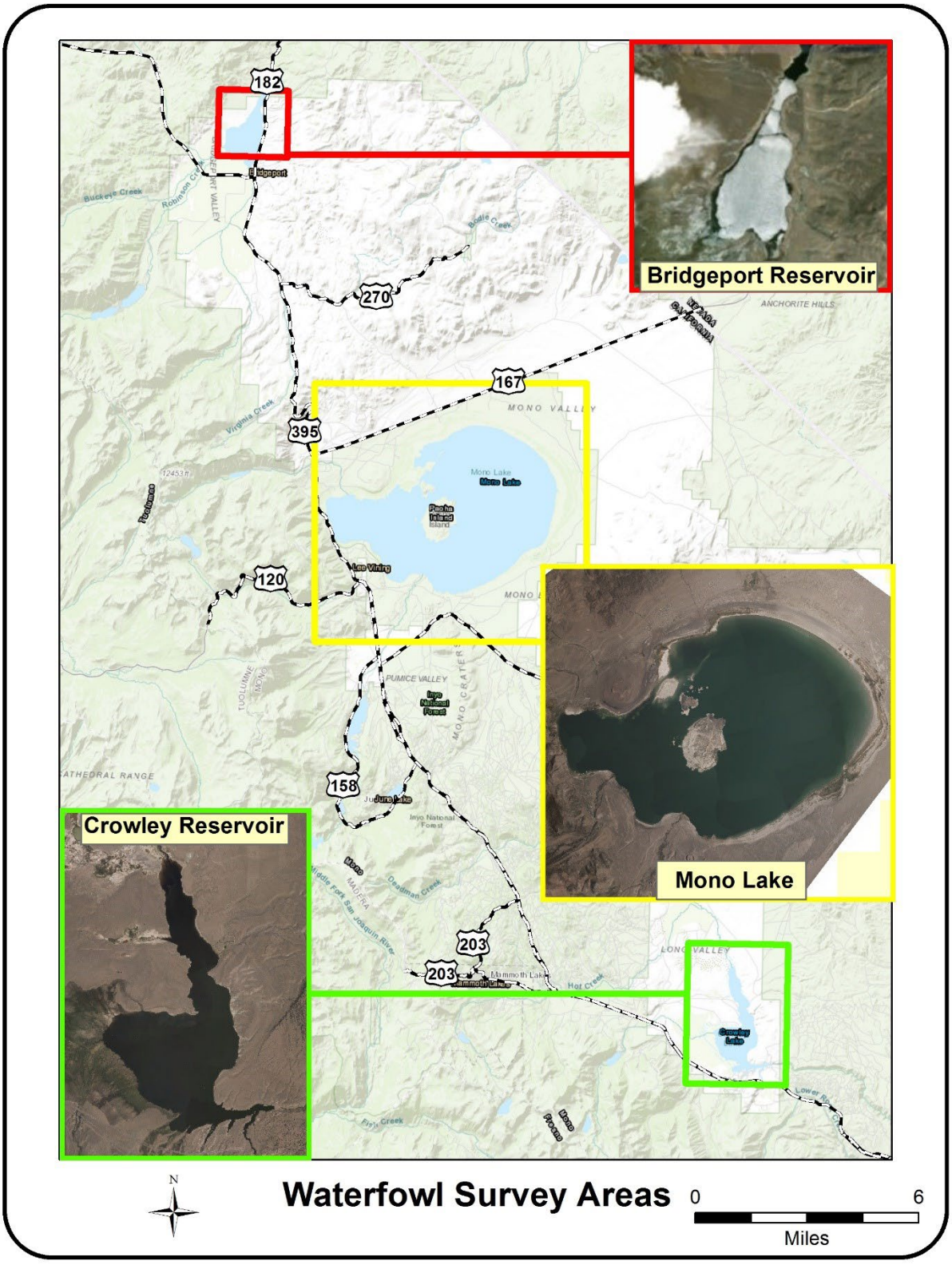

Figure 1. Waterfowl Survey Areas.

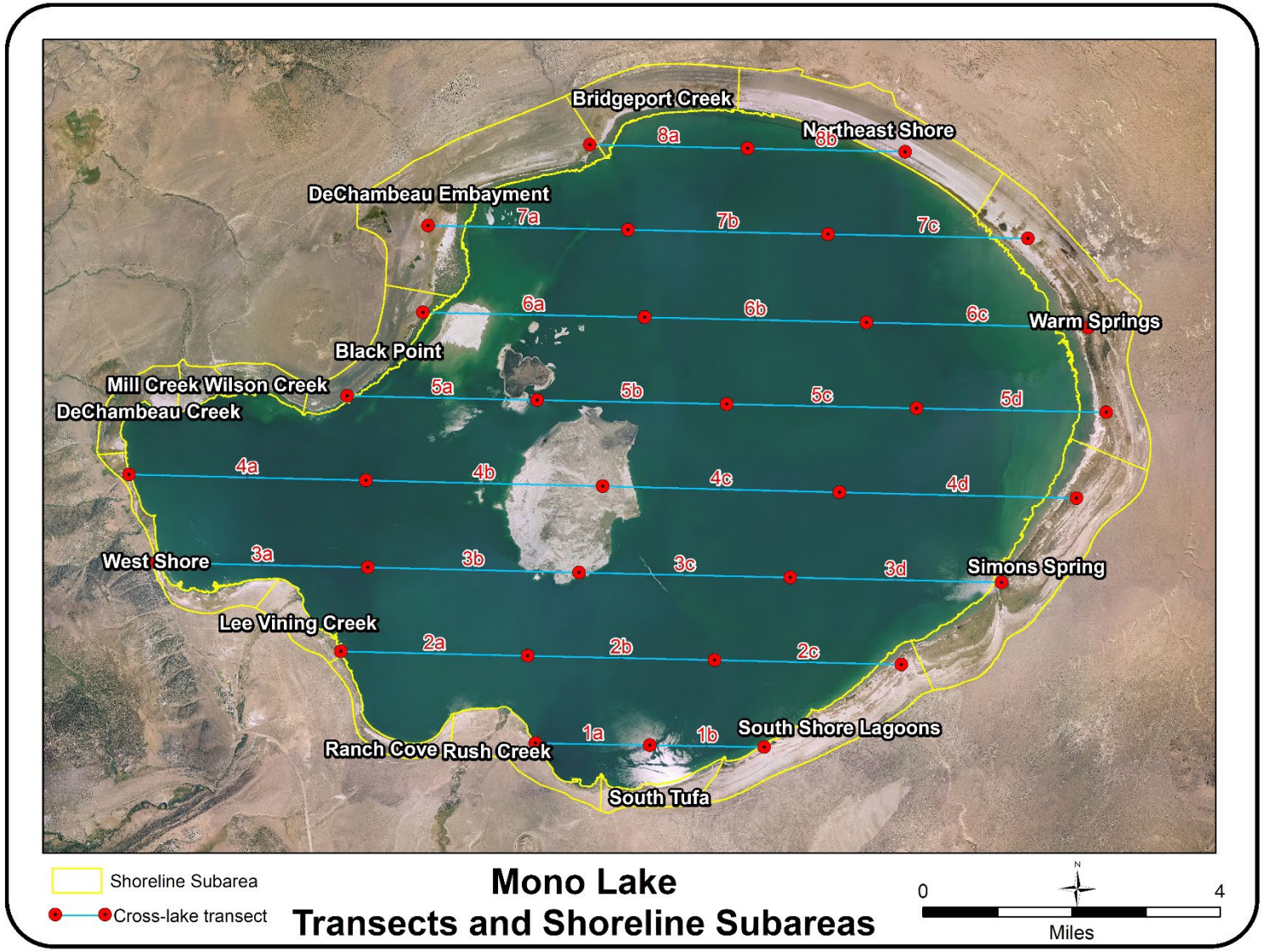

Figure 2. Mono Lake Shoreline Subareas and Cross-lake Transects.

Mono Basin Restoration Ponds

The Mono Basin Restoration Ponds are located on the north side of Mono Lake, near the historic DeChambeau Ranch, and upgradient of the DeChambeau Embayment shoreline area (Figure 3). The Restoration Pond complex consists of the five DeChambeau Ponds and two County Ponds.

The DeChambeau Ponds are a complex of five small artificial ponds of varying size ranging from about 0.7 to 4.0 acres when flooded. The DeChambeau Ponds were initially created at the onset of trans-basin diversions in the 1940s (LADWP 1996a) and restored in the mid-1990s (LADWP 2018). Project goals for the restoration in the 1990s included the creation of seasonal waterfowl habitat consisting of semi-permanent ponds (DEPO1 and DEPO2), and seasonal impoundments (DEPO3, DEPO4 and DEPO5), as well as adjacent seasonal wet meadow and willow habitat (LADWP 1996a, USDA Forest Service 2005). Management has differed from these original goals, as some ponds (DEPO2 and DEPO4) have been continuously inundated and DEPO1 and DEPO5 infrequently flooded. Failing infrastructure has also altered management.

There are two water sources currently supplying water to the DeChambeau Ponds. Most of the water for the DeChambeau Ponds is from Wilson Creek and delivered via an underground pipe averaging 1-2 cubic-feet-second recently (N. Carle, pers. com.). The piped water flows from DEPO1 to DEPO5. The second source is water from a hot artesian source adjacent to DEPO4. Hot spring water is delivered to each of the five ponds through pipes. A leak developed around 2008 or 2009 in the pipe supplying the ponds (N. Carle, pers. com.), and for several years, hot spring water was only delivered to DEPO4. In 2021, repairs to the pipes had restored the ability to deliver artesian water to additional ponds in the DeChambeau Pond complex.

The County Pond complex consists of two ponds – County Pond East (COPOE) and County Pond West (COPOW). The two County Ponds lie in a natural basin and former lagoon that dried as the lake level dropped below 6,405 feet in the 1950s. The County Ponds were temporarily re-flooded on an occasional basis after that time with water diverted from Wilson Creek, until an underground pipeline was installed to deliver water from DEPO4 to the County Ponds (USDA Forest Service 2005) in the late 1990s. A clay sealant was also applied to COPOE to reduce water use and a diverter box at the County Ponds allows some control over water releases to the individual ponds. COPOW has had little open water and poor habitat since 2010 and appearing dry since 2018. COPOE had been the most productive of the restoration ponds for waterfowl until 2018 when infrastructure failure left both County Ponds dry. In summer 2024, both COPOW and COPOE were once again dry.

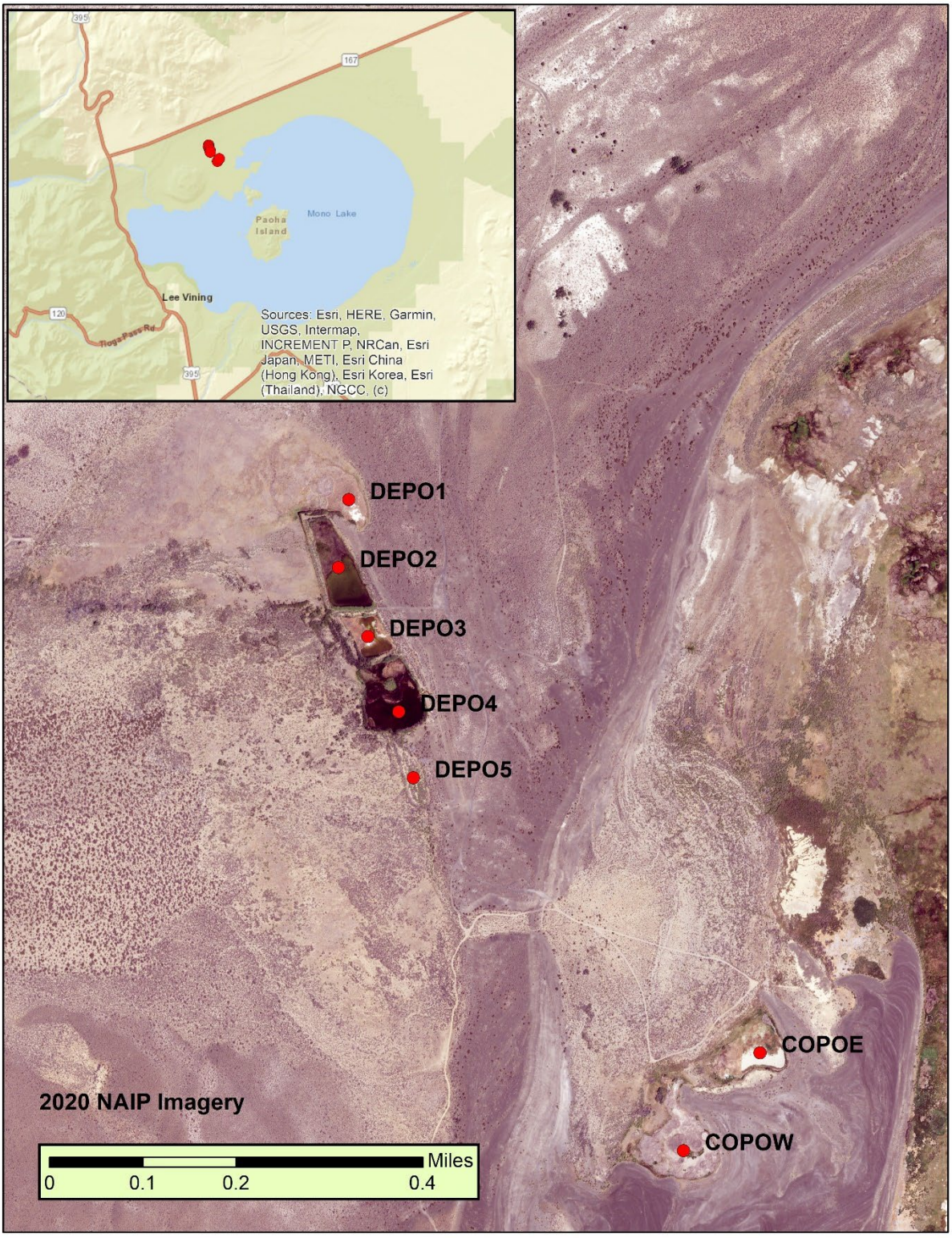

Figure 3. Mono Basin Restoration Ponds.

Bridgeport Reservoir

Bridgeport Reservoir is approximately 22 miles northwest of Mono Lake near the town of Bridgeport (Figure 1). Bridgeport is part of the hydrologically closed Walker River Basin, which spans the California/Nevada border. Bridgeport Reservoir, completed in 1923, provides irrigation water to Smith and Mason Valleys in Nevada (Sharpe *et al.* 2007). Numerous creeks originating from the east slope of the Sierra Nevada drain toward Bridgeport Reservoir. These tributaries are used for upslope irrigation of Bridgeport Valley to support the primary land use of cattle grazing. The creeks directly flowing to the reservoir are: the East Walker River, Robinson Creek and Buckeye Creek. Downstream of Bridgeport Reservoir Dam, the East Walker River continues flowing into Nevada, joining the West Walker River, ultimately discharging into the terminal Walker Lake, Nevada. In Nevada, the Walker River system supports extensive agricultural operations.

The reservoir is rather shallow with a mean depth of 15 feet and a maximum depth of 43 feet (Horne 2003). Due to the shallow-sloping topography of the southwestern portion of the valley, reservoir level greatly influences surface area (House 2021).

Flood-irrigated pastures border the gently sloping south and southwestern portion of Bridgeport Reservoir, while Great Basin scrub is dominant along the more steeply-sloped north arm and east shore. In shallow areas and creek deltas, submergent aquatic vegetation is abundant, including broad beds of water smartweed (*Persicaria amphibia stipulacea*). Marsh, dense wetlands, or woody riparian vegetation are lacking in the immediate vicinity of the reservoir and the Bridgeport Valley. The reservoir is eutrophic due to high nutrient loading and experiences summer blooms of colonial forms of cyanobacteria that form dense floating scum (Horne 2003). Algal blooms in fall frequently result in the issuance of temporary recreational advisories due to the presence of cyanobacteria and associated toxins.

The shoreline of Bridgeport Reservoir was subdivided three shoreline survey areas (Figure 4).

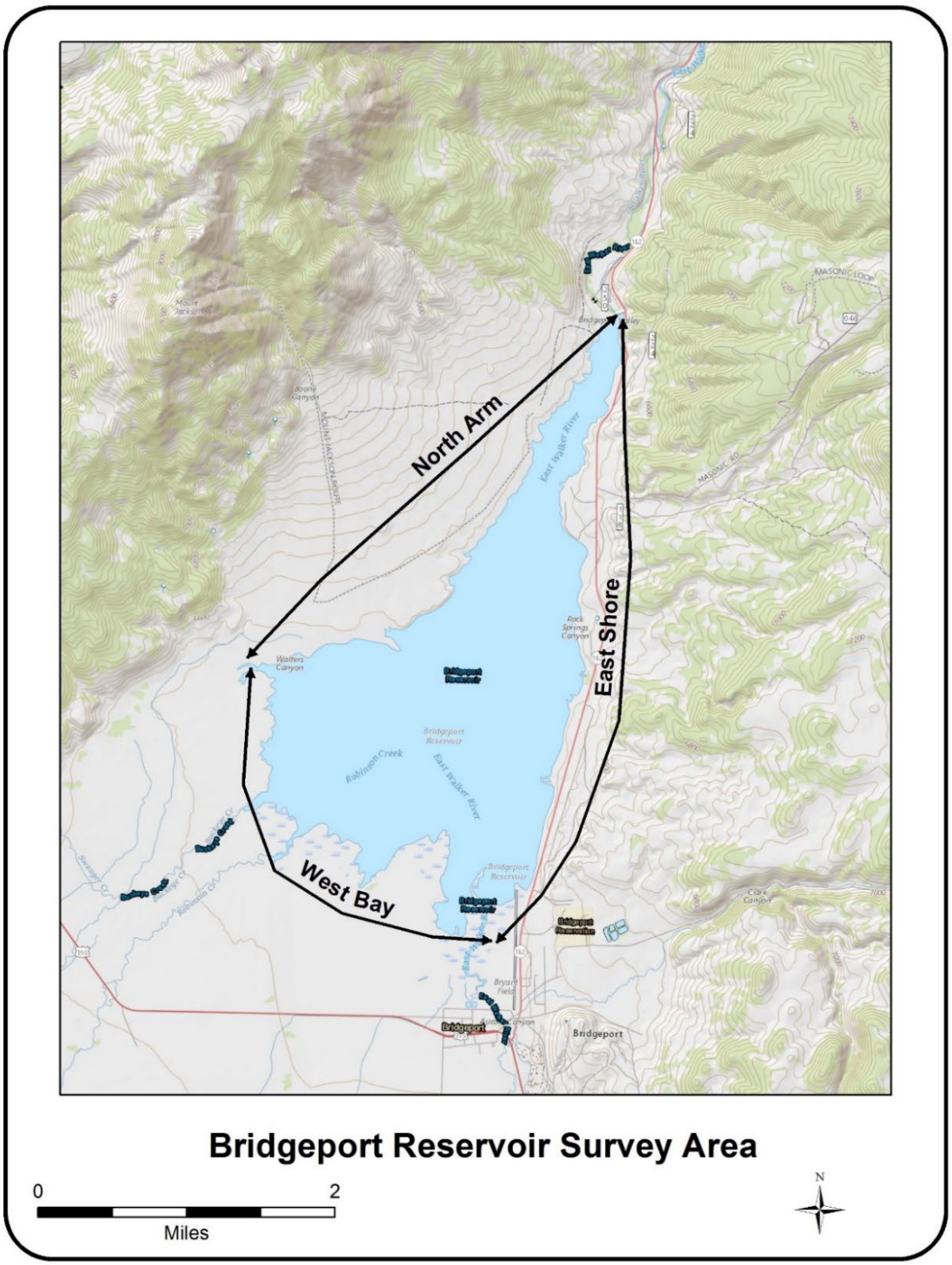

Figure 4. Bridgeport Reservoir Shoreline Subareas.

Crowley Reservoir

Crowley Reservoir is approximately 31 miles southeast of Mono Lake, and 12 miles southeast of the town of Mammoth Lakes (Figure 1). Crowley Reservoir is located in Long Valley, at an elevation of 6,780 feet. Created by the construction of the Long Valley Dam in 1941, Crowley Reservoir is the second largest lake in Mono County, and the largest reservoir in the county, averaging 13.2 square miles. The primary source of freshwater input to Crowley Reservoir is the Owens River. Other freshwater input includes flows from: McGee Creek, Convict Creek, Hilton Creek, and Crooked Creek. Crowley Reservoir also receives spring flow from Layton Springs along the northeast shoreline, and unnamed springs and subsurface flow along the west shore. Crowley has mean depth of 35 feet and a maximum depth of 125 feet (CERL & EMSL 1978).

Crowley Reservoir is eutrophic and experiences summer blooms of the nitrogen-fixing cyanobacteria *Gloeotrichia* in summer, and late-summer and fall season blooms of the cynaobacteria *Aphanizomenon* (Jellison *et al.* 2003). An algal bloom in October 2024 resulted in the issuance of a temporary recreational advisory due to the presence of cyanobacteria and associated toxins. In shallow areas near the deltas, submergent aquatic vegetation is generally abundant, but there was little growth this year as compared to the past several years. Crowley Reservoir is known for supporting a healthy population of midges (Chironomidae).

The shoreline of Crowley Reservoir was subdivided into seven shoreline survey areas (Figure 5).

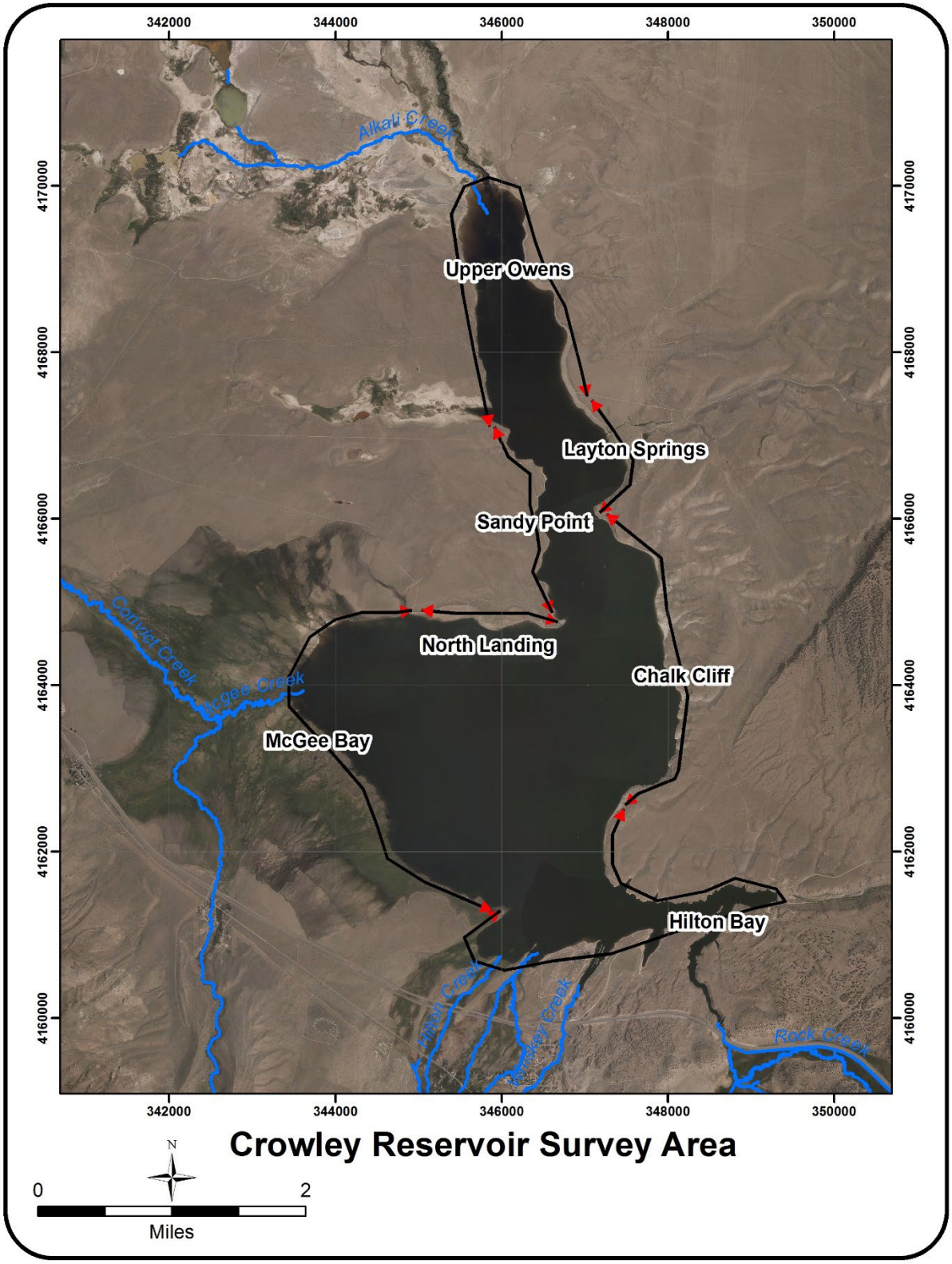

Figure 5. Crowley Reservoir Shoreline Subareas.

Methodologies

Summer Surveys

Summer ground surveys were conducted in the Mono Basin along the shoreline of Mono Lake and at the DeChambeau and County Pond complexes. Nine of the 15 shoreline subareas were surveyed in summer: South Tufa (SOTU), South Shore Lagoons (SSLA), Simons Spring (SASP), Warm Springs (WASP), Wilson Creek (WICR), Mill Creek (MICR), DeChambeau Creek Delta (DECR), lower Rush Creek and Rush Creek Delta (RUCR), and lower Lee Vining Creek and delta (LVCR).

Three summer ground-count surveys were conducted at each of these nine shoreline subareas and all seven restoration ponds in 2024. Surveys were conducted at three-week intervals beginning in mid-June (Table 1). Surveys of the shoreline subareas were conducted by walking at an average rate of approximately 1 mile/hour, depending on conditions, and recording waterfowl species as they were encountered. Surveys started within one hour of sunrise, and all shoreline areas were surveyed over a 4 to 5-day period. The order in which subareas were visited was varied to minimize the effect of time-of-day on survey results. The restoration ponds were surveyed on foot, spending a minimum of 5 minutes at each pond to record any waterfowl and broods present.

For each waterfowl observation, the following was recorded: time of the observation; the habitat type being used; and an activity code indicating how the bird, or birds were using the habitat. Examples of activities recorded include resting, foraging, flying over, nesting, brooding, sleeping, swimming, or calling.

Table 1. Summer Ground Count Survey Dates, 2024.

Subarea	2024 Survey Number and Date		
	Survey 1	**Survey 2**	**Survey 3**
DECR	11-Jun	1-Jul	23-Jul
LVCR	14-Jun	1-Jul	24-Jul
MICR	11-Jun	1-Jul	23-Jul
RUCR	14-Jun	2-Jun	26-Jul
SASP	12-Jun	2-Jul	24-Jul
SOTU	10-Jun	2-Jul	24-Jul
SSLA	10-Jun	28-Jun	22-Jul
WASP	13-Jun	3-Jul	25-Jul
WICR	11-Jun	1-Jul	23-Jul
COPO	11-Jun	1-Jul	25-Jul
DEPO	11-Jun	1-Jul	25-Jul

When conducting summer ground counts at Mono Lake, emphasis was placed on finding and recording all waterfowl broods. Because waterfowl are easily flushed, and females with broods are especially wary, the shoreline was scanned frequently well ahead of the observer to increase the probability of detecting broods. Information recorded for broods included: species, size, GPS coordinates (UTM, NAD 83, Zone 11, CONUS), habitat use, and age. Broods were aged based on plumage and body size (Gollop and Marshall 1954).

Since summer surveys were conducted at three-week intervals, any brood assigned to Class I, using the Gollop and Marshall age classification scheme (which includes subclasses Ia, Ib, and Ic), would be a brood that had hatched since the previous visit. Assigning an age class to broods allowed for a determination of the minimum number of “unique broods” using the Mono Lake wetland and shoreline habitats.

Habitat use was recorded to document habitat use by waterfowl at Mono Lake. Habitat use was recorded using the mapped landtype categories (LADWP 2018). Two additional habitat types: open water near shore (within 50 meters of shore), and open water offshore (>50 meters offshore), were added to the existing classification system to more completely represent areas used by waterfowl.

In previous years, salinity measurements of lake-fringing ponds were taken using an *Extech EC400* Conductivity/TDS/Salinity probe to aid in the classification of fresh versus brackish ponds when recording habitat use. However, this equipment was not providing reliable readings and was not used in habitat classification. Therefore, the presence or

absence of vegetation, proximity to spring sites that provided surface or subsurface freshwater inflow, or proximity to the lake were used to help with classification of ponds.

Fall Surveys

Stantec biologists conducted a total of four, one-week-long waterfowl count surveys on Mono Lake, Crowley Lake and Bridgeport Reservoir starting on September 23, 2024, and ending on November 21, 2024. The goal of each survey was to capture the quantity and species composition of waterfowl, in entirety, on each body of water. These surveys occurred on the weeks of September 23, October 7, October 21, and November 18, 2024. The survey scheduled for the week of November 4 was cancelled due to inclement weather. An initial survey was carried out by the LADWP the week of September 9, 2024, and these data are included in this report. Surveys were either conducted from shore using a *Vortex Diamondback* spotting scope (Bridgeport Reservoir), from a boat using 10x42 binoculars (Mono Lake), or a combination of both (Crowley Lake). Each survey was conducted by two biologists; a boat driver was also present for Mono Lake and Crowley Lake. Each survey began at approximately 0800 hours and was finished by approximately 1400 hours. Conducting waterfowl surveys from a boat presented challenges such as flushing large flocks of waterfowl from shoreline habitat areas from a large distance. This not only made identification and quantification more difficult, but also resulted in waterfowl moving between areas more frequently affecting overall accuracy. Every effort was made to account for these variations in spatial distribution.

Shoreline and open water surveys were conducted on two separate days (Figure 2). The shoreline survey began at the Mono Lake Boat Launch near the Lee Vining Creek delta, and was carried out in a, where possible, continuous clockwise fashion around the shore of the entire lake. During the shoreline surveys, both Stantec biologists made independent counts and species identifications. When a shoreline segment was completed, the biologists compared and rectified counts to reach agreement on species composition and count. The open water surveys on Mono Lake covered nine transects provided by LADWP and were intended to only count Ruddy Ducks. Transects were driven at approximately 5-10 mph with each biologist covering counts from each side of the boat. Unlike the shoreline surveys, data from each biologist were added together for a total count of open water Ruddy Ducks. In addition to Mono Lake proper, the five Dechambeau restoration ponds were surveyed using binoculars from the banks.

Crowley Lake

At Crowley Lake, shoreline surveys were divided into seven lakeshore segments provided by LADWP and carried out in one day. Shoreline surveys began at Crowley Lake Fish camp and were carried out in a continuous clockwise fashion in the same manner as Mono Lake, except at the Upper Owens River delta (UPOW) where the water level was too shallow to survey by boat. Counts for the UPOW lakeshore segment were carried out from a bluff above the delta (37°39'03.4"N 118°44'59.7"W) using at *Vortex Diamondback* spotting scope. Data from the two observers were compared and rectified in the same manner as on Mono Lake.

Bridgeport Reservoir

At Bridgeport Reservoir, shoreline surveys were divided into three lakeshore segments provided by LADWP and carried out in one day. Waterfowl counts were carried out from various points on or near State Highway 182 (Sweetwater Rd) using a *Vortex Diamondback* spotting scope. Data were compared and rectified in the same manner as Mono Lake and Crowley Lake.

Aerial Photography of Waterfowl Habitats

The shoreline configuration of Mono Lake is dynamic, as seasonal and annual changes in lake level influence the development and presence of ponds, the amount of shoreline exposed, and other features important to waterfowl. Due to the dynamic nature of the Mono Lake shoreline, the aerial or satellite imagery studies and subsequent mapping performed at five-year intervals do not adequately capture annual changes that may influence waterfowl use. These still aerial photographs are taken yearly in fall to assess shoreline changes at Mono Lake, particularly in years when aerial imagery is not available.

In 2024, digital photographs were taken from a helicopter to document shoreline conditions at Mono Lake in the summer and fall. In the summer, photos of Mono Lake were taken on July 29, 2024. In the fall, photos of all three waterfowl survey areas (Bridgeport Reservoir, Crowley Lake, and Mono Lake) were taken November 12, 2024. At each waterfowl survey area, representative photos were taken of each shoreline subarea established for use in evaluating the spatial distribution of waterfowl. For reference, the elevation of Mono Lake on August 1 and November 1, 2024 was 6,384.1 and 6,383.1 feet, respectively.

Data Summary and Analysis

Mono Lake Summer Surveys

Waterfowl Community

The summer waterfowl community data summary includes all breeding, migrant, and non-breeding/oversummering species observed in 2024. The 2024 summer waterfowl survey data were summarized by species and summer survey number.

Waterfowl Broods

The total number of broods observed during shoreline surveys is used as an index of waterfowl breeding productivity at Mono Lake. The total number of broods raised at Mono Lake in a year was estimated by removing broods potentially double-counted over the season from all broods recorded. For example, all Class I broods observed over the entire survey period would be included in the total, but older broods (e.g., Class II) observed after the first survey were removed. Older broods were included in the total if no broods of that species had been observed yet.

The calculation of brood parameters included all nesting species except Canada Goose. Canada Goose initiates nesting earlier than the other waterfowl species and family groups can be difficult to approach closely on foot except in areas where they have become habituated to humans. These factors combined with the tendency of this species to be highly mobile has made ageing broods accurately and determining the minimum number of Canada Goose broods less reliable. The spatial distribution of breeding waterfowl was evaluated by calculating the total number of broods observed for each shoreline area in 2024.

Restoration Ponds Summer Surveys

Waterfowl Community

The summer waterfowl community at the restoration ponds includes all breeding, migrant, and non-breeding/oversummering species observed in 2024. The 2024 summer waterfowl survey data at the restoration ponds were summarized by species and summer survey number.

Waterfowl Broods

The total number of broods observed during surveys of the restoration ponds is used as an index of waterfowl breeding productivity and was calculated as described above.

Fall Waterfowl Surveys

Population Size and Species Composition

For Mono Lake data, waterfowl species totals were summed by survey area and survey period. Fall waterfowl totals from 2024 were compared to the long-term 2002 to 2023. The 2024 species total of the most abundant fall migrants were compared to their respective long-term means.

At Bridgeport and Crowley Reservoirs, long-term means were calculated for the 2003 to 2023 period. Fall waterfowl totals from 2024 were compared to the long-term 2002 or 2003 to 2023.

Spatial distribution

The spatial distribution of waterfowl at each of the surveys areas was evaluated by summing the total waterfowl found in each shoreline area over the six fall surveys. For Mono Lake, the 2023 distribution was compared to the long-term 2002 to 2022 trend of proportional distribution of waterfowl at Mono Lake (both offshore on the cross-lake transects and the shoreline areas). The distribution of Ruddy Ducks by survey and cross-lake transect is also presented for Mono Lake.

Waterfowl Population Survey Results

Mono Lake Summer Surveys: Waterfowl Community

In 2024, 1,680 waterfowl and thirteen waterfowl species were observed over the three summer shoreline surveys (Table 2), including six breeding and seven non-breeding species. Waterfowl numbers were highest on Survey 1 and lowest on Survey 2. Of the breeding species, Gadwall was most abundant, comprising 64% of waterfowl detections at Mono Lake in 2024.

In 2023, 585 waterfowl and eight waterfowl species were observed over the entire survey period including seven breeding and one non-breeding species. Of the breeding species, Gadwall was the most abundant and comprised 50% of the breeding waterfowl at Mono Lake (LADWP 2024).

Table 2. Summer Ground Count Waterfowl Detections in 2024.

Mono Lake breeding waterfowl species are in bold type.

	Survey 1	Survey 2	Survey 3	
Species	June 11-14	June 28-July 3	July 22-26	Total Detections in 2024
Greater White-fronted Goose	1			1
Canada Goose	59	57	4	120
Blue-winged Teal	4			4
Cinnamon Teal	16	17	35	68
Northern Shoveler	4			4
Gadwall	509	287	281	1077
Mallard	70	58	142	270
Northern Pintail	5	1	10	16
Green-winged Teal	18	33	43	94
Redhead			2	2
Long-tailed Duck			1	1
Unidentified Dabbling Duck	15		5	20
Common Merganser			1	1
Ruddy Duck	1		1	2
Total Detections per Survey	702	453	525	1680

Mono Lake Summer Surveys: Waterfowl Broods

A total of 100 unique waterfowl broods were found over the entire survey period in 2024, including 12 Canada Goose, 99 dabbling duck, and 1 diving duck broods (Tables 3, 4, and 5). The number of Canada Goose broods is likely an overestimate for the reasons stated above. Dabbling duck broods were found at all shoreline subareas, except Warm Springs. The number of broods was consistently higher at Wilson Creek, except for survey 2 when South Shores Lagoon had the highest number. Other subareas supporting a large proportion of the broods were DeChambeau Creek, Simons Spring, and Rush Creek. Brood numbers were highest for Gadwall with a total of 90 broods found over the entire survey period.

The number of dabbling duck broods produced at Mono Lake has ranged from a low of 26 in 2016 to a high of 74 in 2021 (LADWP 2024). In 2023, the number of broods was 69, which included 62 dabbling duck and 7 Canada Goose broods. As mentioned in last year's report, the total number of broods is mostly strongly correlated with the lake elevation in June. Specifically, increases in brood numbers have only been observed above a threshold of 6,382 feet (LADWP 2024). In June 2024, the lake elevation was 6,383.8 feet.

Table 3. Waterfowl Broods by Shoreline Area, Survey 1.

Includes broods from all age classes.

Breeding Waterfowl Species	Shoreline Areas									
	DECR	LVCR	MICR	RUCR	SASP	SOTU	SSLA	WASP	WICR	Total
Canada Goose	1	0	0	0	0	1	0	0	0	2
Gadwall	2	0	0	1	0	0	3	0	5	11
Mallard	0	0	0	0	0	0	0	0	1	1
Northern Pintail	0	0	0	0	0	0	0	0	0	0
Green-winged Teal	1	0	0	0	0	0	0	0	0	1
Common Merganser	0	0	0	0	0	0	0	0	0	0
Total Broods per Shoreline Area	4	0	0	1	0	1	3	0	6	15

Table 4. Waterfowl Broods by Shoreline Area, Survey 2.

Includes broods from age class I unless the species was seen for the first time in an area.

Breeding Waterfowl Species	Shoreline Areas									
	DECR	LVCR	MICR	RUCR	SASP	SOTU	SSLA	WASP	WICR	Total
Canada Goose	2	0	0	0	0	5	0	0	2	9
Gadwall	5	0	1	1	3	0	18	0	12	40
Mallard	0	0	0	0	1	0	0	0	0	1
Northern Pintail	0	0	0	0	1	0	0	0	0	1
Green-winged Teal	0	0	0	1	1	0	0	0	0	2
Common Merganser	0	0	0	0	0	0	0	0	0	0
Total Broods per Shoreline Area	7	0	1	2	6	5	18	0	14	53

Table 5. Waterfowl broods by Shoreline Area, Survey 3.

Includes broods from age class I unless the species was seen for the first time in an area.

Breeding Waterfowl Species	Shoreline Areas									
	DECR	LVCR	MICR	RUCR	SASP	SOTU	SSLA	WASP	WICR	Total
Canada Goose	0	0	0	0	0	1	0	0	0	1
Gadwall	6	1	0	5	5	2	8	0	12	39
Mallard	0	0	1	1	0	0	0	0	0	2
Northern Pintail	0	0	0	0	0	0	0	0	0	0
Green-winged Teal	0	0	0	0	0	0	0	0	1	1
Common Merganser	0	0	0	1	0	0	0	0	0	1
Total Broods per Shoreline Area	6	1	1	7	5	3	8	0	13	44

Restoration Ponds: Waterfowl Community and Waterfowl Broods

Four ponds were flooded all summer in 2024 (DEPO1, DEPO2, DEPO3 and DEPO4). COPOW, COPOE, and DEPO5 were dry all summer. The open-water habitat in DEPO1 has become reduced as emergent vegetation has expanded, and it has heavy algal growth. The other three DEPO ponds were full when surveyed beginning in mid-June and no significant changes in condition were observed through the summer.

Six species and 40 individuals were seen over the three summer surveys. Gadwall and Ruddy Ducks were the most abundant species (Table 6). Approximately 63% of the ducks were seen in DEPO4. Thirty percent of the ducks were in DEPO 2 and less than 8% were in DEPO3. No waterfowl were observed in DEPO1, DEPO5, COPOW, or COPOE.

Gadwall, Northern Pintail, and Ruddy Duck were the only species that bred at the Restoration Ponds in 2024, and Gadwall and Ruddy Ducks were the most abundant. (Table 6). A total of seven unique waterfowl broods were observed at the Restoration Ponds (Tables 7, 8, and 9) and only in DEPO4. One Canada Goose brood was observed in DEPO2 during the third survey; however, this brood was not included in the total as it was a class III brood that was able to fly and it may have been one of the broods seen at Mono Lake.

In 2023, six species and 55 individuals were observed over the entire survey period. Gadwall and Ruddy Duck were the two most abundant species. There were also eight waterfowl broods observed at the Restoration Ponds with one at DEPO3 and seven at DEPO4. Gadwall and Ruddy Duck were the only species that bred at the ponds, and Gadwall broods were the most abundant (LADWP 2024).

Table 6. Summer Ground Count Waterfowl Detections in 2024.

Restoration pond breeding waterfowl species are in bold type.

	Survey 1	Survey 2	Survey 3	Total Detections in 2024
Species	June 11	July 1	July 25	
Canada Goose			2	2
Cinnamon Teal		2		2
Gadwall	12	4	1	17
Mallard			1	1
Northern Pintail			1	1
Ruddy Duck	4	9	4	17
Total Detections per Survey	16	15	9	40

Table 7. Waterfowl Broods at the Restoration Ponds, Survey 1.

	Restoration Ponds							Total
Breeding Waterfowl Species	DEPO 1	DEPO 2	DEPO 3	DEPO 4	DEPO 5	COPOE	COPOW	
Canada Goose	0	0	0	0	DRY	DRY	DRY	0
Gadwall	0	0	0	1				1
Northern Pintail	0	0	0	0				0
Ruddy Duck	0	0	0	1				1
Total for Restoration Ponds	0	0	0	2	0	0	0	2

Table 8. Waterfowl Broods at the Restoration Ponds, Survey 2.

	Restoration Ponds							Total
Breeding Waterfowl Species	DEPO 1	DEPO 2	DEPO 3	DEPO 4	DEPO 5	COPOE	COPOW	
Canada Goose	0	0	0	0	DRY	DRY	DRY	0
Gadwall	0	0	0	3				3
Northern Pintail	0	0	0	0				0
Ruddy Duck	0	0	0	1				1
Total for Restoration Ponds	0	0	0	4	0	0	0	4

Table 9. Waterfowl Broods at the Restoration Ponds, Survey 3.

	Restoration Ponds							Total
Breeding Waterfowl Species	DEPO 1	DEPO 2	DEPO 3	DEPO 4	DEPO 5	COPOE	COPOW	
Canada Goose	0	1*	0	0	DRY	DRY	DRY	0
Gadwall	0	0	0	1*				0
Northern Pintail	0	0	0	1				1
Ruddy Duck	0	1*	0	1*				0
Total for Restoration Ponds	0	0	0	1	0	0	0	1

Fall Waterfowl Surveys Results

Mono Lake

Waterfowl Population Size and Species Composition

A total of 9 identifiable waterfowl species and 90,344 individuals were detected during the five 2024 Mono Lake fall surveys (Table 10). Northern Shoveler (64,819) were the most abundant species accounting for 71.7% of all waterfowl in 2024 (Table 10) and were five times greater than the long-term mean (Figure 6). Ruddy Duck (12,345) were the second most abundant species accounting for 13.6% of all waterfowl and were 36% greater than the long-term mean (Figure 7). The counts of both Northern Shovelers and Ruddy Ducks maybe inflated owing to the potential of duplicate counting as the birds were flushed upon the arrival of the survey boat and may have relocated to areas that had yet to be surveyed. Unidentified dabbling ducks made up the next greatest proportion of total waterfowl at 10%.

Table 10. Species Totals, 2024 Mono Lake Fall Waterfowl Surveys.

Species	9-Sep	23-Sep	7-Oct	21-Oct	18-Nov	Species Totals
Canada Goose		55	43	35		133
Cinnamon Teal	3		5			8
Common Loon				1		1
Clarks Grebe	3					3
Gadwall	337	347	982	114		1780
Green-winged Teal	60	5				65
Lesser Scaup	2					2
Mallard	199	1218	495	154		2066
Northern Pintail	2					2
Northern Shoveler	14653	14446	19107	10143	6470	64819
Redhead			10			10
Ruddy Duck	654	572	4277	4982	1860	12345
Unidentified Anas sp.	1498	2507	4654	243	200	9102
Western Grebe	1					1
Total	17412	19150	29575	15677	8530	90344

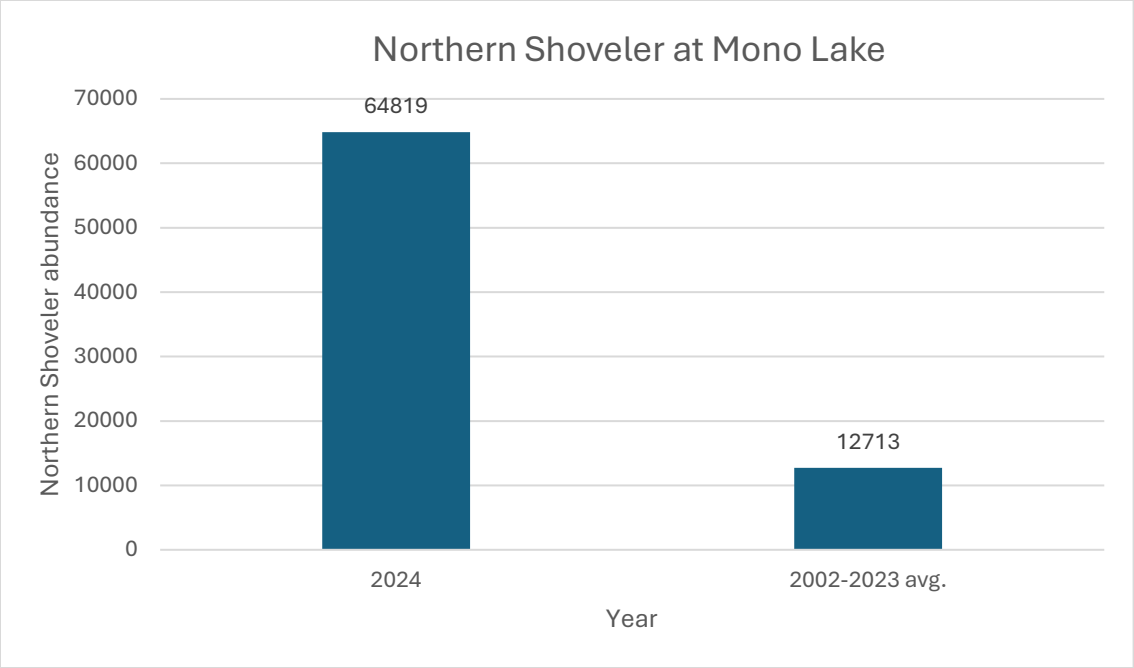

Figure 6. 2024 Northern Shoveler Total Compared to Long Term Mean (2002-2023).

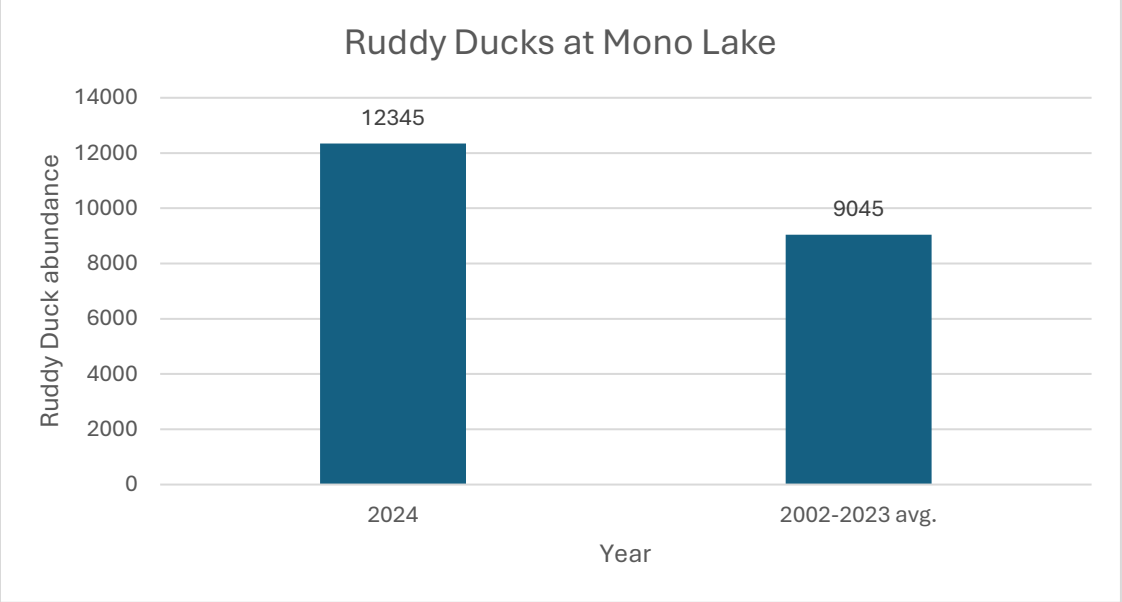

Figure 7. 2024 Ruddy Duck Total Versus Long-Term Mean.

Spatial Distribution

Since 2002, on average, approximately 78% of all fall waterfowl have been recorded on the shoreline surveys (onshore or <250 m from shore), and 23% in offshore areas along the cross-lake transect surveys. The single area of the lake that has supported significantly more waterfowl than any other has been Wilson Creek, accounting for 28% of all waterfowl in fall.

In 2024, large numbers of waterfowl were observed at Wilson Creek, Simons Springs, DeChambeau Creek and Rush Creek Delta (Figure 8) Wilson Creek is typically the main staging area in fall for Northern Shoveler, and frequently the only shoreline location where large numbers of this species are seen (typically several 1,000). Since Northern Shoveler are the dominant species at Mono Lake in fall, their frequent use of Wilson Creek results in this shoreline area supporting a large proportion of all waterfowl. In 2024, Wilson Creek had the greatest number of Northern Shoveler observed during the fall survey period (19,260) followed closely by Simons Springs (17,928).

In 2024, Ruddy Ducks were most numerous (3,027, Table 11) in area covered by cross-lake transect 7A (Figure 2). The West Shore shoreline segment area also had high numbers of Ruddy Ducks observed with 2,534.

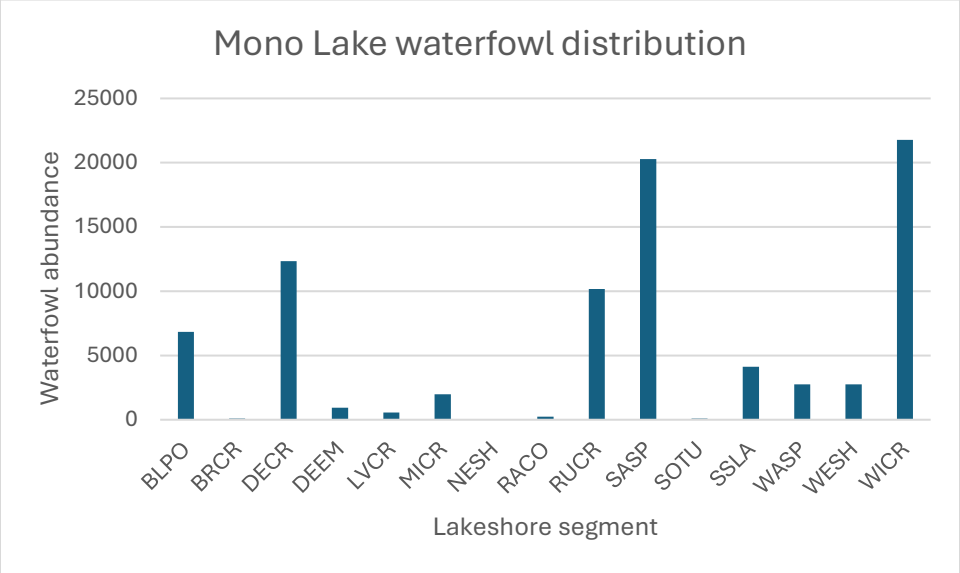

Figure 8. Fall Spatial Distribution of Waterfowl at Shoreline Segments of Mono Lake.

Table 11. Fall Spatial Distribution of Waterfowl at Shoreline Segments of Mono Lake.

Cross-lake subsection	Early Sept	Late Sept	Early Oct	Late Oct	Total
4B		2	58	51	**111**
5A	9	20	264	578	**871**
5B	0	0	47	181	**228**
6A	5	213	176	323	**717**
7A	6	197	1802	1022	**3027**
7B	1	10	96	15	**122**
7C	0	0	0	23	**23**
8A	0	16	79		**95**
8B	0	2	10	75	**87**
8C				63	**63**
Total Offshore	**21**	**460**	**2532**	**2331**	**5344**

Restoration Ponds

Pond conditions were the same in 2024 as in 2023 DEPO5, COPOW, and COPOE remained dry, and DEPO1 algae covered. A total of 24 waterfowl of eight species were seen over the six fall surveys (Table 12). As was the case in the summer, DEPO4 attracted the most waterfowl. The 2024 total of 24 waterfowl over the six surveys was significantly below the 2002-2023 mean of 163.

Table 12. Fall Waterfowl Totals by Pond, 2024.

Species	DEPO1	DEPO2	DEPO3	DEPO4	DEPO5	COPOW	COPOE	Species Total
Bufflehead				1	DRY	DRY	DRY	1
Eared Grebe				1				1
Green-winged Teal				2				2
Lesser Scaup		1						1
Mallard				3				3
Northern shoveler			2					2
Ring-necked Duck			1					1
Ruddy Duck		8		5				13
Pond Totals	0	9	3	12	0	0	0	24

Bridgeport Reservoir

Waterfowl Totals and Species Composition

A total of 12 waterfowl species were identified, and 13,494 individuals recorded at Bridgeport Reservoir over the six fall surveys in 2024 (Table 13). The total number of waterfowl observed in 2024 was 54% lower than the long-term mean of 29,517. Geese and swans comprised approximately 9% of all waterfowl, and of this group, only Canada Goose was seen. Gadwall and Green Winged Teal were the most abundant dabbling ducks, although a large proportion of waterfowl were unidentified due to the long viewing distance.

Table 13. Species Totals, 2024 Bridgeport Reservoir Fall Waterfowl Surveys.

Species	Early Sept	Mid-Sept	Early Oct	Late Oct	Mid-Nov	Species Total
American Widgeon			9			9
Bufflehead					5	5
Canada Goose	145	128	235	465	287	1260
Common Merganser		36	14	11	10	71
Gadwall	992	840	367	23	45	2267
Green-winged Teal	79	23		827	297	1226
Mallard	466	97	83	39	103	788
Northern Pintail	2	8	8	29		47
Northern Shoveler	460	390	365		86	1301
Redhead		2	20			22
Ruddy Duck	161	74	3	81	9	328
Unidentified Anas Sp.	4180	1065	780	120	25	6170
Total	6485	2663	1884	1595	867	13494

Spatial distribution

Of the three subareas at Bridgeport Reservoir, waterfowl numbers were highest in the West Bay throughout the season (Table 14). Waterfowl were found throughout the West Bay, particularly among the deltas and inlets of Buckeye Creek and Robinson Creek. Geese were most often found out on the irrigated pastures and meadows south of the reservoir, away from the water's edge. Waterfowl use in the East Shore subarea occurred primarily in the southern half of this segment area, in proximity to inflow from the East Walker River, where shallow water feeding areas and mudflats occur. In the North Arm, waterfowl were few and scattered along the immediate shoreline area.

Table 14. Bridgeport Reservoir, Spatial Distribution by Survey, 2024.

Survey	EASH	NOAR	WEBA	Total
Early Sept	1786	50	4649	6485
Late Sept	739	35	1889	2663
Mid-Oct	854	18	1012	1884
Late Oct	972	81	542	1595
Mid-Nov	497	1	369	867
Total waterfowl	**4,848**	**185**	**8,461**	**13,494**

Crowley Reservoir

Waterfowl Totals and Species Composition

At Crowley Reservoir a total of 16 waterfowl species were identified, and 44,187 individuals were recorded during the fall surveys in 2024 (Table 15). The total number of waterfowl observed at Crowley Reservoir in 2024 was 10% lower than the long-term mean of 49,384. Northern Shoveler, Mallard, Green Winged Teal, and Gadwall were the most abundant dabbling ducks observed making up 67% of all waterfowl. Ruddy Duck was the most abundant diving duck observed with 7,599 individuals observed.

Table 15. Species totals, 2024 Crowley Reservoir Fall Waterfowl Surveys.

Species	Early Sept	Mid-Sept	Early Oct	Late Oct	Mid-Nov	Species Total
American Widgeon				6	9	15
Bufflehead	13	637	70	138	194	1052
Blue-winged Teal	2		11		22	35
Canada Goose	115	349	22	4	58	548
Cinnamon teal	387		54		13	454
Common Merganser		251		6	5	262
Gadwall	3032	677	310	122	61	4202
Green-winged Teal	1345	1100	623	1169	906	5143
Lesser Scaup				16	58	74
Mallard	2819	2803	1637	2054	613	9926
Northern Pintail	171	400	604	698	54	1927
Northern Shoveler	1258	7452	1273	280	228	10491
Redhead	85	17			130	232
Ring-necked Duck	15		55		14	84
Ruddy Duck	419	1630	2466	2212	872	7599
Tundra Swan					31	31
Unidentified dabbling duck.	1711	150	130		121	2112
Total	11,419	15,466	7,255	6,705	3,389	44,234

Spatial Distribution

During the 2024 surveys, the largest waterfowl concentrations at Crowley Reservoir were in the McGee Bay and Upper Owens River delta area; where 46% of all waterfowl were tallied in each area, totaling 92% of all waterfowl observations (Table 16). Waterfowl in McGee Bay used the entire shoreline area, although higher densities were observed in the area of the shoreline where open cattail marsh existed due to flooding of the shoreline marsh system from the extremely high-water level of the reservoir. The other area of waterfowl concentration was the Upper Owens River delta where flows from the Owens River enter the reservoir.

Table 16. Crowley Reservoir, spatial distribution by survey, 2024.

Survey	CHCL	HIBA	LASP	MCBA	NOLA	SAPO	UPOW	Total
Early Sept	1	419	133	5402	58	51	5355	11419
Late Sept	8	171	142	7700	74	218	7153	15466
Early Oct	6	139	79	3006	152	66	3807	7255
Late Oct	2	398	169	2462	82	6	3586	6705
Mid-Nov	164	445	216	1767	86	159	552	3389
Total	**181**	**1,572**	**739**	**20,337**	**452**	**500**	**20,453**	**44,234**

Aerial Photography of Waterfowl Habitats

Representative photos from each shoreline subarea from Mono Lake, Bridgeport Reservoir, and Crowley Reservoir are compiled in this report. For Mono Lake shoreline subareas, where appropriate, photos from the summer and fall were included. Please refer to Figure 2 for the location of each of the following shoreline subareas at Mono Lake. The descriptions of each shoreline subarea are primarily based on those provided in the 2023 Mono Basin Waterfowl Habitat Restoration Program 2023 Monitoring Report (LADWP 2023).

Mono Lake Shoreline Subareas

Black Point (BLPO)

The Black Point (BLPO) shoreline subarea lies at the base of a volcanic hill on the northwest shore of Mono Lake. The shoreline in this subarea is composed of loose volcanic soils. At lower lake elevations, barren shoreline and alkali meadow predominate. In the western portion of BLPO, dry alkali meadow exists as a linear strip paralleling the shoreline. In the eastern portion of the shoreline subarea are unmapped springs and seepage that support small shallow brackish bays and wet alkali meadow at higher lake levels. Based on past reviews of annual photos, brackish ponds become

more numerous in the BLPO subarea at lake elevations above 6,382 feet, but relatively absent at lake elevations below this level. In 2023, at a lake level of 6383.2 feet, numerous small ponds were present along the Black Point shoreline subarea as shown in the top photo (Figure 9). For reference, the elevation of Mono Lake on July 1 and November 1, 2024 was 6,384.1 and 6,383.1 feet, respectively. The bottom photo (Figure 9) shows the conditions in fall 2024. Figure 10 also compares conditions at BLPO in 2023 and 2024. Figure 10 also compares conditions at BLPO in 2023 and 2024.

Figure 9. Black Point Shoreline Subarea, Western Half (Top Photo: September 18, 2023; Bottom Photo: November 12, 2024).

Figure 10. Black Point Shoreline Subarea, Eastern Half (Top Photo: September 18, 2023; Bottom Photo: November 12, 2024).

Bridgeport Creek (BRCR)

This shoreline subarea is at the terminus of the Bridgeport Creek (BRCR) drainage, however there is typically no surface flow of water in the creek near the lakeshore. There are several springs in this subarea, most of which are slightly brackish and support small brackish ponds. The other wetland resources in the BRCR shoreline subarea include alkaline wet meadow and small amounts of wet meadow and marsh. Waterbird use is often most concentrated at the western end of this subarea, where spring flow has consistently reached the shoreline at all elevations observed. At higher lake elevations, brackish ponds develop along much of the length of this shoreline subarea. With decreasing lake elevations, barren lakebed increases substantially without a subsequent expansion of vegetation, and brackish ponds disappear. Figure 11 (top photo) shows an overview photo of the BRCR drainage and the presence of water near shore in fall. The bottom photo in Figure 11 shows the same area in 2024 during the fall. Figure 12 shows a comparison between 2023 and 2024 conditions at the ”Seeping Springs” area.

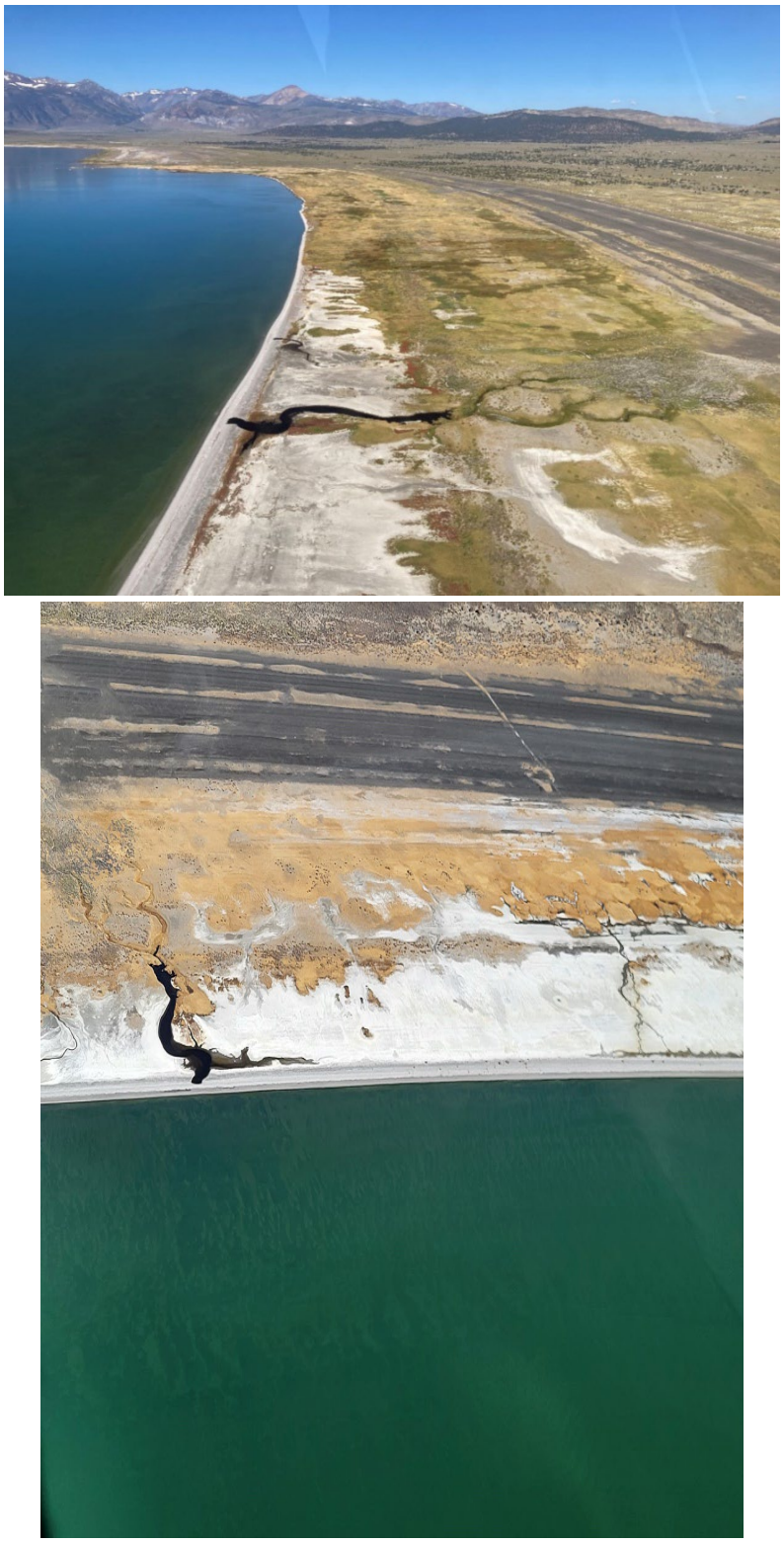

Figure 11. Bridgeport Creek Shoreline Subarea, Eastern Portion (Top Photo: September 18, 2023; Bottom Photo: November 12, 2024).

Figure 12. Bridgeport Creek Shoreline Subarea, Western Portion (Top Photo: September 18, 2023; Bottom Photo: November 12, 2024).

DeChambeau Creek (DECR)

The DeChambeau Creek (DECR) shoreline subarea is along the northwest shore of Mono Lake. Flow in DECR proper is intermittent and does not consistently reach the lakeshore. The DECR shoreline subarea has abundant year-round freshwater resources due to the presence of numerous springs that discharge directly to the lake.

The freshwater springs at DECR support lush wet meadow and riparian scrub habitats. During periods of declining lake level, freshwater mudflats develop due to the extensive spring flow. Wet meadow vegetation will encroach onto exposed mudflats in this area of the shoreline due to the abundance of freshwater spring flow. Increases in barren playa with declining lake elevation have been much less apparent in the DECR subarea as compared to other shoreline subareas due to the slope of the shoreline and the expansion of vegetation onto the mudflats that occurs. However, downcutting of the spring channels and subsequent drying of the shore has occurred at the lowest lake levels observed. During periods of subsequent increasing lake elevations, this wet meadow vegetation, mudflats, and playa has become inundated, leaving little exposed shoreline.

In 2023, due to the extreme runoff year, DeChambeau Creek flowed to the shore of Mono Lake throughout summer and fall. The rise in lake level throughout the spring and summer of 2023 resulted in inundation of shoreline vegetation and very little exposed mudflats.. In 2024, the conditions were similar with the lake elevation starting at 6,383.8 feet on June 1 and rising to 6,384.1 feet by July 1 (Figure 13). The lake level remained unchanged by August 1.

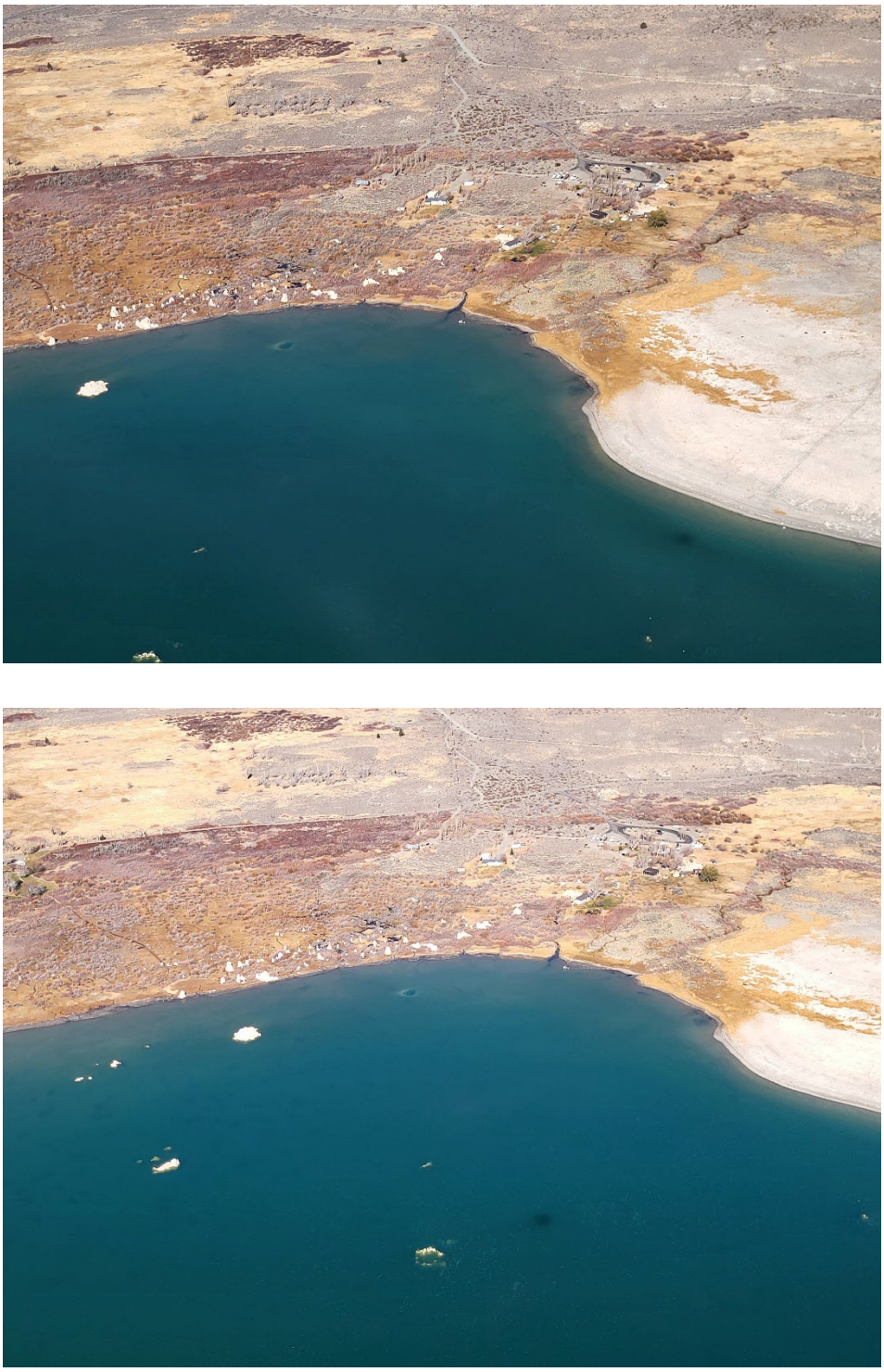

Figure 13. The DeChambeau Creek Subarea (Top Photo: November 12, 2024; Bottom Photo: November 12, 2024).

DeChambeau Embayment (DEEM)

The DeChambeau Embayment (DEEM) subarea lies just east of the DeChambeau Ranch, and the DeChambeau and County restoration ponds. Historically, Wilson Creek discharged to the lake in the DEEM subarea, although there was extensive upstream diversion for irrigation of the DeChambeau Ranch. Past diversions altered the discharge point of Wilson Creek to almost 5 miles west along the shoreline, on the west side of Black Point and at the current “Wilson Creek” shoreline subarea.

The wetland resources in DEEM include alkaline wet meadow, small amounts of marsh, and several small brackish ponds. There are fresh, slightly brackish and moderately brackish springs in this area, the largest of which is Perseverance Spring. Perseverance Spring has discharged directly to the lake at all elevations observed.

The bathymetry of the shoreline and offshore area here is more complex than other subareas. Very shallow sloping topography exists nearshore in the southern portion of the subarea, with a deeper bay just offshore. Pumice blocks litter the entire subarea and are most often visible in the southern portion of this area due to the topography and shallow nearshore waters. At the higher lake elevations observed, the pumice blocks become partially to completely submerged and the shallow nearshore areas expand. As the lake level drops, this shoreline subarea experiences rapid increases in the acreage of barren lakebed and a land bridge forms with Gaines Island. At more extreme low lake levels, such as those observed in 2016, the geographic extent of the pumice blocks in the eastern portion of the subarea are revealed (LADWP 2018). Figure 14 compares the conditions observed in 2023 (top photo) and 2024 (bottom photo). Figure 15 shows an overview of the DEEM subarea.

Figure 14. DeChambeau Embayment (Top Photo: September 18, 2023; Bottom Photo: November 12, 2024).

Figure 15. Overview of the DeChambeau Embayment Subarea (November 12, 2024).

Lee Vining Creek (LVCR)

Lee Vining Creek (LVCR) is the second largest stream in the Mono Basin. LVCR is a woody riparian system that supplies abundant freshwater to its delta year-round. The lower reaches of LVCR and its delta support small patches of wet meadow vegetation along with riparian trees and shrubs. The creek remains confined to the main channel under low flow conditions but inundates the lower floodplain under high flow conditions. Discharge to the lake is “split” by a berm nearshore, and most of the creek flow discharges on the south side of this berm. The north part typically receives a low flow that supports freshwater ponds at some lake levels. At higher lake levels, the delta becomes flooded with lake water, inundating the willows and wet meadow close to shore, resulting in some dieback of willows and freshwater emergent vegetation due to salt water stress. During periods of descending lake elevations, freshwater ponds may form behind littoral bars. At the most recent extreme low lake elevation observed in 2016, extensive drying of the delta meadows occurred. Ria extends offshore beyond the mapping boundary of Lee Vining Creek subarea due to flows from Lee Vining Creek, however this waterfowl resource is not captured by landtype mapping (LADWP 2018).

Bathymetry of the area indicates limited shallow water areas near shore. Shallow sloping areas of water are limited to the delta and areas around the Lee Vining tufa grove to the south, but depths rapidly increase offshore in this area of the lake (LADWP, 2018).

In mid-June, during the first summer survey, the lake level was high and there was no shoreline to navigate past the main channel located on the left side of the photos (Figure 16). At this time, the coyote willow (*Salix exigua*) located along the shoreline was still green. However, by the second summer survey in late-July, the coyote willow had turned brown. By late-July, it was possible to cross the creek and along the shoreline to survey the subarea farther south.

Figure 16. Lee Vining Creek Delta (Top Photo: July 29, 2024; Bottom Photo: November 12, 2024).

Mill Creek (MICR)

Figure 17 shows a comparison of Mill Creek (MICR) in summer (top photo) and fall (bottom photo). MICR is Mono Lake's third largest stream and originates in Lundy Canyon. The Lundy Powerhouse along MICR is operated by Southern California Edison and historically diverted most of the flow off MICR and impacting the lower reaches of MICR. LADWP does not export any water from the MICR system but does hold some water rights.

Much of the MICR riparian system is tree-dominated, but the delta has dense stands of shrub willow, small amounts of wet meadow, and a series of beaver ponds. Freshwater often enters the lake at several points in the delta due to seepage through the loose volcanic soils. Previous bathymetry studies have indicated the creek mouth constitutes the only shallow areas in the MICR delta subarea, and water depths increase rapidly offshore.

During the peak runoff in 2023, debris washed down from upstream blocked the culvert along Mill Creek at Cemetery Road, redirecting most of the creek flow into a former channel to the west (Figure 18, top photo). Figure 18 (bottom photo) shows the debris following the 2023 runoff. Ponds formed along the shoreline at this location and provided some habitat for waterfowl. In other recent high runoff years (i.e. 2017), some water has reached this former channel, but this is the first time since 2002 that it captured most of the flow. The high flow in this former channel resulted in significant downcutting due to a lack of riparian vegetation to stabilize the channel, and a large amount of sediment and some dislodged shrubs flowing into Mono Lake through the summer months until repairs were made to the culvert and road.

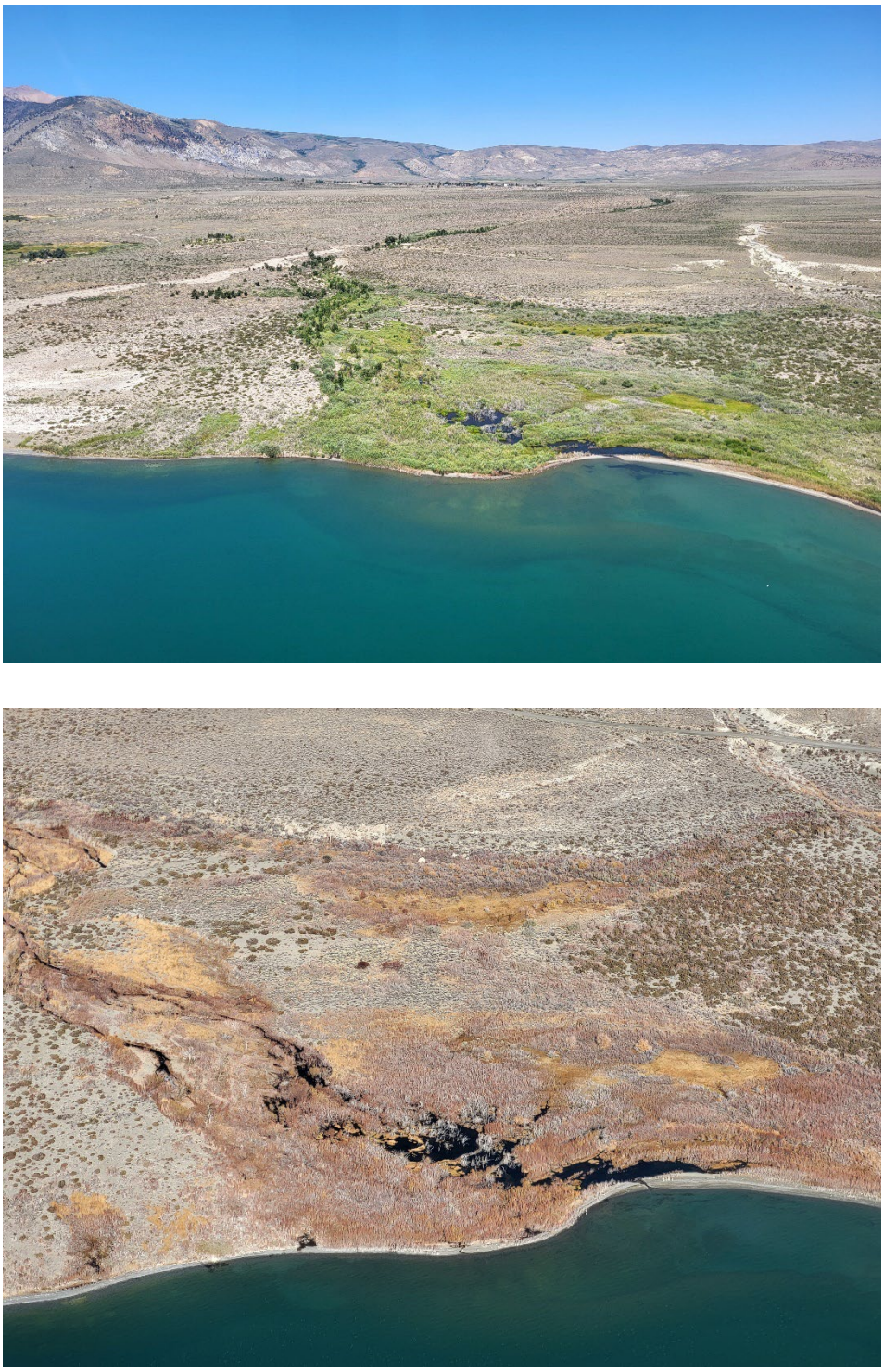

Figure 17. Mill Creek Delta, From the East (Top Photo: July 29, 2024; Bottom Photo: November 12, 2024).

Figure 18. Mid-Summer Flow in a Historic Mill Creek Channel in 2023 Compared to Conditions in 2024 (Top Photo: September 18, 2023; Bottom Photo: July 29, 2024).

Northeast Shore (NESH)

In the Northeast Shore (NESH) subarea, extensive areas of barren playa predominate at most lake elevations as the saline groundwater in this part of the basin prevents the growth of vegetation. Barren playa comprises 99% of the NESH subarea, and only small amounts of alkali meadow are present.

Historically, large perennial brackish ponds were present along the NESH subarea. These historic ponds persisted in depressional areas above the high-water mark and above the target lake level set for Mono Lake. Since 2002, temporary ponds have developed along the length of the shoreline segment, but downslope of the historic ponds. These ephemeral ponds are presumed to be brackish due to the saline nature of the groundwater in the eastern basin. Although there are no known mapped springs in this reach, some are evident (D. House, pers. obs.). Bathymetry studies indicates a very gradual sloped shoreline in this subarea. Figure 19 is an overview of NESH in 2023, including narrow brackish ponds were present along a portion of the shoreline area. Figure 20 is a closeup of some of the ponds that formed along the shoreline in 2024.

Figure 19. Northeast Shore, Looking East (September 18, 2023).

Figure 20. Northeast Shore, Closeup of Ponds Along the Shoreline (November 12, 2024).

Ranch Cove (RACO)

The Ranch Cove (RACO) shoreline area is a relatively small area located between Rush Creek and Lee Vining Creek. The shoreline area is narrow and generally dry, supporting primarily coyote willow, rabbitbrush, upland scrub, and barren playa. The bathymetry data shows a steeply sloped shoreline offshore. This shoreline area has not shown significant changes with lake elevation. Waterfowl resources are limited in this area, and there is no direct spring flow to the lake. Figure 21 shows a general overview of the RACO shoreline area.

Figure 21. Overview of Ranch Cove Shoreline Area, Looking West (July 29, 2024).

Rush Creek (RUCR)

Rush Creek (RUCR) is the largest stream in the Mono Basin. There is a long history dating back to the 1860s of diversion of RUCR flows for irrigation, followed by out of basin water export by LADWP starting in 1941 and resulting in a dry channel in the lower reaches of the creek in some years. Notable large runoff events occurring in 1967, 1969, and the early 1980s, caused substantial incision and scouring due to an absence of riparian vegetation to protect the banks and stabilize the soils. Floodplain incision then drained the shallow groundwater table and left former side channels stranded above the newly incised mainstem channel (SWRCB 1994). Under Decision 1631, LADWP developed a stream restoration plan and has undertaken projects to rehabilitate RUCR (LADWP 1996b). Channel maintenance and flushing flows, referred to as “stream restoration flows” were established to mimic seasonal snowmelt runoff, with the magnitude based on the hydrological conditions for the year (SWRCB 1994).

The wetland resources available at RUCR are primarily meadow and woody riparian vegetation (*Salix* sp.) and the creek supplies abundant freshwater outflow to Mono Lake year-round. Immediately upstream of the delta, the floodplain is a broad meadow supporting scattered shrub willows. At higher lake levels or high creek flows, flooding has extended across the delta mouth. During periods of lake elevation recession, much channel braiding exists in the delta. From 2002 through 2014, side channels distributed water throughout the lower floodplain meadow, creating saturated conditions, freshwater channels, and a stable freshwater pond along the eastern edge. In 2014, headcutting occurred along the mainstem resulting in channel erosion, and side channel abandonment. By the following summer of 2015, pond and channels formerly used by breeding waterfowl in the delta area disappeared as the lower floodplain experienced significant drying.

In 2023, runoff into RUCR was very high all summer and continued to be elevated above the average base flows into fall. The high flows deposited sediments in the delta, dislodged trees and shrubs in the channel, and flooded the delta creating a large freshwater pond. In 2024, the freshwater ponds in the delta received inflow from the mainstem all summer and were present into fall as well (Figure 22).

Figure 22. Rush Creek Delta (Top Photo: July 29, 2024; Bottom Photo: November 12, 2024).

Simons Spring (SASP)

The Simons Spring (SASP) shoreline subarea is in along the southeastern portion of the lakeshore. Located centrally in the subarea is the SASP fault line, a conspicuous feature on the landscape. Several large springs arise from the fault, conducting groundwater to the surface (Rogers *et al.* 1992). The bathymetry map of this area indicates a gradual offshore slope in the western half of the subarea, a steep offshore slope where the tufa towers of the fault line reach shore, and an increasing shallow slope to the east (LADWP 2018). Due to the shoreline gradient in this area, small changes in lake elevation result in large changes in the degree of shoreline flooding or the extent of exposed mudflats or playa.

The combination of high spring flow, shallow shoreline gradient, and the action of longshore currents, makes the SASP shoreline subarea particularly dynamic, particularly west of SASP fault line. Fresh water ponds are a prominent feature of the SASP subarea due to the abundant spring flow in the area, however their presence and condition tends to be ephemeral, especially west of SASP fault. Over the years, longshore currents have resulted in the development of several parallel littoral bars west of the SASP fault line. These littoral bars retain upgradient spring flow and support the creation of ponds, wet meadow, and marsh behind the sandbars. During periods of increasing lake level, lake water inundates areas supporting wetland vegetation upgradient of littoral bars. The vegetation dies back due to salt stress, opening up areas previously grown over with marsh or meadow. During subsequent decreases in lake level, open freshwater ponds develop, supported by inflow from up gradient springs. If the lake level stabilizes, then wetland vegetation will recolonize the open water ponds, decreasing the amount of open water. Many of the freshwater springs in this area reach the lakeshore through breaks in littoral bars, creating extensive mudflats on exposed playa at certain lake levels. Although there may be a physical connection between the mudflats and lake water, the very shallow ponds that form on shore are typically fresh due to the high spring flow and are colonized within 1 to 2 years by wetland vegetation.

Just east of the SASP fault line, permanent to semi-permanent brackish water ponds are generally present year-round. The remainder of the subarea to the east lacks spring flow to the lake and supports alkali wet meadow up gradient and barren playa on shore.

In 2024, the high lake level inundated a section of SASP and, as a result, the survey route was split into two sections (Figure 23). Ponds located at the west end of SASP by Goose Springs (Figure 24) and to the east by Abalos Springs (Figure 25) and a East Samman’s Spring (Figure 26) provided habitat for broods, which were observed during the second and third surveys.

Figure 23. The High Lake Level Inundated a Section of the Shoreline in SASP (July 29, 2024).

Figure 24. Large Pond Located on the Western End of SASP to the East of Goose Springs in Southern Shore Lagoons Area (July 29, 2024).

Figure 25. From Abalos Spring (Left Side of Photo) to the West, a Small Section of Shoreline Remained that Allowed Surveyors to Look for Waterfowl to the West (July 29, 2024).

Figure 26. Ponds to the East in SASP Located Near a Large Tufa Mound by East Samman's Spring (July 29, 2024).

South Shore Lagoons (SSLA)

The South Shore Lagoons (SSLA) is a broad stretch of shoreline with scattered waterfowl habitat features. Waterfowl habitat features include permanent freshwater ponds supported by springs, seasonal to semi-permanent ponds supported by groundwater, and ephemeral brackish ponds. Like Simons Spring, the shoreline configuration in the SSLA subarea is influenced by longshore currents.

At the western border of the subarea, a semi-permanent pond exists along a southwest-northeast trending fault line (Figure 27). The presence of this semi-permanent pond has been a function of lake elevation. At the higher lake elevations observed (approximately 6,383 feet), the pond has been full. Below approximately 6282.5 feet, the pond experiences notable contraction in size and, at elevations below 6,381.9 feet, has been absent.

Sandflat Spring is an isolated freshwater spring supporting two small freshwater ponds- an upper pond, and a lower pond, both partly surrounded by coyote willow (Figure 28). These were open water ponds until 2014, when water speedwell (*Veronica anagallis-aquatica*) and cattails (*Typha* sp.) encroached and enclosed the open water.

At the east end of the subarea is the Goose Springs complex (Figure 29). Goose Springs is a large spring complex that forms a series of interconnected freshwater ponds surrounded by wet meadow and marsh. In some years, the development of a littoral bar downgradient has captured spring flow, creating large onshore ponds that can be either fresh or brackish.

Away from the immediate shoreline in this subarea, the terrain is sandy hummocks with numerous small, depressions supporting alkali meadow in most years. Groundwater levels in this area have been found to be responsive to lake elevation changes (Rodgers *et al.* 1992) due to the high topographic gradient and very permeable soils. In 2006 and 2007 when the lake elevation was at its highest observed (above 6,385 feet), these nearshore depressions filled with groundwater, creating a series of scattered freshwater ponds in the SSLA subarea that were quite attractive to waterfowl.

Figure 29 is a comparison of habitat at the Goose Springs area in 2023 and 2024. In 2024, there was a large pond protected by the shoreline. In 2024, to the east, a large pond replaced the channel in this area that was visible in 2023. Figure 30 shows how the habitat at Goose Springs changed between July and November. Both ponds experienced a noticeable contraction between summer and fall. During the third summer survey, 150 to 160 ducks, over half which were likely age class II broods, were observed swimming from the Goose Springs area.

Figure 27. Semipermanent Pond at Western Edge of South Shore Lagoons (Top photo: July 29, 2024; Bottom Photo: November 12, 2024).

Figure 28. Sand Flat Spring (Top Photo: July 29, 2024; Bottom Photo: November 12, 2024).

Figure 29. Goose Springs (Top Photo: September 18, 2023; Bottom Photo: July 27, 2024).

Figure 30. Goose Springs (Top photo: July 27, 2024; Bottom Photo: November 12, 2024).

South Tufa (SOTU)

The South Tufa (SOTU) subarea is the primary visitor access point to the Mono Lake shoreline, notable for its large display of tufa towers. In the western portion, the shoreline is narrow, the offshore topography steep, and the brackish springs create wet mudflat conditions under most lake levels observed (Figure 31). The eastern portion supported a large pond that was used by a few broods throughout the summer (Figure 32). Water was still present in this pond in the fall.

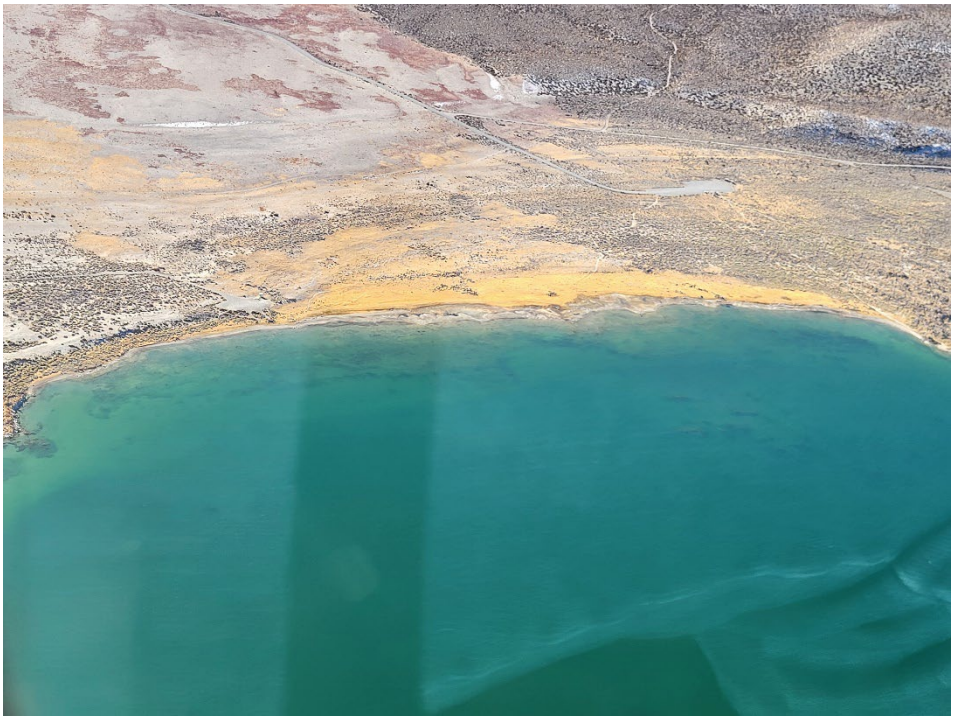

Figure 31. South Tufa, Western Extent (July 29, 2024).

Figure 32. South Tufa, Eastern Extent with the Parking Area Roughly in the Middle of Both Photos (Top photo: July 27, 2024; Bottom Photo: November 12, 2024).

Warm Springs (WASP)

The Warm Springs (WASP) subarea is located on the eastern shore of Mono Lake. The main feature of the WASP subarea is a permanent brackish pond fed by the outflow of Pebble and Twin Warm Springs (referred to as “north pond”). These and other springs in the area support extensive wet alkali meadow and marsh vegetation, primarily around the pond and springheads. The springs in the WASP subarea are slightly to moderately brackish.

The north pond has been present at all lake elevations observed. Some expansion and contraction have occurred, with the pond at its largest extent in 2006. This pond has been the most reliable place in the WASP subarea to find waterfowl (Figure 33). To the south of north pond, there was a large pond that had waterfowl present during the summer surveys (Figure 34).

Due to the very gradual sloping shoreline in this area, small changes in lake elevation result in large differences in the amount of exposed playa on shore. Longshore action also shapes this shoreline area as evidenced by the prominent littoral bars creating the north pond and ponds downgradient. During periods of declining lake elevation, seepage of water from the north pond through the loose sandy soil results in the development of ephemeral brackish ponds downgradient of the north pond as was noted in 2010 (LADWP 2018).

Feral horse activity at Mono Lake continues to be high in the WASP subarea. WASP was severely grazed again this year, and virtually all wetland vegetation along spring channels and ponds had been consumed. The meadows were grazed down to almost zero stubble, and bare patches of compacted soil were present in areas formerly supporting wetland vegetation.

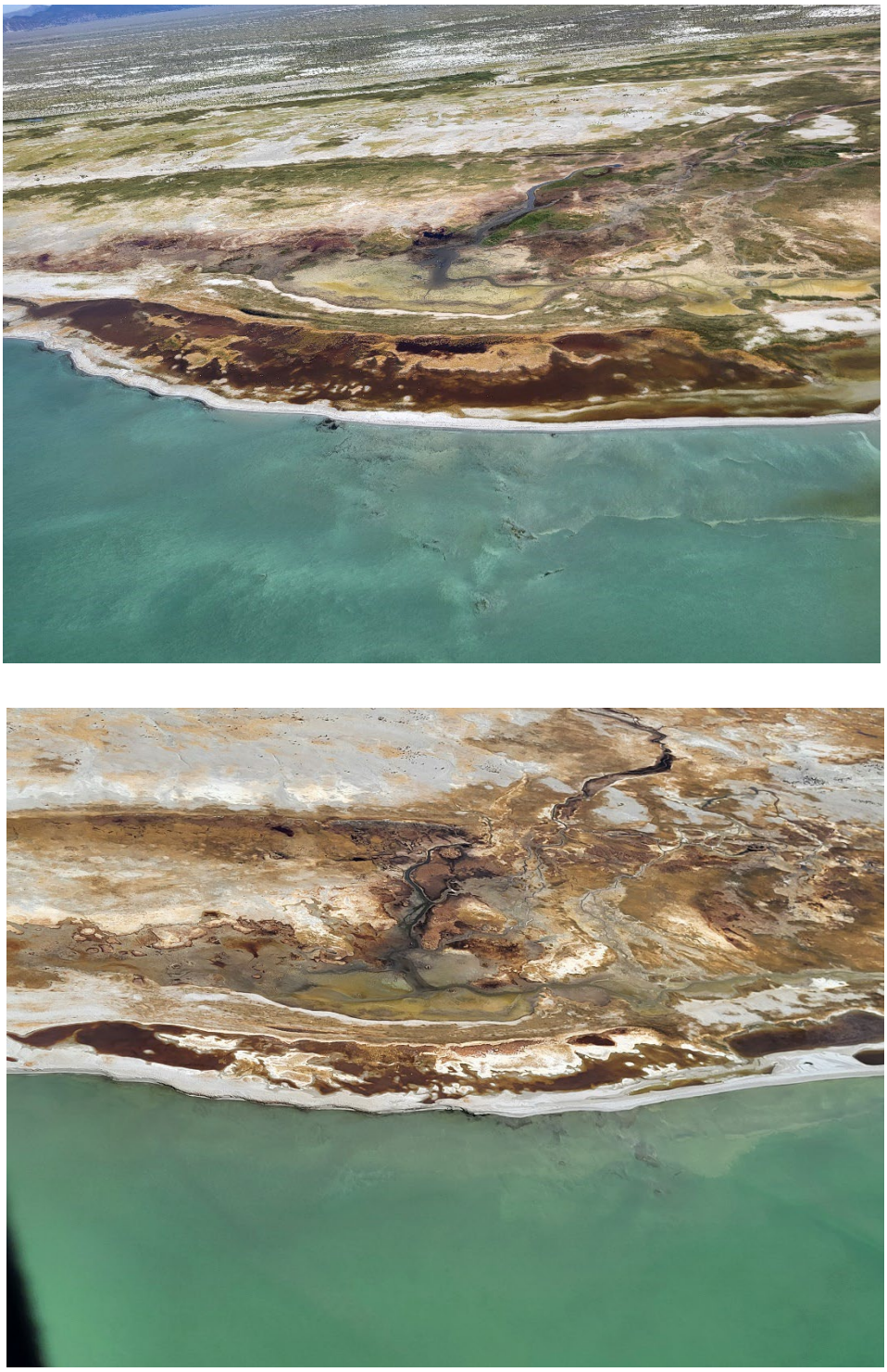

Figure 33. North Pond at Warm Springs (Top Photo: July 27, 2024; Bottom Photo: November 12, 2024).

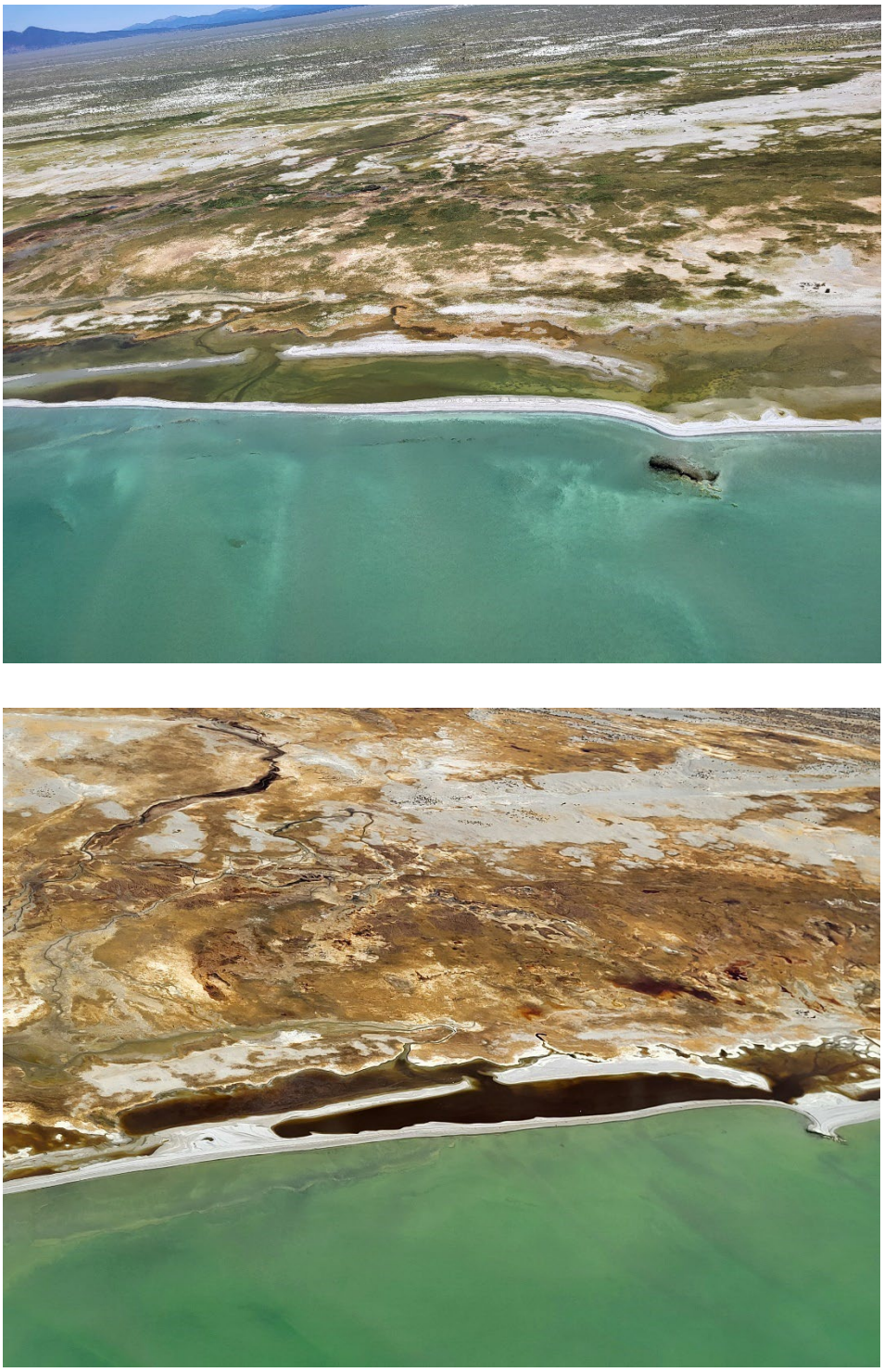

Figure 34. Warm Springs, South of the North Pond (Top photo: July 27, 2024; Bottom photo: November 12, 2024).

West Shore (WESH)

Much of the West Shore (WESH) subarea is located immediately east of Highway 395, along a steep fault scarp. Although some shallow gradient areas exist along the southern boundary, most of this shoreline area is steeply sloping lakeward. Several fractured rock gravity springs (LADWP 1987) and two small drainages, Log Cabin Creek and Andy Thom Creek provide freshwater resources along the length of this shoreline subarea, although ponds are lacking. A very narrow beach exists along much of the length and becomes inundated at higher lake elevations. Significant changes have not been noted in the configuration of this shoreline subarea with lake elevation changes. The area supports lush wetland resources, but waterfowl use is limited (Figures 35 and 36).

Figure 35. West Shore, Looking West (November 12, 2024).

Figure 36. West Shore, looking west (November 12, 2024).

Wilson Creek (WICR)

Wilson Creek (WICR), along the northwest shore, is one of the best and most important waterfowl habitat areas at Mono Lake. WICR supports a large expanse of wet meadow, multiple freshwater springs, and mudflats. The WICR subarea has the second highest median spring flow of the monitored springs (LADWP 2018). Due to the shoreline configuration and presence of large tufa towers, this subarea also has two protected bays. Submerged pumice blocks are present throughout the shallows of the eastern portion of the subarea. The bathymetry indicates a very gentle sloping topography throughout the protected bays and all along the shoreline (LADWP 2018). Due to the sheltered nature of the bay, the spring flow, and shallow waters near shore, the hypopycnal layer may be extensive in this area. The spring flow and shallow waters also lend toward the formation of mudflats, which have been present at most lake elevations observed. At the lowest elevation observed (2016), the retreat of shoreline resulted in some loss of the protection of the bays, however, mudflats were still prominent due to the high spring flow. The extreme low lake elevation observed in 2016 allowed an opportunity to visualize the near shore topography and the significance of spring flow to WICR bay (LADWP, 2018). The topography is very gently sloping throughout the entire bay, extending out beyond the mouth of the bay and east of Tufa Mound spring. The high spring flow in this area combined with the sheltered nature of the bay is conducive to creating hypopycnal conditions. Even at higher lake elevations, such as in 2012, hypopycnal conditions would likely occur across the bay except under windy conditions, due to the high spring flow and contribution from Wilson Creek to the west in 2012. The shallow, protected areas in the bay would make food more accessible to waterfowl. The high spring flow conditions combined with the sheltering of the bay and shallow waters support ideal feeding and loafing conditions for waterfowl at Mono Lake.

In 2024, the pond seen in 2023 became inundated (Figure 37). Figure 38 shows the changing conditions of the bay between July and November. Between summer and fall, the berm around the pond in WICR bay became more prominent. In 2024, several broods were observed throughout the bay and to the east of Tufa Mound Spring (Figure 39).

Figure 37. Freshwater Pond in Wilson Creek Bay (Top Photo: September 18, 2023; Bottom Photo: July 27, 2024).

Figure 38. Freshwater Pond in Wilson Creek Bay (Top Photo: July 27, 2024; Bottom Photo: November 12, 2024).

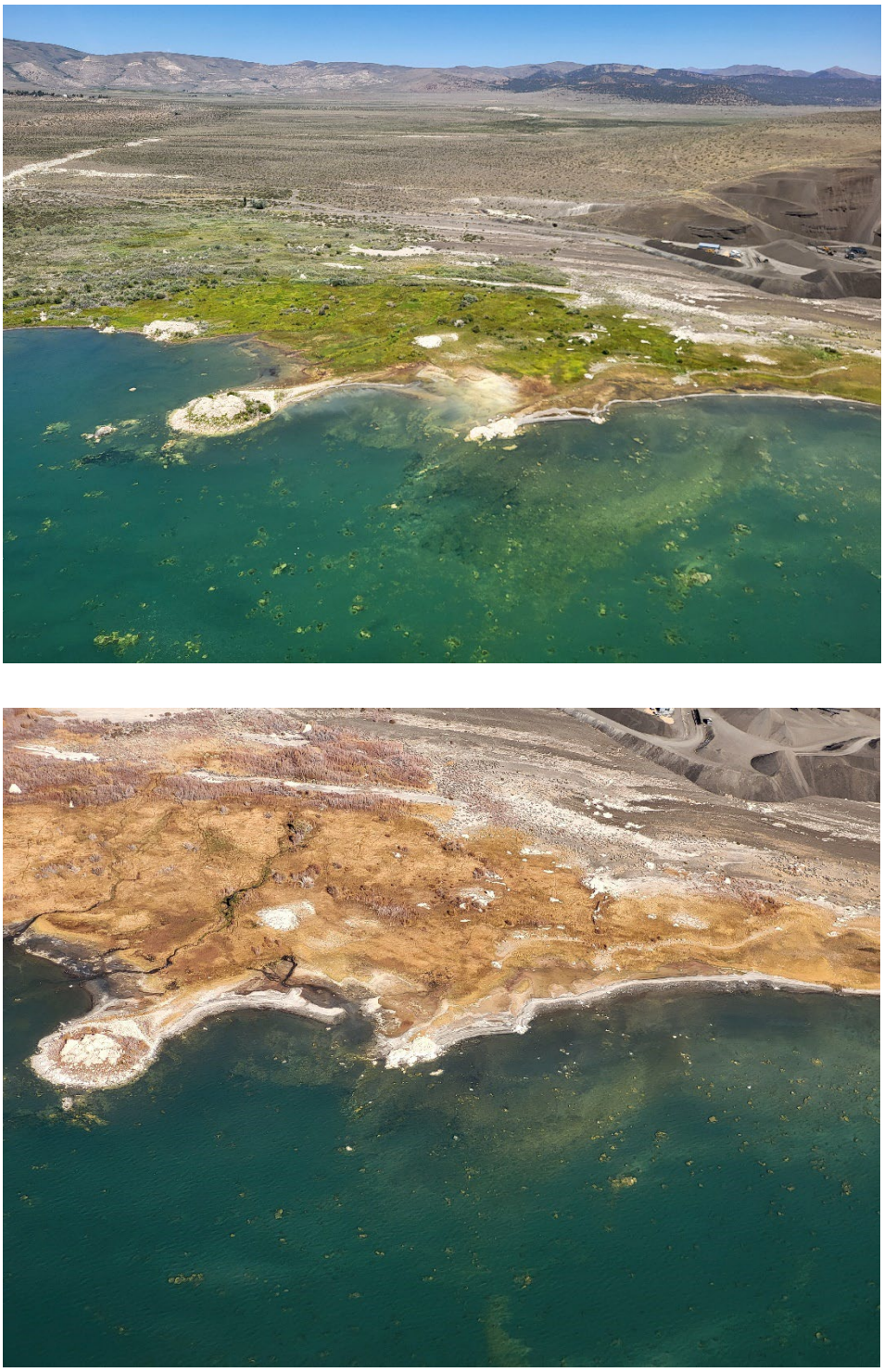

Figure 39. Wilson Creek, East of Tufa Mound Spring to the Left in the Photo (Top Photo: July 27, 2024; Bottom Photo: November 12, 2024).

Bridgeport Reservoir Shoreline

Please refer to Figure 4 for the location of each shoreline subareas at Bridgeport Reservoir. All three shoreline segments at Bridgeport Reservoir: North Arm, West Bay, and East Shore are shown in Figure 40.

The North Arm seen at the far end of the photo is in the narrowest part of the reservoir and includes primarily sandy beaches bordered by upland vegetation. The West Bay receives freshwater inflows from Buckeye and Robinson Creeks and the East Walker River, creating extensive mudflat areas adjacent to these creek inflow areas, especially when the water level in the reservoir is higher. The West Bay also receives seepage and runoff from the adjacent irrigated pastures. The East Shore includes some mudflat and meadow areas in the vicinity of the East Walker River, but most of the East Shore area is bordered by Great Basin scrub or exposed reservoir bottom.

Figure 40. Conditions at Bridgeport Reservoir in 2024 (November 12, 2024).

Crowley Reservoir Shoreline Subareas

Please refer to Figure 5 for the location of each of the following shoreline subareas at Crowley Reservoir. The major source of freshwater input to Crowley Reservoir is the Owens River. Other freshwater input includes flows from McGee and Convict Creeks, Layton Springs, and subsurface flow from other springs along the west shore. Vegetation communities immediately surrounding Crowley Reservoir include irrigated pasture, wet meadow, Great Basin scrub, alkali meadow, and mudflats.

Chalk Cliffs (CHCL)

The Chalk Cliffs (CHCL) subarea lacks freshwater inflow areas and wetland habitats, and is dominated by sandy beaches adjacent to steep, sagebrush-covered slopes. (Figures 41 and 42).

Figure 41. Chalk Cliffs, Northern Extent (November 12, 2024).

Figure 42. Chalk Cliffs, Southern Extent (November 12, 2024).

Hilton Bay (HIBA)

The Hilton Bay (HIBA) shoreline area includes Big Hilton Bay to the north and Little Hilton Bay to the south (Figure 43). The HIBA subarea, surrounded by meadow and sagebrush habitat, receives small amounts of freshwater input from Hilton Creek, Whiskey Creek, and area springs. Pelican Point, on the right side of the photo, is a favored sleeping and loafing area for waterbirds including waterfowl.

Figure 43. Hilton Bay Conditions, Looking West (November 12, 2024).

Layton Springs (LASP)

The Layton Springs (LASP) shoreline subarea is bordered by upland vegetation and a sandy beach. LASP provides freshwater input at the southern border of this lakeshore segment. The high reservoir level resulted in flooding of rabbitbrush, sagebrush and meadow along much of the length of this shoreline area (Figures 44 and 45). These flooded stands of shrubs seemed particularly attractive to waterfowl in fall.

Figure 44. Layton Springs, Looking South (November 12, 2024).

Figure 45. Layton Springs, Looking Southeast (November 12, 2024).

McGee Bay (MCBA)

The McGee Bay (MCBA) shoreline subarea supports the best waterfowl habitat at Crowley Reservoir (Figures 46 and 47). McGee Creek and Convict Creek supply perennial freshwater flow to this area of Crowley. At most reservoir levels, vast mudflats and wetlands occur along the west shore due to the low gradient slope of the shoreline and input from springs and subsurface flow from up-gradient irrigation.

Figure 46. McGee Creek Shoreline Subarea North of Pelican Point, Southern Extent (November 12, 2024).

Figure 47. McGee Creek Shoreline Subarea, Northern Extent (November 12, 2024).

North Landing (NOLA)

The North Landing (NOLA) subarea is influenced by subsurface flows and supports meadow, wet meadow and mudflat habitats (Figure 48). The depression was still full in fall at Sandy Point, but in the past, it has only attracted low numbers of waterfowl.

Figure 48. North Landing, looking west (November 12, 2024).

Sandy Point (SAPO)

Most of the length of Sandy Point (SAPO) subarea is bordered by short cliffs or upland vegetation (Figure 49). Small areas of meadow habitat occur in this area, and limited freshwater seepage occurs at Green Banks Bay.

Figure 49. Sandy Point, Looking North Towards the Owens River Delta (November 12, 2024).

Upper Owens River (UPOW)

The Upper Owens River (UPOW) receives direct flow from the Owens River, the largest source of freshwater input to Crowley Reservoir (Figures 50 and 51). Except at high reservoir levels, this subarea includes a large area of exposed reservoir bottom, and variable amounts of mudflats.

Figure 50. Upper Owens Delta, Looking North (November 12, 2024).

Figure 51. Upper Owens Delta, Looking North (November 12, 2024).

Literature Cited

[CERL & EMSL] Corvallis Environmental Research Laboratory and Environmental Monitoring and Support Laboratory. 1978. U.S. Environmental Protection Agency National eutrophication survey. Working Paper Series. No. 743. Report on Lake Crowley, Mono County, California, EPA Region IX.

Gollop, J. B, and W. H. Marshall. 1954. A guide for aging duck broods in the field. Mississippi Flyway Council. Tech. Sect. Report.

Horne, A. J. 2003. Report on Bridgeport Reservoir beneficial use impairment: limnology in the summer-fall 2000 and comparisons with 1989. Report prepared for Lahontan Regional Water Quality Control Board. South Lake Tahoe.

House, D. 2021. Fall waterfowl use of Bridgeport Reservoir, Mono County, California. Western Birds 52(4): 278–295.

Jehl, J. R. 2002. Waterfowl populations at Mono Lake, California 2001. Hubbs Sea World Institute. Technical Report 2002-330. Prepared for Los Angeles Department of Water and Power.

Jellison, R., K. Rose and J. M. Melack. 2003. Assessment of internal nutrient loading to Crowley Lake, Mono County. Final Report to the State Water Resources Control Board.

Los Angeles Department of Water and Power (LADWP). 1987. Mono Basin geology and hydrology. Prepared by Aqueduct Division Hydrology Section. March 1987.

Los Angeles Department of Water and Power (LADWP). 1996a. Mono Basin waterfowl habitat restoration plan. Prepared for the State Water Resources Control Board. In response to Mono Lake Basin Water Right Decision 1631.

Los Angeles Department of Water and Power (LADWP). 1996b. Mono Basin stream and stream channel restoration plan. Prepared for the State Water Resources Control Board. In response to Mono Lake Basin Water Right Decision 1631.

Los Angeles Department of Water and Power (LADWP). 2018. Mono Basin Waterfowl Habitat Restoration Program Periodic Overview Report. Prepared by Deborah House and Motoshi Honda for the State Water Resources Control Board. May 2018.

Los Angeles Department of Water and Power (LADWP). 2024. Mono Basin Waterfowl Habitat Restoration Program 2023 Monitoring Report. Prepared by Deborah House for the State Water Resources Control Board. April 2024.

Rogers, D.B., S.J. Dreiss and D.P. Groeneveld. 1992. Near-Shore Groundwater and Salt-Flat Processes at Mono Lake, White Mountain Research Station Symposium, 4, 367–395.

Sharpe, S. E., M. E. Cablk, and J. M. Thomas. 2007. The Walker Basin, Nevada and California: physical environment, hydrology, and biology. Desert Research Institute Publication No. 41231. May 2007. Revision 01 May 2008.

State Water Resources Control Board (SWRCB). 1994. Mono Lake Basin water right decision 1631.

U.S.D.A. Forest Service. 2005. Decision Memo. Pond 3-Barrow Pit Pond Wildlife Habitat Improvement. Inyo National Forest. Mono County, CA. July 18, 2005.

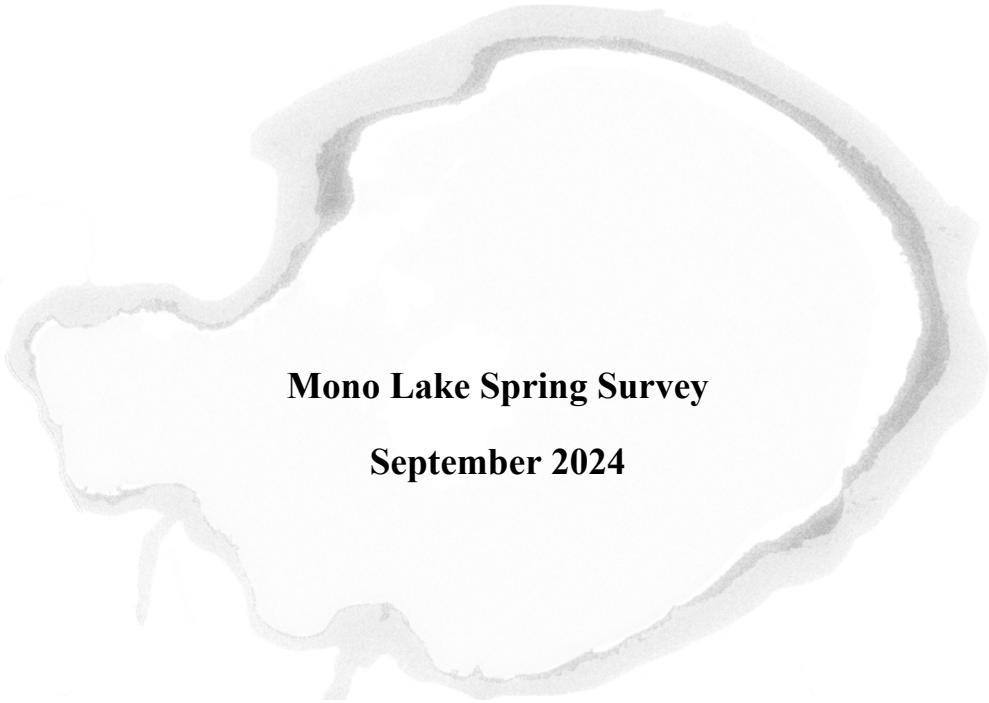

Mono Lake Spring Survey

September 2024

Eastern Sierra Environmental and Water Rights Group

Water Operations Division

Los Angeles Department of Water and Power

Summary

The 2024 Mono Lake Spring Survey was conducted September 16 through September 20, 2024, to measure the flow rates and the basic water quality of spring water flowing into Mono Lake. The survey, which is conducted every 5 years, is part of Los Angeles Department of Water and Power's (LADWP) environmental mitigation monitoring efforts of the lake. This survey complies with the terms and conditions of LADWP water right License Nos. 10191 and 10192 as set forth in the State Water Resources Control Board Decision 1631 and Order No. 98-05 and per LADWP's Waterfowl Habitat Restoration Plan of 1996. LADWP's Eastern Sierra Environmental Group's staff, along with hydrographers from LADWP's Northern District Office, participated in the survey.

The spring locations on the shores of Mono Lake are presented in **Map 1** and the survey data (*flow*, *temperature*, *electrical conductivity*, etc.) are listed in **Table 1**. The spatial distributions of *flow*, *temperature*, and *electrical conductivity* values are displayed in **Maps 2, 3, and 4**, respectively. Parameters such as temperature and conductivity help indicate the flow mechanisms by which water seeps to the surface and the presence of deep saline zones in the aquifer due to salt intrusion. Parametric data are presented as bar charts geographically positioned at their approximate spring locations on the maps.

The presence of sulfur strands, hydrogen sulfide gas, and tufa towers at each spring are also presented in **Table 1**. These features indicate the presence of volcanic activity and calcium saturation at or near the springs. Photographs of each spring site surveyed are included in the **Album** section of the report. Dense vegetation and high water levels (compared to Spring Survey 2019) made it difficult to access some spring sources. All accessible sites were surveyed using a hand-held Global Positioning System (GPS) using longitudinal and latitudinal coordinates from the 2014 spring survey.

Mono Lake surface water elevation on September 16th at the start of this year's survey was 6383.51 feet (USGS Datum), which was 0.96 feet higher than when the 2019 spring survey was conducted. A comparison of the spring flows between the 2019 and 2024 surveys are presented in **Table 2**, which includes 2 newly discovered springs (*Perseverance NW and Gull Bath (East 2.0)*). Each new spring is located within 30 feet of the springs that bear the same root name (i.e. *Perseverance NW* is within 30 feet of Perseverance). Of the 38 spring sites surveyed, 29 springs flowed to Mono Lake totaling approximately **10.5 cfs**. Six sites exhibited no flow or flow too small to be measured. One spring was dry, and one was indistinguishable due to excess

water in the area. It is likely that the decreased total spring flow shown in **Table 2** is due to the submerged springs at the Gull Bath site.

Some spring data is unavailable for certain sites, which are indicated in **Table 1**. Sandpiper was not found and was therefore determined to be dry. County Park No. 4.5 was also not found due to large amounts of water in the area, which made it difficult to discern whether there was a distinct second spring. In addition, spring sites *Hot Tufa Tower, Perseverance NW, Martini,* and *Villette* were completely submerged and were visually assessed to be "bubbling" as indicated in the table below.

Fourteen sites exhibited increases in flow compared to the 2019 spring survey, including flow from new springs. Seventeen sites exhibited decreases in flow. Flow at 2 sites remained the same, not including trace flow comparisons. Overall, flow from the springs into Mono Lake in 2024 increased by approximately **1.32 cfs** compared to that measured in the 2019 spring survey.

The next spring survey is scheduled for the Fall of 2029.

Physical Location

Map 1: Spring Locations

Springs in Mono Lake seep groundwater to the surface when the pressure on groundwater in the underlying aquifer becomes so high that it overcomes the gravitational pressure keeping it down. Pressure builds up in the aquifer via two mechanisms: *elevation gradient flow* and *hydrothermal flow*. High elevation gradient flow exists where runoff infiltrates into the aquifer from high nearby elevations like the Sierra Nevada Mountains. High hydrothermal flow is the convection of groundwater due to volcanic activity which forces groundwater up to the cooler surface. Springs are scattered throughout the shores of Mono Lake except in the northeast, likely due to low elevation gradient and limited hydrothermal activity. Increased volcanic activity and increased runoff from local mountains can attribute to increased spring flow and also the manifestation of new springs. The landscape of Mono Lake Basin, including the key mountain ranges surrounding the Lake is presented in **Map 5**.

Two new springs were discovered during this year's spring survey. *Gull Bath (East 2.0)* is located on the Northwest shore, while *Perseverance NW* is located on the North shore. The apparition of these springs is likely attributed to the Extreme-Wet 2023 Runoff Year, coming after three years of Dry, Dry-Normal, and Normal years from May 2020 to April 2023. This is consistent with past findings. According to the 2019 Spring Survey Report, three new springs

were observed during the 2019 survey due to increased runoff during the two years leading up to the 2019 survey, coming after four years of drought.

Two existing springs were not found this year. *Sandpiper* is located on the Southeast shore and *County Park No. 4.5* is located on the Northwest shore.

Geophysical Analysis

Map 2: Flow Rate Measurements

The points of measurement at each spring site varied by accessibility due to vegetation density. Generally, the flow rate (as well as temperature and conductivity) of spring water was measured as soon as the water channelized on the surface. Hydrographers measured the flow at spring sites via one of three methods: current meter, v-notch weir, and estimation. A current meter equipped with a positive displacement sensor was used to measure the flow rate by measuring the water velocities at subsections within spring flow channels. A v-notch weir was used when the depths of the spring flow channels were too low to measure flow rate accurately with the current meter. When the flow or depth of the spring flow channels was too low to measure flow rate using a current meter or v-notch weir, hydrographers visually estimated the flow.

The largest increase in flow from 2019 to 2024 occurred at springs on the north and northwest shores. Increases in flow in the northern spring – *Coyote Marsh* – and in the northwestern springs – *County Park No. 1, County Park No. 3, County Park No. 4, County Park No. 5, County Park No. 8,* and *County Park No. 9* – are likely attributed to the same phenomenon that caused the apparition of three new springs in the same areas (i.e. high infiltration from runoff over the past two years after four years of drought).

Relatively little flow was observed from springs on the east and north shores, which is comparable to the lack of flow in that area in 2019. On the east shore, this phenomenon is likely due to the low elevation gradient between the east shore of Mono Lake and the Excelsior Mountains east of the lake (the expanse of land between Mono and Excelsior is over 15 miles), which results in low groundwater recharge. The Bodie Hills to the north, likewise, contribute a low amount of groundwater recharge, which is indicated by low spring activity on the north shore. This is due generally to less rainfall, sediments with low permeability (reducing vertical groundwater fluxes), and the low groundwater surface.

On the south shore, low spring activity is apparent; however, there is actually a high gradient of flow to this area from the Mono Craters. This results in an intermediate amount of groundwater recharge from the deep water table, which likely never manifests into springs on the surface. Rather, a significant amount of the groundwater recharges the lake directly underground.

Map 3: Temperature Measurements

Temperature was measured by inserting an electronic temperature probe into the spring flow channels or ponding areas near the eye of springs so long as the probe was kept suspended in water. Most temperature measurements taken throughout the springs at Mono Lake varied around 10-20 °C. The measurements taken at *Southern Comfort* on the south shore, however, was at 31.7 °C. In addition, springs on the east shore – *Twin Warm*, *Bug Warm*, and *Warm B* – all had temperature readings ranging from 28.4 to 33.4 °C. The warm springs in these areas are likely driven by hydrothermal (based on the high temperature measurements) and fault activity (based on the close proximity of the east shore to fault lines). Although temperature is generally indicative of flow mechanism, various factors can affect temperature readings in the field, including but not limited to the flow rates, vegetation densities, and shading at the points of measurement. High temperature readings may also be attributed to the ponding of spring water, which results in more sun exposure due to the low flows of springs in the area.

Map 4: Conductivity Measurements

Conductivity was measured either by collecting spring water in a bottle and subsequently inserting an electronic conductivity meter into the bottle or inserting the electronic conductivity probe into the spring flow channel or ponding area. The conductivity measurements throughout the springs of Mono Lake exhibit noticeable trends. The southwest, west, and northwest shores exhibit relatively low conductivity levels (36-368 µS/cm), except for *Gull Bath (East)* and *Gull Bath (East 2.0)*, which flowed directly into the lake and were therefore highly saline; the southeast shore has relatively moderate conductivity levels (262-741 µS/cm); the north shore has moderately high conductivity levels (444-1715 µS/cm); and the south and east shores have relatively high conductivity levels (1254-2420 µS/cm, excluding *Hot Tufa Tower*, which flowed directly into Mono Lake and was therefore highly saline).

High conductivity in water is caused by the presence of salts that promote a high electrical current, which also contributes to high levels of total dissolved solids (TDS). The

relative levels of conductivity respective to their shores help indicate the origins of groundwater seepage.

Generally, eastern shores have higher conductivity than western shores. This is caused by the significant freshwater recharge from the Sierra Nevadas Mountains in the west. Since saline water is denser than freshwater, it sinks below freshwater when it flows into Mono Lake and the aquifer underneath it. There is generally stratification between freshwater and saline water throughout the lake, where salinity increases with depth (although evaporation exposes salt crusts at the surface), with some mixing between strata. The influx of freshwater essentially pushes (overcuts) the saltwater towards the east. This phenomenon results in the high conductivity values evident on the eastern shores and low values on the western shores. The low levels of conductivity at springs on the western shores are also attributed to a high elevation gradient with the Sierra Nevada Mountains, resulting in minimal exposure to salts at the surface.

Groundwater on the southeast shore has moderate conductivity levels indicating that there is likely salt exposure to the shallow groundwater table due to evaporation. Higher conductivity measurements in the north shore are also likely attributed to further shallow groundwater activity. The low flow from these springs indicate that there is likely more of a retention time for water to be exposed to salts.

Hydrothermally driven groundwater typically carries sodium bicarbonate-chloride and other related salts, which explains the high levels of conductivity in the south and east shores, which have high temperatures at springs. Hydrothermal activity is likely a main mechanism in bringing groundwater to the surface in these areas. Thus, at these springs, high levels of conductivity correlate to high temperatures.

Map 1. 2024 Mono Lake Spring Survey Spring Locations

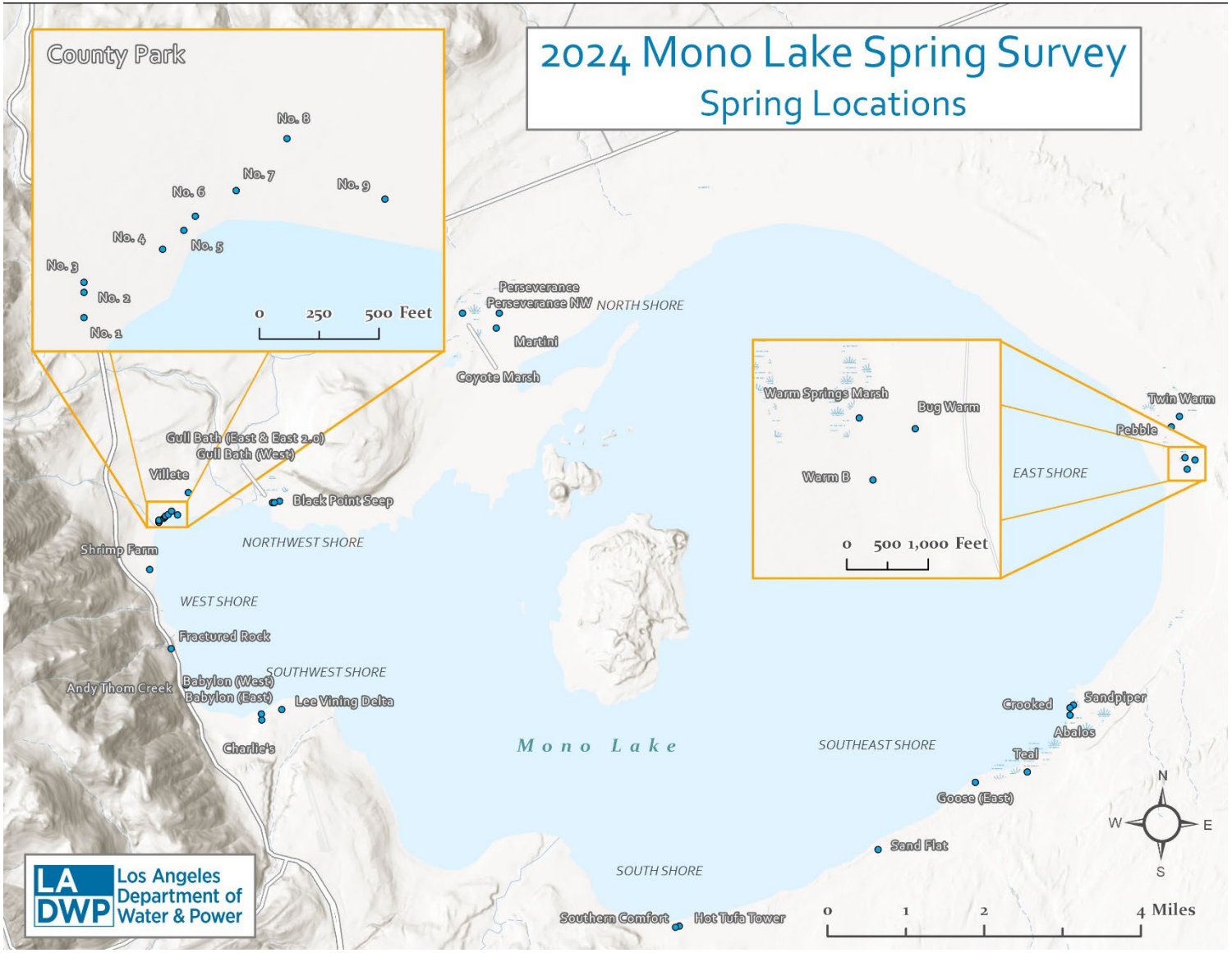

Map 2. 2024 Mono Lake Spring Survey Flow Measurements

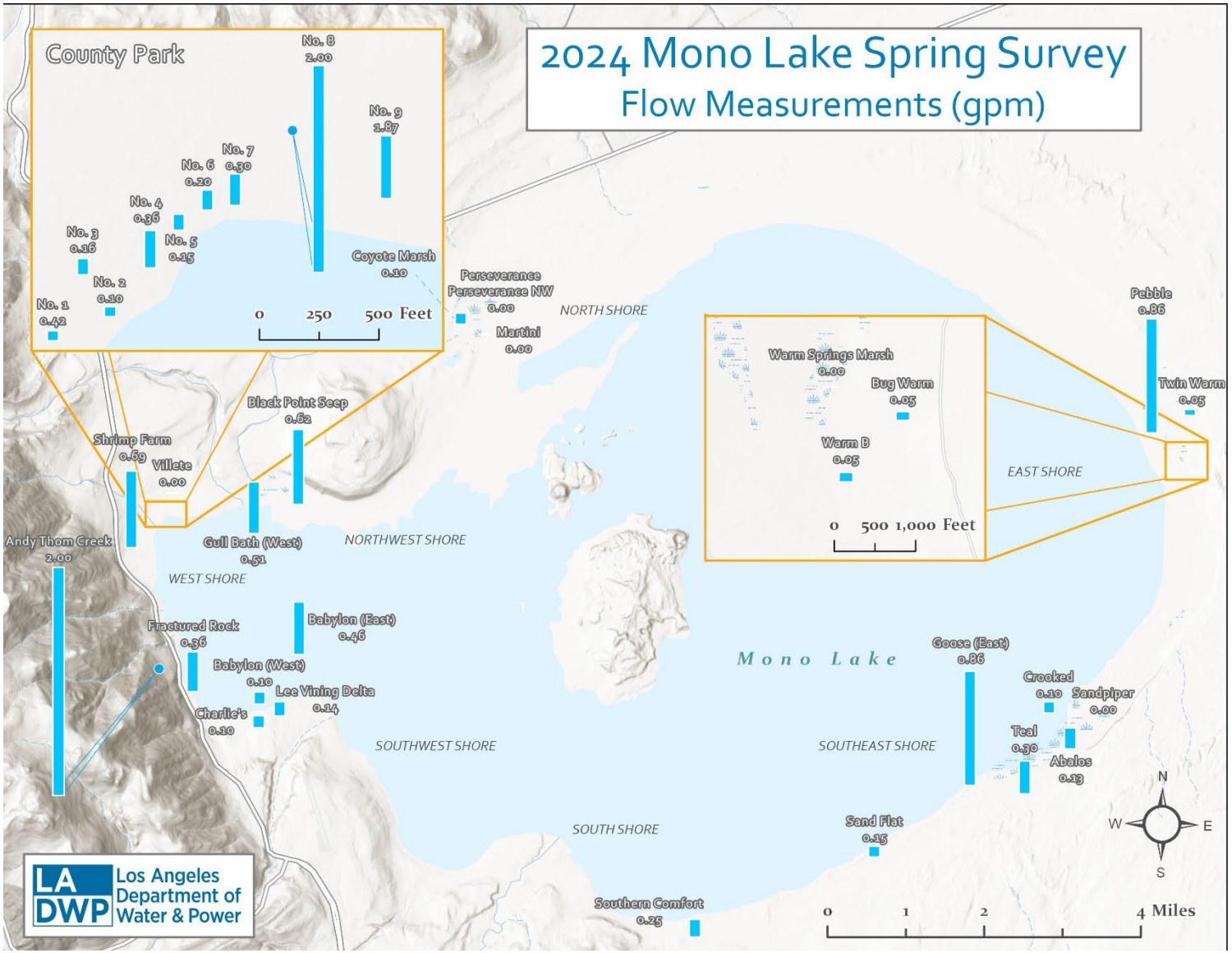

Map 3. 2024 Mono Lake Spring Survey Temperature Measurements

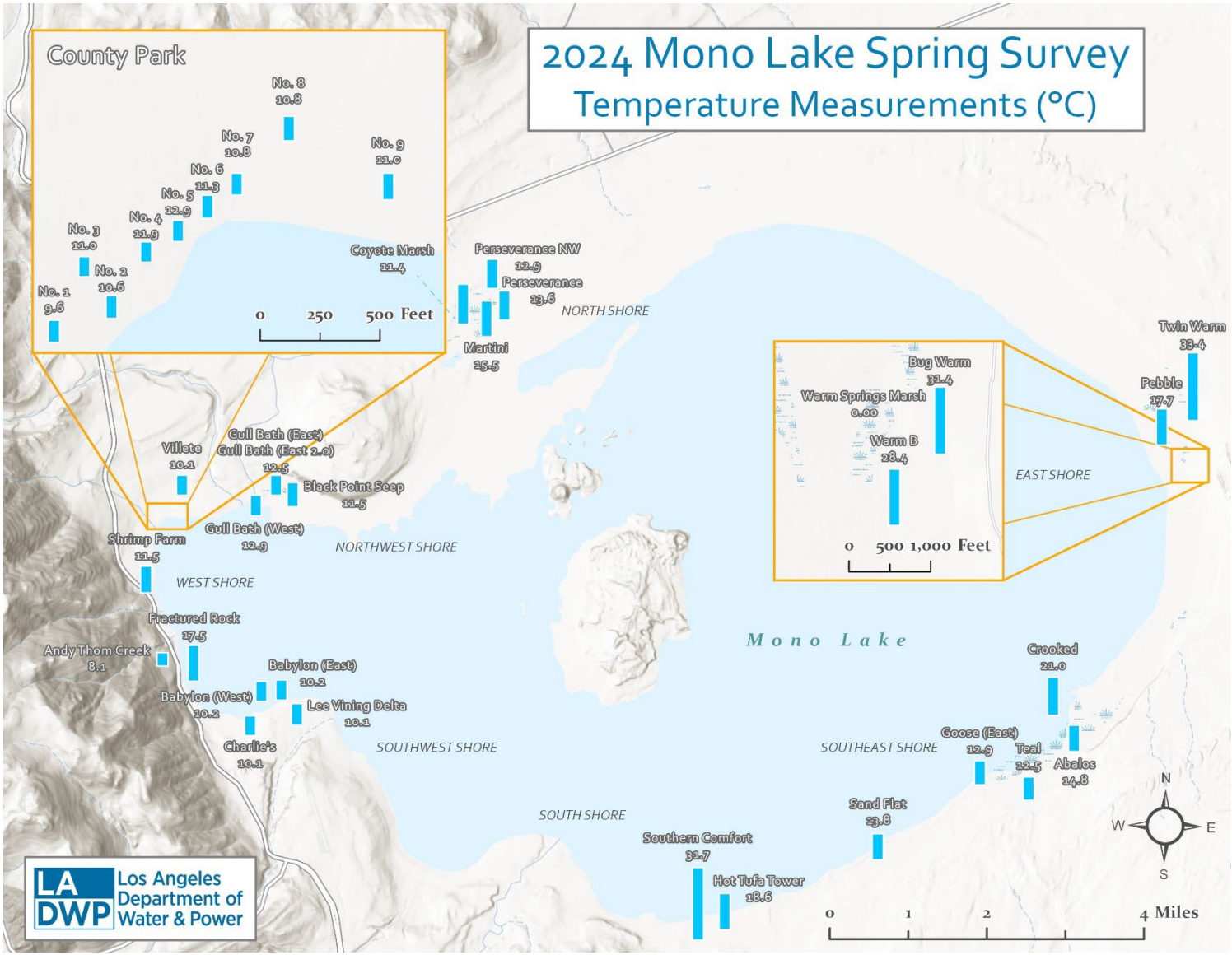

Map 4. 2024 Mono Lake Spring Survey Conductivity Measurements

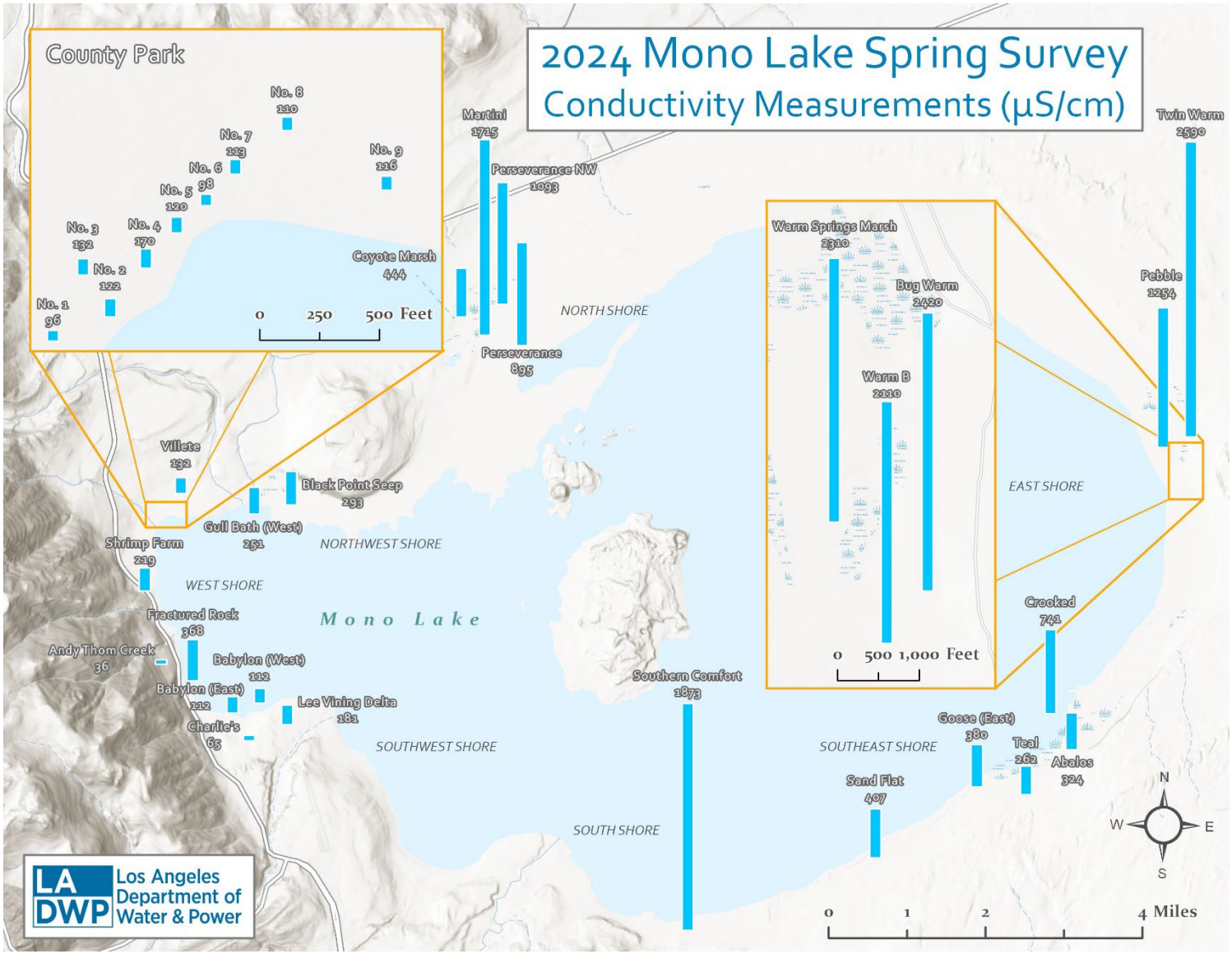

Map 5. Mono Lake Basin Landscape

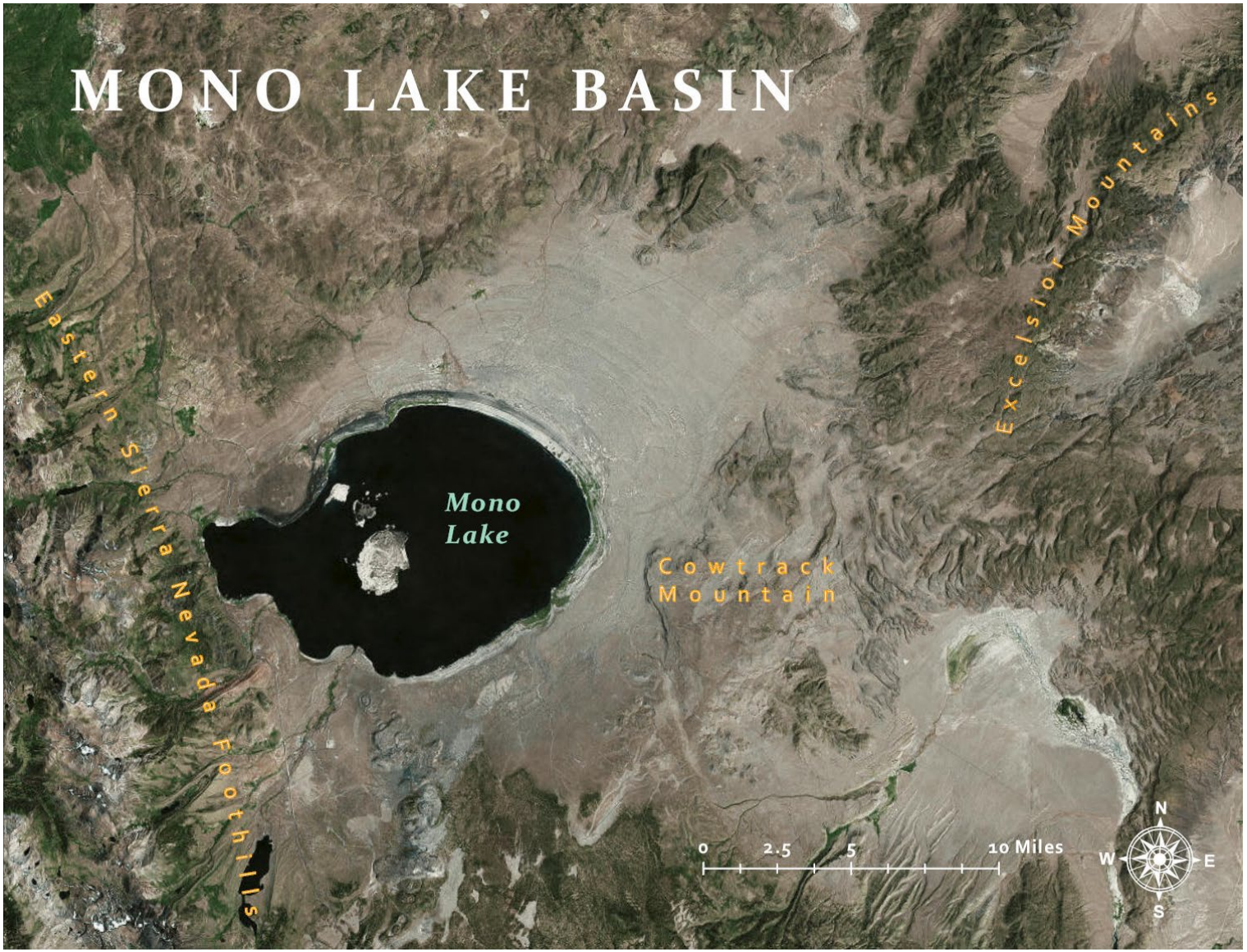

Table 1. 2024 Mono Lake Spring Survey Data

2019 ID	Spring	Flow (cfs)	Measurement Method	Temp. (°C)	Elec. Cond. (uS/cm)	Sulfur Strands	H2S Gas	Tufa Tower	Clarity	WGS Coordinates Latitude	Longitude
South Shore											
M01	Hot Tufa Tower	0.2	Estimate	18.6	51,300	No	No	Yes	Clear	N 37° 56.481'	W 119° 01.321'
M02	Southern Comfort	0.25	Estimate	31.7	1,873	No	No	Yes	Slight Haze	N 37° 56.465'	W 119° 01.375'
Southeast Shore											
M03	Sand Flat	0.15	Estimate	13.8	407	No	No	Yes	Clear	N 37° 57.376'	W 118° 58.555'
M04	Sandpiper				Dry					N37 59.024"	W118 55.861"
M05	Goose (East)	0.86	Current Meter	12.9	380	No	No	Yes	Clear	N 37° 58.145'	W 118° 57.214'
M06	Teal	0.30	Estimate	12.5	262	Yes	No	Yes	Clear	N 37° 58.273'	W 118° 56.491'
M07	Crooked	0.10	Estimate	21.0	741	No	No	No	Clear	N 37° 58.996'	W 118° 55.887'
M08	Abalos	0.13	Estimate	14.8	324	No	No	Yes	Slight Color	N 37° 58.912'	W 118° 55.905'
East Shore											
M09	Warm B	0.05	V-notch	28.4	2110	No	No	No	Clear	N 38° 01.772'	W 118° 54.224'
M10	Warm Springs Marsh	Trace	Estimate	19.3	2310	No	No	No	Clear	N 38° 01.792'	W 118° 54.366'
M11	Twin Warm	0.05	Estimate	33.4	2590	No	No	Yes	Clear	N 38° 02.131'	W 118° 54.568'
M12	Pebble	0.86	V-notch	17.7	1254	No	No	Yes	Clear	N 38° 02.249'	W 118° 54.457'
M13	Bug Warm	0.05	V-notch	31.4	2420	No	Yes	Yes	Clear	N 38° 01.668	W 118° 54.328'
North Shore											
M14	Perseverance	Trace	Estimate	13.6	895	No	Yes	No	Clear	N 38° 03.232'	W 119° 04.034'
M14.5	Perseverance NW	Trace	Estimate	12.9	1093	No	Yes	No	Clear	New Spring Beside M14	
M15	Coyote Marsh	0.10	Estimate	11.4	444	No	No	No	Slight Color	N 38° 03.222'	W 119° 04.550'
M16	Martini	Trace	Estimate	15.5	1715	No	Yes	Yes	Clear	N 38° 03.069'	W 119° 04.072'
Northwest Shore											
M17	Gull Bath (East)	2.00	Estimate	12.5	23,500	No	No	Yes	Clear	N 38° 01.075'	W 119° 07.131'
M17.5	Gull Bath (Weast)										
M18	Gull Bath (West)	0.51	Current Meter	12.9	251	No	No	Yes	Clear	N 38° 01.073'	W 119° 07.160'
M19	Villette	Trace	Estimate	10.1	131.9	No	No	No	Slight Color	N 38° 01.164'	W 119° 08.346'
M20	County Park No. 1	0.10	Current Meter	9.6	95.5	No	No	Yes	Clear	N 38° 00.827'	W 119° 08.748'
M21	County Park No. 2	0.10	Estimate	10.6	122	No	No	Yes	Clear	N 38° 00.846'	W 119° 08.708'
M22	County Park No. 3	0.16	Current Meter	11.0	132.3	No	No	Yes	Clear	N 38° 00.852'	W 119° 08.707'
M23	County Park No. 4	0.36	Current Meter	11.9	170.2	No	No	Yes	Clear	N 38° 00.875'	W 119° 08.681'
M23.5	County Park No. 4.5				No Source Found					Beside M23	
M24	County Park No. 5	0.15	Estimate	12.9	119.8	No	No	Yes	Clear	N 38° 00.889'	W 119° 08.663'
M25	County Park No. 6	0.20	Estimate	11.3	98.4	No	No	Yes	Clear	N 38° 00.899'	W 119° 08.652'
M26	County Park No. 7	0.30	Estimate	10.8	113.3	No	No	Yes	Clear	N 38° 00.917'	W 119° 08.618'
M27	County Park No. 8	2.00	Current Meter	10.8	110.3	No	No	No	Clear	N 38° 00.953'	W 119° 08.574'
M28	County Park No. 9	0.56	Current Meter	11.0	116.1	No	No	No	Clear	N 38° 00.914'	W 119° 08.487'
M29	Black Point Seep	0.62	Current Meter	11.5	293	No	No	Yes	Clear	N 38° 01.093'	W 119° 07.062'
West Shore											
M30	Shrimp Farm	0.69	Current Meter	11.5	219	No	No	No	Clear	N 38° 00.304'	W 119° 08.859'
M31	Fractured Rock	0.36	Current Meter	17.5	368	No	No	No	Clear	N 37° 59.031'	W 119° 08.314'
M32	Andy Thom Creek	2.00	Current Meter	8.1	36.2	No	No	No	Clear	N 37° 59.432'	W 119° 08.535'
Southwest Shore											
M33	Lee Vining Delta	0.14	Current Meter	10.1	181	No	No	Yes	Clear	N 37° 58.783'	W 119° 06.962'
M34	Babylon (West)	0.10	Estimate	10.2	112.2	No	No	Yes	Clear	N 37° 58.727'	W 119° 07.245'
M34.5	Babylon (East)	0.46	Current Meter	10.2	112.1	No	No	Yes	Clear	Beside M34	
M35	Charlie's	0.10	Estimate	10.1	64.6	No	No	No	Clear	N 37° 58.661'	W 119° 07.241'

Table 2. Mono Lake Spring Survey 2019/2024 Flow Comparison

2024 ID	Spring	Flow (cfs)		
		2019	2024	Difference (+/-)
South Shore				
M01	Hot Tufa Tower	Submerged	Submerged	0
M02	Southern Comfort	No Flow	0.25	+0.25
Southeast Shore				
M03	Sand Flat	0.10	0.15	+0.05
M04	Sandpiper	0.37	No Flow	-0.37
M05	Goose (East)	1.38	0.86	-0.52
M06	Teal	0.75	0.30	-0.45
M07	Crooked	0.30	0.10	-0.20
M08	Abalos	0.20	0.13	-0.07
East Shore				
M09	Warm B	0.06	0.05	-0.01
M10	Warm Springs Marsh	Trace	Trace	0
M11	Twin Warm	0.09	0.05	-0.04
M12	Pebble	0.03	0.86	+0.83
M13	Bug Warm	0.05	0.05	0
North Shore				
M14	Perseverance	Trace	Trace	0
M14.5	Perseverance NW	Did not Exist	Trace	0
M15	Coyote Marsh	Trace	0.10	+0.10
M16	Martini	Trace	Trace	0
Northwest Shore				
M17	Gull Bath (East)	1.80	Submerged	-1.80
M17.5	Gull Bath (Weast)	Did not Exist	Submerged	0
M18	Gull Bath (West)	0.23	0.51	+0.28
M19	Villette	Trace	Trace	0
M20	County Park No. 1	0.06	0.10	+0.04
M21	County Park No. 2	0.14	0.10	-0.04
M22	County Park No. 3	0.07	0.16	+0.09
M23	County Park No. 4	0.10	0.36	+0.26
M23.5	County Park No. 4.5	0.12	No Flow	-0.12
M24	County Park No. 5	Did Not Measure	0.15	+0.15
M25	County Park No. 6	0.87	0.20	-0.67
M26	County Park No. 7	0.53	0.30	-0.23
M27	County Park No. 8	1.85	2.00	+0.15
M28	County Park No. 9	0.25	0.56	+0.31
M29	Black Point Seep	0.65	0.62	-0.03
West Shore				
M30	Shrimp Farm	0.77	0.69	-0.08
M31	Fractured Rock	0.53	0.36	-0.17
M32	Andy Thom Creek	2.57	2.00	-0.57
Southwest Shore				
M33	Lee Vining Delta	0.32	0.14	-0.18
M34	Babylon	0.17	0.10	-0.07
M34.5	Babylon 2.0	0.04	0.46	+0.42
M35	Charlie's	0.10	0.10	0
Total		14.49	11.81	-2.69

Album

M01 – Hot Tufa Tower

M02 – Southern Comfort

M03 – Sand Flat

M04 – Sandpiper

M05 – Goose (East)

M06 – Teal

M07 – Crooked

M08 – Abalos

M09 – Warm B

M10 – Warm Springs Marsh

M11 – Twin Warm

M12 - Pebble

M13 – Bug Warm

M14 – Perseverance

M14.5 – Perseverance NW

M15 – Coyote Marsh

M16 – Martini

M17 – Gull Bath (East)

M17.5 – Gull Bath (East 2.0)

M18 – Gull Bath (West)

M19 – Villete

M20 – County Park No. 1

M21 – County Park No. 2

M22 – County Park No. 3

M23 – County Park No. 4

M24 – County Park No. 5

M25 – County Park No. 6

M26 – County Park No. 7

M27 – County Park No. 8

M28 – County Park No. 9

M29 – Black Point Seep

M30 – Shrimp Farm

M31 – Fractured Rock

M32 – Andy Thom Creek

M33 – Lee Vining Delta

M34 – Babylon (West)

M34.5 – Babylon (East)

M35 – Charlie’s